

Metal-Based Chemosensors for Important Bioanalytes

THÈSE N° 4796 (2010)

PRÉSENTÉE LE 15 OCTOBRE 2010

À LA FACULTÉ SCIENCES DE BASE

LABORATOIRE DE CHIMIE SUPRAMOLÉCULAIRE

PROGRAMME DOCTORAL EN CHIMIE ET GÉNIE CHIMIQUE

ÉCOLE POLYTECHNIQUE FÉDÉRALE DE LAUSANNE

POUR L'OBTENTION DU GRADE DE DOCTEUR ÈS SCIENCES

PAR

Sébastien ROCHAT

acceptée sur proposition du jury:

Prof. K. Johnsson, président du jury

Prof. K. Severin, directeur de thèse

Prof. P. J. Dyson, rapporteur

Prof. C. Hartinger, rapporteur

Prof. B. König, rapporteur



ÉCOLE POLYTECHNIQUE
FÉDÉRALE DE LAUSANNE

Suisse
2010

“There is nothing like looking, if you want to find something. You certainly usually find something, if you look, but it is not always quite the something you were after.”

J. R. R. Tolkien, *The Hobbit*

Acknowledgements

The Claude & Giuliana Foundation is gratefully acknowledged for having generously provided financial support for this research work.

During the many years I spent at EPFL, I had the chance to meet many remarkable and admirable people. It was a real pleasure to spend time by their side, and this thesis owes them a lot.

First, I would like to thank my supervisor Prof. Kay Severin for all his support, guidance, direction, enthusiasm and encouragement. I never failed to leave a meeting with Kay without feeling truly motivated and encouraged and I have found his help and advice invaluable over the last four years.

I would like to express my gratitude to the members of the jury (Prof. Paul J. Dyson and Prof. Kai Johnsson from EPFL, Prof. Burkhard König from University of Regensburg, and Prof. Christian G. Hartinger from University of Vienna), who kindly accepted to dedicate some of their time to evaluating of this work. Sabine Hauert and Adrien Lawrence are gratefully acknowledged for proof-reading this manuscript.

I have had the good fortune to work with a number of great people in the Severin group throughout my PhD studies. The Severin group is a great place to work and I would like to thank the current members (Mariano Fernández-Zúmel, Barnali Dutta, Mirela Pascu, Julie Risse, Alexander Tskhovrebov, Katrin Thommes, Clément Schouwey, Justus Tönnemann, Bo Ram Lee, Gregor Kiefer, Anton Granzhan, Euro Solari, Thomas Riis-Johannessen, Fidi Zaubitzer, Erin Sheepwash, Burçak İçli, Sebastian Mirtschin and Vera Janowski) and those from a distant past (Céline Olivier, Davinia Fernández-González, Joffrey Wolf, Christian “Jonny” Albrecht, Andrey Buryak, Nicolas Christinat, Christian Schüttler, Dalit Rechavi-Robinson, Evgeny Katayev, Elvira Krasniqi, Karthik Naganathan, Charlotte Buron) for the many enjoyable hours spent having lunch, a coffee or a beer, chatting and of course working. Special thanks to Zacharias Grote for having introduced me to the wonderful world of metallocrown complexes (at

the time when I was still a clumsy student), and particularly to Jie Gao (now in Shanghai) for an extremely fruitful collaboration.

Outside the lab, I wish to thank the 'Sat' team, which made the end of weeks extremely enjoyable: Ryan Dykeman, Tom Woods, Annabelle Gillig, Ludivine Rielle, Céline Fellay, Filippo De Simone, Jean-Yves Wach, Cyril Portmann, among others.

Merci beaucoup à tous ceux qui oeuvrent “dans l'ombre” afin de nous faire bénéficier des meilleures conditions de travail: l'équipe du magasin (Gladys Pasche, Annelise Carrupt, Giovanni Petrucci) pour laquelle il n'y a jamais de problème, uniquement des solutions, Martial Rey, qui entretient les spectromètres RMN comme ses plantes vertes, Francisco Sepulveda et Laure Menin qui effectuent les analyses de spectrométrie de masse, et Christina Zamanos-Epreman ainsi qu'Anne-Lene Odegaard pour les tâches administratives.

Je remercie ici Ana Borges et Sophie Nallet, qui ont eu l'excellente idée de commencer leurs études de chimie un jour d'octobre 2001, et qui se trouvèrent être mes voisines dans un laboratoire du *Collège Propédeutique*. Ensuite, elles ont poursuivi leurs études par un doctorat qu'elles achèvent presque en même temps que moi: Ana, Sophie, merci pour tous les moments passés ensemble! On en a partagé des vertes et des pas mûres pendant ces années, mais ç'aurait été bien moins fun sans vous!

Un mot aussi pour les autres chimistes (et ingénieurs) qui ont étudié au Poly entre 2001 et 2006 - entre autres, Brian Bromley, François Boo, Simone Bonazzi: c'est un plaisir d'avoir passé tous ces bons moments avec vous!

Concernant la *Fine Equipe*, composée d'Antoine Berthoud, Kevin Hänni, Adrien Lawrence et Laélia Tomassini: merci pour tous ces week-ends 'culturels' à travers l'Europe non-francophone, ce seront des souvenirs pour la vie!

Dans ma liste viennent ensuite les Neuchâtelois: toujours disponibles - malgré mes réponses aléatoires à leurs sollicitations - et motivés à venir rendre visite à Lausanne: David, Jacques, Alex (qui fut aussi mon colocataire pendant trois ans), Nicolas, Mathieu, Georges, Jean-Ma et Anne-Ju, et tous les autres pour qui j'ai une pensée mais pas suffisamment d'espace pour l'exprimer! Longue vie à notre joyeuse équipe, nous qui venons de fêter nos dix ans de “vie commune”!

Finalement, je remercie mes parents, Marie-Jeanne et Jean-Louis, ma soeur Aurélia et toute ma famille pour leur soutien inconditionnel (tant moral que financier) et leurs encouragements tout au long de ces années.

Pour terminer, j'aimerais remercier Sabine, simplement pour toujours être à mes côtés.

Abstract

This work describes different strategies for the detection of biologically relevant analytes. The main goal was to achieve sensing in water, which is a prerequisite for application to real biological samples. In several cases, we could demonstrate that our systems were also working in blood serum, a notoriously complex medium containing proteins, sugars and salts, which can potentially interfere with our sensors.

Our first analyte of choice was the lithium cation. Owing to its therapeutic uses in the field of psychology, it represents an appealing target, and an efficient chemosensor for lithium ions may find numerous uses in biomedical investigations. The first strategy that will be presented involves the use of organometallic macrocycles carrying fluorescent reporting units. These compounds were found to be potent ionophores and display a very high selectivity for lithium ions. Upon careful choice of constituent building blocks, a chemosensor displaying good affinity, selectivity, and solubility was obtained. The sensor allowed the detection of lithium ions in water and in human serum by simple fluorescence measurements (Chapter 2).

Other approaches for the detection of lithium ions will be presented in Chapter 3. Instead of covalently attaching fluorescent dyes to the lithium binding unit, fluorophores that can bind in a non-covalent fashion were employed. Assays based on easily available constituents were devised. They allowed the sensing of lithium ions in the sub-millimolar concentration range.

In Chapter 4, the pattern-based sensing of micromolar concentrations of small peptides in water will be described. Small peptides are ubiquitous in biology, and they are involved in many essential processes such as neurotransmission, blood pressure regulation or oxidative stress mitigation. It will be demonstrated that their selective detection can be accomplished by arrays of differential sensors: instead of building a selective sensor for a given analyte, a series of cross-reactive, unsophisticated sensors could be employed. Their differential response (fingerprint) for various analytes was

interpreted *via* statistical methods. As a result, low micromolar concentrations of many short peptides (as well as mixtures thereof) could be measured in water and in human serum samples.

In the last part (Chapter 5), the sensing properties of a sensor array will be compared with those of a dynamic combinatorial library (DCL). The DCL contains the same elements as the sensor array, but they are mixed in one pot. It is shown that the DCL can outperform the sensor array in many situations, but that an excessive complexity can be detrimental to its resolution.

Keywords

Sensors • Fluorescence spectroscopy • Metallamacrocycles • Self-assembly • Ruthenium • Lithium • Peptide • Indicator displacement assay • Combinatorial chemistry • Sensor array

Résumé

Ce travail décrit différentes stratégies développées afin de détecter diverses molécules importantes d'un point de vue biologique. L'un des objectifs est de parvenir à la détection des molécules ciblées en milieu aqueux, ce qui représente un passage obligé dans la perspective d'aboutir à la détection en milieu biologique réel.

La première substance dont la détection sera présentée est le cation lithium. Son emploi dans le traitement de divers troubles psychologiques en fait un analyte de choix. Un senseur simple et efficace pour le lithium peut ouvrir d'intéressantes perspectives pour la recherche biomédicale, notamment en ce qui concerne le développement de médicaments à partir de lithium. Tout d'abord, des chémosenseurs fluorescents sélectifs pour le cation lithium seront décrits (Chapitre 2). Constituées de macrocycles organométalliques auxquels des marqueurs fluorescents ont été attachés, ces molécules peuvent, sous certaines conditions, être la fois solubles dans l'eau, sélectives pour le cation lithium, et donner une réponse sous forme d'une modulation de l'intensité de fluorescence. Comme il le sera démontré, ces macrocycles sont également capables de détecter le lithium dans du sérum issu de sang humain.

Au Chapitre 3 seront présentées des approches simplifiées pour la détection de lithium. En utilisant des colorants fluorescents qui s'attachent de façon non-covalente au récepteur macrocyclique, de nombreuses étapes de synthèse sont évitées, et le système obtenu permet la détection de lithium en milieu aqueux à des concentrations submillimolaires. L'un des avantages de ces systèmes est qu'ils font usage de molécules simples, généralement disponibles dans le commerce.

Au Chapitre 4, la détection de petits peptides de concentration micromolaire en milieu aqueux sera présentée. Les peptides sont omniprésents dans tout système et processus biologique. Par exemple, ils interviennent dans la régulation de la pression sanguine, dans des phénomènes de neurotransmission, ou encore dans la gestion du stress oxydant. Dans le cas que nous présentons, les senseurs sélectifs sont

abandonnés au profit d'ensembles de senseurs différentiels. Une série de senseurs peu sophistiqués, possédant une réactivité croisée pour les différents analytes d'intérêt peut être employée. La discrimination entre différents peptides est effectuée au moyen d'algorithmes de reconnaissance de formes (*pattern recognition*) qui permettent d'attribuer à chaque analyte sa propre empreinte. Au final, la discrimination de petits peptides (ainsi que de mélanges de peptides) à des concentrations micromolaires sera réalisée, en solution aqueuse tout comme en solution contenant du sérum humain.

Finalement, le Chapitre 5 propose de comparer les capacités en termes de discrimination d'un ensemble de senseurs et d'une bibliothèque combinatoire dynamique (BCD). Une BCD contient les mêmes éléments qu'un ensemble de senseurs, à la différence près que tous sont mélangés dans une même solution. Il en résulte un système plus simple à employer et analyser qu'un ensemble de senseurs. Il sera montré que la librairie possède des capacités analytiques supérieures à l'ensemble de senseurs, à condition qu'une trop grande complexité ne porte pas atteinte à sa résolution.

Mots Clefs

Senseurs • Spectroscopie de fluorescence • Métallamacrocycles • Auto-assemblage • Ruthénium • Lithium • Peptide • Analyse par déplacement d'indicateur • Chimie combinatoire • Ensemble de senseurs

Contents

Acknowledgements	v
Abstract	vii
Résumé	ix
Contents	xi
Abbreviations and Symbols	xv
1 General Introduction	1
1.1 Definition of a Chemosensor	3
1.2 Integrated Chemosensors	3
1.3 Conjugated Chemosensors	5
1.4 Sensing Ensembles	9
1.4.1 Definition and Examples	9
1.4.2 Sensor Arrays	11
1.4.3 Dynamic Combinatorial Libraries as Sensors	14
1.4.4 Chemometrics	15
2 Conjugate Chemosensors for the Detection of Li⁺	19
2.1 Pharmacology of Lithium Ions	21
2.2 Chemosensors for Lithium Ions	21
2.3 Design Strategy: Metallacrown Complexes	24
2.4 Towards Water-Soluble Fluoroionophores	29
2.4.1 Macrocycles Based on (<i>p</i> -cymene)Ru Fragments	29
2.4.2 Macrocycles Based on Modified Ru Fragments	33

2.5	A Fluorescence Sensor for Lithium Ions in Water and Serum	39
2.6	Conclusions	42
3	Simple Assays for the Detection of Li⁺	45
3.1	Introduction	47
3.2	A Ditopic Receptor for Lithium and HPTS	47
3.3	Sensing of Lithium through its Stabilizing Effect on Macrocyclic Receptors	57
3.4	Conclusions	64
4	Sensor Arrays for Small Peptides	65
4.1	Introduction	67
4.2	Building an Array of Fluorescence Sensors	69
4.3	Discrimination of Small Peptides	73
4.3.1	Dipeptides in Water	73
4.3.2	Bradykinin and Kallidin	79
4.3.3	Carnosine and Homocarnosine Solutions in Serum	80
4.4	Conclusions	83
5	Sensor Arrays vs. Dynamic Combinatorial Libraries	85
5.1	Introduction	87
5.1.1	Sensor Arrays and Dynamic Combinatorial Libraries	87
5.1.2	Linear Discriminant Analysis	88
5.2	Discrimination of Peptides with a Sensor Array and with a DCL	90
5.3	Conclusions	96
6	General Conclusions	99
7	Experimental Section	105
7.1	General and Instrumentation	107
7.1.1	General	107
7.1.2	Instrumentation	107
7.1.3	Purchase of Compounds	108
7.1.4	Software	109
7.2	Syntheses	110
7.2.1	Organometallic Complexes	110
7.2.2	Dihydropyridine-based Bridging Ligands	113
7.2.3	Syntheses of Trimeric Complexes	123
7.2.4	Other Syntheses	135

7.3	Lithium Detection with Conjugate 12-Metallacrown-3 Complexes	137
7.3.1	NMR Studies for K_a Determination	137
7.3.2	Fluorescence Measurements	138
7.4	Lithium Detection with Supramolecular Assays	140
7.4.1	Assay based on the HPTS Fluorophore	140
7.4.2	Assay based on the Calcein Blue Fluorophore	141
7.5	Sensor Arrays for Small Peptides	143
7.5.1	General	143
7.5.2	Metal/Dye Titrations	143
7.5.3	Fluorescence Assays with Dipeptides	144
7.5.4	Fluorescence Assays with Bradykinin and Kallidin	144
7.5.5	Fluorescence Assays with Carnosine and Homocarnosine	146
7.5.6	Data Processing	146
7.6	Sensor Arrays versus Dynamic Combinatorial Libraries	147
7.6.1	General	147
7.6.2	Sensing of Peptides with DCL Sensors	147
7.6.3	Sensing of Peptides with the Sensor Array	148
A	Sensor Arrays for Small Peptides	149
A.1	Fluorescence Titration Experiments	151
A.2	Multivariate Analyses	165
A.2.1	Sensing of Ten Dipeptides in Water	165
A.2.2	Sensor Array Reduction	168
A.2.3	Sensing of Bradykinin and Kallidin	174
A.2.4	Sensing of Carnosine and Homocarnosine in Serum	177
A.3	Linear Discriminant Functions provided by the LDAs	181
A.4	Kinetic Profiles	187
B	Sensor Arrays vs. Dynamic Combinatorial Libraries	189
B.1	LDA Score Plots	191
	Bibliography	201
	Curriculum Vitae	219

Abbreviations and Symbols

AcO	acetate
Al	arsenazo I
a.u.	arbitrary units
BK	bradykinin
BODIPY	4,4-difluoro-4-bora-3a,4a-diaza-s-indacene (boron-dipyrromethene)
br	broad
ⁿ Bu	<i>n</i> -butyl
°C	degree Celsius
<i>ca.</i>	<i>circa</i> , about
CAB	calcein blue
CAL	calcein
calcd	calculated
cbz	carbobenzyloxy
<i>cf.</i>	<i>confer</i> , compare to
CHES	2-(cyclohexylamino)ethanesulfonic acid
Cp*	η ⁵ -pentamethylcyclopentadienyl
cyclen	1,4,7,10-tetraazacyclododecane
cymene	1-methyl-4-(1-methylethyl)benzene
d	doublet
δ	chemical shift
dansyl	<i>N,N</i> -dimethylaminonaphthalene-1 sulfonyl
DCL	dynamic combinatorial library
dd	doublet of doublets
DHP	2,3-dihoxypyridine
DMF	<i>N,N</i> -dimethylformamide

DMSO	dimethyl sulfoxide
<i>e.g.</i>	<i>exempli gratia</i> , for example
em	emission
en	ethylenediamine
ESI	electrospray ionisation
Et	ethyl
<i>et al.</i>	<i>et alia</i> , and others
ex	excitation
g	gram
h	hour
HEPES	4-(2-hydroxyethyl)piperazine-1-ethanesulfonic acid
HOMO	highest-occupied molecular orbital
HPLC	high performance liquid chromatography
HPTS	8-hydroxy-1,3,6-pyrenetrisulfonic acid
Hz	Hertz (s^{-1})
<i>i. e.</i>	<i>id est</i> , that is
<i>J</i>	coupling constant
K_a	association constant
KD	kallidin
kJ	kilojoule
λ	wavelength (nm)
LDA	linear discriminant analysis
LUM	lumazine
LUMO	lowest-unoccupied molecular orbital
m	multiplet
<i>m</i>	meta
M	molar ($\text{mol} \cdot \text{L}^{-1}$)
m/z	mass-to-charge ratio
MAA	<i>N</i> -methylantranilic acid
MCB	methylcalcein blue
Me	methyl
Mes	mesityl (1,3,5-trimethylphenyl)
mg	milligram
mL	milliliter
mm	millimeter
mM	millimolar ($\text{mmol} \cdot \text{L}^{-1}$)

mmol	millimole
μm	micrometer
μM	micromolar ($\mu\text{mol} \cdot \text{L}^{-1}$)
μmol	micromole
mV	millivolt
NFR	nuclear fast red
nm	nanometer
NMR	nuclear magnetic resonance
o	ortho
OTf	triflate, trifluoromethanesulfonate
p	para
PCA	principal component analysis
PET	photoinduced electron transfer
Ph	phenyl
PPi	pyrophosphate
ppm	parts per million
ⁱ Pr	isopropyl
quint	quintet
rac	racemate
ref	reference
rpm	revolutions per minute
s	singlet
sept	septuplet
t	triplet
TEA	triethyl amine
TFA	trifluoroacetic acid
UV	ultraviolet
UV/Vis	UV/Visible
vol	volume
vs.	versus, against
wt	weight
XO	xlenol orange

Note: usual abbreviations are used for amino acids.

1

General Introduction

Synopsis

In this opening chapter, an elementary introduction to the concept of chemosensors is presented. The sensing methodologies, which will be employed in the following chapters, are described and illustrated with selected examples from the recent literature.

1.1 Definition of a Chemosensor

A CHEMOSENSOR can be regarded as “a receptor that interacts with an analyte producing a detectable change in a signal”.^[1] Optical reporters (for fluorescence or UV/Vis spectroscopy) have been widely used in this context,^[2–14] owing to a usually fast and convenient implementation. The instrumentation required for the use of such techniques is relatively simple and cheap, which makes this type of sensors quite appealing. In addition to optical methods, electrochemical techniques have also been employed.^[6, 9] In this introduction, we will focus on optical sensors, since they will be extensively used and studied in the next chapters.

Chemosensors can be classified into three main categories, which are described in the following sections.

1.2 Integrated Chemosensors

When the signaling unit is part of the binding unit (and vice-versa), the sensor is referred to as an integrated chemosensor.^[11, 15] The most ancient examples of this class of compounds are pH indicators, where a change in the protonation state of a colored molecule results in a change in coloration.

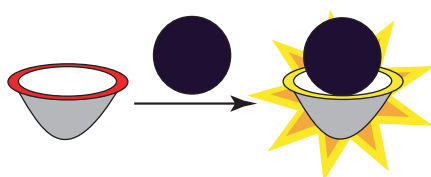
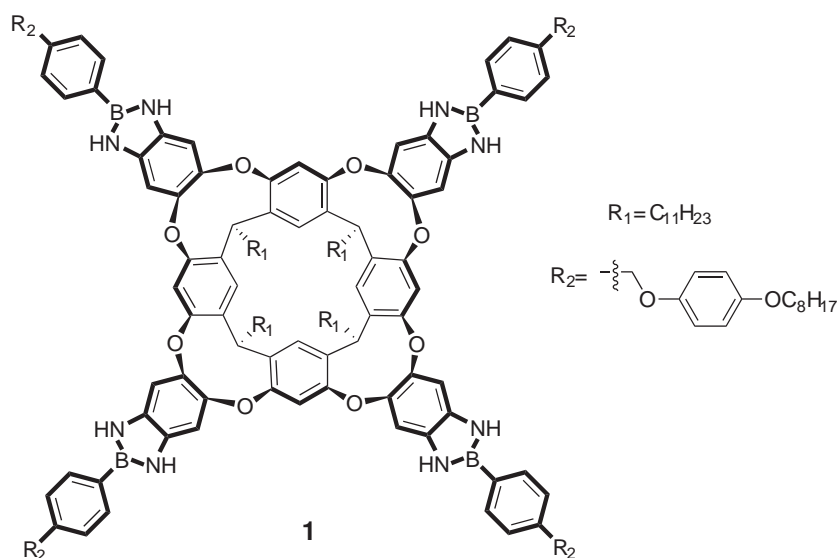


Figure 1.1 – Representation of an integrated chemosensor: The binding unit (grey cup) is also a fluorophore, and the complexation of the substrate (ball) modifies the emission intensity (switching it on).

With the rise of supramolecular chemistry, compounds such as crown ethers, cryptands and carcerands were developed,^[6] which are able to capture various analytes in a selective fashion. These receptors can be used as sensors when they simultaneously behave as signaling units. Several sensors for cations were elaborated based on this type of platform.^[11] For example, boron-containing resorcinarene **1**, which was very recently described by Kubo *et al.*, is able to indicate the presence of alkyltrimethylammonium ions by a change in its fluorescence properties.^[16] Compound **1** is selective for

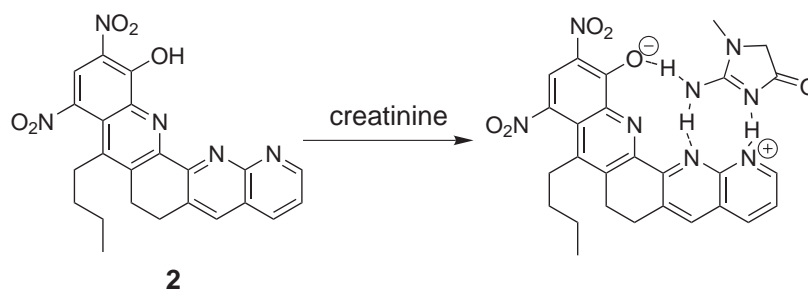
small ammonium salts and no response is observed for bulky tetraalkylammonium ions such as NEt_4^+ or N^nBu_4^+ .



Scheme 1.1 – Resorcinarene **1**, which can act as a sensor for alkyltrimethylammonium ions.^[16]

Another example is the sensor **2**, which was developed by Bell *et al.*^[17] (Scheme 1.2), and which is able to extract creatinine from water into organic solvents. Upon binding of creatinine, receptor **2** undergoes a rearrangement (proton shift), which induces a strong change in the UV/Vis spectrum.

Although some successes were reported with sensors of this type, their nature makes them difficult to modify. If one tries to improve the binding of analytes, it is very likely one will simultaneously modify the photophysical properties of the dye, or vice-versa. Therefore, optimization and customization of this type of sensor is difficult to achieve.^[4]



Scheme 1.2 – Binding of creatinine to the designed receptor **2**.^[17]

1.3 Conjugated Chemosensors

These types of sensors are made of a *binding unit*, which is selective for the desired analyte, and a *reporting unit*, which role is to signal the absence or presence of analyte at the binding unit. A spacer physically connects the binding and the signalling units. The *signalling unit-spacer-receptor* triad was extensively used in the context of supramolecular analytical chemistry. It makes the design of a sensor much more flexible than the “integrated sensor” approach, given that the various parts can be separately optimized and tuned before being combined to form the desired sensor. In order to work properly, a transduction mechanism must exist, which allows the reporting unit to sense and indicate binding events occurring at the receiving unit (Figure 1.2).

Fluorescence appears to be a method of choice for the formation of conjugated sensors, essentially because photoinduced electron transfer (PET) mechanisms offer the possibility to design off-to-on sensors for a large variety of analytes.

The mechanism of photoinduced electron transfer was extensively studied,^[11, 15, 18] and is depicted in Figure 1.2 for the case where a cation (ball) controls the fluorescence behaviour of a sensor. The binding site possesses an electron donating moiety (indicated by a D), and the fluorophore plays the role of an electron acceptor.

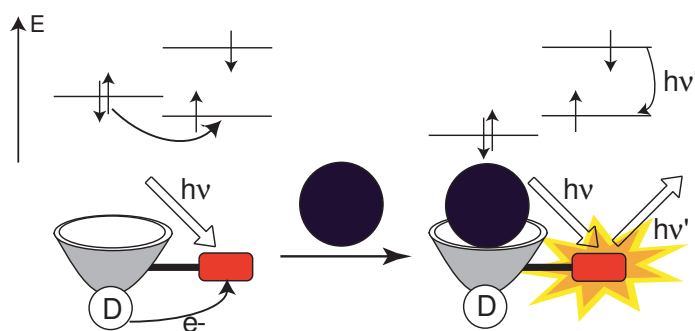


Figure 1.2 – Working principle of a conjugate PET sensor. Bottom: The binding subunit (grey cup) is separated from the fluorescent subunit (red rectangle) by a spacer (black line). The system also contains an electron donating moiety (D). Binding of the substrate (ball) modifies the energy of the electron donor, which switches on the emission of the dye. Top: Representation of the molecular orbitals involved in the PET process.

When the fluorophore is irradiated at the appropriate wavelength, an electron of its highest-occupied molecular orbital (HOMO) is promoted to the lowest-unoccupied molecular orbital (LUMO). When no guest occupies the binding site, PET can occur from the HOMO of the donor (indicated by D in Figure 1.2) to the one of the fluorophore (after excitation, and before emission takes place), thus quenching the fluorescence.

When a cation occupies the receptor, the redox potential of the donor is increased, so that the relevant HOMO becomes lower in energy than that of the fluorophore. The PET process is no longer possible, and the fluorescence is turned on. As will be discussed in Chapter 2, 4d transition metals also exhibit redox activity, and can therefore be involved in PET mechanisms.

Although many existing optical sensors work with the PET mechanism, numerous other phenomena can be involved,^[5] resulting in analyte-induced changes in fluorescence or colorimetric properties (Table 1.1).

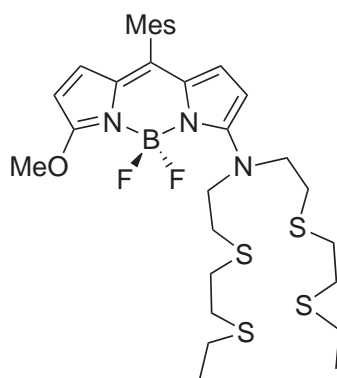
Table 1.1 – Optical response mechanism involving supramolecular interactions between chemosensors and analytes.^[5]

Mechanism	Chromophore	Fluorophore
Proton transfer	✓	✓
Tautomerism	✓	✓
Skeletal isomerism	✓	✓
Charge transfer	✓	✓
Polarization	✓	✓
Solvent displacement		✓
Conformational restriction		✓
Quenching by guest		✓
Internal charge transfer (ICT)		✓
Twisted internal charge transfer (TICT)		✓
Resonance energy transfer (RET)		✓
Photoinduced electron transfer (PET)		✓

Over the years, the *signaling unit-spacer-receptor* paradigm was extensively studied and applied,^[2, 11–13, 18–21] with a particular emphasis on sensors for alkali or alkaline earth metal cations,^[22–29] transition metals,^[28, 30–41] anions,^[7, 8, 10, 42–44] sugars,^[45] and neutral organic species.^[5, 46, 47]

Domaille *et al.* recently reported a fluorescent PET sensor for Cu⁺ (**3**, Scheme 1.3).^[31] The selective detection of guests is performed by thioether-rich side-arms (binding site) tethered to a boron-dipyrromethene fluorophore (abbreviated BODIPY). In the absence of any guest at the binding site, the fluorescence of the BODIPY fluorophore is essentially quenched. This quenching is attributed to an electron transfer from the amine bearing the BODIPY core. Upon cation binding (Cu⁺ in H₂O, pH 7.0) by the thioether side-arms, a dramatic increase in fluorescence is observed. In this case, the amino group is coordinated to the metal cation, and the lone pair formerly involved in fluorescence quenching is no longer available. The high selectivity observed for Cu⁺

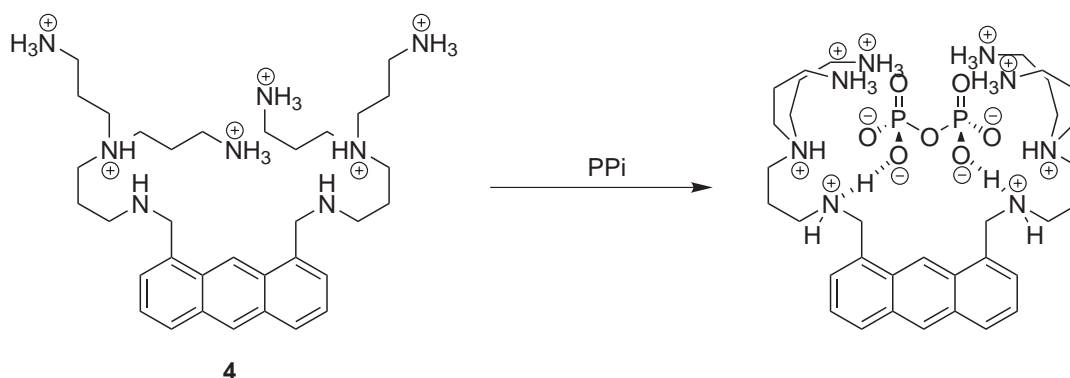
is attributed to the *soft-soft* interactions between the thioether functions and the Cu^+ cation.

**3****Scheme 1.3** – Fluorescent PET sensor **3** for Cu^+ .^[31]

Live-cell experiments showed that chemosensor **3** is membrane-permeable and that changes in the levels of Cu^+ within living cells can be sensed by confocal microscopy imaging. Applications such as studying intracellular redox chemistry of copper in brain or immune systems can be envisioned, which is remarkable since the translation of a sensor from a chemical system to a biological living one is a notoriously difficult task to achieve.

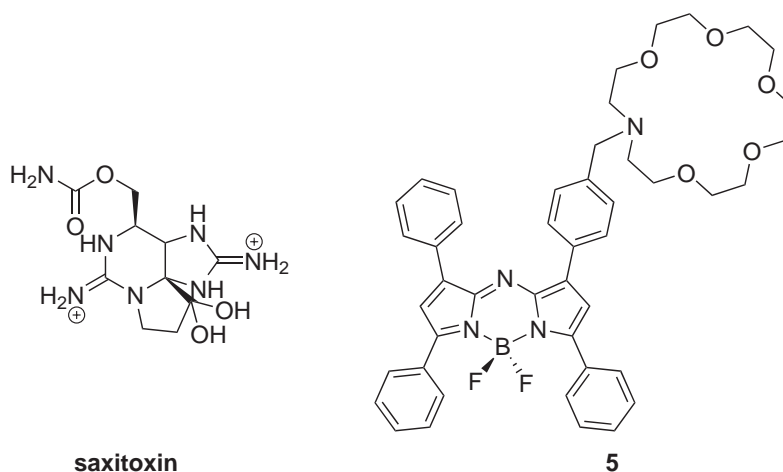
A fluorescent PET sensor for the pyrophosphate anion was reported by the group of Czarnik.^[44] The design principle of sensor **4** is very similar to that of cation sensor **3** described above: the fluorophore (anthracene) is linked to the binding site (made of two *tris*(3-aminopropyl)amine residues) *via* a spacer (Scheme 1.4). Sensor **4** displays good affinity and selectivity for the pyrophosphate anion, as indicated by fluorescence titration experiments. Again, the “free” receptor is very weakly fluorescent, given that the quenching of fluorescence by the amino groups is very efficient. In the presence of pyrophosphate at the binding site, an enhancement of the fluorescence is observed, reflecting the electronic rearrangement induced by capturing the anion. Remarkably, the preorganisation of the sensor allows for a good discrimination for pyrophosphate towards phosphate anion.

Gawley *et al.* presented compound **5** as a selective, fluorescent PET sensor for the neurotoxin saxitoxin.^[46] The typical features of a PET sensor are easily recognizable (Scheme 1.5), although the interaction mechanism between the crown ether receptor and the saxitoxin itself is much less straightforward. More complex interactions are



Scheme 1.4 – Binding pattern of receptor **4** with pyrophosphate anion (PPi) by means of hydrogen-bonding interactions.^[44]

speculated to occur between the analyte and the fluorophore, quenching the PET process in the presence of saxitoxin.



Scheme 1.5 – Saxitoxin, together with sensor **5**, which is able to detect it down to submillimolar concentrations.^[46]

These examples and many others show that the very modifiable receptor-spacer-indicator scheme has been widely applied, and research in this area is still flourishing. However, these sensors can prove rather difficult to develop. One can mention tedious synthesis, solubility issues or poor selectivity, for instance, as recurrent problems associated with this methodology. The next section presents a completely different approach to chemical sensing, which aims at overcoming these weaknesses.

1.4 Sensing Ensembles

1.4.1 Definition and Examples

In contrast to the examples of chemosensors discussed so far, there is no requirement of covalent bonding between the binding and the signaling units in the case of a sensing ensemble. More particularly, in the approach known as “indicator displacement assay” (IDA), a preliminary self-assembly of a receptor and an indicator is required. The targeted analyte, possessing a higher affinity for the receptor than the indicator, is able to displace the latter from the binding site. This displacement event induces a change in the colorimetric or fluorescence properties of the indicator, as shown in Figure 1.3. This method was first applied by Inouye^[48] and Shinkai,^[49] who developed sensing ensembles for acetylcholine. In the last 15 years, the field was further developed and numerous applications were found in the research groups of Eric Anslyn^[1, 3, 50], of Luigi Fabbrizzi,^[51, 52] as well as in ours.^[53]

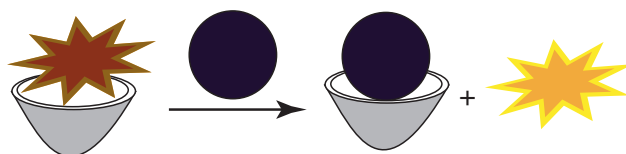
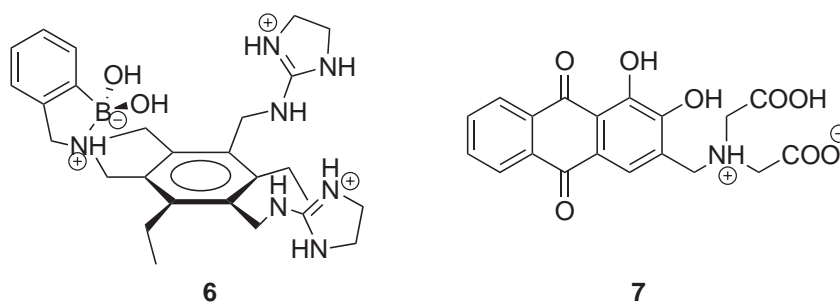


Figure 1.3 – Working principle of an indicator displacement assay: upon binding of the analyte (ball), the indicator (star) is expelled from the receptor (grey cup), which translates into a change in color or fluorescence.

The general strategy for the development of such a sensing ensemble is to build a selective receptor for the analyte of interest. One then needs to find an indicator possessing approximately the same functional groups than the analyte. The indicator-receptor interaction can be quantified, and the sensing conditions can be tuned, in order to obtain the best response for the sensing of the analyte.^[50] Anions have been widely studied as targets for indicator displacement assays. Since many commercially available dyes are anionic themselves, competitive binding with analytes is likely to occur.

An example of sensing ensemble is provided by Piatek *et al.*, who used compound **6** together with the dye alizarin complexone (**7**) to detect malate (hydroxybutanedioate) and tartrate (2,3-dihydroxybutanedioate) anions in beverages.^[54, 55] The receptor features a boronic acid moiety, which confers a good affinity to vicinal diols, and guanidinium groups which improve the affinity for carboxylates (Scheme 1.6). It was

observed that alizarin complexone (**7**) possesses some affinity for receptor **6**, but is efficiently displaced by tartrate and malate anions.

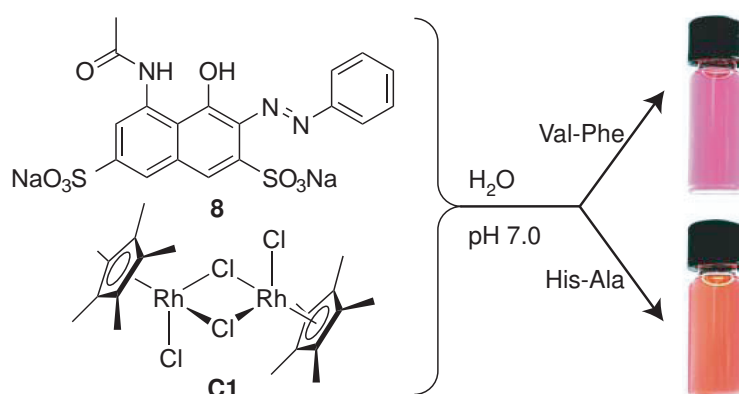


Scheme 1.6 – A chemosensing ensemble for tartrate and malate anions: the receptor **6** and the alizarin complexone indicator (**7**).

Similar systems were developed for the detection of many different analytes such as inositol-1,4,5-triphosphate,^[56] adenosine triphosphate,^[57, 58] guanosine monophosphate^[59] and triphosphate,^[60] caffeine,^[61] aspartate,^[62] glutamate,^[63] histidine,^[64–66] short peptides,^[67] phosphates,^[68–72] pyrophosphate,^[52, 73, 74] phosphoesters,^[75] 2,3-bisphosphoglycerate,^[76] halides,^[77] gluconic acid,^[78, 79] α -hydroxyacids,^[80, 81] (poly)carboxylates,^[54, 55, 82–85] carbonate,^[86] heparin,^[87] thiols,^[88] nitric oxide,^[89, 90] among others. Enantioselective detection of amino acids was achieved,^[91, 92] and high-throughput screening was proposed to optimize sensing ensembles.^[93]

The use of transition metals as receptors is of notable interest. This approach, which was in particular pioneered by Fabbrizzi *et al.*,^[10, 51, 52, 63, 66, 82, 83, 86] was exploited in our group to build a sensor for histidine- or methionine-containing short peptides.^[65] Here, the simplification of the sensing ensemble goes a step further: both the indicator and the rhodium-based receptor are commercially available. The colorimetric sensing ensemble is made of the dye azophloxin (**8**) and organometallic complex $[\text{Cp}^*\text{RhCl}_2]_2$ (**C1**). The addition of an analyte, which is able to bind to the Cp^*Rh fragment, leads to the replacement of the dye and to a change of color. In particular, it was observed that short peptides containing histidine or methionine close to their N-terminus are able to completely displace the dye: when the dipeptide His-Ala is used as analyte, the red color of azophloxin is visible; however, if Val-Phe is used as analyte, the purple color of the $[\text{Cp}^*\text{Rh}\text{-azophloxin}]$ adduct is visible. In summary, naked-eye detection of histidine or methionine containing peptides could be achieved with this simple sensing ensemble (Scheme 1.7).

The sensors or sensing ensembles described so far made successful use of Emil Fischer's “lock-and-key” principle.^[94] However, a conceptually different approach was



Scheme 1.7 – A chemosensing ensemble for sequence-selective detection of histidine- and methionine-containing peptides in water.^[65]

developed over the last decade, which aimed at abandoning the usually complicated and sometimes serendipitous synthesis of highly selective receptors. This is the principle behind the concept of sensor arrays, which is described in the next section.

1.4.2 Sensor Arrays

Inspiration for building arrays of differential sensors was provided by the extraordinary performances achieved by the senses of taste and smell in mammals. It was established that our olfactory and gustatory systems are made of several hundreds of cross reactive sensors, which do not display high selectivity for specific analytes. Instead, the composite response of the sensor array is interpreted and recorded as a given odor or flavor.^[95] Pattern-based recognition of analytes was recognized as an interesting alternative to more classical detection methods.^[96] Indeed, there are several classes of analytes (including many bioanalytes such as peptides, nucleotides or sugars), which proved to be tough targets for analyte-selective chemosensors, but which could be efficiently analysed by sensor arrays.

A remarkable feature of pattern-based sensors is that the individual sensor units can be rather unsophisticated as long as they give a differential response upon interaction with the analyte. Furthermore, pattern-based sensors can be used for classes of analytes, whereas normal chemosensors are generally used for one particular analyte. Cross-reactive sensor arrays can be employed to detect analytes in the gas phase or in solution. Gas-phase sensors are known as “electronic noses”,^[97] in analogy to the pattern-based sensing of the olfactory system.^[98–100] Research in the area of electronic noses is quite advanced and sensors for different applications such as

food and beverages analyses,^[101–105] follow-up of chemical processes,^[106] or toxic gas detection^[107–109] have been developed and are commercially available.^a

These systems usually rely on arrays of different materials that undergo modifications of their properties when they are exposed to analytes. Cross-reactivity arises from the variety of materials being used. Several types of sensors have been developed,^[98] which include sensors based on conducting polymers, metal oxide semiconductors, piezoelectric devices, optical fluorescence and amperometric gas sensors. The output signals are generally treated with pattern recognition algorithms.^[110]

A remarkable “smell-seeing” device was proposed by Rakow and Suslick, which allows detection of various gases and mixtures by an array of metalloporphyrin sensors. Strong color changes occur upon exposure to various analytes, which make it possible to visually interpret the response of the sensor.^[111] The sensor array is made of different metalloporphyrins fixed in silica gel, and unique “color fingerprints” of vapours down to a few hundreds parts per billion can be obtained (Figure 1.4). This concept was extended by the same group to the detection of toxic gases,^[107, 108, 112, 113] as well as to the analysis of coffee aromas.^[101]

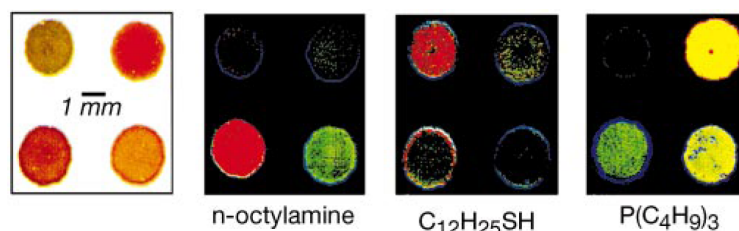


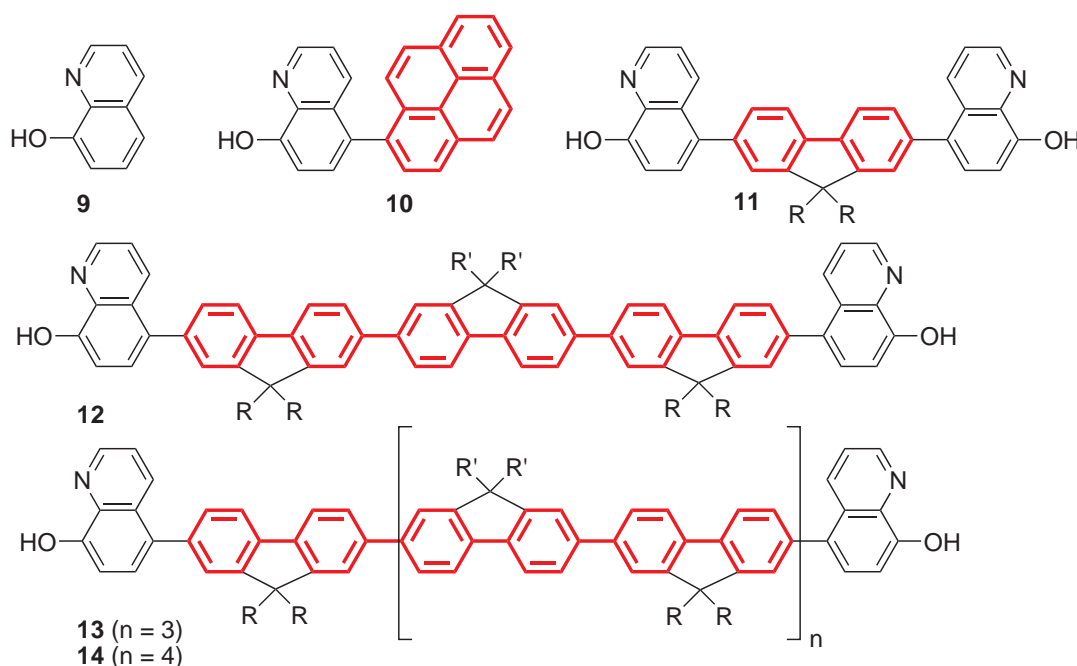
Figure 1.4 – Color fingerprint for different analytes (1.8 ppm): The response of a minimal array of four metalloporphyrins is shown for *n*-octylamine, dodecanethiol and tri-*n*-butylphosphine. (Reprinted by permission from Macmillan Publishers Ltd: Ref. [111], copyright 2000).

The pattern-based recognition of analytes in solution is less developed, but the field has advanced substantially over the last years. Sensors that display an electronic signalling mechanism are referred to as “electronic tongues”.^[114–121] They have found applications for the analyses of food and beverages, and of biological fluids. The construction of electronic tongues typically requires the fabrication of specialized sensor hardware and electrode systems. This is in contrast to pattern-based sensors, which are based on UV/Vis or fluorescence spectroscopy.^[95, 122–124] These techniques are appealing because standard equipment can be used for the signal readout (e.g., plate readers).

^aFor example, see: www.osmetech.com

Cross-reactive sensors with a colorimetric or a fluorescence response have been described for the solution-based detection of cations,^[125–140] anions^[141–145] and ion pairs,^[146] of organic amines^[147–153] and carboxylates,^[154–159] of nitrated explosives,^[160–162] nucleotides,^[142, 163–167] steroids,^[156, 168, 169] alkaloids,^[170] carbohydrates,^[165, 171–178] amino acids,^[179, 180] peptides,^[181–188] and proteins,^[184, 189–201] among others. It has also been demonstrated that sensor arrays of this kind can be used for the classification of beverages.^[127, 158, 159, 171, 175, 202] Furthermore, recent studies showed that cell classification into normal, cancerous and metastatic is achievable with conjugated polymer-based sensor arrays.^[203, 204]

For example, Palacios *et al.* reported a sensor array for the detection of metal ions.^[128] The array consists in a series of 8-hydroxyquinoline receptors linked to different conjugated fluorophores **9** - **14** (Scheme 1.8).



Scheme 1.8 – Hydroxyquinoline-based differential sensors **9** - **14**. R = *rac*-2-ethylhexyl, R' = *n*-hexyl. The extended conjugated chromophore is shown in red color.^[128]

Upon coordination of a metal cation to the hydroxyquinoline receptor, the fluorescence of the conjugated fluorophore is modified in a differential fashion (Figure 1.5). Pattern recognition methods (see section 1.4.4) are used to estimate the discriminating ability of the array, as well as the individual contribution of each sensor. This approach allows qualitative discrimination between 10 cations with high accuracy. As a real-world

example, the capacity of the sensor array to discriminate between a series of enhanced soft drinks, based on their Ca^{2+} , Mg^{2+} and Zn^{2+} contents, was presented.

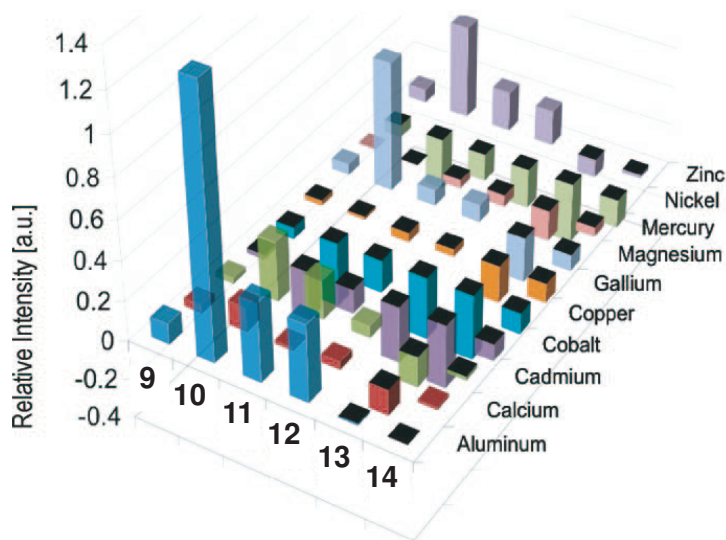


Figure 1.5 – Response patterns generated by the sensors (numbered 9 - 14) displayed in Scheme 1.8 ($\lambda_{\text{em}} = 525 \text{ nm}$) in the presence of 10 different metal cations. The black tops in the graph indicate negative responses (Adapted with permission from ref. [128]. Copyright 2008 American Chemical Society).

By examining Figure 1.5, it is clear that no individual sensor gives a selective response towards a particular cation. On the other hand, it is also evident that the array gives very different responses for each analyte. This underlines the basic principle of a sensor array: perfect selectivity is not required, but a differential response of a series of sensors towards different analytes is necessary.

1.4.3 Dynamic Combinatorial Libraries as Sensors

The use of dynamic combinatorial libraries (DCLs) as sensing systems is closely related to the use of sensor arrays (roughly speaking, a DCL can be considered as the one-pot version of an array). Assemblies can be formed in a reversible fashion when a series of receptors and indicators are mixed. If there is cross-reactivity (*i.e.*, each receptor-indicator combination can theoretically be present), a dynamic combinatorial library is obtained.^[205-210] A DCL is a complex equilibrium between several interacting species. Upon perturbation of the library (*e.g.*, by addition of an analyte), a re-equilibration process takes place and modifies the composition of the library. If this modification can be transduced into a measurable signal, sensing of the analyte becomes possible. Several studies have been published by our group, which take

advantage of the properties of DCLs.^[166, 183, 186, 188, 211, 212] The general protocol used in these studies is quite simple: A DCL is constituted by mixing one or several metal complexes (the receptor(s)) with several dyes. After equilibration, the UV/Vis spectrum reflects the composition of the library. When an analyte such as a peptide^[180, 183, 186, 213] or a nucleotide^[166] is added, the DCL rearranges in an analyte-specific fashion, which results in a change in the UV/Vis spectrum (Figure 1.6). In this case, the whole spectrum represents a fingerprint for a given analyte, and can be analyzed by pattern recognition procedures.

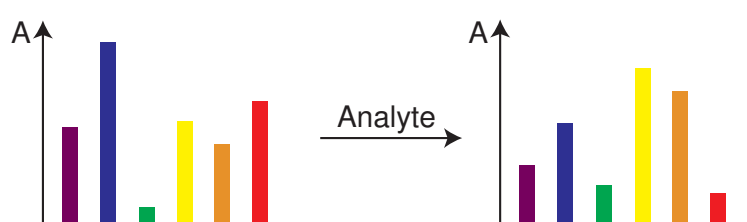


Figure 1.6 – Principle of a DCL sensor: a dynamic mixture of colored (or fluorescent) compounds undergoes an analyte-induced re-equilibration. The change in color (or in fluorescence) can be related to the presence of an analyte, its concentration, and its nature. Here, the absorbances measured at 6 wavelengths are represented by the 6 colored bars.

Other research groups applied this sensing principle to the simultaneous detection of tartrate and malate in solution,^[157] citrate and Ca^{2+} in flavored vodkas,^[158] or to the sensing of analytes such as diamines,^[150] histamine,^[148] and proteins.^[192]

In a recent publication, Margulies and Hamilton presented a sensing ensemble based on G-quadruplexes.^[192] A library of compounds is obtained when guanine-rich DNA single strands tagged with different fluorophores are mixed together: using DNA strands carrying 3 different fluorophores, an ensemble of 21 different G-quadruplexes can be generated, each one of them possessing distinct fluorescence properties. Upon addition of a protein, its non-specific interactions with the various G-quadruplexes result in a unique fluorescence signature. With this method, it was demonstrated that five different proteins could be detected owing to the specific change they induce to the emission response of the sensing ensemble.

1.4.4 Chemometrics

When sensor arrays or dynamic combinatorial libraries are employed as chemosensors, they usually provide high-dimensionality data sets, which are difficult to interpret quantitatively. Chemometrics is the application of statistical and mathematical methods to

interpret multivariate data and extract useful information.^[110, 214] The two methods that our group uses routinely are principal component analysis (PCA) and linear discriminant analysis (LDA).^[215]

Principal component analysis is a non-supervised method used to reduce the dimensionality of a data set in order to make it easier to interpret. The non-supervised character of the method implies that it does not “know” which data points should belong to the same cluster, but it tries to classify them according to their similarities. The fact that analyte-clusters naturally arise is evidence of the discriminating efficiency of the data set, and allows to qualitatively differentiate one sample from another. The data analysis consists in calculating orthogonal eigenvectors (the principal components) lying in the direction of the maximum variance in the data set. Principal components are generated in such a way that the first one contains the highest degree of variance, and the other principal components follow by order of decreasing variance. In most of the cases that will be developed in the following chapters, two or three principal components were enough to concentrate 95% of the total variance, thus considerably reducing the dimensionality of the data set, while ensuring a minimal loss of information.

Linear discriminant analysis is a supervised method, which implies that there is a prior knowledge on which data points belong together. The routine tries to form clusters of similar analytes, and to maximize the separation between these clusters. As for PCA, the analysis is performed by finding the linear combination of sensor responses that best describe similarities and differences between analytes. Functions that are linear combinations of discriminating variables are created and used to describe the existing data set. They are of the general form:

$$F_z = A + \sum_{b=1}^p c_b \cdot Z_b \quad (1.1)$$

Where A represents a constant, c the classification coefficients and Z the variables (in the case where p variables are used). The F_z 's are the discriminant scores, which are used to predict group membership. The generated scores (or factors) are classified by order of importance, and 2 or 3 scores are usually enough to describe 95% of the total variance.

LDA is frequently considered as giving overly optimistic classification results. In order to obtain more realistic evaluation of a system, one can use a *jack-knife validation*. This routine excludes one observation from the original set, and uses the remaining $(n - 1)$ observations to estimate the discriminant functions. The group membership of

the omitted observation is determined based on these functions, and the method is repeated, successively excluding each observation. The proportion of correct classification of excluded observations gives an estimate for the success of the discrimination. Going a step further, it is also possible to exclude several observations from the data set (the *hold-out sample*), and then calculate the discriminant functions with the remaining observations (the *training sample*). The observations belonging to the *hold-out sample* can then be classified. A successful classification of the unknown samples within the proper clusters ensures the predictability and quality of a statistical model and, consequently, of a sensing system.

2

Conjugate 12-Metallacrown-3 Complexes for the Selective Detection of Lithium Ions

Synopsis

In this chapter are introduced the pharmacology of the lithium ion, as well as some of the properties, that make it so challenging to detect. The chemosensors that were developed by other research groups are reviewed, and our approach based on metallacrown complexes is introduced. The syntheses of a series of fluorescent dihydroxypyridine ligands are described, as well as the reactions of these ligands with $[(p\text{-cymene})\text{RuCl}_2]_2$ or $[(\text{C}_6\text{H}_5\text{CH}_2\text{NMe}_2\text{H})\text{RuCl}_2]_2\text{Cl}_2$, which resulted in the formation of 12-metallacrown-3 complexes. These complexes were found to possess strong affinity and selectivity for lithium ions. By a judicious choice of the fluorophore and the arene π -ligand, a macrocycle was obtained that could be used in aqueous solution to selectively and quantitatively detect lithium ions by fluorescence spectroscopy.

Part of the work presented in this chapter was published in: S. Rochat, Z. Grote, K. Severin, *Org. Biomol. Chem.* **2009**, 7, 1147-1153, and in: S. Rochat, K. Severin, *Chimia* **2010**, 64, 150-152.

2.1 Pharmacology of Lithium Ions

AUSTRALIAN PSYCHIATRIST John Cade is referred to as the father of the use of lithium salts in the treatment of psychotic excitement.^[216] In 1949, he reported the calming effects of lithium salts on patients suffering from acute mania.^[217] The potential value in psychiatry was rapidly acknowledged and since the mid-1960s, lithium drugs have been widely used for patients suffering from bipolar disorders. It must be noted, however, that the use of lithium was delayed due to accounts from the USA of deaths caused by lithium toxicity in cardiac patients.^[218] Therefore, it was only in 1970 that the US Food and Drug Administration approved lithium for the treatment of mania.^[219] Since then, and despite the development of alternative drugs, lithium has remained the gold standard for the treatment of acute episodes and the prevention of relapses.^[220–223] Recent studies suggest that lithium salts could also be of interest for the treatment of amyotrophic lateral sclerosis (ALS)^[224, 225] and of Alzheimer's disease.^[226–228] It was even speculated whether lithium could become the “aspirin of the brain”.^[229] Apart from applications in the field of neurology and psychiatry, lithium salts have been proposed to treat skin diseases and certain viral infections.^[220, 222]

An important problem occurring with lithium treatment comes from the fact that the efficient concentrations in blood range from 0.5 mM to 1.5 mM, which is very close to the concentrations where side-effects and toxicity arise.^[230–232] Furthermore, a concentration of 5.0 mM can result in death. This potential toxicity makes the control of concentration of prime importance during treatment periods. In view of their pharmacological relevance, it is not surprising that considerable efforts have been devoted towards the development of sensors for lithium ions.^[230, 232] In fact, a recent review about the pharmacological action of lithium salts concludes that “...progress in lithium research has been hampered by the unavailability of a sensitive and specific Li⁺ spectroscopic tool.”^[233]

2.2 Chemosensors for Lithium Ions

The lithium ion represents a challenging analyte. First, it is very well solvated, and a potent ionophore is required in order to extract it from water (the hydration energy of Li⁺ is $-519 \text{ kJ} \cdot \text{mol}^{-1}$).^[234] Second, lithium usually appears in environments where poten-

tially competing ions such as Na⁺, K⁺ or Mg²⁺ are present in high concentrations.^[230, 235] A good selectivity for Li⁺ is therefore required. Finally, if the goal is to detect lithium in a homogeneous aqueous solution, a water soluble sensor is necessary, which strongly limits the number of potential candidates. Many of the receptors and sensors, which were reported in the past, are based on organic macrocycles, and were used in organic solvents.^[23, 25, 26, 230, 232, 236–255] Furthermore, although there are several publications about fluoroionophores for Li⁺ in organic solvents,^[23, 25, 26, 230, 237–240, 243, 244, 247–249] only a few studies - summarized thereafter - report sensors working in homogeneous aqueous solution.^[24, 256, 257]

Caballero *et al.* have developed the ferrocene-anthracene dyad **15**,^[257] which can be used in mixtures of acetonitrile and water (70:30) at pH 5.0 to detect lithium ions with good selectivity over other cations (Figure 2.1). A fluorescence enhancement could be observed in the presence of Li⁺, which was attributed to the concomitant effect of protons on the imine bridge, and of Li⁺ captured by the ferrocene fragment.

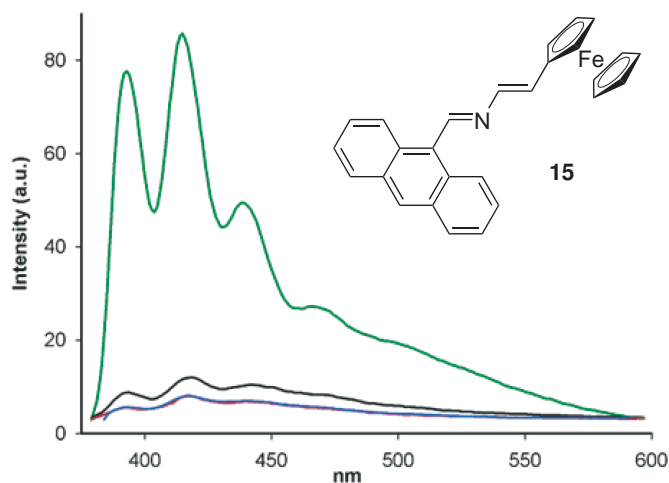
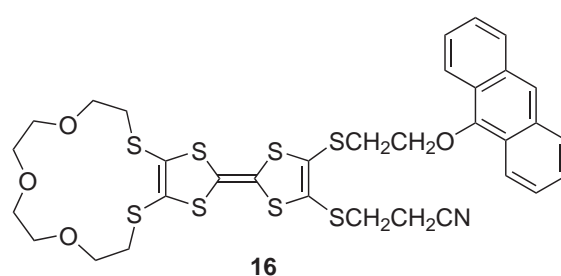


Figure 2.1 – Fluorescence spectra of **15** ($2.5 \cdot 10^{-5}$ M, in CH₃CN/H₂O, 70:30) at: pH = 7.0 (red), pH = 5.0 (black), pH = 7.0 in the presence of Li⁺ (blue), and pH = 5.0 in the presence of Li⁺ (green). (Adapted with permission from ref. [257]. Copyright 2004 American Chemical Society).

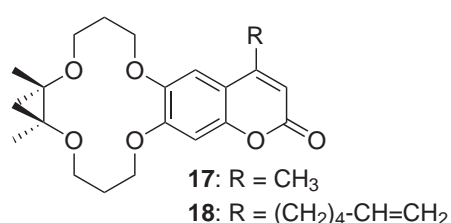
Liu *et al.* presented crown ether derivative **16** (Scheme 2.1), which acts as a dual sensor for Li⁺ ions and singlet oxygen (¹O₂).^[256] Fluorescence measurements showed that the emission intensity of compound **16** was very weak, due to efficient PET from the tetrathiafulvalene unit to the anthracene fluorophore. In the presence of singlet oxygen, an enhancement of the emission intensity was observed. Oxidation of the

tetrathiafulvalene was assumed to inhibit the PET process, and to result in an emission increase. After subsequent addition of Li^+ to the system, fluorescence was further enhanced, which can be explained by additional restriction of PET by the presence of the cation in the crown receptor. Interestingly, addition of Li^+ alone does not affect the fluorescence of compound **16**. The presence of $^1\text{O}_2$ is therefore required to trigger the detection of Li^+ . This system was used in mixtures of water and tetrahydrofuran (20:80, pH 7.0) and alkali metals other than lithium did not induce any measurable change in fluorescence.



Scheme 2.1 – Crown ether annelated tetrathiafulvalene derivative with anthracene moiety **16**, which was used for the simultaneous sensing of $^1\text{O}_2$ and Li^+ .^[256]

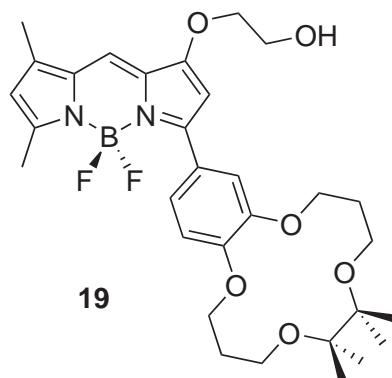
Fluorescent probe **17** was presented by Citterio *et al.* as a sensor for Li^+ ions in water.^[24] The use of a coumarin fluorophore rendered the probe pH-insensitive over a broad pH range. In addition to that, it was found that the tetramethyl 14-crown-4 binding site possessed a good selectivity for Li^+ over other cations. The fused compound **17** was therefore quite successful in detecting Li^+ in aqueous solutions. Nevertheless, a small quantity of MeOH (1%) was required in order to solubilize the sensor, and its synthesis was affected by poor yields. The analogous compound **18** was immobilized on a membrane, allowing the formation of a so-called optode (optical sensor), which was able to detect lithium ions in aqueous solutions with high accuracy.



Scheme 2.2 – Chemical structures of the Li^+ -selective fluoroionophores **17** and **18**.^[24]

The same group recently reported fluoroionophore **19** (Scheme 2.3), which can be covalently immobilized on a porous glass support.^[258] The recognition unit is again a

14-crown-4 ether, and the fluorophore is a BODIPY derivative. Compound **19** allows measuring therapeutically relevant concentrations of Li⁺ in aqueous solutions with an improved sensitivity and selectivity compared to sensor **18**.



Scheme 2.3 – Chemical structure of fluoroionophore **19**.^[258]

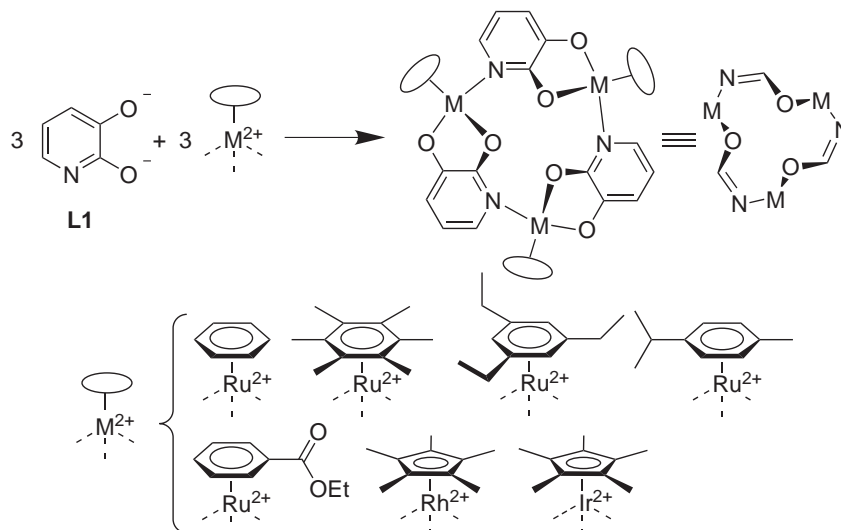
None of the above-mentioned examples features a chemosensor, which is soluble in 100% water. Regarding the numerous clinical applications mentioned earlier (section 2.1, p.21), as well as the widespread use of lithium in industrial fields (particularly in batteries),^[259] we expect that the needs for monitoring Li⁺ levels in biological or environmental samples will be constantly increasing. In the following sections, we report efforts to address the triple challenge of solubility, selectivity, and sensitivity. In particular, we will describe a fluorescent conjugated chemosensor, that allows the detection of low millimolar concentrations of lithium in water or serum with excellent selectivity over Na⁺ or Mg²⁺.^[22, 260]

2.3 Design Strategy: Metallocrown Complexes

As recognition units for our lithium sensor, we decided to use 12-metallocrown-3 complexes.^[53, 261–264] This class of compounds has been investigated extensively by our group,^[265–275] and by others.^[276–279] They can easily be obtained by self-assembly of half-sandwich complexes of Ru(II), Rh(III), or Ir(III) with organic ligands featuring the 2,3-dihydroxypyridine motif.^[263, 264] Organometallic half-sandwich complexes such as [(*p*-cymene)RuCl₂]₂ (**C2**) or [Cp*RhCl₂]₂ (**C1**) are commercially available or easily accessible, either by reaction of cyclohexa- or cyclopentadienes with MCl₃ · xH₂O (M = Ru, Rh, Ir),^[280, 281] or by arene exchange.^[282] Dimeric compounds of this type are remarkably stable: solids can be handled without a protective atmosphere, and solutions are only moderately air sensitive. They are soluble in many organic solvents,

as well as in water, by formation of monomeric aqua complexes. The π -ligands usually act as ancillary ligands, and the remaining three coordination sites can be used for the coordination of anionic or neutral ligands. The fact that these coordination sites are very labile^[283, 284] is decisive, since lability is required for the systems to undergo error correction during self-assembly processes.

Formation of trinuclear macrocycles proceeds when chloro-bridged organometallic dimers react with 2,3-dihydroxypyridine ligands (DHP, **L1**) in the presence of a base (Scheme 2.4). The macrocycles are usually well soluble in organic solvents, and they display characteristic ¹H NMR signatures: since the complexes possess a high symmetry, only one set of signals is observed for the bridging ligands as well as for the π -ligands. When *p*-cymene is used as π -ligand, one observes two signals for the methyl protons of the isopropyl side chain. This indicates that the methyl groups are diastereotopic. The metal centers are thus chiral and epimerization is slow compared to the NMR time scale. Since only one set of signals is observed, the self-assembly process is completely diastereoselective (a racemic mixture of $M_R M_R M_R$ and $M_S M_S M_S$ is obtained).



Scheme 2.4 – Top: Self-assembly of organometallic complexes of the general formula $[(\pi\text{-ligand})M(\mathbf{L1})]_3$ and their 12-metallacrown-3 scaffold. Bottom: Examples of metal fragments, which can be used for the formation of trinuclear metallamacrocycles.

Complexes of the general formula $[(\pi\text{-ligand})M(\mathbf{L1})]_3$ represent analogues of organic 12-crown-3 ethers. The first examples of organometallic analogues of crown ethers were published in 1989, and consisted of a manganese-based mimic of 12-crown-4,^[285] and of an iron-based mimic of 9-crown-3, respectively.^[286] Since then,

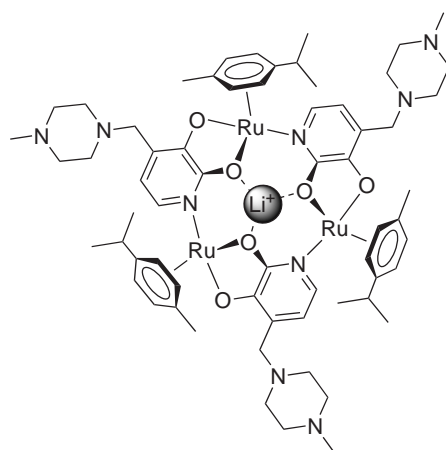
numerous metallacrowns have been reported, from small 8-member molecular wheels up to 60-metallacrown-20 complexes.^[262] Not surprisingly, 12-metallacrown-3 complexes (Scheme 2.4) can accommodate small cations next to the three adjacent oxygen atoms, similarly to their organic counterparts. Several lithium and sodium adducts have been isolated, and the selectivity for these small cations was found to be largely dependent on the steric requirements of π -ligands. Furthermore, certain conditions were found to enable accommodation of Li⁺ only.^[273] Competition experiments revealed that the host-guest complexes are extremely stable, and that association constants are comparable to that of cryptands.^[274, 275] Several reasons were cited in order to explain this exceptional affinity:^[274, 275] (a) The receptors are highly preorganized and rigid. (b) The energetic costs for desolvation of the donor atoms is very small because the binding site is well shielded by the π -ligands. (c) The salts are bound as ion pairs, with the anion occupying the fourth coordination site of the Li⁺ or Na⁺ ion. In addition to that, theoretical data show that the partial negative charges on the O-donor atoms of the metallamacrocycle are larger than those on the O-donor atoms of 12-crown-3 (-0.88 versus -0.59).^[269] Electrostatic reasons can therefore also be invoked to explain the strikingly high affinity of 12-metallacrown-3 complexes for small cations.

Coordination of guest molecules to the binding site of macrocycles is fairly easy to detect by ¹H NMR spectroscopy: upon binding of Li⁺ or Na⁺, the aromatic signals of pyridine and arene are shifted towards higher chemical shifts. If all the macrocycles in solution are not occupied by a cationic guest, two sets of signals can be observed, one corresponding to the “free” receptor, and the other one corresponding to the adduct. The fact that the cation exchange is slow on the NMR time scale makes the quantification of adduct formation (*i.e.*, determination of the association constant) very easy. Interestingly, the presence of a cation at the binding site can also be detected electrochemically: in the presence of Li⁺, the metal centers are more difficult to oxidize, which can be measured by cyclic voltammetry experiments.^[273, 274]

The fact that ion pairs are captured in organic apolar solvents was exploited to build a sensor for the fluoride anion:^[270] a macrocycle was designed, which could accommodate only the small F⁻ anion together with Li⁺ in its binding pocket. The presence of fluoride can be followed by electrochemical measurements (in the presence of F⁻, the macrocycle is significantly easier to oxidize).

Water-soluble 12-metallacrown-3 complexes were obtained by using modified dihydroxypyridine ligands (Scheme 2.5).^[267, 268] The solubility is conferred by appended amino groups, which can be easily added to dihydroxypyridine ligands by Mannich reactions.^[287-290] Protonation of these groups in water at neutral pH enhances the solu-

bility of the trimeric macrocycles. Synthesis of water soluble metallacrown complexes is remarkably simple: all that is required is to mix the organometallic dimeric complexes and bridging ligands in water at neutral pH in the presence of a buffer, or in methanol in the presence of a base. When performed in water, self-assembly affords quantitative yields of the desired trimeric species.^[267, 268] Strong affinity for Li^+ ions persists even in a polar solvent such as water, and still depends on the π -ligands. Complex **M1**, for example, is able to bind lithium ions in aqueous solution with a binding constant of $K_a = 5.8 (\pm 1.0) \cdot 10^4 \text{ M}^{-1}$ (Scheme 2.5),^[267] whereas sodium ions are bound with much lower affinity ($K_a = 5.0 (\pm 1.0) \text{ M}^{-1}$).



Scheme 2.5 – Representation of the Li^+ adduct of complex **M1** with view along the C_3 symmetry axis.

A simple “naked-eye” chemosensor for low millimolar concentrations of Li^+ was devised:^[267] When FeCl_3 was added to an aqueous solution of receptor **M1**, fast decomposition of the macrocycle occurred, and resulted in an immediate color change from orange to dark brown. In the presence of Li^+ ions, this reaction was kinetically inhibited and addition of FeCl_3 led to no immediate color change (Figure 2.2).

In order to convert macrocyclic receptors into fluoroionophores, our strategy was to attach a fluorophore to the 2,3-dihydroxypyridine ligands. Upon formation of a macrocycle, the fluorescence is expected to be quenched due to electron transfer from the transition metals. In the presence of lithium ions, however, the transition metals are more difficult to oxidize ($\Delta E \sim 300 \text{ mV}$),^[273, 274] and the quenching effect is expected to be reduced (Scheme 2.6). The detection of Li^+ can therefore be performed by a simple fluorescence measurement. The modular nature of the macrocycles allows for the organic ligand and organometallic complex to be separately modified until an optimal combination is found.

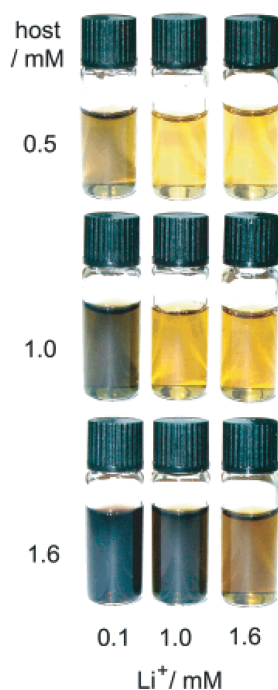
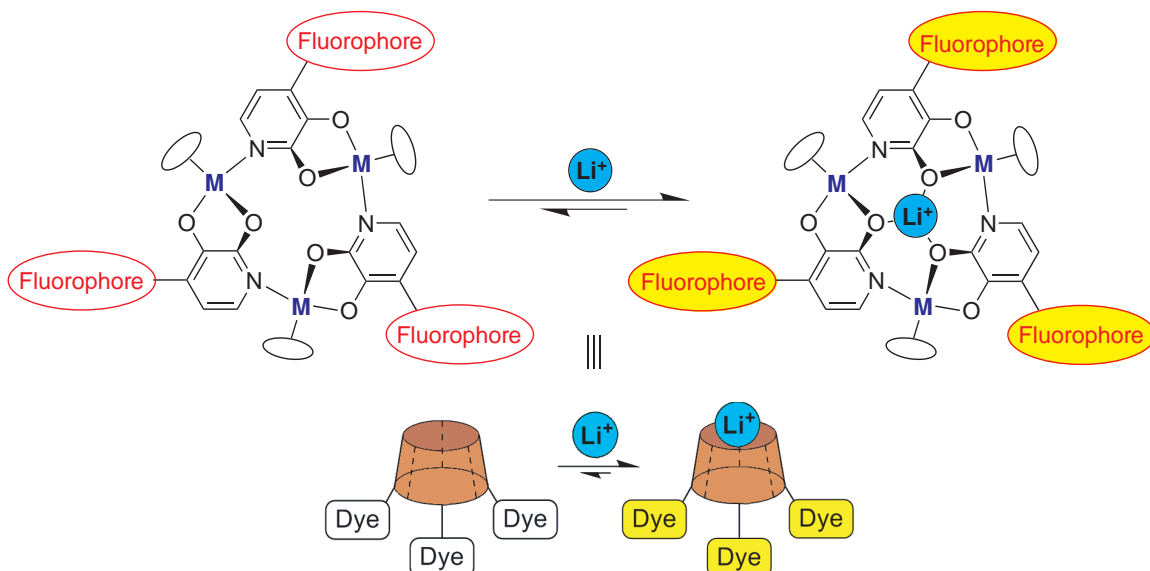


Figure 2.2 – Photos of aqueous solutions containing different concentrations of macrocycle **M1** (0.5, 1.0, and 1.6 mM) and different lithium concentrations (0.1, 1.0, and 1.6 mM) after addition of an excess of FeCl₃. A brown color is observed for solutions in which receptor **M1** is not saturated with Li⁺. (Reproduced with permission from ref. [267]. Copyright 2004 American Chemical Society).

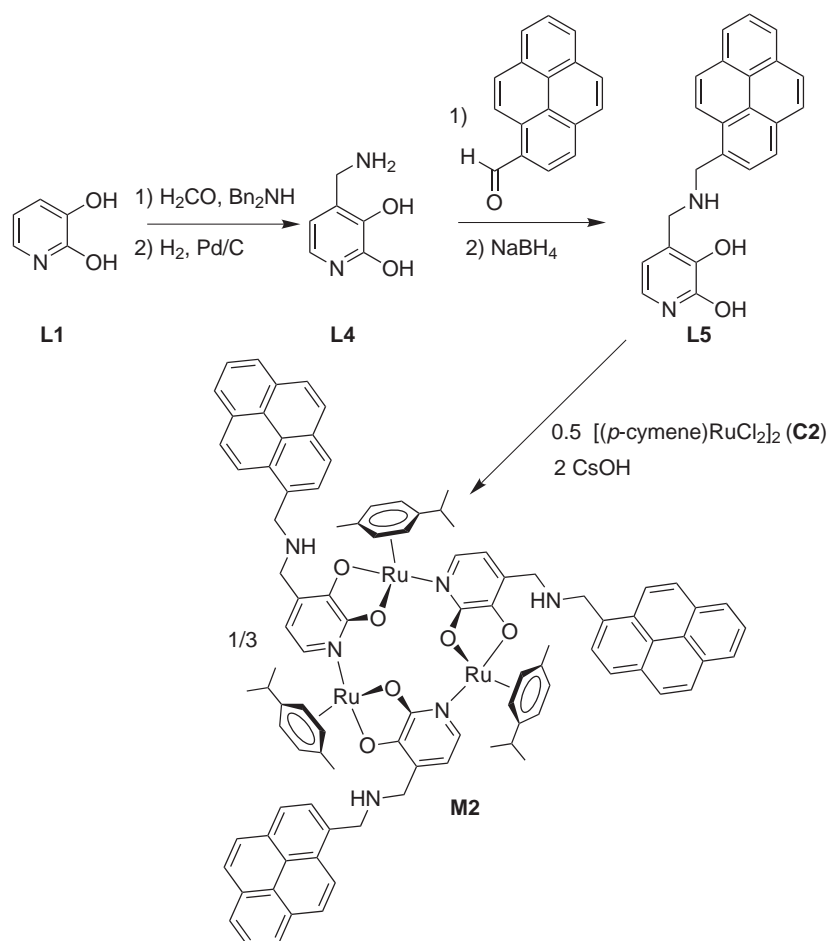


Scheme 2.6 – Sensing of Li⁺ ions by a 12-metallacrown-3 based sensor. The fluorescence is turned on upon coordination of lithium at the binding site. M = transition metal.

2.4 Towards Water-Soluble Fluoroionophores

2.4.1 Macrocycles Based on (*p*-cymene)Ru Fragments

The first fluorescent 12-metallacrown-3 complex that was prepared was tagged with pyrene fluorophores. The organic bridging ligand **L5**, carrying the pyrene moiety was obtained by reductive amination of 1-pyrenecarboxaldehyde with 4-aminomethyl-2,3-dihydroxypyridine (**L4**). The latter was prepared by a Mannich reaction of commercial 2,3-dihydroxypyridine (**L1**) with dibenzylamine, followed by hydrogenolysis over Pd/C (Scheme 2.7).



Scheme 2.7 – Synthesis of organic bridging ligand **L5**, followed by self-assembly of macrocycle **M2**.

Complex **M2** was then obtained by reaction of bridging ligand **L5** with the chloro dimer [(*p*-cymene)RuCl₂]₂ (**C2**) in methanol in the presence of a base (CsOH). After filtration, the product was separated from the residual salts by washing with methanol.

Macrocycle **M2**, which contains the highly hydrophobic pyrene fluorophore, was only moderately soluble in benzene and in dichloromethane. To evaluate the affinity of **M2** for lithium cations, the complexation of Li⁺ was studied using ¹H NMR spectroscopy. 12.5 μL of a 100 mM LiCl stock solution in CD₃OD were added to 487.5 μL of a solution of complex **M2** in C₆D₆. (Final concentrations: [**M2**] = 5.0 mM; [Li⁺] = 2.5 mM). After stirring for 5 minutes, the ¹H NMR spectrum of the solution was examined. It showed that macrocycle **M2** was still present, but it also displayed a new set of signals. The two sets of signals had the same intensity, and we attributed the new set to the Li⁺ adduct (Figure 2.3).^a The peaks of the Li⁺ adduct were slightly shifted and in some cases strongly broadened (aromatic *p*-cymene signals) compared to those of complex **M2**. More detailed complexation studies were not performed due to the poor solubility of the macrocycle in polar solvents. However, it was concluded that the presence of sterically demanding fluorophores on the macrocycle does not prevent Li⁺ from reaching the binding site.

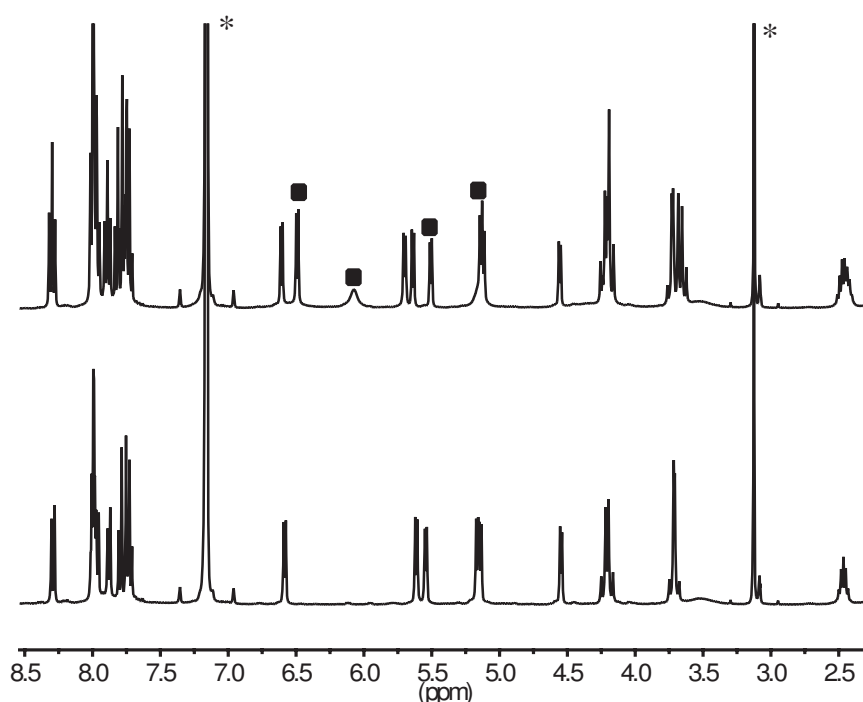
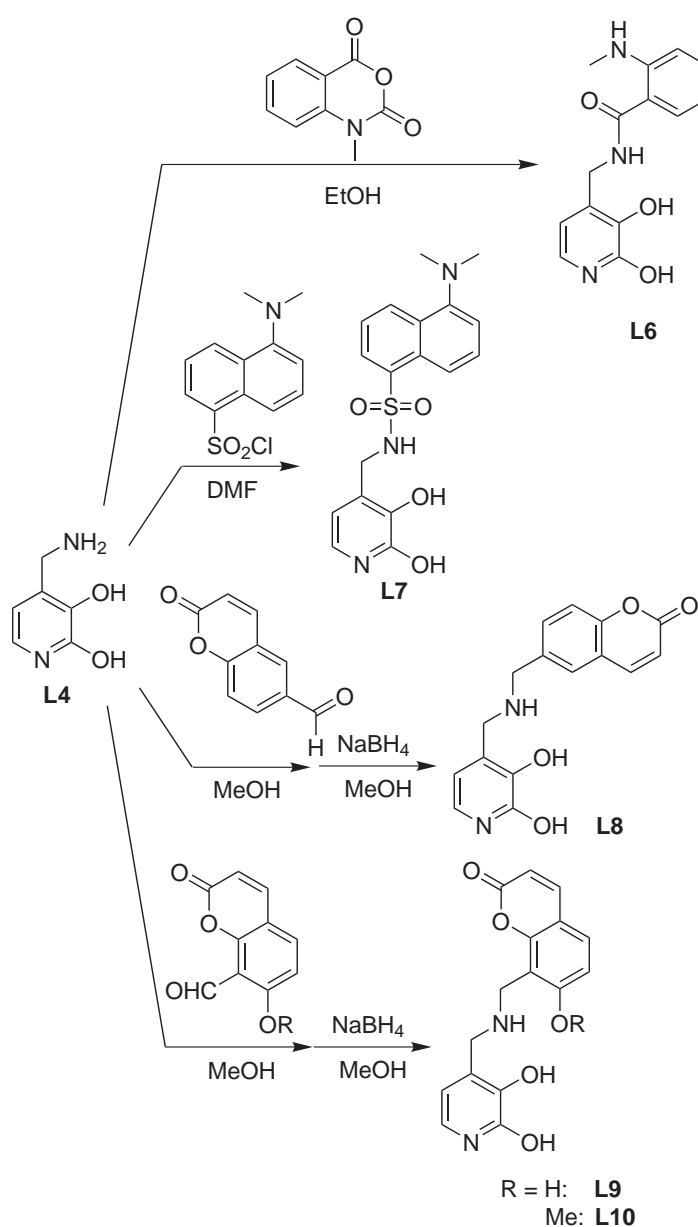


Figure 2.3 – Bottom: region of the ¹H NMR spectrum of the receptor **M2** (5.0 mM) in C₆D₆ containing 2.5 vol% CD₃OD. Top: receptor **M2** in the presence of 0.5 equivalent (2.5 mM) of LiCl. The peaks labeled with ■ indicate the presence of signals corresponding to the pyridine and/or *p*-cymene of the macrocycle–Li⁺ adduct. The asterisks indicate the solvents peaks.

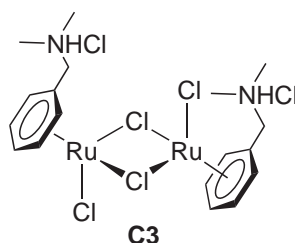
^aThe fact that two sets of signals are observed indicates that the exchange of Li⁺ is slow compared to the NMR time scale, as reported in previous studies (see for example ref. [264]).

Two approaches were pursued in order to obtain more soluble complexes. First, a series of ligands bearing less lipophilic fluorophores was synthesized. In all cases, ligand **L4** was used as starting material: ligand **L6** was obtained by reaction between **L4** and *N*-methylisatoic anhydride, resulting in the formation of an amide bond; **L7** was formed by reaction of **L4** with dansyl chloride (dansyl = 5-dimethylaminonaphthalene-1-sulfonyl), resulting in a sulfonamide linkage; ligands **L8** - **L10** were formed in two steps by reductive amination between **L4** and the respective formylcoumarin derivative (Scheme 2.8).



Scheme 2.8 – Synthesis of ligands **L6-L10**.

Conjointly, a modified π -ligand was used in order to enhance the solubility of the macrocycle in water. Together with standard [(*p*-cymene)RuCl₂]₂ (**C2**), we synthesized amino-substituted [(C₆H₅CH₂NMe₂H)RuCl₂]₂Cl₂ (**C3**, scheme Scheme 2.9).^[291] The tertiary amino groups of the arene π -ligand were expected to enhance the solubility of the resulting macrocycles in water. Chloro dimer **C3** was obtained by reaction of the corresponding diene ammonium salt with hydrated RuCl₃. The diene itself was obtained by a Birch reduction of commercially available *N,N*-dimethylbenzylamine, followed by protonation of the amino group.



Scheme 2.9 – Representation of the dimeric complex **C3**.

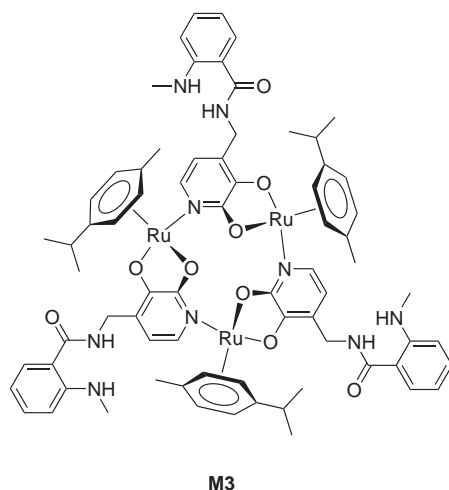
As described below, organic ligands **L6** - **L10** were combined with ruthenium arene chloro dimers **C2** and **C3** in order to form 12-metallacrown-3 complexes. Their solubility properties and lithium affinity depend on both the π -ligand and the fluorophore (as summarized in Table 2.1)

Table 2.1 – Macrocycles that were obtained by combination between organometallic chloro complexes **C2** or **C3** with various organic ligands. The most polar solvent (or combination) able to dissolve significant amounts of the macrocycle is indicated (H₂O refers to buffer solutions at pH 7.0 or 8.0).

Macrocycle	Ru fragment	Bridging ligand	Solubility
M1 ^a	C2	L2	H ₂ O
M2	C2	L5	C ₆ H ₆
M3	C2	L6	MeOH
M4	C3	L1	H ₂ O
M5	C3	L2	H ₂ O
M6	C3	L5	CH ₂ Cl ₂
M7	C3	L6	MeOH/H ₂ O 1:1
M8	C3	L7	MeOH/H ₂ O 7:3
M9	C3	L8	H ₂ O
M10	C3	L10	H ₂ O

^aThe use of the non-fluorescent receptor **M1** will be presented in Chapter 3.

Complex **M3** was synthesized by the reaction of ligand **L6** with $[(p\text{-cymene})\text{RuCl}_2]_2$ (**C2**) in methanol in the presence of CsOH. After removal of the solvent, the complex was extracted from the residual salts with chloroform, and isolated by precipitation upon addition of hexane (Scheme 2.10).



Scheme 2.10 – Macrocycle **M3**.

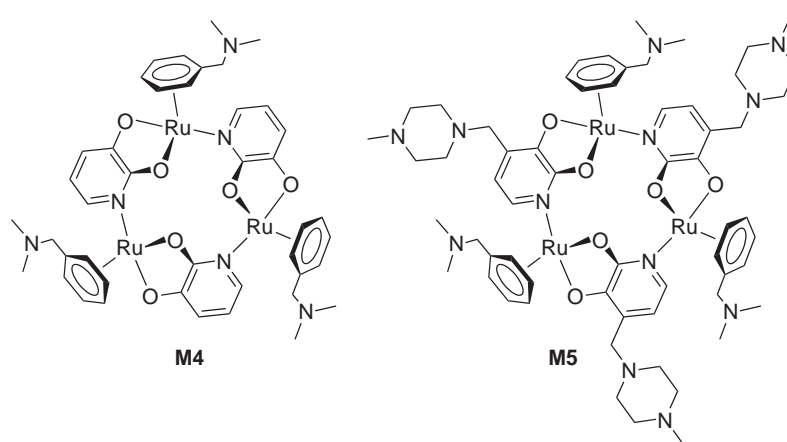
It was observed that macrocycle **M3** was soluble in methanol (unlike **M2**), but that its solubility was considerably reduced upon addition of water to the solution. Therefore, investigations on complex **M3** were not pursued further, and from this point, our efforts focused on using the modified ruthenium chloro dimer **C3** as building block for our sensors.

2.4.2 Macrocycles Based on Modified Ru Fragments

Self-Assembly with Non-Fluorescent Ligands

In order to verify that 12-metallacrown-3 complexes could be formed with modified ruthenium fragment $[(\text{C}_6\text{H}_5\text{CH}_2\text{NMe}_2\text{H})\text{RuCl}_2]_2\text{Cl}_2$ (**C3**), the syntheses of simple macrocycles **M4** and **M5** were performed (Scheme 2.11). Analogous complexes made from widely used $[(p\text{-cymene})\text{RuCl}_2]_2$ had been synthesized and extensively studied in our laboratory,^[53, 264, 267, 269, 271, 272, 274, 275] and similar procedures were developed for synthesis with complex $[(\text{C}_6\text{H}_5\text{CH}_2\text{NMe}_2\text{H})\text{RuCl}_2]_2\text{Cl}_2$. For the preparation of complex **M4**, commercially available 2,3-dihydroxypyridine (**L1**) was stirred in methanol with complex **C3** in the presence of CsOH. After evaporation of the solvent, the macrocycle was extracted with dichloromethane and precipitated by addition of hexane. Interestingly, complex **M4** was found to be soluble in water at neutral pH, which was not the case

for the similar macrocycle based on the (*p*-cymene)Ru fragment.^[274, 275] The synthesis of complex **M5** was performed in the same manner, using organic ligand **L2**, that had been prepared by a Mannich reaction of 2,3-dihydropyridine, formaldehyde and *N*-methylpiperazine.^[267] As in the case of complex **M4**, macrocycle **M5** was found to be well soluble in water at neutral pH. This was expected since the methylpiperazine side-chains can be protonated, enhancing the solubility of the macrocycle.

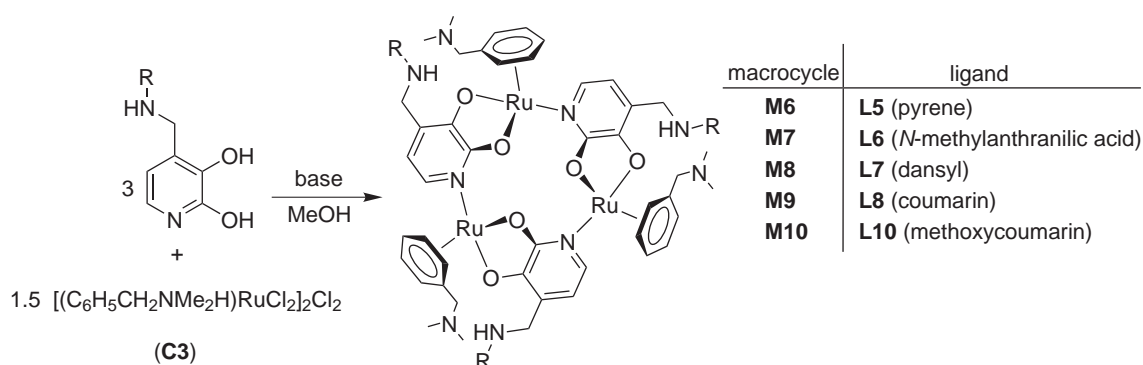


Scheme 2.11 – Macrocycle **M4** and **M5** (neutral forms).

Furthermore, macrocycles **M4** and **M5** could be obtained by self-assembly directly in water (in the presence of a buffer) by mixing appropriate amounts of the building blocks (ligands **L1** or **L2** with chloro dimer **C3** in H₂O pH 8.0, 100 mM phosphate). In this case, the reaction is essentially quantitative and can be followed by ¹H NMR if it is performed in deuterated solvent. NMR also allowed to study the affinity of receptors **M4** and **M5** for Li⁺ ions. When the macrocycles were dissolved in water (phosphate buffer, pH 8.0) in the presence of an excess of Li⁺, a new set of signals appeared, which was attributed to the adduct. Smaller signals corresponding to the uncomplexed receptors **M4** and **M5** were also visible, which made it possible to estimate the association constants as $K_a(\text{Li}^+) = 3.2 (\pm 0.3) \cdot 10^3 \text{ M}^{-1}$ for receptor **M4**, and $K_a(\text{Li}^+) = 1.2 (\pm 0.6) \cdot 10^3 \text{ M}^{-1}$ for receptor **M5**. The error on the second value is relatively important, since the ¹H NMR spectrum was considerably broadened after addition of LiCl, and therefore contained few suitable signals. Still, these results are important since they indicate that complex $[(\text{C}_6\text{H}_5\text{CH}_2\text{NMe}_2\text{H})\text{RuCl}_2]_2\text{Cl}_2$ (**C3**) is well adapted to the self-assembly of 12-metallacrown-3 complexes, and that in spite of additional positive charges, the corresponding receptors still possess a good affinity for Li⁺ ions.

Self-Assembly with Fluorescent Ligands

A series of syntheses was undertaken, the goal of which was the formation of macrocycles **M6** - **M10**. These were obtained by reaction of organic bridging ligands **L5** - **L10** with ruthenium complex $[(C_6H_5CH_2NMe_2H)RuCl_2]_2Cl_2$ (**C3**) in methanol, in the presence of CsOH or Cs₂CO₃ (Scheme 2.12).



Scheme 2.12 – Synthesis of macrocycles **M6** - **M10**. The corresponding fluorophores are indicated.

Macrocycle **M6**, which contains the pyrene fluorophore, was prepared in the same manner as macrocycle **M2** described in Scheme 2.7. No significant improvement in terms of solubility was observed compared to the analogous complex **M2**, which features *p*-cymene as π -ligand.

We then decided to focus on the less lipophilic ligands **L6** - **L10**. When ligand **L6** was mixed with $[(C_6H_5CH_2NMe_2H)RuCl_2]_2Cl_2$ in methanol in the presence of CsOH, macrocycle **M7** was formed. After evaporation of the solvent, the complex was extracted with dichloromethane and isolated by precipitation. Macrocycle **M7** was found to be soluble in organic solvents (MeOH, CH₂Cl₂, CHCl₃), as well as in a 1:1 mixture of methanol and buffered water (pH 7.0 - 8.0, 50 mM phosphate). ¹H NMR studies for this complex were made difficult by a considerable broadening of the signal upon addition of lithium salts, and by several overlaps between the signals of the macrocycle, and those of the lithium adduct. However, the fact that the spectrum undergoes important changes (broadening, shift of the signals) led us to be confident that a good affinity between compound **M7** and Li⁺ exists. Taking advantage of the relatively good solubility properties of the complex, a series of fluorescence experiments was performed. First, we observed that the fluorescence of the *N*-methylantranilic acid dye was almost completely quenched upon formation of the macrocyclic receptor. This was an expected effect of the Ru(II) centers, which are able to quench the

fluorescence by electron transfer. However, the quenching seemed particularly strong in the present case: at the maximum intensity, the fluorescence decreased by a factor of approximately 3000. Second, a small but significant recovery of the fluorescence was observed when Li⁺ was present in solution. This turn-on was very weak: When 4.0 mM Li⁺ was added to a 2.0 mM solution of **M7** in a 1:1 mixture of methanol and water (final phosphate concentration: 50 mM), the fluorescence intensity increased by a factor of 1.3 ($\lambda_{\text{ex}} = 350 \text{ nm}$, $\lambda_{\text{em}} = 507 \text{ nm}$, Figure 2.4). We propose that the “turn-on” response of receptor **M7** upon the binding of Li⁺ is due to the reduced ability of the Ru centers to quench the fluorescence of the fluorophores. This assumption is supported by electrochemical measurements, which have shown that Ru-based metallacrown complexes are significantly more difficult to oxidize in the presence of Li⁺.^[273, 274]

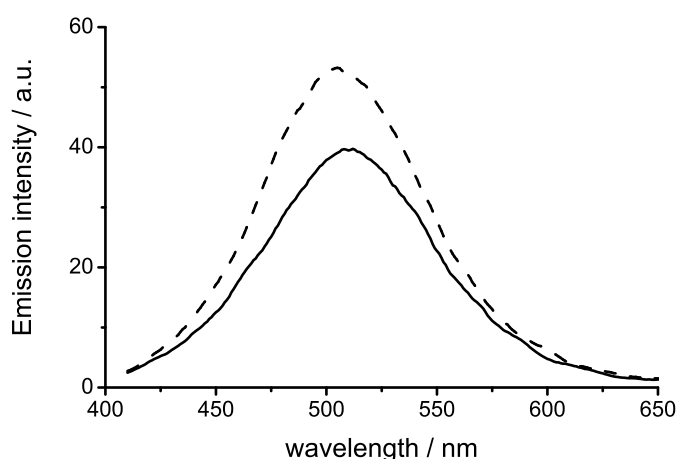


Figure 2.4 – Emission spectra of macrocycle **M7** (2.0 mM) in methanol/water (1:1, pH 7.0, 50 mM phosphate buffer) in absence of Li⁺ (solid line), and after equilibration with 4.0 mM Li⁺ (dashed line). Excitation wavelength: 350 nm.

Complex **M8**, bearing dansyl fluorophores, was synthesized by reaction of **L7** with $[(\text{C}_6\text{H}_5\text{CH}_2\text{NMe}_2\text{H})\text{RuCl}_2]_2\text{Cl}_2$ in methanol in the presence of Cs_2CO_3 . After removal of the solvent, the complex was extracted from the residual salts with dichloromethane and isolated by precipitation. Macrocycle **M8** turned out to be soluble in aqueous methanol (containing up to 30% H_2O) but not in pure water. The ^1H NMR spectra of solutions containing **M8** and various concentrations of LiCl unequivocally indicated a strong affinity between the macrocycle and Li⁺. The association constant was determined by NMR measurements: a 1.5-fold excess of LiCl (3.0 mM) was added to a solution of macrocycle **M8** (2.0 mM) in $\text{CD}_3\text{OD}/\text{D}_2\text{O}$ (9:1, pD 7.0, 10 mM phosphate buffer). After stirring for 5 minutes, the ^1H NMR spectrum was recorded. A new set of signals, corresponding to the Li⁺ adduct, was visible together with the signals corresponding to

uncomplexed receptor **M8**. The ratio of the two species was determined by integration of selected signals. From that, the association constant was calculated as $K_a(\text{Li}^+) = 6.4 (\pm 0.6) 10^3 \text{ M}^{-1}$. The water content of the solution could be increased to 30% if HEPES buffer was used, since phosphate salts show a limited solubility in MeOH/H₂O. The fluorescence of complex **M8** was again strongly reduced compared to that of the free ligand **L7**. Still, solutions of complex **M8** displayed a pronounced fluorescence signal centered at 547 nm when excited at 360 nm. This signal increased in intensity when LiCl was added to the solution (Figure 2.5), as was reported in the case of **M7**. This time, however, the increase in emission intensity was more pronounced.

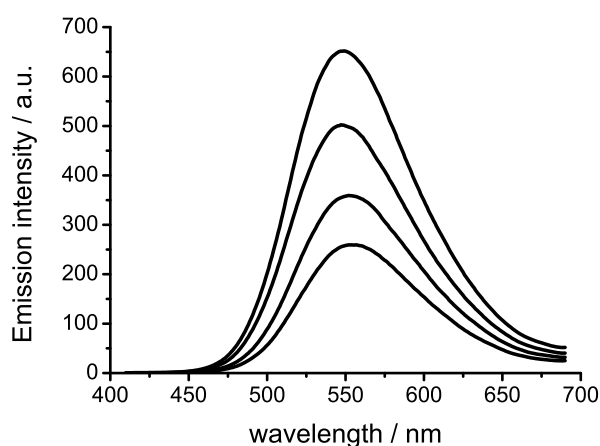


Figure 2.5 – Increase of the emission signal of macrocycle **M8** (2.0 mM) in methanol/water (9:1, pH 7.0, 10 mM phosphate buffer) upon the addition of LiCl (0.0, 0.5, 1.5 and 3.0 mM). Excitation wavelength: 360 nm.

The next series of fluorescent ligands that were investigated are based on the coumarin fluorophore. Commercially available coumarin was formylated in basic solution in the presence of chloroform.^[292] Ligand **L8** was prepared by reductive amination of amino-substituted dihydroxypyridine **L4** with 6-formylcoumarin. Ligand **L8** proved difficult to purify with standard techniques, and semi-preparative reversed-phase HPLC was used. Since only small quantities of purified product were available, synthesis of macrocycles in methanol in the presence of base was not attempted. However, macrocycle **M9** could be formed by self-assembly of ruthenium complex **C3** with ligand **L8** directly in water in the presence of a buffer (pH 8.0, 100 mM phosphate). The formation of macrocycle **M9** could be observed by ¹H NMR when the self-assembly was performed in D₂O. It has to be noted, however, that the ¹H NMR spectrum displayed several extra peaks in addition to the expected signals of **M9**. It appears likely that the reaction leads to side products. Nevertheless, when lithium

ions were present in solution, the ¹H NMR spectrum displayed a new set of signals, corresponding to the adduct. Having this first water soluble macrocycle in hands, we investigated its fluorescence properties. The overall fluorescence was extremely weak – although still detectable – in the absence of Li⁺ in solution. Upon stepwise addition of LiCl, an increase in the fluorescence signal was observed. This increase was not very pronounced: the increase factor estimated for the situation where the receptor is saturated with Li⁺ is 1.35 (Figure 2.6).

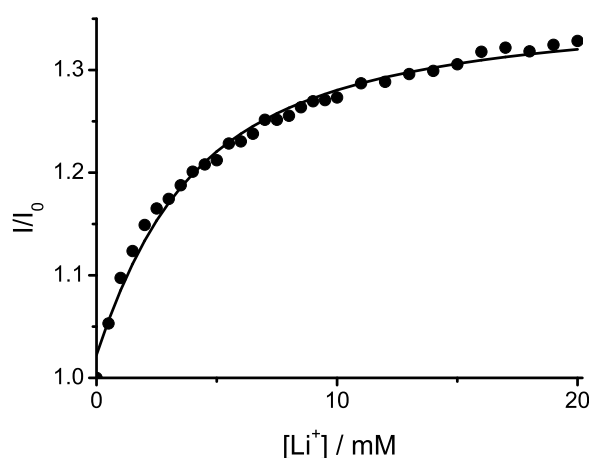


Figure 2.6 – Relative emission intensity of $[(C_6H_5CH_2NMe_2)Ru(L8)]_3$ (2.0 mM in H₂O (pH 7.0)) as a function of Li⁺ concentration. The curve was obtained by fitting the data to a 1:1 binding model. $\lambda_{ex} = 495$ nm, $\lambda_{em} = 523$ nm.

The titration data were fitted with the nonlinear least square curve-fitting program WinEQNMR^[293] using a 1:1 binding model^b to calculate the association constant: $K_a(Li^+) = 3.5 (\pm 1.0) \cdot 10^2 M^{-1}$.

Macrocycle **M9** represents a first success towards a sensor for Li⁺ in water. However, the fact that the ¹H NMR spectrum was not perfect, the weak fluorescence, and the limited emission intensity increase upon Li⁺ coordination encouraged us to search for different ligands. Based on the results obtained with complex **M9**, several important conclusions could be drawn: 1) coumarin-based fluorophores represent a suitable option; 2) an amino group between the fluorophore and the dihydroxypyridine confers additional solubility in water, and 3) the modified π -ligand carrying additional amino groups is necessary to ensure a good solubility.

Ligand **L9** was synthesized by reductive amination of dihydroxypyridine derivative **L4** and 8-formyl-7-hydroxycoumarin. The purification was the most problematic step,

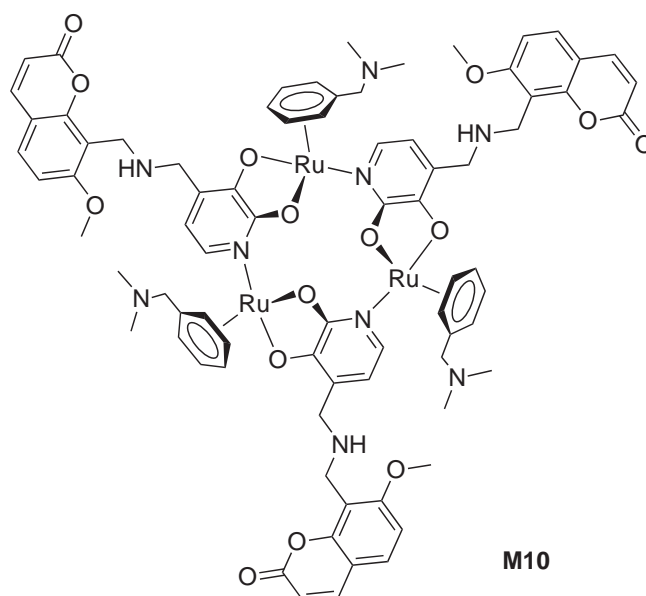
^bDue to steric reasons, the binding site of a 12-metallacrown-3 complex can only accommodate one cation.

and it required the use of semi-preparative HPLC. When self-assembly of ligand **L9** and organometallic complexes **C2** or **C3** was attempted in water or in methanol, the resulting solution contained a mixture of species (as observed by ^1H NMR). The complicated mixtures could not be separated, and no corresponding macrocycle was isolated. We attributed these problems to the hydroxycoumarin moiety, which is likely to interact with Ru centers during the self-assembly process. This led us to synthesize ligand **L10**, which is the *O*-methylated equivalent of **L9**. Reductive amination of dihydroxypyridine derivative **L4** and 8-formyl-7-methoxycoumarin formed ligand **L10**, which was purified by reversed phase HPLC. In the next section, we show how ligand **L10** was used to build a selective fluorescent sensor for Li^+ , which was used in buffered aqueous solutions and in human serum.

2.5 A Fluorescence Sensor for Lithium Ions in Water and Serum

Complex **M10** was synthesized by the base-assisted reaction of bridging ligand **L10** with $[(\text{C}_6\text{H}_5\text{CH}_2\text{NMe}_2\text{H})\text{RuCl}_2]_2\text{Cl}_2$ (**C3**) in methanol, followed by extraction with dichloromethane. The complex is soluble in water at neutral pH. It was therefore possible to generate macrocycle **M10** by simply mixing two equivalents of ligand **L10** with complex **C3** in water (pH 8.0, 100 mM phosphate buffer). The *in situ* reaction is essentially quantitative and further host-guest experiments were performed without prior isolation of macrocycle **M10** (Scheme 2.13).

When 2 equivalents of LiCl were added to an aqueous solution of complex **M10**, the ^1H NMR spectrum showed new signals for the Li^+ adduct along with small signals for remaining **M10** (Figure 2.7). From the ratio of the two species, a value of $K_a(\text{Li}^+) = 8.3 (\pm 0.3) \cdot 10^2 \text{ M}^{-1}$ was calculated. This value is similar to what had been observed for water-soluble (*p*-cymene)Ru-derived metallocrown complexes.^[267] The same experiment performed with a large excess of NaCl instead of LiCl allowed us to estimate the binding constant for sodium as $K_a(\text{Na}^+) = 6 (\pm 3) \cdot 10^{-1} \text{ M}^{-1}$, thus indicating a remarkable $\text{Li}^+:\text{Na}^+$ selectivity of 3 orders of magnitude. Previous investigations had shown that organometallic 12-metallocrown-3 complexes have a negligible affinity for K^+ . Binding studies with K^+ were therefore not performed. Due to its solubility in water, complex **M10** was selected for more detailed fluorescence investigations. Solutions of complex **M10** displayed a fluorescence signal at 480 nm when excited at 382 nm. Upon incremental addition of LiCl to an aqueous solution of **M10**, an increase



Scheme 2.13 – Fluoroionophore **M10** (neutral form).

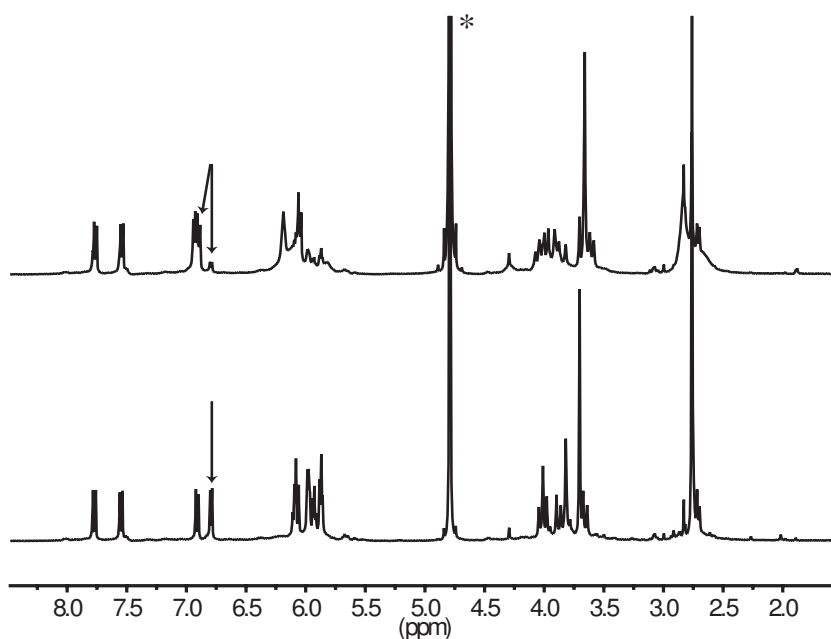


Figure 2.7 – Bottom: ¹H NMR spectrum of receptor **M10** (5.0 mM) in D₂O (pD 8.0, 100 mM phosphate buffer). Top: receptor **M10** in the presence of 2 equivalents of LiCl. The arrows indicate signals of the pyridine ring; in the presence of Li⁺, these signals are slightly downfield shifted, and some “empty” receptor is still visible. The asterisk indicates the water peak.

in the fluorescence was observed (Figure 2.8). Kinetic measurements showed that the response was very quick and that a stable signal was obtained after 1 minute.^c The data were fitted to a 1:1 binding model with the help of the non-linear least square curve-fitting program WinEQNMR.^[293] The obtained value of $K_a(\text{Li}^+) = 7.4 (\pm 0.6) \cdot 10^2 \text{ M}^{-1}$ was in good agreement with the NMR studies.

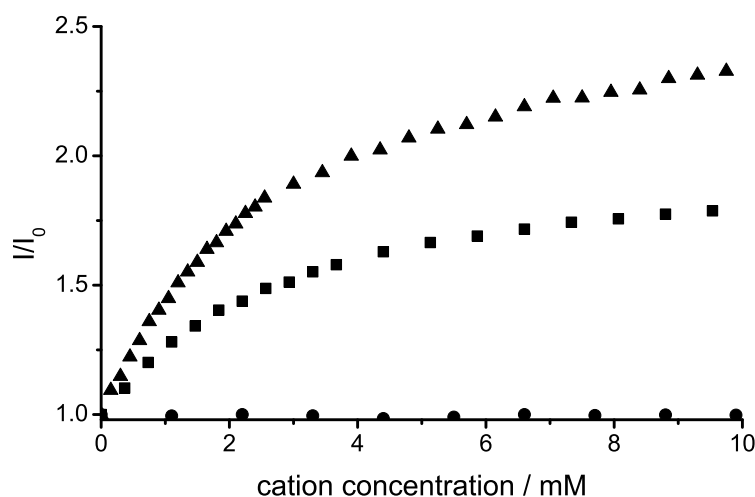


Figure 2.8 – Relative fluorescence intensity at 480 nm (excitation at 382 nm) for solutions containing metallacrown complex **M10** (2.0 mM) and variable amounts of LiCl (\blacktriangle and \blacksquare) or NaCl (\bullet). The data labeled with \blacksquare and \bullet were obtained in water (100 mM phosphate buffer, pH 8.0), whereas the data labeled with \blacktriangle were obtained in serum after removal of proteins.

In biological samples such as serum, the Na^+ concentration can be more than 100 times higher than the pharmacologically relevant Li^+ concentration of around 1.0 mM. For potential applications, it is therefore of prime importance that the sensor displays a very good selectivity for Li^+ over Na^+ . Fluorescence titration experiments with NaCl instead of LiCl showed that complex **M10** is indeed highly specific (Figure 2.8). Only a minor increase (less than 15%) in fluorescence was observed for Na^+ concentrations of up to 140 mM. Mg^{2+} is another potentially interfering ion,^[233] but sensor **M10** showed a negligible response for concentrations of up to 3.0 mM, which is much higher than the biological relevant concentration.

Encouraged by the results obtained in water, we investigated whether metallacrown sensor **M10** could be used in a more complex environment such as human serum. Blood serum contains numerous salts, glucose, hormones, and proteins (with albumin, transferrin and immunoglobulins representing 90% of the total weight).^[235]

^cDepending on the nature of the (π -ligand) M fragment and its steric requirements, 12-metallacrown-3 complexes may display very slow Li^+ binding kinetics. See for example ref. [265] and ref. [269].

The latter were expected to interfere with our sensor due to autofluorescence and competitive coordination to the (arene)Ru complexes. Consequently, large proteins were removed prior to analysis by a simple precipitation procedure.^[294] Fluorescence measurements were then performed with samples that contained different concentrations of LiCl. The results were similar to what was observed for water: the presence of Li⁺ resulted in a concentration-dependent increase in fluorescence (Figure 2.8). The signal to noise ratio was sufficient for quantitative measurements in the biologically interesting concentration range of 0.5 – 3.0 mM. Fitting of the binding isotherm gave an association constant of $K_a(\text{Li}^+) = 8.3 (\pm 0.6) \cdot 10^2 \text{ M}^{-1}$, and the increase in fluorescence was slightly more pronounced than for the measurements performed in water.

2.6 Conclusions

In this chapter are reported the syntheses and host-guest properties of fluorescent (arene)Ru-based 12-metallacrown-3 complexes. The solubility of the complexes was found to depend strongly on the arene π -ligand, as well as on the appended fluorophore. In order to obtain water soluble complexes, several solubilizing amino groups were needed: both on the arene π -ligand and in the spacer connecting the dihydroxypyridine to the fluorophore. Moreover, the appended fluorophores could not be too lipophilic, to avoid compromising the solubility of the macrocycles.

Two water soluble complexes (**M9** and **M10**) were obtained by combining a Ru complex carrying an amino-substituted π -ligand with coumarin and methoxycoumarin fluorophores, respectively. Although both complexes act as “turn-on” fluorescence sensors, **M10** was the most interesting one for the following reasons: its fluorescence was more intense than that of **M9** (even if the quenching by the Ru centers was still very efficient); its emission intensity nearly doubles in the presence of Li⁺; its association constant $K_a(\text{Li}^+)$ is higher than that of **M9**; and the self-assembly process allows the *in situ* formation of pure **M10**, which was not the case for complex **M9**.

Complex **M10** can be used to quantify low millimolar concentrations of the pharmacologically important lithium ion. The sensor can be formed *in situ* from ligand **L10** and $[(\text{C}_6\text{H}_5\text{CH}_2\text{NMe}_2\text{H})\text{RuCl}_2]_2\text{Cl}_2$ (**C3**), both of which are straightforward to synthesize. A key advantage of **M10** is the high affinity and selectivity for Li⁺, which allows working in purely aqueous solution in the presence of an excess of Na⁺, or in a complex matrix such as serum. A current limitation is the modest increase in signal intensity (up to 2.5-fold) and the low overall fluorescence. It should be possible, however, to overcome these limitations by changing the nature of the (π -ligand)M fragment and the fluorophore.

Nevertheless, as was shown by the examples presented above, the solubility of the sensors remains the main issue, which must be kept in mind when modifications are considered.

3 Simple Assays for the Fluorometric Detection of Lithium Ions in Aqueous Solution

Synopsis

In this chapter are presented simple ruthenium-based assays for the selective detection of lithium ions in buffered aqueous solution or in deproteinized serum by fluorescence spectroscopy. A water-soluble metallacrown complex served as the recognition unit of the sensing ensembles. The metallacrown complex could be obtained *in situ* by mixing solutions of complex $[(p\text{-cymene})\text{RuCl}_2]_2$ with a dihydroxypyridine bridging ligand. The addition of the fluorescent dyes 1-hydroxypyrene-3,6,8-trisulfonic acid (HPTS) or Calcein Blue (CAB) to the metallacrown complex resulted in a quenching of the fluorescence, either by formation of a non-covalent aggregate (HPTS) or by destruction of the metallacrown structure (CAB). Significantly increased fluorescence was observed for solutions containing lithium ions. Mixtures containing $[(p\text{-cymene})\text{RuCl}_2]_2$, the dihydroxypyridine ligand, and either HPTS or CAB could therefore be used as turn-on fluorescence sensors for lithium ions.

The work presented in this chapter was a collaboration between Jie Gao and the author (equal contribution from both sides), and part of it was published in: J. Gao, S. Rochat, X. Qian, K. Severin, *Chem. Eur. J.* **2010**, *16*, 5013-5017.

3.1 Introduction

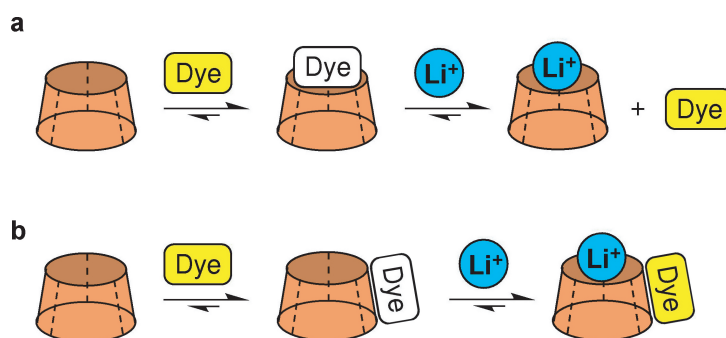
FIRST SUCCESS towards the development of fluorescent sensors, which are able to detect lithium ions in water, is reported in Chapter 2. In particular, complex **M10**, carrying the methoxycoumarin fluorophore, displays a very good selectivity for Li^+ , and could also be used in the presence of numerous potentially interfering species present in human blood serum (cf. section 2.5, p. 39). However, fluoroionophore **M10** has two disadvantages. First of all, the synthesis of the functionalized dihydropyridine ligand **L10** (six steps) and the Ru complex with an amine side chain **C3** (three steps) requires substantial synthetic efforts. Second, the overall fluorescence of the sensor is very weak, and the Li^+ -induced turn-on is not highly pronounced.

In this chapter, we describe two conceptually different approaches to sense lithium ions with a metallocrown complex. We will show that it is possible to obtain turn-on fluorescence sensors for lithium ions by simply mixing readily available starting materials in buffered aqueous solution. The sensors display a significantly improved sensitivity, which allows sensing Li^+ in the submillimolar concentration range.

3.2 A Ditopic Receptor for Lithium and HPTS

The functionalization of a 12-metallocrown-3 complex with a covalently bound fluorophore while maintaining its solubility in water turned out to be a difficult and time-consuming task (see Chapter 2).^[22] We therefore considered the possibility of using a fluorescent dye bound to the macrocyclic receptor in a noncovalent fashion. In principle, such a sensing ensemble can operate by two different mechanisms. If the dye is bound at — or close to — the binding site of the lithium ion, the addition of Li^+ would lead to a displacement of the dye and to a change of its optical properties (Scheme 3.1a). Sensors of this kind are typically referred to as indicator displacement assays (IDAs) and many examples have been described in the literature (see section 1.4). Alternatively, the metallocrown can act as a ditopic receptor for the dye and the metal ion (Scheme 3.1b). If there is some type of “communication” between the two guests, a modulation of the fluorescence properties is possible.

To implement such a sensing scheme, we decided to focus on receptor **M1**. It had been extensively studied in our laboratory, and it is able to bind lithium ions in



Scheme 3.1 – A dye is bound to a Li⁺ receptor through noncovalent interactions, resulting in partial quenching of its fluorescence. A change in fluorescence may be observed if Li⁺ displaces the dye (a), or if the ternary complex between the receptor, Li⁺, and the dye has different optical properties than the receptor–dye complex (b).

aqueous solution with a binding constant of $K_a = 5.8 (\pm 1.0) \cdot 10^4 \text{ M}^{-1}$ (Figure 3.1),^[267] whereas sodium ions are bound with much lower affinity ($K_a = 5.0 (\pm 1.0) \text{ M}^{-1}$). Another interesting feature of complex **M1** is that its synthesis is very easy, and can be done by dissolving the corresponding dihydroxypyridine ligand **L2** and commercially available $[(p\text{-cymene})\text{RuCl}_2]_2$ (**C2**) in a buffer at neutral pH. The macrocycle is then formed by self-assembly in nearly quantitative yield.^[267]

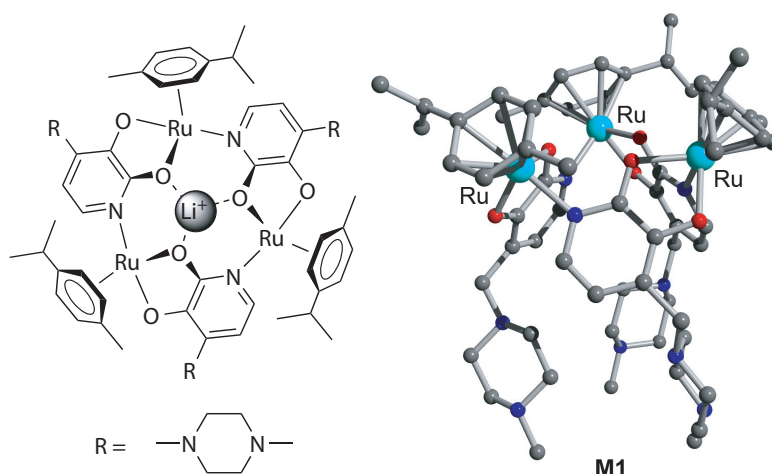


Figure 3.1 – Left: representation of the Li⁺ adduct of complex **M1** with view along the C₃ symmetry axis; right: ball-and-stick representation of the molecular structure of complex **M1** in the crystal with view from the side (based on data from reference [267]).

We then had to find a fluorescent dye, which binds to the receptor in a noncovalent fashion. Complex **M1** was expected to exist as a polycation at neutral pH (protonation of the piperazine side chains). To maximize electrostatic interactions, a polyanionic fluorescent dye seemed to be best suited. Furthermore, the dye could not contain strong metal binding groups, which could lead to the destruction of the metallacrown receptor. Finally, the dye needed to be commercially available to make the assay as simple as possible. The commonly used fluorescent dye 8-hydroxy-1,3,6-pyrenetrisulfonate (HPTS) meets the above-mentioned criteria. In addition, it possesses a high quantum yield and its fluorescence is not sensitive to oxygen.^[295] When a buffered aqueous solution of complex **M1** was mixed with a solution of HPTS, the fluorescence emission intensity at 520 nm ($\lambda_{\text{ex}} = 462 \text{ nm}$) was strongly reduced. The change in fluorescence was a first indication that a complex between the trimeric receptor and HPTS was formed. To quantify the interaction between complex **M1** and HPTS, a fluorescence titration experiment was performed (Figure 3.2).

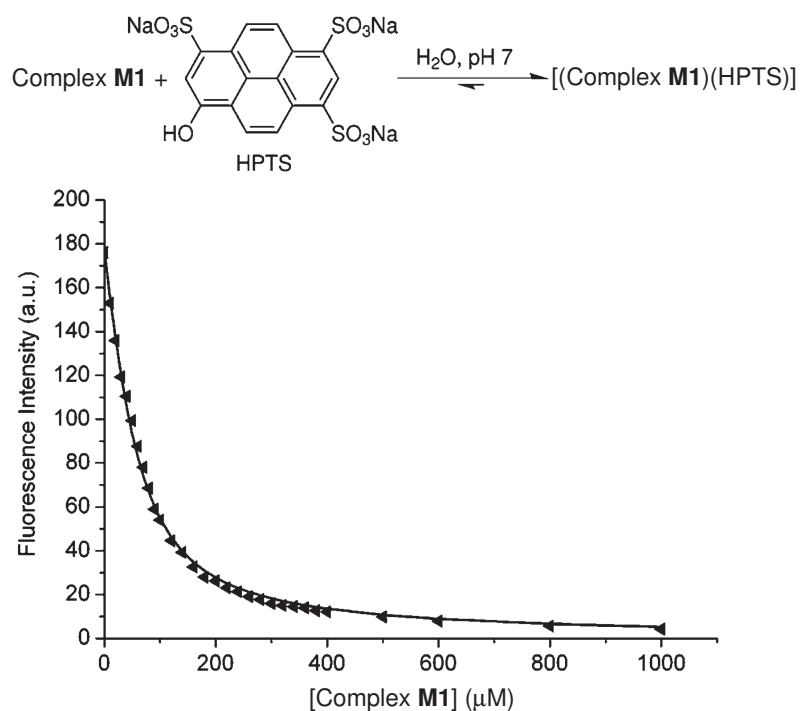


Figure 3.2 – Fluorescence emission intensity at 520 nm ($\lambda_{\text{ex}} = 462 \text{ nm}$) of a solution of HPTS (50 μM) upon addition of complex **M1** (0 – 1000 μM). The curve was obtained by fitting the data to a 1:1 binding model.

Fitting of the data to a 1:1 binding algorithm resulted in an association constant of $K_a = 3.4 (\pm 0.3) \cdot 10^4 \text{ M}^{-1}$, and the 1:1 stoichiometry of the aggregate was confirmed by a Job plot.

Neither the sulfonate groups nor the hydroxy group of HPTS were expected to show a strong affinity to the Ru centers. It therefore seemed unlikely that HPTS would destroy the metallacrown complex. This assumption was supported by ¹H NMR spectroscopy. When increasing amounts of HPTS were added to a buffered D₂O solution of complex **M1**, the signals of trimer **M1** shifted but the number and the multiplicity of the signals remained the same (Figure 3.3). The data of the ¹H NMR titration also gave a clear indication of the binding mode. Strong differences in the chemical shifts were observed for the signals of the protons of the *p*-cymene π -ligand, whereas much smaller changes were found for the N-CH₂ protons, and a negligible shift for the N-CH₃ protons (Figure 3.4). These results suggest that HPTS is bound to the aromatic π -ligand(s) of complex **M1**, and not to the piperazine side chains. The interaction between HPTS and the π -ligands is likely mediated by hydrophobic effects. We have not attempted to derive a binding constant by fitting of the NMR data because a precipitate was observed at higher concentrations (starting for [HPTS] = [M1] \sim 1 mM).

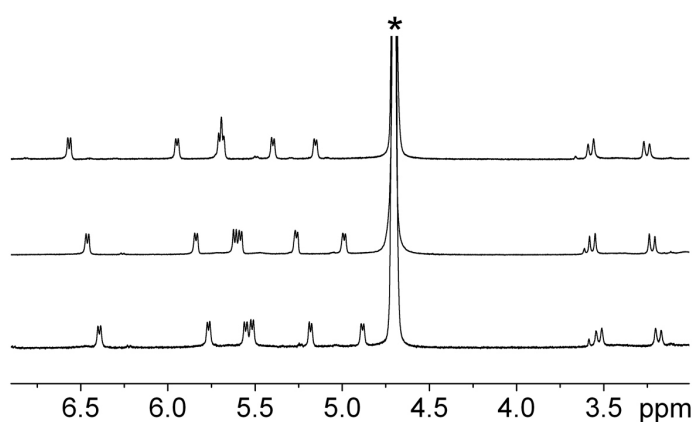


Figure 3.3 – Part of the ¹H NMR spectrum of complex **M1** (1.0 mM) in D₂O (20 mM phosphate buffer, pH 7.0) in the absence (top), in the presence of 0.5 mM HPTS (middle), or in the presence of 1.0 mM HPTS (bottom). The solvent peak is denoted by an asterisk. Complex **M1** was prepared *in situ* by mixing appropriate amounts of [(*p*-cymene)RuCl₂]₂ and ligand **L2**.

Next, we investigated whether the addition of lithium ions to the aggregate between complex **M1** and HPTS would result in a change of fluorescence. This was indeed the case. Addition of LiCl (0 – 20 mM) to a buffered aqueous solution containing the metallacrown complex **M1** (1.0 mM) and HPTS (0.5 mM) resulted in a pronounced recovery of the fluorescence signal with $I/I_0 = 6.6$ at [Li⁺] = 20 mM (Figure 3.5). The

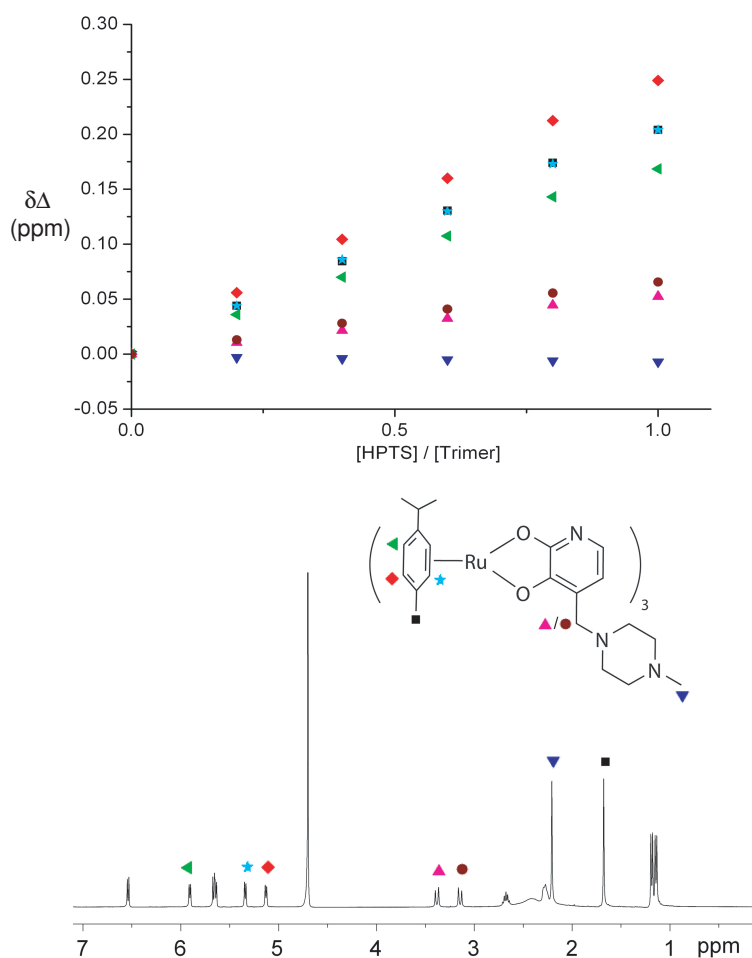


Figure 3.4 – Top: changes of the chemical shifts of selected 1H NMR signals of complex **M1** (1.0 mM) in D_2O (20 mM phosphate buffer, pD 7.0) in the presence of various amounts of HPTS. Bottom: 1H NMR spectrum of complex **M1** in the absence of HPTS and a drawing of the structure showing the assignment of the respective signals (the annotation of the three aromatic CH protons of the cymene π -ligand is arbitrary).

data could be fitted to a 1:1 binding model, which is in line with the known ability of 12-metallacrown-3 complexes to form monoadducts with Li^+ .^[267–279] The apparent binding constant derived from the fitting procedure was $K_a = 2.3 (\pm 0.2) \cdot 10^3 M^{-1}$. This value is only slightly lower than what has been observed for complex **M1** in the absence of buffer and dye.^[267] The strong binding of Li^+ suggests that complex **M1** is able to act as a ditopic receptor for HPTS and Li^+ , and that the complexation of the two guests is largely independent of each other.

The assumption that Li^+ and HPTS are bound independently was supported by the

following control experiment: First, receptor **M1** was saturated with Li⁺ by addition of an excess of LiCl. Subsequently, a fluorescence titration experiment with HPTS was performed. As expected, the decrease in fluorescence was less pronounced than in experiments with free receptor **M1**, but the binding constant of HPTS obtained by fitting of the resulting isotherm ($K_a = 1.9 (\pm 0.2) \cdot 10^4 \text{ M}^{-1}$) was similar to that obtained without Li⁺ ($K_a = 3.4 (\pm 0.3) \cdot 10^4 \text{ M}^{-1}$) (Figure 3.6). The presence of bound Li⁺ was thus not detrimental to the complexation of HPTS.

Taken together, these experiments indicate that the sensing ensemble operates according to the mechanism depicted in Scheme 3.1b and not *via* a Li⁺-induced dye displacement as shown in Scheme 3.1a. The “communication” between HPTS and Li⁺ must be mediated *via* the macrocyclic receptor since LiCl alone did not affect the fluorescence of HPTS. Cyclic voltammetry studies showed that complex **M1** was more difficult to oxidize if bound to a Li⁺ ion (Figure 3.7): For the “free” receptor **M1**, a first oxidation was observed at around $E_{1/2} = 380 \text{ mV}$. Upon saturation with Li⁺, Ru complex **M1** is more difficult to oxidize. Precise values for the difference in half potentials ($\Delta E_{1/2}$) were not measured due to the irreversible nature of the redox transitions. As a result, fluorescence quenching by electron transfer from the metallocrown complex to HPTS is more difficult in the presence of Li⁺, which is in line with the observed increase in fluorescence upon addition of Li⁺. Inner filter effects do not contribute to the observed fluorescence changes since receptor **M1** and its lithium adduct show identical UV/Vis spectra.

Based on the results summarized above, we were able to devise a simple assay for the detection of lithium ions by fluorescence spectroscopy.^[296] The sensor was assembled *in situ* by mixing dihydroxypyridine ligand **L2**^[287–290] with dimer [(*p*-cymene)RuCl₂]₂ (**C2**) and the dye HPTS in buffered aqueous solution (Scheme 3.2). The addition of LiCl^a to this sensing ensemble resulted in a significant increase in fluorescence intensity. The sensitivity of the assay was sufficient for the sensing of Li⁺ in the submillimolar concentration range with very good selectivity over competing metal ions such as Na⁺ and Mg²⁺ (Figure 3.8).

Subsequently, we have explored the possibility of using the sensing ensemble in a complex biological fluid such as human blood serum. Proteins were expected to interfere with the self-assembly of receptor **M1**, notably because histidine and methionine residues have a high affinity for the (*p*-cymene)Ru fragment.^[181] Therefore, larger proteins were removed from the serum by a simple precipitation procedure.

^aPrevious results with receptor **M1** and different Li_nX salts had shown that the nature of the anion Xⁿ⁻ does not affect the binding of Li⁺ in an aqueous solution (see ref. [267]).

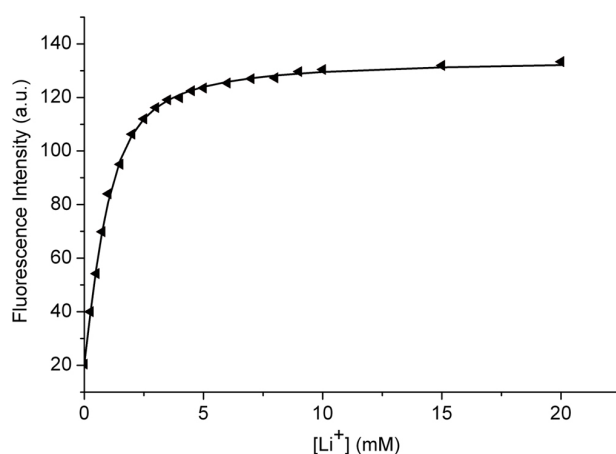


Figure 3.5 – Fluorescence emission intensity at 520 nm ($\lambda_{\text{ex}} = 462$ nm) of a solution of HPTS (0.5 mM) and complex **M1** (1.0 mM) upon addition of Li^+ (0 – 20 mM) in HEPES buffer (100 mM, pH 7.0). Complex **M1** was prepared in situ by mixing appropriate amounts of $[(p\text{-cymene})\text{RuCl}_2]_2$ and ligand **L2**. The curve was obtained by fitting the data to a 1:1 binding model.

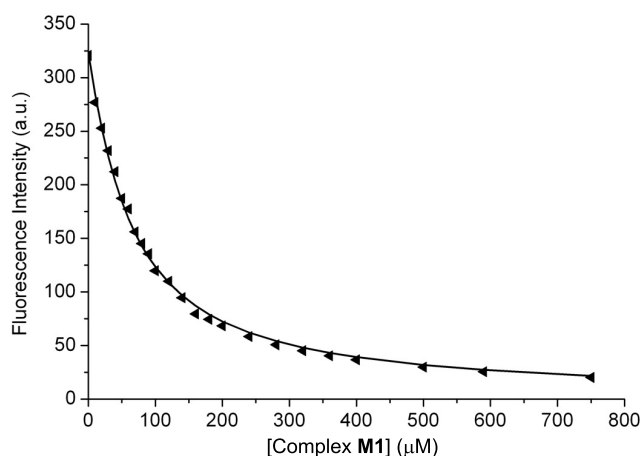


Figure 3.6 – Fluorescence emission intensity at 520 nm ($\lambda_{\text{ex}} = 462$ nm) of a solution of HPTS (25 μM) upon addition of complex **M1** (0 - 750 μM) saturated with Li^+ . The data were recorded in HEPES buffer (20 mM, pH 7.0) containing 5.0 mM LiCl. The curve was obtained by fitting the data to a 1:1 binding model.

Fluorescence measurements with 3:1 mixtures of deproteinized serum and buffered water containing the sensing ensemble and variable amounts of Li^+ showed an enhancement of the fluorescence with increasing amounts of Li^+ (Figure 3.9). The derived binding constant of $K_a = 1.2 (\pm 0.1) \cdot 10^3 \text{ M}^{-1}$ was similar to that obtained for plain buffer. However, the maximum signal intensity was reduced ($I/I_0 = 3.2$ at $[\text{Li}^+] = 20 \text{ mM}$). Still,

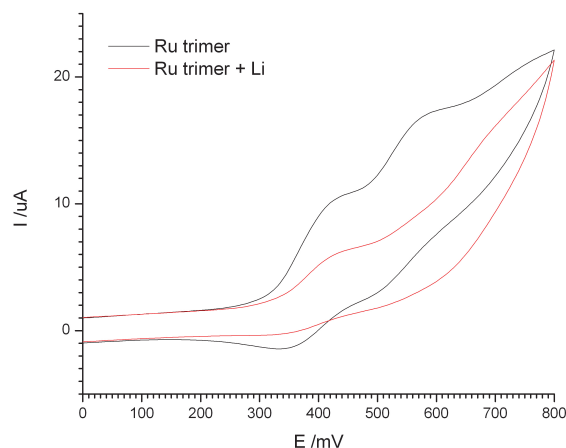
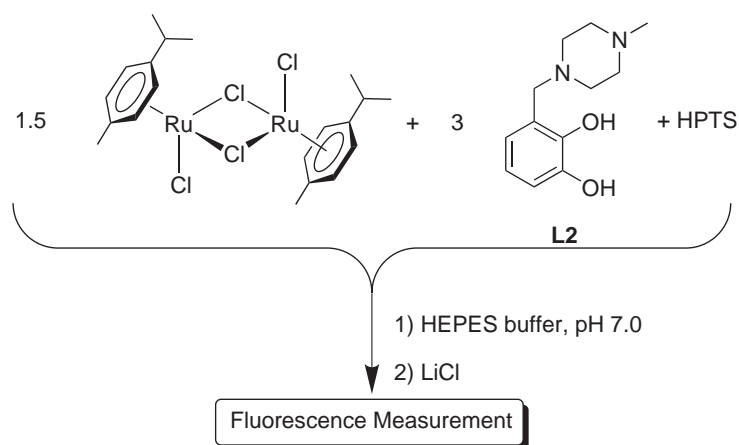


Figure 3.7 – Cyclic voltammogram of a solution of complex **M1** (“Ru trimer”) in the absence and in the presence of LiCl ($[\mathbf{M1}] = 1.0 \text{ mM}$, $[\text{LiCl}] = 0$ and 10 mM , $[\text{HEPES}] = 50 \text{ mM}$, $\text{pH } 7.0$).



Scheme 3.2 – A turn-on fluorescence sensor for Li⁺ is generated *in situ* by reaction of $[(p\text{-cymene})\text{RuCl}_2]_2$ with ligand **L2** and dye HPTS.

the sensing ensemble could be used to sense Li⁺ in the pharmacologically important concentration range of 0.5 to 1.5 mM.

In summary, the presented assay overcomes several limitations, which are often associated with chemosensors for lithium ions. The assay utilizes the known Li⁺ receptor **M1**, but it is based on a conceptually novel signal transduction mechanism. The key to success was the realization that complex **M1** is able to act as a ditopic receptor for Li⁺ and the fluorescent dye HPTS. Consequently, it was possible to obtain the sensor by self-assembly, circumventing the need for the time-consuming modification of the

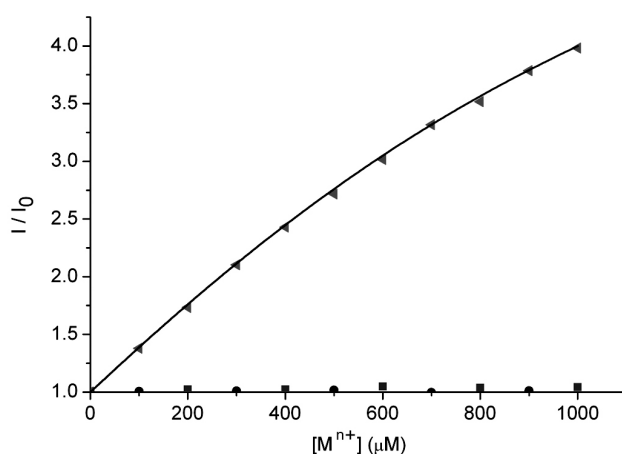


Figure 3.8 – Relative fluorescence intensity at 520 nm ($\lambda_{\text{ex}} = 462$ nm) for solutions containing $[(p\text{-cymene})\text{RuCl}_2]_2$ (1.5 mM), ligand **L2** (3.0 mM), and HPTS (0.5 mM) in the presence of variable amounts of Li^+ (\blacktriangle), Mg^{2+} (\blacksquare) and Na^+ (\bullet) in H_2O (100 mM HEPES, pH 7.0).

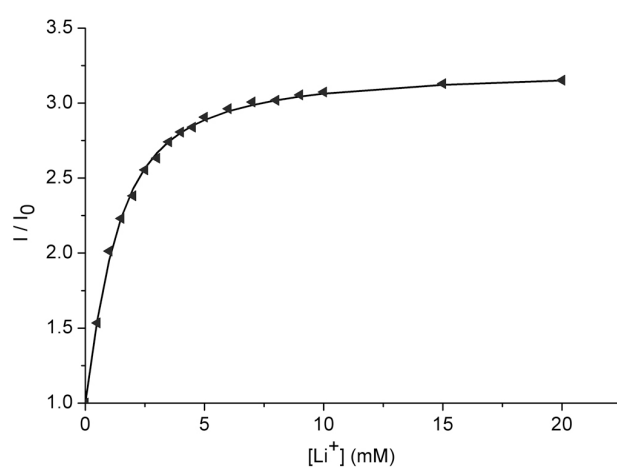


Figure 3.9 – Relative fluorescence intensity at 520 nm ($\lambda_{\text{ex}} = 462$ nm) for solutions containing $[(p\text{-cymene})\text{RuCl}_2]_2$ (1.5 mM), ligand **L2** (3.0 mM), and HPTS (0.5 mM) in the presence of variable amounts of Li^+ in a mixture of H_2O (100 mM HEPES, pH 7.0) and deproteinized serum (1:3). The curve was obtained by fitting the data to a 1:1 binding model.

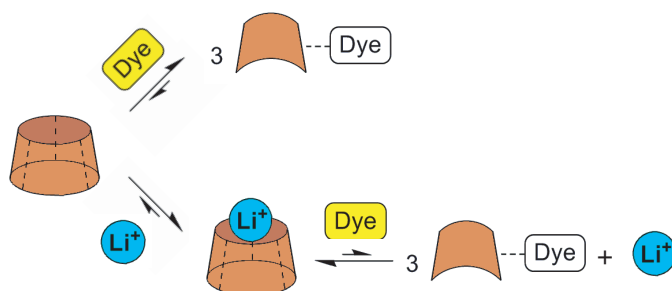
receptor scaffold. The assay allows the sensing of sub-millimolar concentrations of Li^+ in buffered aqueous solution with high selectivity. It should also be pointed out that minimal synthetic efforts are required. Apart from the dihydroxypyridine ligand **L2**, all reagents for the assay are commercially available. Ligand **L2**, on the other hand, can be obtained in one step by a simple Mannich reaction.^[287–290] One drawback of the assay

is its response time: due to the slow binding kinetics of receptor **M1**, several hours at room temperature are required until equilibration.^b Furthermore, large amounts of proteins should be avoided because they can decompose the metallamacrocyclic receptor. Despite these restrictions, the assay^[296] represents a simple but powerful analytical tool for sensing lithium ions in an aqueous solution.

^bThe equilibration time depends on the concentrations. With a receptor concentration of [**M1**] = 1.0 mM and a LiCl concentration of 1.0 mM, 3 h are required until equilibration, as shown by kinetic experiments.

3.3 Sensing of Lithium through its Stabilizing Effect on Macrocyclic Receptors

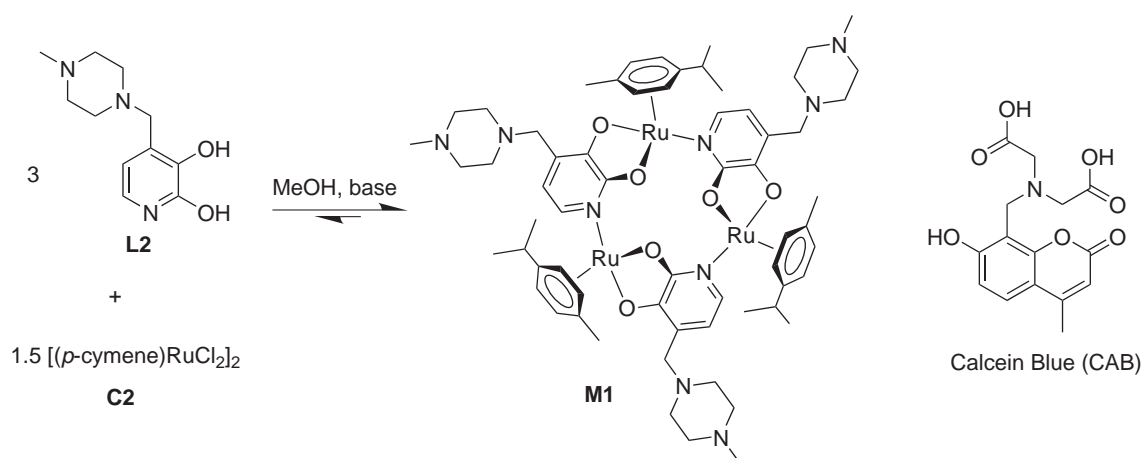
A different approach for sensing of Li^+ is depicted in Scheme 3.3. The same macrocyclic receptor **M1**, which was used in the former section, is employed. The addition of a fluorescent dye with a high affinity for ruthenium leads to partial destruction of the metallacrown complex accompanied by a quenching of the fluorescence. In the presence of Li^+ , a stable adduct $[\mathbf{M1} + \text{Li}^+]$ is formed. If the adduct $[\mathbf{M1} + \text{Li}^+]$ is less prone to destruction by the fluorescent dye than the “free” receptor **M1**, a difference in fluorescence should be observed.



Scheme 3.3 – The addition of a fluorescent dye to a trimeric receptor leads to a partial destruction of the trimer and to a quenching of the fluorescence. In the presence of lithium ions, the destruction of the receptor is less pronounced and an increased fluorescence is observed.

To implement such a sensing scheme, we have used the metallacrown complex **M1** as the receptor. This complex can be formed either *in situ* by mixing commercially available $[(p\text{-cymene})\text{RuCl}_2]_2$ with dihydroxypyridine ligand **L2** in aqueous buffer, or in methanol in the presence of a base (Scheme 3.4).^[267] Organic ligand **L2** is accessible by a simple Mannich reaction between dihydroxypyridine and *N*-methylpiperazine. As fluorescent dye, we have decided to employ commercially available Calcein Blue (CAB). Previous studies in our group had shown that this dye has a high affinity for organometallic halfsandwich complexes such as the $(p\text{-cymene})\text{Ru(II)}$ fragment, and that its fluorescence is nearly completely quenched upon coordination to the metal.^[181]

In order to study the interaction of macrocycle **M1** with CAB, we performed a fluorescence titration experiment, in which a variable amount of **M1** (0 – 130 μM) was added to a fixed quantity of CAB (30 μM) in water (20 mM phosphate buffer, pH 7.0). A quenching of the fluorescence was observed as the concentration of **M1** increased, which we attribute to binding of CAB to the ruthenium centers and simultaneous



Scheme 3.4 – Synthesis of trimeric receptor **M1** and structure of the fluorescent dye Calcein Blue.

destruction of **M1** (Figure 3.10). Fitting the data to a 1:1 binding model afforded an equilibrium constant of $K = 8.2 (\pm 0.8) \cdot 10^5$.

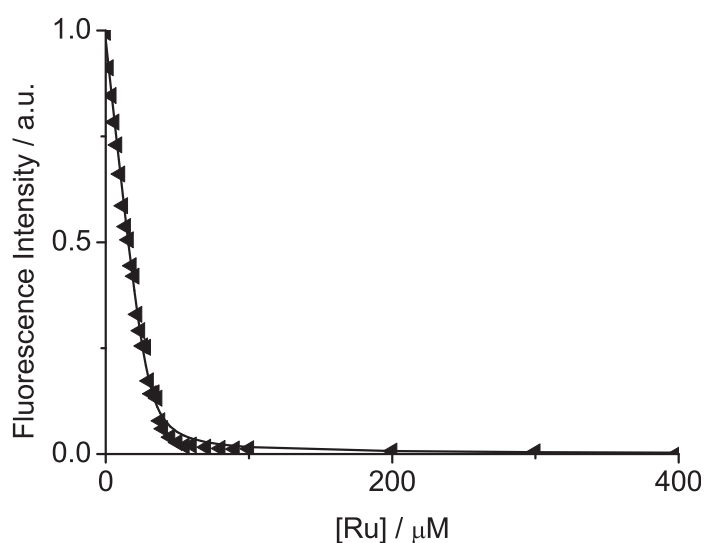


Figure 3.10 – Relative fluorescence intensity at 443 nm of a solution of Calcein Blue (30 μM) in the presence of various amounts of macrocycle **M1**. The indicated Ru concentration refers to the actual concentration of Ru(II) (*i.e.*, 3 times the concentration of **M1**). The solutions were equilibrated 24 hours at 25°C in H₂O (pH 7.0, 20 mM phosphate buffer), and the excitation wavelength was 364 nm. The curve was obtained by fitting the data to a 1:1 binding model.

The assumption that CAB binds to the ruthenium centers and destroys macrocycle **M1** is supported by analyses of ¹H NMR spectra recorded during a similar experiment. When a solution containing **M1** (2.0 mM) and CAB (6.0 mM) was stirred at room

temperature, ^1H NMR spectra recorded after different time intervals showed a progressive disappearance of the signals corresponding to **M1** and the appearance of peaks corresponding to pyridone ligand **L2**, which is released by the reaction (Figure 3.11). Signals corresponding to species formed by interaction between the Ru half-sandwich complex and CAB were also observed. It appears that several new species are formed by mixing **M1** and CAB, which is not surprising since CAB possesses several coordinating sites.

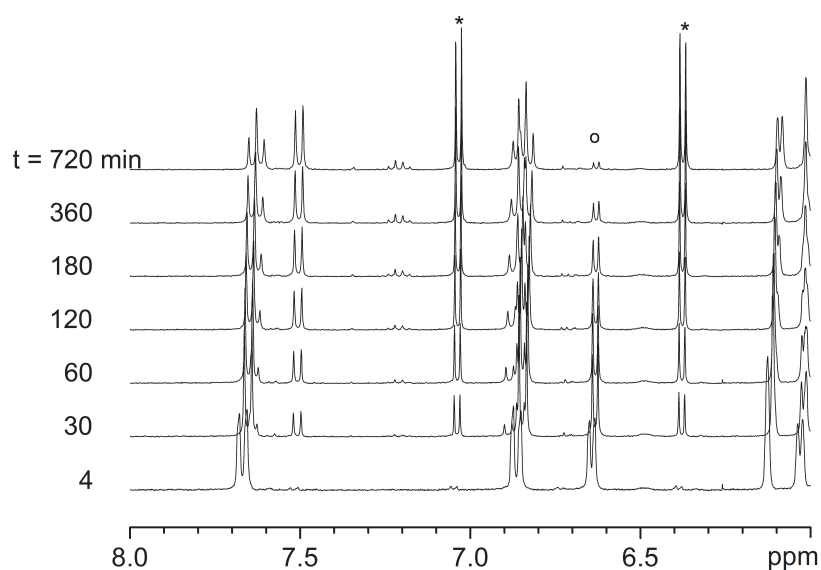


Figure 3.11 – Part of time-dependant ^1H NMR spectra of a mixture containing macrocycle **M1** (2.0 mM) and fluorescent dye Calcein Blue (6.0 mM) in D_2O (20 mM phosphate buffer, pD = 7.0). Asterisks indicate signals corresponding to pyridone ligand **L2**, and the circle indicates a peak corresponding to **M1**.

Next, we investigated whether the presence of Li^+ in solution would influence the stability of the macrocycle towards CAB-induced degradation. The following two-step experiment was performed: First, an aqueous solution (20 mM phosphate buffer, pH 7.0) containing macrocycle **M1** (4.0 mM) and excess LiCl (8.0 mM) was equilibrated at room temperature for 2 hours. At this point, ^1H NMR measurement revealed a quantitative formation of the adduct $[\text{M1}+\text{Li}^+]$, whose spectrum is well distinguishable from the one corresponding to **M1**. Second, an equivalent volume of an aqueous solution of CAB (12.0 mM) was added to this solution, and the reaction was monitored by ^1H NMR (Figure 3.12). From the time-dependant ^1H NMR spectra it is clear that the host-guest complex $[\text{M1}+\text{Li}^+]$ is considerably more stable in the presence of CAB than macrocycle **M1**. Even after a reaction time of 12 h, a very large amount of $[\text{M1}+\text{Li}^+]$ was still visible (about 85% of the initial quantity), whereas in the case where no lithium

was present (Figure 3.11), the signals corresponding to **M1** had almost completely disappeared. It was found that a reaction time of several days was necessary to obtain a complete disappearance of the peaks corresponding to [**M1**+Li⁺].

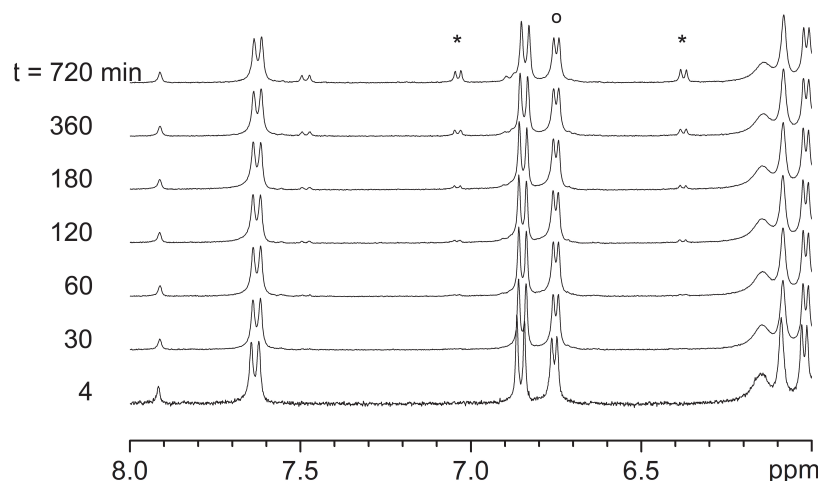


Figure 3.12 – Part of time-dependant ¹H NMR spectra of a sample prepared by mixing equivalent volumes of a solution containing **M1** (4.0 mM) and LiCl (8.0 mM) with a solution containing CAB (12 mM). Asterisks indicate signals corresponding to the pyridone ligand **L2**, and the circle indicates a peak corresponding to [**M1**+Li⁺]. No peak corresponding to **M1** is visible. The spectra were recorded in D₂O (20 mM phosphate buffer, pD = 7.0).

Hoping that the Li⁺-induced difference in reactivity would be translated into a difference in fluorescence, we studied the fluorescence response of our systems. A preliminary control experiment showed that the fluorescence of CAB was not influenced by the presence of LiCl. Then, a two-step experimental setup with various concentrations of LiCl and fixed concentrations of **M1** and CAB was devised as follows: a water solution (pH 7.0, 20 mM phosphate buffer) containing 2.0 mM of **M1** and LiCl (0, 1.0, 2.0 or 4.0 mM, respectively) was equilibrated at room temperature for 2 hours. A portion of this solution (50 μL) was then poured into a water solution containing CAB (2950 μL, 76.1 μM) to initiate the degradation reaction. The fluorescence intensity was measured in a time-resolved fashion for 12 hours ($\lambda_{\text{ex}} = 364 \text{ nm}$, $\lambda_{\text{em}} = 443 \text{ nm}$). As expected, the assay performed in the absence of Li⁺ resulted in a relatively fast quenching of the fluorescence, reflecting the complexation of CAB to the ruthenium centers. An abrupt decrease of the fluorescence of about 20% directly after both solutions were mixed is attributed to an inner filter effect: UV/Vis measurements revealed that a solution of macrocycle **M1** significantly absorbs light at 364 nm, which is also the excitation wavelength that was employed. Part of the excitation energy is then not transmitted to CAB but absorbed by **M1**. Surprisingly, when Li⁺ was present,

a pronounced quenching was also observed during the reaction, although the signal was still well distinguishable from the one recorded in the absence of Li^+ (Figure 3.13).

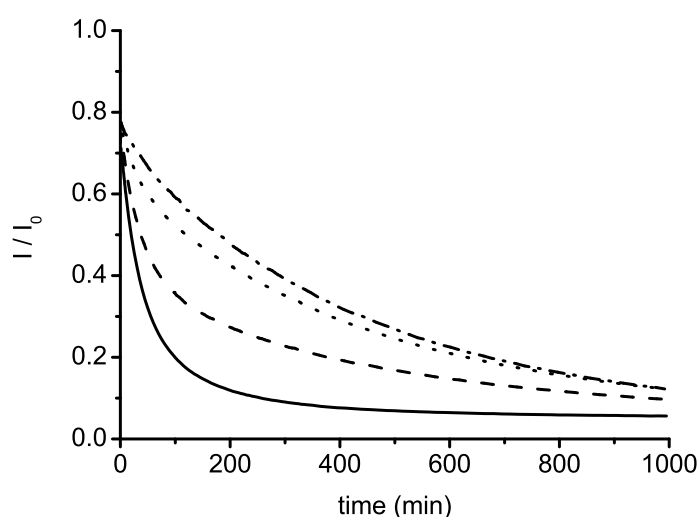


Figure 3.13 – Relative fluorescence intensity at 443 nm for the reaction between macrocycle **M1** ($33.3 \mu\text{M}$) and CAB ($75 \mu\text{M}$), after the stock solution of **M1** (2.0 mM solution) was equilibrated with various quantities of LiCl (solid line, 0.0 mM ; dashed line, 1.0 mM ; dotted line, 2.0 mM ; dash dotted line, 4.0 mM). The data were obtained at 25°C in H_2O ($\text{pH } 7.0$, 20 mM phosphate buffer), and the excitation wavelength was 364 nm .

Two factors can explain this unexpected quenching phenomenon, which seems quite contradictory to what was observed by ^1H NMR: a) It is likely that one Ru center can bind to more than one CAB molecule. This would result in a more pronounced quenching even if a relatively small amount of Ru centers are made available by the reaction; b) The absorbance at 364 nm mentioned above was found to be increasing during the course of the reaction, which points to the formation of compounds which deprive the fluorophore of exciting light (timewise increase of the inner filter effect). In spite of these unavoidable side-effects, it was still possible to differentiate the curves corresponding to different concentrations of Li^+ . Furthermore, it was observed that the ratio of these curves relative to the curve corresponding to the solution containing no lithium was constant (within the experimental error) in the range $310 - 370$ minutes. This allows to measure the relative fluorescence intensity in this time-window without taking the absolute variations of fluorescence into account (Figure 3.14).

A series of experiments involving various Li^+ concentrations was performed in order to obtain a more accurate view of the performance of our sensing ensemble. The

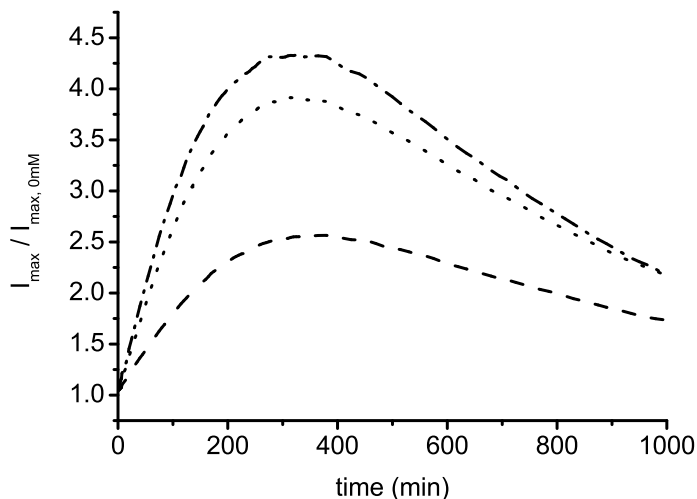


Figure 3.14 – Relative fluorescence intensity ratios between the curves displayed in Figure 3.13: the dashed line indicates the ratio between the curves corresponding to 1.0 and 0.0 mM LiCl, the dotted line to the ratio between the curves corresponding to 2.0 and 0.0 mM LiCl, and the dash dotted line to the ratio between the curves corresponding to 4.0 and 0.0 mM LiCl.

procedure described above was used, and the final mixtures containing CAB, **M1** and Li⁺ were stirred for 5.5 hours before their fluorescence was measured ($\lambda_{\text{ex}} = 364 \text{ nm}$). The obtained binding isotherm (Figure 3.15) was fitted to a 1:1 binding model to obtain an apparent binding constant of $K_a(\text{Li}^+) = 2.5 \pm (0.3) \cdot 10^4 \text{ M}^{-1}$, which indicates that our system is well suited for the detection of Li⁺ in the low millimolar range.

Biological samples usually contain many potentially interacting cations such as Na⁺ (up to 150 mM in blood), K⁺ (up to 5 mM), Mg²⁺ or Ca²⁺ (both up to 1 mM). It is therefore of prime importance to assess the selectivity of our sensor towards these compounds. The buffer used in the frame of this study (pH 7.0, 20 mM phosphate) contains more than 30 mM K⁺ and no signal corresponding to a [**M1**+K⁺] adduct was observed by ¹H NMR. Influence of K⁺ on the behaviour of the sensor can therefore be neglected. Furthermore, fluorescence experiments were conducted in the same manner as indicated above with NaCl (up to 150 mM), CaCl₂ and MgCl₂ (up to 5.0 mM). None of these assays showed any significant fluorescence increase, thus indicating a very high selectivity for the detection of Li⁺, even in the presence of high concentrations of potentially competing cations.

In summary, we have developed a simple assay, made of macrocycle **M1** and fluorophore Calcein Blue, which can detect the presence of Li⁺ ions in aqueous solutions.

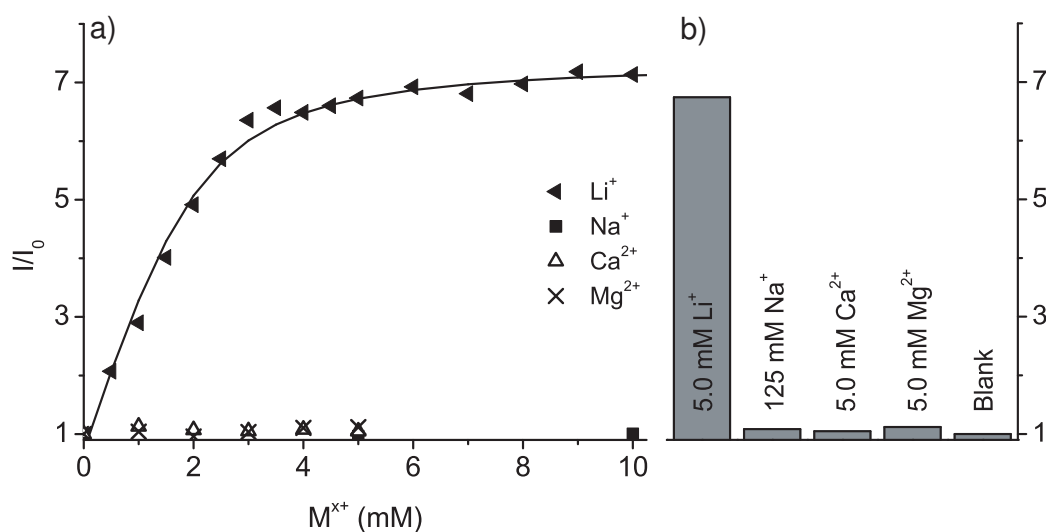


Figure 3.15 – a) Binding isotherms of the system made of **M1** and CAB in the presence of various cations in water. The curve was obtained by fitting the data to a 1:1 binding model. b) Emission intensities of the sensing ensemble in the presence of Li^+ , Ca^{2+} , Mg^{2+} (5.0 mM), and Na^+ (125 mM).

The sensing principle relies on the additional stabilization conferred by Li^+ to the macrocyclic receptor **M1**. As observed by ^1H NMR spectroscopy, degradation of **M1** by CAB, which occurs relatively quickly, is nearly inhibited when the receptor is saturated with Li^+ . This phenomenon was partially translated into a fluorescence signal: the degradation reaction in absence of Li^+ resulted in a pronounced quenching of the fluorescence of CAB, whereas in the presence of Li^+ , this quenching was reduced, as a result of the degradation reaction being prevented. It is, however, unfortunate that a complete suppression of the quenching of the fluorescence was not achieved, contrary to what could be expected based on ^1H NMR experiments.

3.4 Conclusions

Salts containing lithium ions are frequently used drugs for patients suffering from bipolar disorder. Furthermore, Li⁺-based drugs are investigated for neurodegenerative diseases such as Alzheimer's or amyotrophic lateral sclerosis (ALS). In this context it is desirable to have a spectroscopic tool, which allows the selective detection of lithium ions in an aqueous environment. There have been numerous attempts to prepare colorimetric or fluorescence sensors for Li⁺ in homogeneous solution. However, the reported sensors typically show limitations such as low solubility in purely aqueous solution, difficult synthesis, or a lack of selectivity and/or sensitivity. We have developed two assays, which overcome the above-mentioned limitations. The assays utilize a known Li⁺ receptor, but they are based on conceptually novel signal transduction mechanisms with non-covalently bound fluorescent dyes (CAB or HPTS). In terms of sensitivity, the HPTS-based assay is particularly appealing. It allows sensing sub-millimolar concentrations of Li⁺ in buffered aqueous solution with high selectivity. It should also be pointed out that minimal synthetic efforts are required. Apart from dihydroxypyridine ligand **L2**, all reagents for the assay are commercially available. Ligand **L2**, on the other hand, can be obtained in one step by a simple Mannich reaction. One drawback of these assays is their response time: due to the slow binding kinetics of receptor **M1**, 2-3 hours at room temperature are required until equilibration, and the second assay needs additional time for the degradation reaction to proceed. Furthermore, large amounts of proteins should be avoided because they can decompose the macrocyclic receptor. Despite these restrictions, the assays should be of interest as a simple but powerful analytical tool for sensing lithium ions in an aqueous environment.

4 Cross-Reactive Sensor Arrays for the Detection of Peptides in Aqueous Solution by Fluorescence Spectroscopy

Synopsis

A simple but powerful method for the sensing of peptides in aqueous solution was developed. The transition-metal complexes $[\text{Cp}^*\text{RhCl}_2]_2$, $[(p\text{-cymene})\text{RuCl}_2]_2$, and $[(\text{en})\text{PdCl}_2]$ were combined with six different fluorescent dyes to build a cross-reactive sensor array. The fluorescence response of the individual sensor units was based on competitive complexation reactions between the peptide analytes and the fluorescent dyes. The collective response of the sensor array in a time-resolved fashion was used as an input for multivariate analyses. A sensor array composed of only six metal–dye combinations was able to differentiate ten different dipeptides in buffered aqueous solution at a concentration of $50\ \mu\text{M}$. Furthermore, the cross-reactive sensor could be used to obtain information about the identity and the quantity of the pharmacologically interesting dipeptides carnosine and homocarnosine in a complex biological matrix, such as protein depleted human blood serum. The sensor array was also able to sense longer peptides, which was demonstrated by differentiating mixtures of nonapeptide bradykinin and decapeptide kallidin.

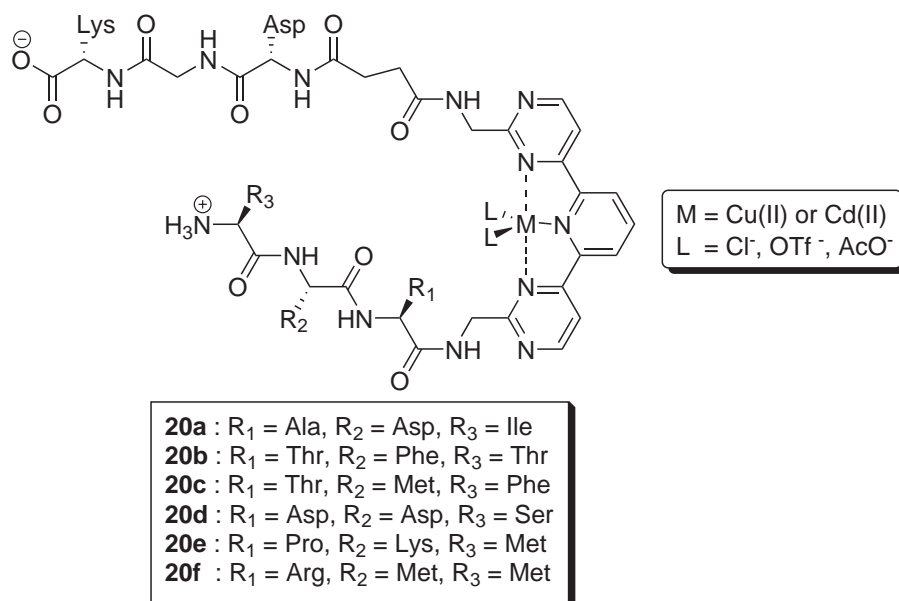
Jie Gao is gratefully acknowledged for having performed the fluorescence measurements involving palladium complexes. The work presented in this chapter was published in: S. Rochat, J. Gao, X. Qian, F. Zaubitzer, K. Severin, *Chem. Eur. J.* **2010**, *16*, 104-113, and in: S. Rochat, K. Severin, *Chimia* **2010**, *64*, 150-152.

4.1 Introduction

SHORT PEPTIDES AND PROTEINS are elusive targets for chemosensors. The design of selective receptors for analytes of this kind, which possess multiple binding sites, requires preorganization of multiple complementary moieties. The synthetic task is therefore rendered prohibitively complicated. Additional difficulties come from the intrinsic flexibility of peptides, as well as from the fact that peptides are usually present in complex fluids, containing numerous, sometimes very similar, compounds. It is therefore not surprising that many successful sensors for peptides are based on pattern recognition protocols.^[184]

Efforts towards the selective detection of peptides were essentially limited to analytes possessing histidine side chains,^[297] which could be targeted owing to their affinity for metal cations, although methionine^[65] and tryptophan^[298] were also found to be relevant targets. Peptides possessing no interacting side-chain are therefore challenging analytes, since they must be differentiated based on minute differences in reactivity or structure.

For the pattern-based analysis of short peptides, two conceptually different approaches have been described. Anslyn and McDevitt *et al.* have generated libraries of synthetic receptors containing Cu(II) and Cd(II) ions. The receptors were either immobilized on a silicon microchip array^[187] or used in homogeneous solution.^[185] The UV/Vis response of the sensor collection was used to differentiate tri- and tetrapeptides as well as the neurotransmitter peptides α -neurokinin (a decapeptide) and substance P (an undecapeptide). Good discrimination was achieved in buffered aqueous solution at peptide concentrations of 13^[187] and 267 μ M,^[185] respectively. A drawback of these systems, however, is the fact that considerable synthetic efforts were required to prepare the receptors. Indeed, the synthesis of a library of compounds (displayed in Scheme 4.1) was necessary to perform discrimination of short peptides in solution. The members of the library have a metal-binding ligand with two appended peptide chains. The metal center imparts selectivity toward peptides terminating in His. One peptide arm was consistently Lys-Gly-Asp, while the second was variable in order to provide the differential recognition character. Although the library made of **20a** - **20f** achieved successful peptide discrimination, it is desirable to reduce the synthetic efforts while maintaining the analytical power.



Scheme 4.1 – Library developed by Wright *et al.* for the discrimination of short peptides in solution.^[185]

Our group reported colorimetric sensors that were obtained by mixing CuCl₂ and NiCl₂ with three dyes in buffered water.^[183, 186, 188] The resulting solutions were composed of complicated mixtures of metal–dye complexes. Upon addition of the peptide analyte, a characteristic change in the UV/Vis spectrum was observed. The peptide was then identified with the help of multivariate analyses. The advantage of this method is its simplicity. Zaubitzer *et al.* showed how mixtures of two related peptide hormones (angiotensin I and angiotensin II, ten- and eight-amino acid peptides, respectively) can be distinguished at concentrations of 20 μM with a sensing ensemble made of commercially available metal salts and dyes (Figure 4.1). However, only a single UV/Vis spectrum is used as the data input (the composite spectrum of all metal–dye–peptide complexes), which potentially compromises the resolution that can be achieved.^a

Here we describe an alternative approach to sense peptides with metal–dye complexes. Sensor arrays with up to 14 individual sensor units were created by combination of metal complexes with dyes. The dyes showed strong luminescence, and fluorescence spectroscopy could be used for the analysis. Instead of 3d transition-metal ions, we used 4d transition-metal complexes of rhodium, ruthenium, or palladium. These compounds showed high binding constants and moderately fast exchange kinetics. As a result, it was possible to perform measurements at very low analyte concentrations and in a time-resolved fashion. The sensor arrays were found to display a remarkable

^aSee Chapter 5 for further discussion on the capacities of such sensing systems.

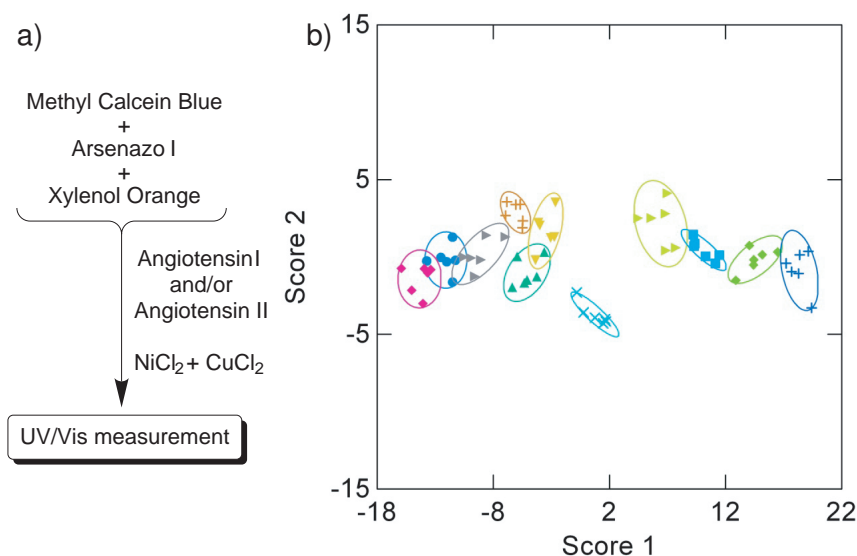


Figure 4.1 – a) Experimental setup for the sensing of the peptide hormones angiotensin I and angiotensin II. The data from UV/Vis measurements were evaluated by multivariate analysis. b) Score plots of LDA showing discrimination between different mixtures of angiotensin I and angiotensin II. $[\text{angiotensin I}]_{\text{tot}} = (20 - x) \mu\text{M}$, $[\text{angiotensin II}]_{\text{tot}} = x \mu\text{M}$; $x = 20$ (maroon, \blacklozenge), 18 (blue, \bullet), 16 (grey, \blacktriangleright), 14 (orange, $+$), 12 (green, \blacktriangle), 10 (yellow, \blacktriangledown), 8 (light blue, \times), 6 (light green, \blacktriangleright), 4 (light blue, \blacksquare), 2 (green, \blacklozenge), 0 (dark blue, $+$). Adapted from ref. [183] with permission of The Royal Society of Chemistry.

discriminatory power. An excellent differentiation of dipeptides was achieved at concentrations as low as 20 – 50 μM . This includes peptides composed of amino acids without coordinating side chains, a challenging class of analytes for metal-based receptors. Furthermore, it was shown that mixtures of the nonapeptide bradykinin and the decapeptide kallidin can be distinguished, and that the dipeptides carnosine and homocarnosine can be analyzed in a complex matrix, such as human serum.

4.2 Building an Array of Fluorescence Sensors

The basic design principle of our cross-reactive sensor array is shown in Figure 4.2. The peptide analytes compete with fluorescent dyes for the coordination to metal complexes. When coordinated to the metal complexes, the fluorescence of the dyes is significantly reduced. The fluorescence intensity is therefore an indication of the proportion of metal–dye complex being formed for a given metal–dye–peptide combination. For the minimal sensor array shown in Figure 4.2, two different fluorescent

dyes were combined with two metal complexes to give a 2×2 array. Larger arrays can be obtained by increasing the number of dyes and/or the number of metal complexes. The identification and/or quantification of the peptide analytes can be achieved by analyzing the fluorescence response of the sensor array with pattern-recognition protocols.

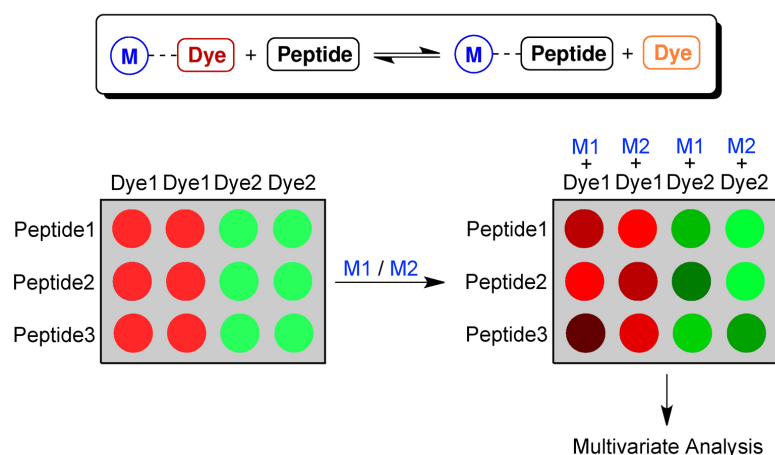


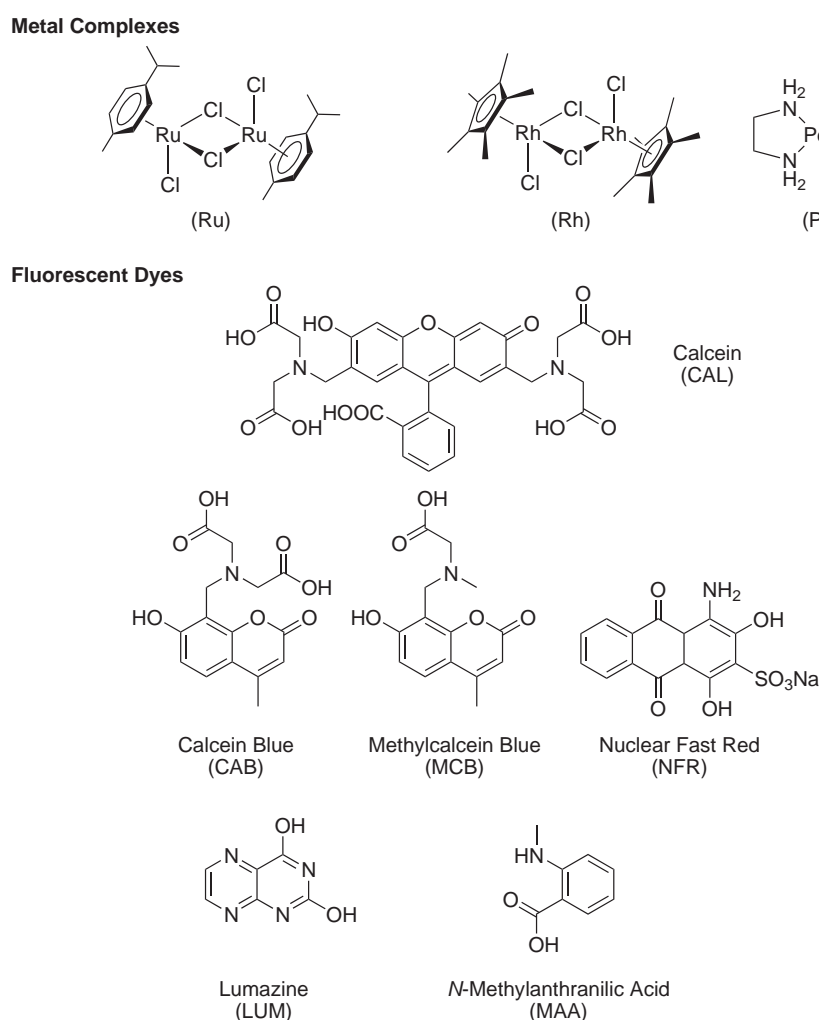
Figure 4.2 – Basic principle of a sensor array based on competition reactions of peptide analytes and metal–dye complexes.

To implement such a sensor scheme, we had to identify metal complexes with the following characteristics: 1) they should be water soluble and inert towards oxidation; 2) they should bind to peptides with high affinity; 3) they should show reasonably fast ligand exchange kinetics; and 4) they should quench the fluorescence of metal-binding dyes. For practical purposes, we were furthermore interested in having metal complexes that are either commercially available or easy to synthesize. Simple 3d transition-metal halides (e.g., CuCl_2) might fulfill the above-mentioned criteria. However, we decided to focus on 4d transition-metal complexes, because they potentially show higher binding constants to peptide analytes.

Previous experiments from our laboratory showed that the organometallic complex $[\text{Cp}^*\text{RhCl}_2]_2$ (**C1**) was well suited for competitive assays with dyes and peptides.^[65] The commercially available rhodium chloro dimer is soluble in water (aqua complexes are formed) and the solutions are not air sensitive. Importantly, this complex showed a good binding affinity to peptides, albeit with a strong preference for those containing histidine or methionine.^[65] The coordination chemistry of the arene complex $[(p\text{-cymene})\text{RuCl}_2]_2$ (**C2**) is known to be similar to that of $[\text{Cp}^*\text{RhCl}_2]_2$,^[263] and studies by Beck and Sheldrick showed that the (*p*-cymene)Ru fragment is able to bind to

peptides.^[299-304] The complex $[(p\text{-cymene})\text{RuCl}_2]_2$ was therefore used as the second metal constituent for our sensor array. The third and final metal component that we chose was $[(\text{en})\text{PdCl}_2]$ (**C4**, en = ethylenediamine). Again, there was strong evidence that this metal complex is able to bind to peptides, in particular due to the detailed studies of Kostić and others on Pd(II)-induced peptide hydrolysis.^[305-319] To the best of our knowledge, there was no precedence for the utilization of (en)Pd or (p-cymene)Ru complexes in the context of indicator displacement assays.

The structures of the fluorescent dyes that we used for the sensor are depicted in Scheme 4.2. They are all commercially available and possess donor groups that are suited for the complexation to transition metals.



Scheme 4.2 – Metal complexes and fluorescent dyes used in this study.

To obtain quantitative information about the binding affinities of the dyes to the three metal complexes, we performed fluorescence titration experiments in buffered

aqueous solution (100 mM phosphate buffer, pH 7.0) with a fixed amount of dye and a variable amount of metal complex. The binding constants were obtained by fitting of the binding isotherms. The case of Nuclear Fast Red (NFR) titrated by Ru is illustrated in Figure 4.3 (for the other metal/dye combinations, see Appendix A.1). In most cases, a 1:1 binding model provided a reasonably good fit. For Calcein (CAL), it is likely that $[M_2(\text{CAL})]$ complexes are formed as well, but it was difficult to obtain an accurate binding constant for the coordination of the second metal, because the fluorescence was nearly fully quenched by the first metal.

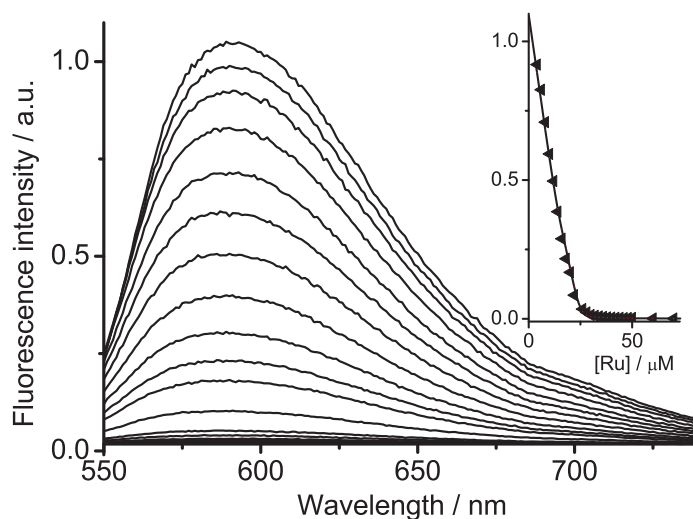


Figure 4.3 – Fluorescence emission spectra of a solution of Nuclear Fast Red (50 μM) upon addition of complex $[(p\text{-cymene})\text{RuCl}_2]_2$ ($[\text{Ru}] = 0 - 100 \mu\text{M}$). The excitation wavelength was 540 nm. The spectra were recorded in H_2O (100 mM phosphate buffer, pH 7.0) after equilibration for two days in the dark. Inset: emission intensity at 590 nm of a solution of Nuclear Fast Red (50 μM) upon addition of complex $[(p\text{-cymene})\text{RuCl}_2]_2$ ($[\text{Ru}] = 0 - 100 \mu\text{M}$). The curve was obtained by fitting the data to a 1:2 binding model.

When comparing the binding constants for the three different metal complexes, it is apparent that the values for a given dye generally increase in the order $K_1(\text{Pd}) < K_1(\text{Ru}) < K_1(\text{Rh})$, except in the case of Nuclear Fast Red (Table 4.1). Overall, the binding constants span more than four orders of magnitude, which is advantageous for the analysis of peptides possessing very different binding affinities to metal complexes. No pronounced quenching was observed when solutions of Rh or Ru were added to Lumazine (LUM) and *N*-Methylantranilic Acid (MAA). Therefore, these combinations were not taken into account for our sensor array.

Table 4.1 – Binding constants for the complexation of the fluorescent dyes to the metal complexes.

Fluorescent Dye	Metal Complex	K_1 [M^{-1}] ^a
CAL	Rh	$7.6 (\pm 0.8) \cdot 10^6$
CAL	Ru	$1.9 (\pm 0.2) \cdot 10^6$
CAL	Pd	$6.2 (\pm 0.6) \cdot 10^5$
CAB	Rh	$> 10^7$
CAB	Ru	$1.6 (\pm 0.2) \cdot 10^6$
CAB	Pd	$1.2 (\pm 0.1) \cdot 10^5$
MCB	Rh	$> 10^7$
MCB	Ru	$1.8 (\pm 0.2) \cdot 10^7$
MCB	Pd	$2.2 (\pm 0.2) \cdot 10^5$
NFR	Rh	$1.6 (\pm 0.2) \cdot 10^6$
NFR	Ru	$> 10^7$
NFR	Pd	$> 10^7$
LUM	Pd	$7.8 (\pm 0.8) \cdot 10^4$
MAA	Pd	$8.6 (\pm 0.9) \cdot 10^3$

^aThe binding constants were calculated by numerical fitting of the binding isotherms obtained from fluorescence titration experiments. The titrations were performed in buffered aqueous solution (100 mM phosphate buffer, pH 7.0)

4.3 Discrimination of Small Peptides

4.3.1 Dipeptides in Water

Next, we studied the sensor response to dipeptides for some selected metal–dye combinations. For this purpose, an aqueous solution of the dye was mixed with the respective peptide. The competition reaction was then initiated by adding a stock solution of the metal complex and the fluorescence response was recorded as a function of time. The data for a mixture of [(en)PdCl₂] (Pd) and Lumazine (LUM) and the analytes Met-Leu, His-Ala, and Ser-Gly are shown in Figure 4.4. The final concentrations for these reactions were: [Pd] = [LUM] = 25 μM, [peptide] = 50 μM. In all cases, an initial decrease in fluorescence intensity was observed. However, within a few minutes the fluorescence signal started to increase. After one hour, a steady state was nearly reached with a fluorescence signal that was only slightly weaker than that of the free dye. These data suggest that the Pd complex reacts faster with Lumazine than with peptides (initial decrease of the signal), but peptides bind stronger to the metal than Lumazine and ultimately displace the dye (subsequent increase of the signal).

A different situation was encountered for reactions with [(en)PdCl₂], Calcein Blue

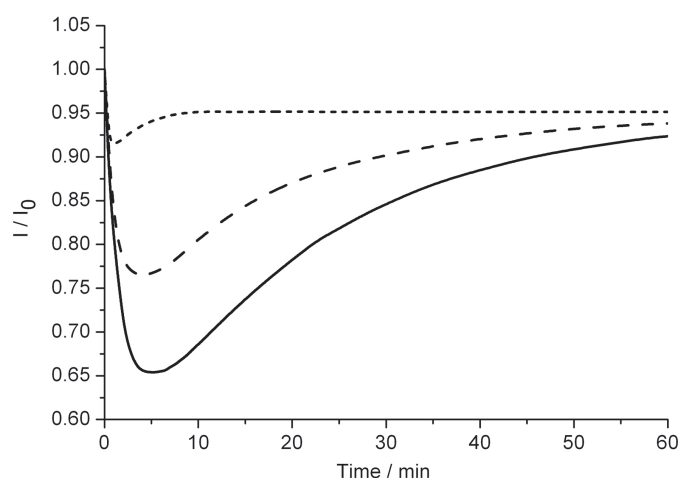


Figure 4.4 – Relative fluorescence emission intensity at 460 nm for the reaction of [(en)PdCl₂] (25 μM) and Lumazine (25 μM) in the presence of Met-Leu (50 μM, dotted line), His-Ala (50 μM, dashed line), and Ser-Gly (50 μM, solid line). The data were obtained at 25°C in H₂O (100 mM phosphate buffer, pH 7.0). The excitation wavelength was 328 nm.

(CAB), and the peptides Trp-Gly, Val-Phe and Phe-Pro (Figure 4.5). A steady decrease of the fluorescence signal was observed for all three peptides for the first 20 min. A minor increase in signal intensity occurred for Trp-Gly and Val-Phe over the last 30 min, but for Phe-Pro the signal continued to decrease. The data show that the reaction rate for the complexation of Calcein Blue to Pd is slower than that of Lumazine, and that the peptides are less-efficient competitors for the binding to the metal. Kinetic profiles similar to that shown in Figure 4.5 were found for the Rh and Ru sensors (the competition reactions were slower for Ru than for Rh). Some representative examples are shown in Appendix A.4.

From the results of these competition experiments, it is evident that for some metal–dye–peptide combinations, larger differences in fluorescence intensity are observed at the beginning of the reaction, whereas other combinations show more pronounced differences at the end. Consequently, the sensing of peptides was best achieved by time-resolved measurements.

To test the scope of our sensor array, ten different dipeptides were used. The binding kinetics of the fourteen metal–dye combinations shown in Table 4.1 were measured in the presence of each dipeptide. The assays were performed as follows: Metal complexes ($[M]_{\text{final}} = 25 \mu\text{M}$) were added to solutions containing the respective dye ($[\text{dye}]_{\text{final}} = 25 \mu\text{M}$) and peptide ($[\text{peptide}]_{\text{final}} = 20$ or $50 \mu\text{M}$) to initiate the

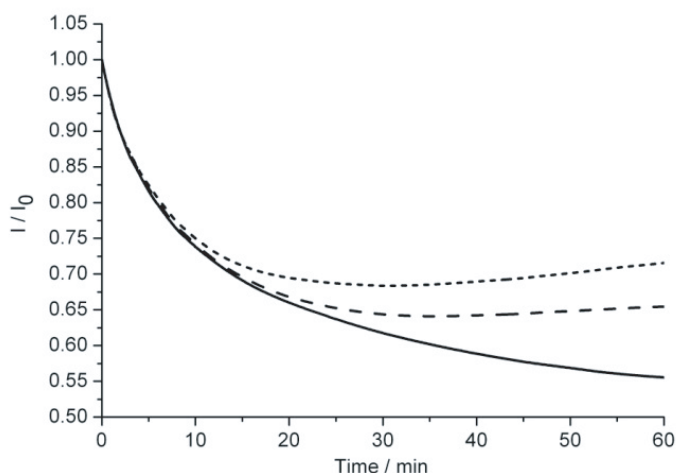


Figure 4.5 – Relative fluorescence emission intensity at 440 nm for the reaction of $[(en)PdCl_2]$ ($25 \mu M$) and Calcein Blue ($25 \mu M$) in the presence of Trp-Gly ($50 \mu M$, dotted line), Val-Phe ($50 \mu M$, dashed line) and Phe-Pro ($50 \mu M$, solid line). The data were obtained at $25^\circ C$ in H_2O (100 mM phosphate buffer, $pH 7.0$). The excitation wavelength was 336 nm .

competition reactions. The fluorescence signal at the emission maximum (Table 4.2) was measured at regular time intervals, and each reaction was repeated four or six times. An inspection of the fluorescence response revealed that 1) the fluorescence signal before the addition of the metal complex was stable over time and independent of the peptide, thus indicating that no dye-peptide interactions occur, and 2) a pseudo-equilibrium state was reached one hour after metal complex addition in most of the cases.

Table 4.2 – Excitation and emission wavelengths of the fluorescent dyes.

Fluorescent Dye	Excitation [nm]	Emission [nm]
CAL	493	520
CAB	336	440
MCB	363	445
NFR	540	590
LUM	328	460
MAA	325	439

For the statistical analyses, we chose to take the fluorescence intensities of each metal–dye–analyte combination at 5, 20, and 60 min as input values. This choice allowed us to take into account kinetic differences (5 and 20 min values) as well as variations of the pseudo-steady-states (60 min value). Figure 4.6 shows a qualitative

view of the sensor response at 60 min. It is apparent that peptides containing amino acids with coordinating side chains, in particular His-Ala and Met-Leu, are able to displace a larger fraction of the dyes and thus give stronger signals. The least-coordinating peptide was found to be Phe-Pro: it does not compete efficiently with the fluorescent dyes for the complexation to the metals, resulting in almost completely quenched fluorescence signals.

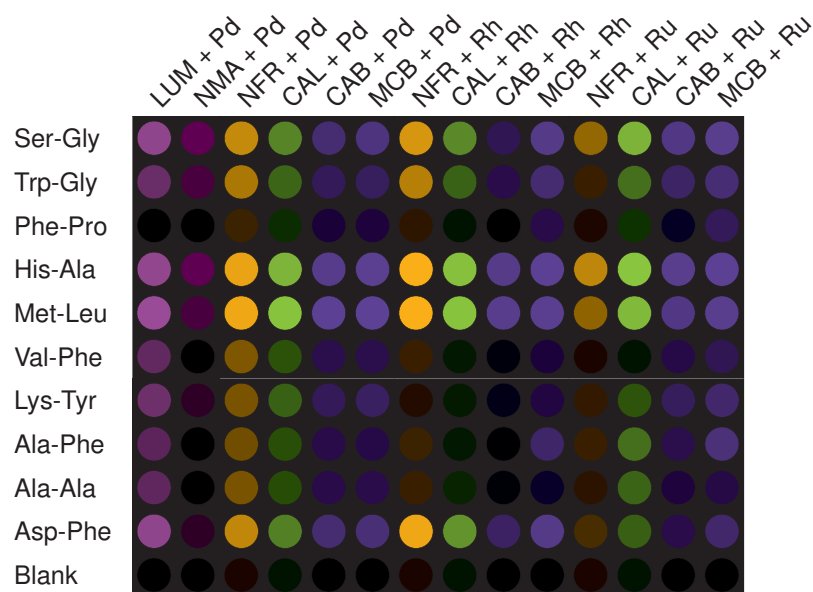


Figure 4.6 – Graphic representation of the relative fluorescence intensities after 60 min of solutions containing the indicated dyes, peptides and metal complexes ($[M] = 25 \mu\text{M}$, $[\text{dye}] = 25 \mu\text{M}$, $[\text{peptide}] = 50 \mu\text{M}$, 100 mM phosphate buffer, pH 7.0). The colors approximately match the wavelengths at maximum emission intensities, and the brightness corresponds to the fluorescence intensities of the samples. The brightness was calculated by assuming that the signal of the free dye was 100% and that of a “blank” sample without peptide was 0%.

To evaluate the discriminatory power of our sensor array, a principal component analysis (PCA)^[110] was performed. PCA allows to reduce the multidimensional sensor array data to only two or three dimensions with minimal loss of variance. The resulting score plots are shown in Figure 4.7. The first three principal components are displayed, accounting for 94% of the total variance. All analytes are grouped in well-separated clusters. The analytes that appear close to each other are the ones that possess the weakest interaction with the metal complexes: Ala-Ala, Val-Phe, Phe-Pro, and Ala-Phe. Despite their weak displacement abilities, these analytes are still well separated from the blank sample. Interestingly, the main principal component (factor 1) correlates with

the affinity of the peptide to the metal complexes: the blank sample shows the lowest values (factor 1 = $-6.27 (\pm 0.06)$), close to those of the dipeptides possessing aliphatic side chains. As qualitatively observed in Figure 4.6, the peptide appearing closest to the blank on the factor 1 axis is Phe-Pro (at a concentration of $50 \mu\text{M}$, factor 1 = $-3.83 (\pm 0.05)$), whereas the peptides containing strongly coordinating His or Met residues appear with the highest values (His-Ala: factor 1 = $11.53 (\pm 0.05)$; Met-Leu: factor 1 = $11.43 (\pm 0.12)$). The dipeptides with other, weakly interacting side chains are found in between. Also of importance is the fact that the 20 and the $50 \mu\text{M}$ samples of Val-Phe and Ala-Ala appear well separated on the score plots, which underlines the possibility of obtaining information about the nature *and* the concentration of the analytes.

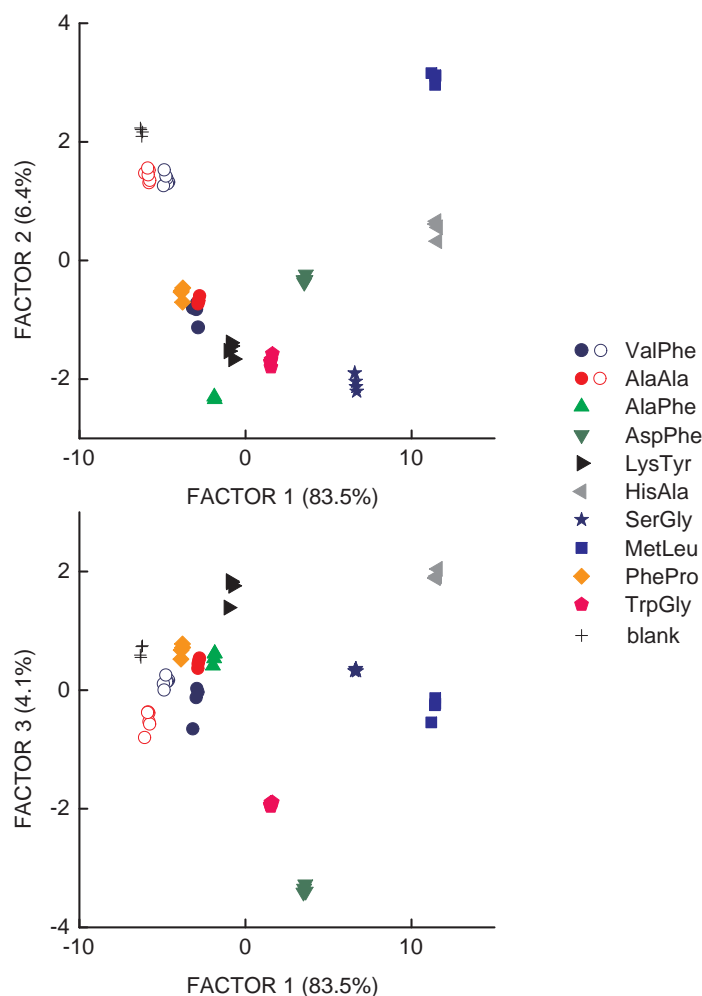


Figure 4.7 – PCA score plots for the discrimination of ten dipeptides. The peptide concentrations were $50 \mu\text{M}$ (filled symbols) or $20 \mu\text{M}$ (open symbols). The input data for the PCA were obtained from a sensor array comprised of the 14 metal–dye combinations listed in Table 4.1.

In addition to the PCA, the same data set was used to perform a linear discriminant analysis (LDA),^[110] which also resulted in a good separation of each analyte. The model was built by using a stepwise variable selection algorithm. A “jack-knifed matrix” validation procedure was performed, where one measurement at a time was randomly omitted. The remaining data were used as the training set for the LDA, and the omitted observation could be evaluated. In our case, all data were classified correctly (see Appendix A.2 for detailed results).

The PCA of our data set allowed to establish which of the fourteen metal–dye combinations brought the most information for the discrimination of the peptides. For our analysis, we focused on principal component 1 (factor 1), which contains more than 80% of the total variance. The component loadings to factor 1 of the three measurements at 5, 20 and 60 min of each metal–dye mixtures were combined, thus affording fourteen contributions (see the Appendix A.2 for details). A comparison of the resulting values allowed us to identify the six metal–dye combinations that contribute most significantly to the discriminating power: Pd/NFR, Pd/CAB, Rh/NFR, Rh/CAL, Pd/MCB and Rh/CAB (MCB = Methylcalcein Blue).^b Sensors involving Ru were found to contribute less, plausibly because of the slower exchange kinetics.

To verify that the reduced sensor array was still able to give good separation, multivariate analyses were performed with the fluorescence data obtained from the selected six metal–dye combinations. Both PCA and LDA resulted in complete discriminations of all peptides. It is clear from the PCA score plots, as well as from the contribution of the variables to the principal components, that the variance was further concentrated in factor 1. However, this effect was expected (the sensors accounting most for factor 1 were selected), the discrimination still works satisfyingly, and the loss of resolution is minimal. A “jack-knifed matrix” validation procedure was performed in the same manner as in the case of the entire sensor array, and the classifications were correct in all cases. Furthermore, if only 60% of the data were used to build discriminant functions, the remaining 40% were subsequently classified with complete accuracy (see Appendix A.2). Successful cross-validation procedures ensure the predictability and quality of our sensing system.

^bThis number of six metal–dye combinations was arbitrarily chosen. According to the vast amount of experimental data available, it is likely that several sensor subsets exist that would also afford a good discrimination.

4.3.2 Bradykinin and Kallidin

Encouraged by the results obtained for the discrimination of dipeptides, we investigated whether the sensor array was able to discriminate mixtures of longer peptides. We chose the closely related plasma peptides bradykinin (Arg-Pro-Pro-Gly-Phe-Ser-Pro-Phe-Arg, BK) and kallidin (Lys-bradykinin, KD). Both peptides are hormones belonging to the kinin group. Kinins are important inflammatory mediators that induce pain and oedema.^[320] Kallidin can be converted into bradykinin by aminopeptidases. The peptides also show vasodilatory effects, and at the cellular level they influence glucose and chloride release as well as neurotransmitter transport.^[321] Kinins are degraded by angiotensin I-converting enzymes (ACE), and it was suggested that ensuring a high micromolar level of BK in plasma by inhibition of cleavage enzymes could provide cardioprotective effects.^[322] Our goal was to discriminate aqueous solutions containing various kallidin/bradykinin ratios, where the total amount of peptide was kept constant at 50 μM . It should be pointed out that this was a challenging task because both peptides lack His or Met amino acids with strongly coordinating side chains. Consequently, relatively weak signals were obtained in competition reactions with metal–dye combinations. A short pre-screening of the fourteen metal–dye combinations listed in Table 4.1 revealed that the following six mixtures were best at discriminating BK from KD: Rh/MCB, Rh/CAB, Rh/CAL, Pd/CAB, Pd/NFR and Pd/LUM. This selection was made by comparing the fluorescence signals obtained when the different metal–dye mixtures were reacted with BK or KD: only the combinations affording significant differences between the two analytes were chosen (see Appendix A.2). These mixtures were then used for time-resolved sensor array analyses. The assay was performed as follows: an aqueous solution of the respective fluorescent dye was added to a solution containing either the pure kinin or a mixture of KD and BK in the ratios 20:80, 40:60, 60:40, or 80:20. The competition reaction was then initiated by adding a stock solution of the metal complex, and the fluorescence response was recorded as a function of time. The solutions contained 50 μM of peptide (100 mM phosphate buffer, pH 7.0). For the Rh-based assays, the final concentrations were $[\text{dye}] = [\text{Rh}] = 10 \mu\text{M}$, whereas concentrations of $[\text{dye}] = [\text{Pd}] = 20 \mu\text{M}$ were used for the Pd-based experiments (the amount of dye and metal was semi-optimized in the prescreening). Each reaction was repeated four times, and the fluorescence signals measured after different time intervals were used as input for the multivariate analysis. The score plot of a PCA is shown in Figure 4.8. The different peptide mixtures appear in distinct clusters. The factor 1 axis is clearly correlated with the presence or absence of any analyte, whereas

the various peptide mixtures are separated along the factor 2 axis. Furthermore, the analytes are classified along the factor 2 axis according to their composition: the higher the mole ratio of bradykinin, the higher the position of the corresponding cluster along this axis. This type of correlation could be used to create calibration curves, which would allow the KD/BK ratios of samples with unknown composition to be determined. By analyzing the contribution of each sensor to the principal components, one observes that Rh-based sensors contribute mostly to factor 1, whereas Pd-based sensors are more correlated to factor 2 (see Appendix A.2).

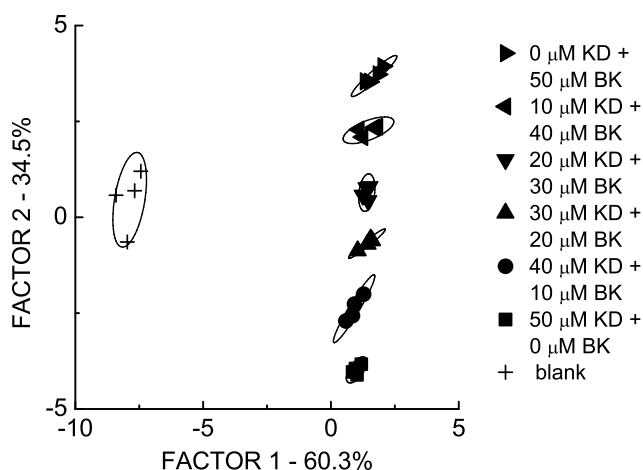


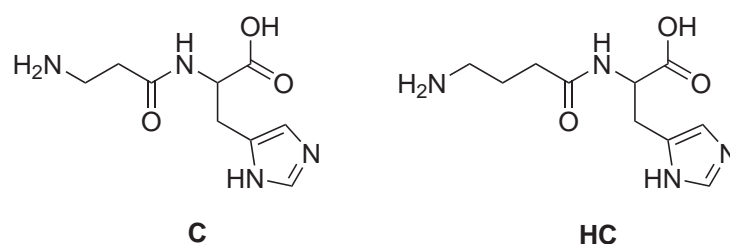
Figure 4.8 – Two-dimensional PCA score plot for the discrimination of aqueous solutions containing different concentrations of kallidin (KD) and bradykinin (BK). The input data for PCA were obtained from a sensor array composed of the following six metal–dye combinations: Rh/MCB, Rh/CAB, Rh/CAL, Pd/CAB, Pd/NFR and Pd/LUM.

In order to assess the predictability of our sensor in this case, a LDA-based “jack-knifed” validation procedure was applied, and resulted in a correct classification in all cases.

4.3.3 Carnosine and Homocarnosine Solutions in Serum

Finally, we investigated whether the sensor array could be used in a more complex environment such as human serum. As analytes, we chose the dipeptides carnosine (β -alanyl–histidine) and homocarnosine (γ -aminobutyryl–histidine). Carnosine (C) is a naturally occurring dipeptide that was initially isolated from meat extracts. Several metabolic functions are known, including antioxidant^[323, 324] and hydroxyl-radical

scavenging effects,^[325] metal-ion chelation^[326] and pH regulation.^[327] Carnosine can be found in high concentrations in the brains and muscles of mammals, whereas the related homocarnosine (HC) can be found in cerebrospinal fluid and brain.^[323] The two dipeptides are usually very short-lived in human plasma, due to the presence of restriction enzymes (carnosinases) which degrade them to their constituent amino acids.^[328] Carnosinase deficiency, resulting from a rare genetic disorder,^[329] was identified as the cause of abnormal carnosine and homocarnosine levels in body fluids (micromolar instead of nanomolar concentrations in blood).^[328, 330–334] People suffering from this metabolic disorder show severe symptoms such as developmental delay and mental retardation. In addition, reduced carnosinase activity was also detected in patients suffering from Parkinson's disease, multiple sclerosis and cerebrovascular disease.^[335]



Scheme 4.3 – Carnosine (C) and homocarnosine (HC).

Our goal was to selectively detect carnosine and homocarnosine in the micromolar concentration range. Blood serum contains large amounts of salts, sugars, hormones and proteins. The latter were expected to interfere with our metal receptors, so a simple precipitation technique with acetonitrile was used to remove them. The deproteinized serum would still contain non-negligible quantities of other potentially interfering substances, including micromolar concentrations of histidine and methionine.^[336] To counterbalance the effect of these strong chelators, we decided to perform the competition reactions with slightly higher metal concentrations (200 – 500 μM , determined by preliminary tests). The final assays were carried out as follows: deproteinized serum samples were spiked with different quantities of carnosine or homocarnosine, an aqueous solution of the respective fluorescent dye was added, and the competition reaction was initiated by adding a stock solution of the metal complex. The reduced sensor array, which we had already used for the dipeptide analysis was employed (sensors: Pd/NFR, Pd/CAB, Rh/NFR, Rh/CAL, Pd/MCB, and Rh/CAB). As before, the fluorescence response was recorded as a function of time. The final solutions contained 25% (v/v) serum, 25% (v/v) buffered water (100 mM phosphate buffer, pH 7.0), and 50% (v/v) acetonitrile. Each reaction was repeated four

times, and the fluorescence signals after 5, 20, and 60 min were used as input for the multivariate analysis. The score plot of a PCA is shown in Figure 4.9. The data for the two peptides at four different concentrations (25, 50, 75, and 100 μM) appear in well-separated groups with no apparent overlap. An analysis of the respective contributions of the sensors to the principal components indicates that all the sensors contribute significantly to both factor 1 and factor 2. The peptides themselves are separated along the factor 1 axis (49.1% of the total variance), whereas most of the concentration information is described by factor 2 (36.9% of the total variance). A LDA with a cross-validation routine resulted in a correct assignment of all data when one measurement was omitted at a time and then reclassified. When only 80% of the data were used as the training set, the remaining data were also classified correctly (see Appendix A.2).

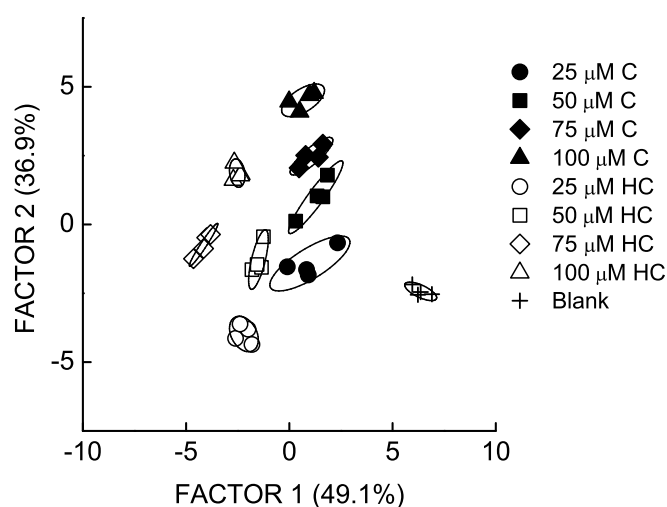


Figure 4.9 – Two-dimensional PCA score plot for the discrimination of various concentrations of carnosine (C) and homocarnosine (HC). The input data for the PCA were obtained from a sensor array composed of the following six metal–dye combinations: Pd/NFR, Pd/CAB, Rh/NFR, Rh/CAL, Pd/MCB and Rh/CAB.

These results demonstrate that a sensor array composed of metal–dye complexes is able to analyze structurally very similar molecules in a complex matrix. One should note, however, that the matrix in our experiments was always the same. For a real application, one would have to consider that the matrix could change (e.g., the blood composition varies from one person to another). These changes could affect the response of the sensors independently of the concentration of analytes of interest.

4.4 Conclusions

Cross-reactive sensor arrays can be constructed from fluorescent dyes and simple 4d transition metal complexes. Sensor arrays comprising only six metal–dye combinations displayed a remarkable analytical power: samples containing low-micromolar concentrations of dipeptides were identified with high accuracy, and mixtures of the nonapeptide bradykinin and the decapeptide kallidin could be distinguished. Furthermore, it was possible to obtain information about the identity and quantity of the pharmacologically interesting dipeptides carnosine and homocarnosine in a complex biological matrix. A key advantage of our approach is its simplicity: all components of the sensor array are commercially available (if necessary, the metal complexes can be easily synthesized), and the individual sensors are rapidly obtained by mixing stock solutions of the respective reagents. The modular nature of our array makes it easy to optimize a sensor for a particular sensing problem, by varying the nature and/or the amount of the dyes and metal complexes. Furthermore, the approach should be well suited for parallelization and automatization.

5

Pattern-Based Sensing with Metal-Dye Complexes: Sensor Arrays versus Dynamic Combinatorial Libraries

Synopsis

In this chapter, we describe colorimetric sensors for peptides which are based on the dyes Methyl Calcein Blue, Arsenazo I, and Xylenol Orange, and the metal salts CuCl_2 and NiCl_2 . Two different approaches were followed: (1) Sensors based on dynamic combinatorial libraries of metal-dye complexes were created by mixing dyes with metal salts in one pot. The optical response of these libraries was analyzed by measuring the spectral changes of the mixtures upon addition of the peptide analytes at six selected wavelengths. (2) A sensor array was created from the six possible metal-dye combinations. The six individual sensors were analyzed at one wavelength, and the resulting data was used as the input for a multivariate analysis. Both types of sensors were evaluated for their ability to differentiate 13 different di- and tripeptides. The sensors based on dynamic combinatorial libraries gave in most cases better results than the sensor array. Furthermore, it was found that libraries of intermediate complexity perform best as sensors.

The work presented in this chapter was published in: S. Rochat, K. Severin, *J. Comb. Chem.* **2010**, *12*, 595-599.

5.1 Introduction

5.1.1 Sensor Arrays and Dynamic Combinatorial Libraries

A COMPLEX between a synthetic receptor and a dye can be used as a chemosensing ensemble, given that the displacement of the dye by an analyte leads to a change in color or fluorescence. Sensors of this type are commonly referred to as indicator displacement assays (IDAs).^[3] Transition metal complexes have been used very successfully as receptor units in IDAs.^[59, 65, 66, 68, 73, 76, 82, 83, 86, 88, 89, 337–339] In the presence of a dye and an analyte, a dynamic mixture of metal-dye and metal-analyte complexes is established (Figure 5.1a). Fluorescence or UV/Vis spectroscopy can then be used to obtain information about the equilibrium, and thus about the identity and/or quantity of the analyte.

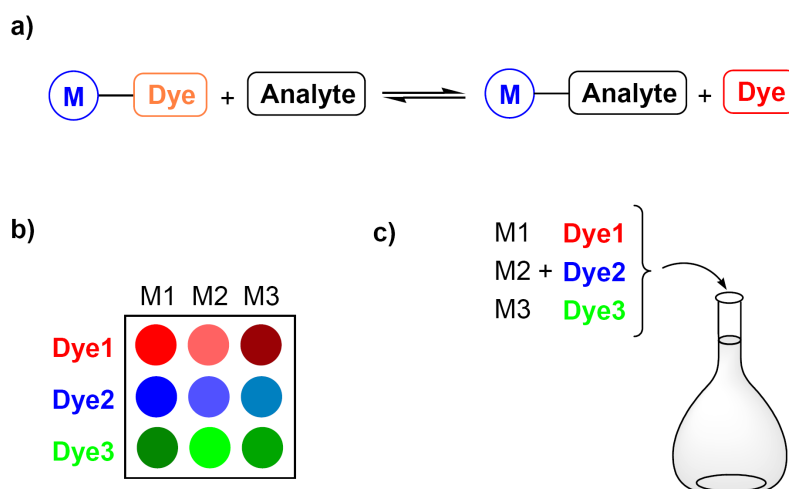


Figure 5.1 – (a) Basic principle of a metal-based indicator displacement assay. (b) A sensor array based on the combination of different metal complexes with different dyes. (c) A sensor based on a dynamic combinatorial library of metal-dye complexes. M = metal complex.

The analytical power of IDAs can be increased if they are performed in an array format.^[1] In such an array, several IDAs are performed in parallel, and the recognition of the analyte is then achieved by a pattern-based analysis of the response of the entire array. Sensor arrays of metal-based IDAs have been created by mixing different dyes with different metal complexes (Figure 5.1b),^[143, 145, 155, 163, 179, 181, 182, 185, 187, 260] or by utilization of one metal-dye combination at different pH values.^[176, 180]

Another way to increase the analytical power of displacement assays is to perform several IDAs simultaneously in one pot (Figure 5.1c).^[157, 158, 166, 183, 186, 188, 212] This approach results in the formation of a dynamic combinatorial library (DCL)^[205, 206, 208–210] of metal-dye complexes. The optical response of a DCL is likewise analyzed with pattern-recognition protocols.

The sensors described above have fundamental differences. In a sensor array, each metal-dye combination is analyzed separately by UV/Vis or fluorescence spectroscopy. This measurement is typically done at the wavelength, where the largest changes are observed. For a DCL sensor, on the other hand, the information about the analyte is distributed over the entire spectrum, and the absorption (or emission) at multiple wavelengths is used as the data input for a pattern-based analysis. Consequently, it is sufficient to record a single UV/Vis or fluorescence spectrum for a DCL sensor (once the sensor is calibrated). Sensor arrays and DCL sensors based on metal-dye complexes may also differ on the molecular level. Each sensing unit of an array will contain homoleptic complexes of type $[(M)_n(Dye)_m]$. A DCL sensor, on the other hand, may also contain heteroleptic complexes such as $[(M_1)(Dye)(M_2)]$ or $[(M)(Dye_1)(Dye_2)]$. These heteroleptic complexes can participate in displacement reactions with analytes and can help to differentiate them. DCL sensors therefore have two distinct advantages: only one optical measurement is needed, and heteroleptic complexes can contribute to the analysis. However, there is also one drawback: since multiple IDAs are performed simultaneously in one pot, it is likely that the spectra of the different dyes and of the metal-dye complexes show significant overlap. This spectral overlap is expected to result in some loss of resolution.

From the arguments outlined above it is clear that both types of metal-dye sensors, arrays and DCLs, have advantages and disadvantages. It thus appears interesting to perform a direct comparison of the two approaches for a particular sensing problem. The results of such an investigation are reported below. As a case study, we chose to compare the discriminating abilities of a sensor array and of DCL sensors toward a series of di- and tripeptides combining only four different amino acids. Interestingly, DCL sensors were found to perform significantly better than sensor arrays for most cases studied.^[213]

5.1.2 Linear Discriminant Analysis

As mentioned in section 1.4.4, linear discriminant analysis (LDA) can be used to separate classes of objects, or assign new objects to appropriate classes.^[110] One way to evaluate

the goodness of fit of the discriminant function is to assess the *hit rate*, i.e. the proportion of observations classified correctly. However, if the same data set is used to assess the hit rate, that was used to determine the discriminant function, the estimate of prediction accuracy will be biased upwards. This problem is usually solved by parting the data set into a holdout and a training sample: the holdout sample can be used to validate the predictive performance of the discriminant function established by using the training sample.

When a more accurate estimation of the quality of a LDA is necessary (i.e., when one needs to compare different models), Wilks' lambda can be used.^[215, 340, 341] Wilks' lambda (Λ) represents the ratio of intraclass versus interclass variances, and can also be expressed as a function of the eigenvalues of the model. Its value is always comprised between 0 and 1. The smaller the value, the better the model. On the other hand, a value of $\Lambda = 1$ indicates that all clusters are overlapping.

$$\Lambda = \frac{|\mathbf{W}|}{|\mathbf{V}|} = \prod_i \frac{1}{1 + \lambda_i} \quad (5.1)$$

\mathbf{W} is the within-group variance matrix, \mathbf{V} is the total variance matrix, and λ_i is the i^{th} eigenvalue.

There is no threshold value for Λ , which indicates when a discrimination can be considered as satisfactory. Assessing the quality of a discrimination also depends on the number of classes, samples, and variables. Wilks' lambda is related to a F -statistic test, which can be represented as the ratio of two variances: the total variance of the sample, and the residual variance (the amount left unexplained by the model):

$$F = \frac{\text{explained variance}}{\text{unexplained variance}} = \frac{\text{between-group variability}}{\text{within-group variability}} \quad (5.2)$$

When this ratio is large, it suggests that a large proportion of the variance can be explained by the regression model; when the ratio is close to 1, the conclusion is that the model is probably not significant. More formally, the F -ratio can be expressed as a function of Wilks' lambda:

$$F = \frac{1 - \Lambda^{1/t}}{\Lambda^{1/t}} \cdot \frac{df_2}{df_1} \quad (5.3)$$

with

$$df_1 = p\nu_H \quad (5.4)$$

$$df_2 = wt - 0.5(p\nu_H - 2) \quad (5.5)$$

and

$$w = \nu_E + \nu_H - 0.5(p + \nu_H + 1) \quad (5.6)$$

$$t = \sqrt{\frac{p^2\nu_H^2 - 4}{p^2 + \nu_H^2 - 5}} \quad (5.7)$$

where p , ν_H and ν_E are defined as:

$$p = \text{number of variables (dimension)} \quad (5.8)$$

$$\nu_H = \text{degrees of freedom for hypothesis (i.e., number of classes - 1)} \quad (5.9)$$

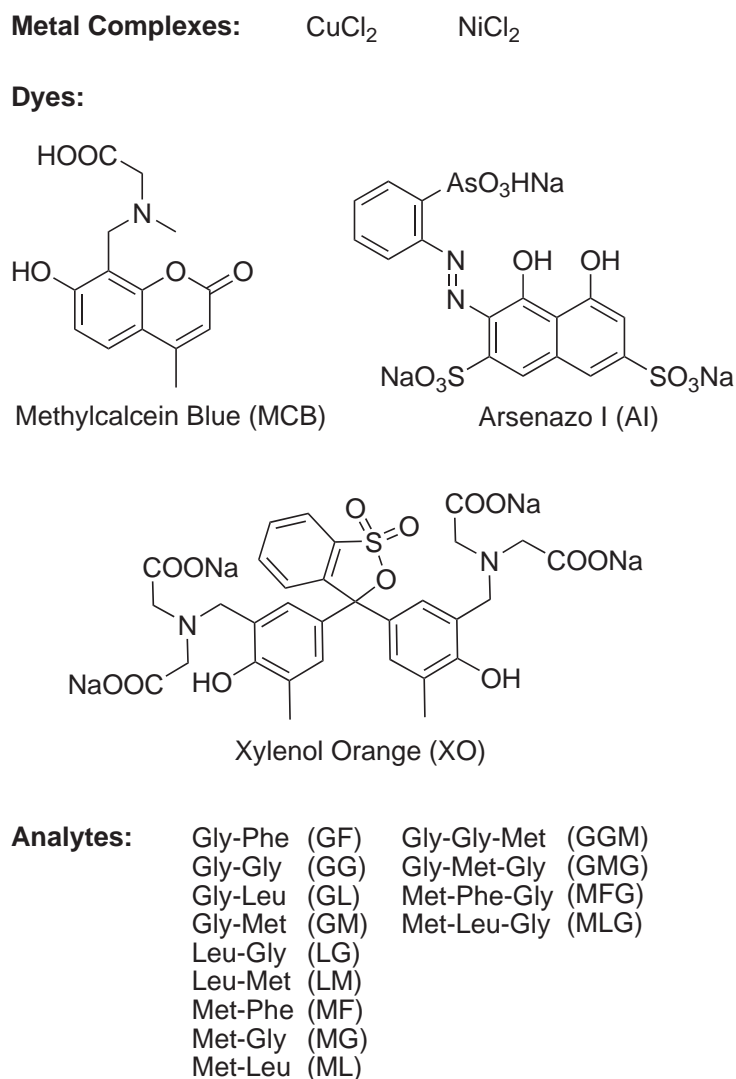
$$\nu_E = \text{degrees of freedom for error (i.e., } \Sigma(\text{class} \cdot \text{replicates in the class))} \quad (5.10)$$

Critical values for F have been calculated^[340] and can be used to determine whether a statistical model is significant (i.e., if the null hypothesis implying that there is no difference across the classes can be rejected). It must be noted, however, that the F -ratio can be misleading in some cases: for example, it can be very high if only one analyte is very different, and the others are grouped and not well separated. On the other hand, the F -ratio can be low if all the analytes behave slightly differently, but are nonetheless very well separated. The F -ratio must therefore be employed while being aware of these limitations.

5.2 Discrimination of Peptides with a Sensor Array and with a DCL

For our study we decided to use a colorimetric DCL sensor, which was recently developed by our group.^[183] It is composed of the dyes Methylcalcein Blue (MCB), Arsenazo I (AI), and Xylenol Orange (XO), and the metal salts CuCl_2 (Cu) and NiCl_2 (Ni, Scheme 5.1). When the five components are mixed in buffered aqueous solution, a dynamic mixture of homo- and heteroleptic metal-dye complexes is formed. The sensor can be used

for the colorimetric detection of peptides, as evidenced by an analysis of the peptide hormones angiotensin I and angiotensin II.^[183]



Scheme 5.1 – The metal complexes, the dyes, and the peptide analytes used in this study.

For the creation of a sensor array, we used the same five components to make a total of six sensors composed of all possible metal-dye combinations. The readout of the six sensors was performed at the wavelength, where the largest spectral change was observed upon complexation of the dye to the respective metal (spectrophotometric titrations of the dyes and the metal salts are described in ref. [183]). The following values were used: MCB/Cu: 372 nm, AI/Cu: 492 nm, XO/Cu: 584 nm, MCB/Ni: 376 nm, AI/Ni: 532 nm, and XO/Ni: 592 nm.

The DCL sensor and the sensor arrays were then employed for the sensing of di- and tripeptides. The analytical task was the differentiation of the 13 peptides listed in Scheme 5.1 at a concentration of 1.0 mM.

For the analysis with the DCL sensor, the UV/Vis spectrum of the library was recorded for each of the 13 analytes after equilibration (10 replicates each). The initial data contained 93 values for each measurement (absorbance values in the region $\lambda = 332 - 700$ nm, with intervals of 4 nm). To determine the wavelengths which contribute most to the differentiation of the peptides, an internal variable selection algorithm of the software package Systat^[342] (version 11) was applied. This allowed reducing the data set to 6 values for each measurement. The reduced data set was then used as the input for a linear discriminant analysis (LDA).^[110] LDA was chosen as a method because it allows to obtain quantitative information about the quality of the classification. This information is very useful for comparing different sensors. One should note, however, that LDA tends to give “overoptimistic” results when compared to unsupervised methods such as principal component analysis (PCA).

For the analysis of the sensor array, the optical response of the six different sensors was recorded for each of the 13 peptides. As in the case of the sensor array, 10 independent measurements were performed for each peptide. The resulting data was also classified by an LDA.

A graphic representation of the two analyses in form of two-dimensional score plots is shown in Figure 5.2. It is evident that the resolution of the DCL sensor is superior to that of the sensor array. The qualitative assessment is confirmed by a cross-validation analysis, in which 33% of the cases are removed from the data set and then reclassified using the remaining data as a training set. For the sensor array, the cross-validation procedure results in a correct classification in 96% of the cases, whereas 98% is obtained for the DCL sensor (averaged results of 10 independent executions of the cross-validation routine).

One can note that the first two scores of the sensor array contain 89% of the total variance. In the case of the DCL sensor, 97% of the total variance is found for the first two scores. The higher dispersion of the sensor array data is not unexpected, since the displacement assays are performed independently from each other and not in one pot. Still, the dimensionality of the sensor array data is low compared to what has been observed for some other systems.^[127, 142, 152, 171, 198]

The complexity of a DCL sensor, that is, the number of its constituent components, is expected to influence the analytical power of the system. Reducing the complexity substantially should lead to a loss in resolution. However, it is not clear whether

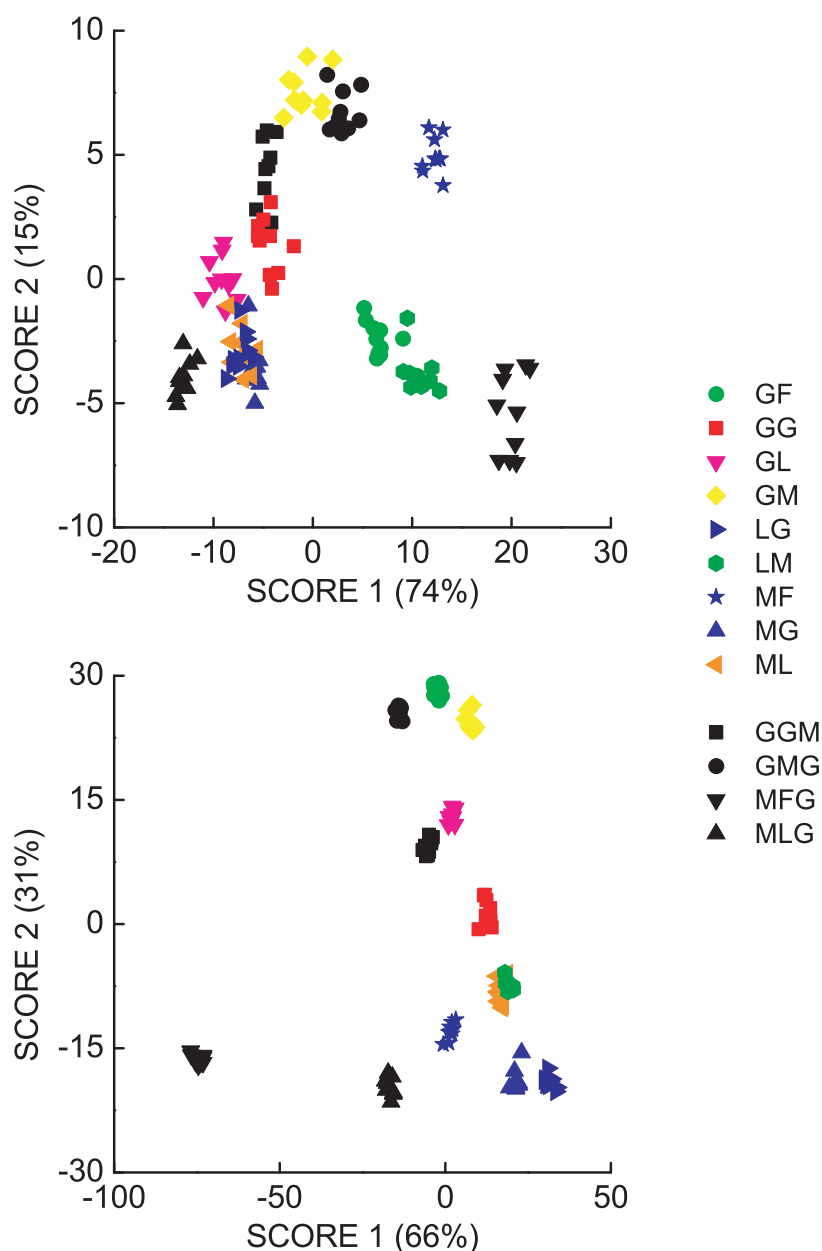


Figure 5.2 – LDA score plots generated from the data of the sensor array composed of six individual metal-dye sensors (top), or the data of the DCL sensor made by mixing the dyes MCB, AI, and XO with the metal complexes CuCl_2 and NiCl_2 (bottom). Both sensors were used for the differentiation of 13 di- and tripeptides in buffered aqueous solution at a concentration of 1.0 mM.

DCL sensors of high complexity (more dyes and metals) are necessarily better. To address this point, we have examined the performance of DCL sensors containing fewer components than our original 3-dye-2-metal sensor. Systematically, we have omitted one, two, or three components, and the resulting DCLs were then evaluated

for their ability to differentiate the 13 peptides used before. To characterize the quality of the sensor, we have performed cross-validation procedures in all cases. As a second criterion for comparison, we have examined the *F*-ratios associated to Wilks' lambda values for the different analyses. As mentioned in section 5.1.2 (p. 88), *F*-values can be used to determine whether a statistical model is significant, and larger *F*-values indicate a better model and analysis.^[215, 340] A summary of the results is given in Table 5.1.

Table 5.1 – Analysis of 13 di- and tripeptides with DCL sensors of different composition and with the sensor array described in the main text. The percentage of correct cross-validation and the *F*-value associated to each discriminant model are indicated.

Entry	Dye(s)	Metal Salt(s)	% cross-validation	<i>F</i> -value
1	Al + XO	CuCl ₂ + NiCl ₂	100	510
2	MCB + Al + XO	NiCl ₂	100	423
3	MCB + XO	CuCl ₂ + NiCl ₂	100	325
4	XO	NiCl ₂	100	238
5	MCB + XO	CuCl ₂	100	220
6	Al	CuCl ₂ + NiCl ₂	100	209
7	MCB + Al	NiCl ₂	100	154
8	Al + XO	NiCl ₂	100	154
9	Al	NiCl ₂	100	141
10	MCB + XO	NiCl ₂	100	133
11	MCB + Al	CuCl ₂ + NiCl ₂	99	661
12	MCB + Al + XO	CuCl ₂	99	230
13	MCB + Al	CuCl ₂	99	190
14	MCB	CuCl ₂	99	121
15	MCB + Al + XO	CuCl ₂ + NiCl ₂	98	254
16	Al	CuCl ₂	98	209
17	XO	CuCl ₂ + NiCl ₂	98	194
18	Al + XO	CuCl ₂	98	105
19	MCB	CuCl ₂ + NiCl ₂	96	161
20	Sensor Array		96	92
21	XO	CuCl ₂	87	63
22	MCB	NiCl ₂	81	60

Interestingly, the quality of the analysis was found to increase in most cases when one component was removed from the original 5-component DCL sensor. All sensors made from two dyes and two metal salts, for example, gave a better discrimination than the full library (Table 5.1, entries 1, 3 and 11 vs. entry 15). Further reduction in complexity to 3 or 2 components typically resulted in a loss of quality as shown by comparison of the *F*-values (Figure 5.3). The score plots associated with the

combinations listed in Table 5.1 which are not discussed in detail here, are given in Appendix B.1.

Quite surprising was the performance of some of the sensors composed of just one metal and one dye. The combination of NiCl_2 with XO, for example, resulted in a sensor, which gave 100% correct classification in the cross-validation procedure and an F -value of 238 (Table 5.1, entry 4 and Figure 5.4). Consequently, it performs significantly better than the sensor array with only 96% correct classification and an F -value of 92 (Table 5.1, entry 20).^a

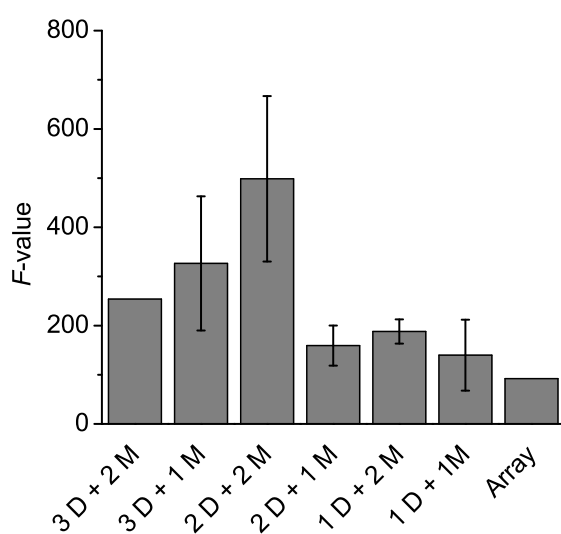


Figure 5.3 – Comparison of the F -values for multivariate analyses of DCL sensors composed of a different number of dyes (D) and metal salts (M). The F -value of the sensor array is given for comparison.

At first hand, it may appear paradoxical that a mini-DCL sensor composed of just NiCl_2 and XO is superior to an array of six individual sensors, one of which is based on a mixture of the very same components: NiCl_2 and XO. However, only one wavelength is taken into account for each of the six sensors of the array (592 nm for XO/Ni), whereas six wavelengths are used for the analysis of the mini-DCL sensor. A buffered aqueous solution of NiCl_2 , XO, and the peptide analyte is expected to contain metal-dye complexes of the stoichiometry $[\text{Ni}(\text{XO})]$ and $[\text{Ni}_2(\text{XO})]$ ^b, metal-peptide complexes, and possibly heteroleptic metal-dye-peptide complexes. The system is thus more complex than the idealized displacement assay shown in Figure 5.1a, which assumes that the dye and a 1:1 metal-dye complex are the only colored species. An analysis of the

^aA comparison of the F -factors is legitimate because the format of the data input is the same for the DCL sensors and for the sensor array (13 analytes, 10 replicates, 6 wavelengths).

^bSpectrophotometric titrations had shown that the dominant species in mixtures of XO and NiCl_2 are complexes with the stoichiometry $[\text{Ni}(\text{XO})]$ and $[\text{Ni}_2(\text{XO})]$ (see ref. [183]).

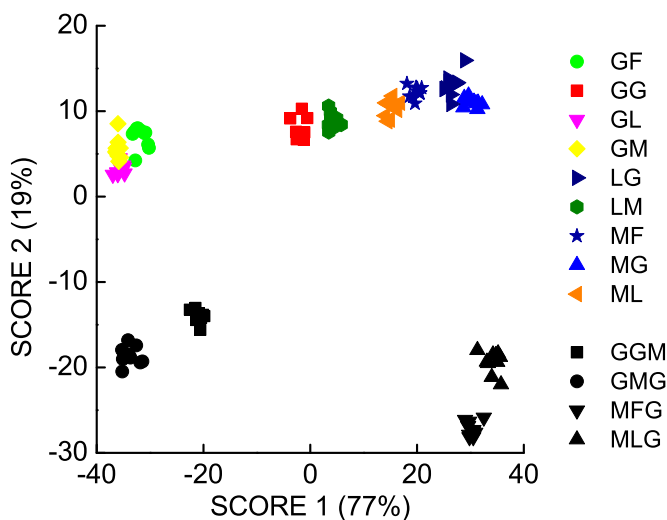


Figure 5.4 – LDA score plot generated from the data of a sensor made from XO and NiCl₂. The sensor was used for the differentiation of 13 di- and tripeptides in buffered aqueous solution at a concentration of 1.0 mM.

XO/Ni sensor at only one wavelength neglects the information that is provided by the inherent complexity of the system (multiple colored species, the concentration of which depends on the nature of the analyte).^c In this regard it is easy to understand that a pattern-based analysis of the XO/Ni sensor is better than a single-wavelength analysis. It is surprising, however, that the information provided by the five other sensors of the array (MCB/Cu, Al/Cu, XO/Cu, MCB/Ni, and Al/Ni) is not sufficient to outperform the simple DCL sensor composed of NiCl₂ and XO.

5.3 Conclusions

DCL sensors containing one, two, or three dyes (XO, Al, MCB) as well as one or two metal salts (CuCl₂, NiCl₂) were used to differentiate short peptides. The analytical power of the DCL sensors was compared with that of a sensor array made from six separate metal-dye mixtures (MCB/Cu, Al/Cu, XO/Cu, MCB/Ni, Al/Ni, XO/Ni). DCL sensors of intermediate complexity (e.g., 4-component sensors) were found to give better results than the full library made from all five components. This finding will be of interest for future studies in this area because it shows that *more is not necessarily better*. Interestingly, most DCL sensors including very simple 2-component systems performed better than the sensor array. However, the fact that these results cannot be easily

^cFor a discussion about the advantages of higher order complexes in IDAs see ref. [155].

generalized must be acknowledged. For example, chemically rather homogeneous analytes were used, and different results may be obtained with a more diverse set of analytes. However, the results clearly show that the one-pot-one-spectrum approach of DCL sensors represents a potentially very attractive alternative to the more common sensor array approach.

6

General Conclusions

THREE DIFFERENT STRATEGIES have been presented for the detection of the biologically relevant Li^+ ion in aqueous solution (Figure 6.1). All these approaches are based on 12-metallacrown-3 complexes, which act as selective receptors for Li^+ .

PET sensors were developed, where ruthenium-based metallacrowns were labelled with fluorescent dyes (Figure 6.1a). The main issue turned out to be solubility: several amino groups were required to obtain a water-soluble macrocycle (at neutral pH, the amines are protonated, which confers their solubility to the macrocycles), and the fluorophores needed to be of limited hydrophobicity. On the other hand, fluorophores containing functional groups that may interfere with the self-assembly of macrocycles (*i.e.*, that possess strong affinity for ruthenium centers) had to be avoided. The most successful system was found to be ruthenium-based macrocycle **M10**, featuring methoxycoumarin as fluorophore and an amino substituted π -ligand. This compound is water-soluble, and it can be obtained *in situ* by combination of its building blocks in buffered aqueous solution. Compound **M10** possesses a strong affinity for Li^+ (with an affinity constant of *ca.* 10^3 M^{-1}) as well as a good selectivity over potentially interfering ions such as Na^+ or K^+ . Its fluorescence intensity depends on the concentration of Li^+ , which allows detection of lithium ions in the pharmacologically relevant range (0.5 - 1.5 mM). The macrocycle is stable in blood serum (after removal of proteins), and can thus be employed as a lithium sensor in complex biological samples.

The development of sensor **M10** came at the price of tedious and time-consuming syntheses. An alternative approach involving non-covalent interactions between the binding and signalling units was devised. Simple macrocycle **M1** was employed, which is made by self-assembly of $[(p\text{-cymene})\text{RuCl}_2]_2$ and ligand **L2**. Depending on the fluorophore that was employed, the sensing of Li^+ was achieved by two different mechanisms: a) when HPTS was used, it interacted with macrocycle **M1** without disrupting it. The fluorescence was modulated as a function of the presence of Li^+ at the binding site (Figure 6.1b). This simple assay was found to have a detection limit of less than 100 μM . b) when Calcein Blue was used, its strong affinity for ruthenium led to the destruction of the macrocyclic receptors, and to a strong quenching of the fluorescence. In the presence of lithium at the binding site, the macrocycle was efficiently stabilized and its destruction by Calcein Blue considerably slowed down (Figure 6.1c). This resulted in an attenuated quenching of the fluorescence, which allowed to detect Li^+ down to low millimolar concentrations.

A different approach to chemical sensing is described in the second part of this work: instead of designing selective sensors, we developed arrays of cross-reactive dif-

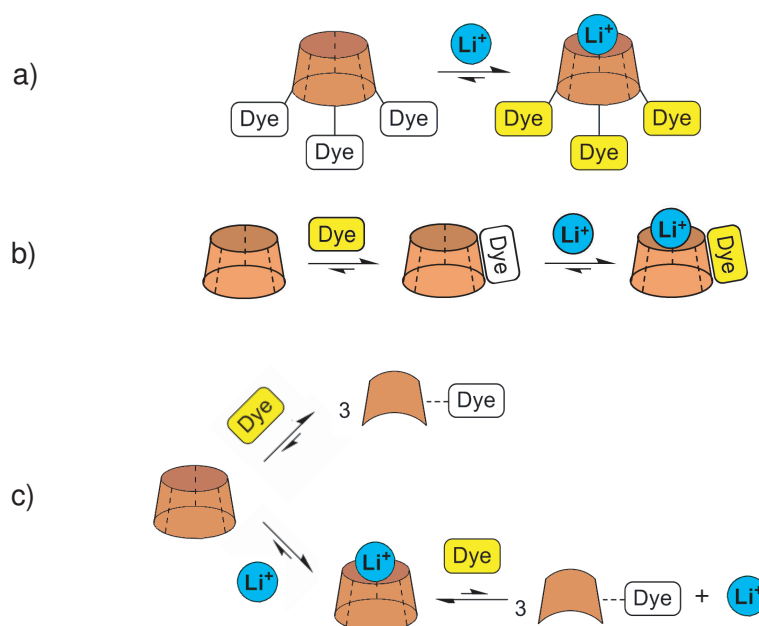


Figure 6.1 – Three different methods for the detection of Li^+ ions. a) a conjugated PET sensor; b) a ditopic sensor for Li^+ and a fluorophore (HPTS); c) detection through the stabilizing effect of Li^+ on the receptor. All systems result in a fluorescence turn-on in the presence of Li^+ .

ferential sensors for the detection and discrimination of small peptides. By combining fluorescent dyes such as Methylcalcein Blue, Calcein Blue, Calcein, Nuclear Fast Red, Lumazine and *N*-methylantranilic acid with metal fragments ($[(p\text{-cymene})\text{RuCl}_2]_2$, $[\text{Cp}^*\text{RhCl}_2]_2$ and $[(\text{en})\text{PdCl}_2]$), sensor arrays were generated (Figure 6.2). Their use for the discrimination of dipeptides in deproteinized serum, as well as for the discrimination of mixtures of longer peptides was demonstrated. The differential responses of the sensor arrays were interpreted with the help of pattern-recognition software, and resulted in the detection of peptides in the low micromolar range.

Finally, the performance of a sensor array was compared with the performance of a dynamic combinatorial library (DCL) for the discrimination of a series of related small peptides. The array was composed of combinations of the three dyes Methylcalcein Blue, Arsenazo I and Xylenol Orange, and the metal salts CuCl_2 and NiCl_2 . The DCL was prepared by mixing the five constituents, and sub-libraries were prepared by removing one or several constituents. The different systems were tested for the discrimination of 13 di- and tripeptides. Two important conclusions could be drawn: a) Generally, the DCL outperforms the sensor array; b) Increasing the complexity of the DCL generally increases the quality of its performances, but only until a certain threshold. When numerous species are present in the mixture, the resulting UV/Vis spectrum is the sum

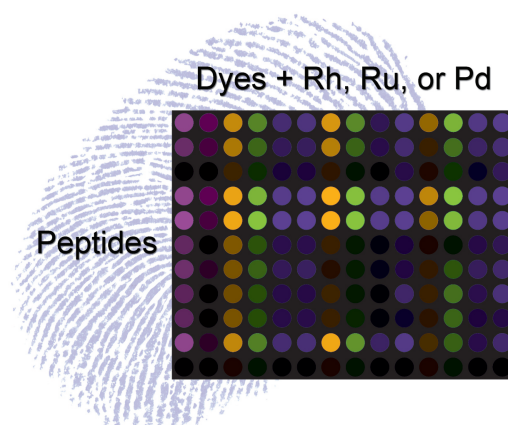


Figure 6.2 – Representation of a sensor array for peptides. Each row corresponds to the fingerprint of a given dipeptide.

of many different contributions, that can potentially cancel each other. In such a case, the advantage of a multicomponent system is annihilated by the averaging of its UV/Vis spectrum.

In summary, we have shown that simple systems can achieve complex sensing tasks: self-assembled macrocycles made of easily accessible building blocks can detect the elusive lithium ion, whereas mixture of commercially available dyes and metal compounds can form sensor arrays or dynamic combinatorial libraries with a high potential to detect small peptides down to low micromolar concentrations. These systems were found to work well in water at neutral pH and in deproteinized human serum, paving the way to applications involving real biological or environmental samples.

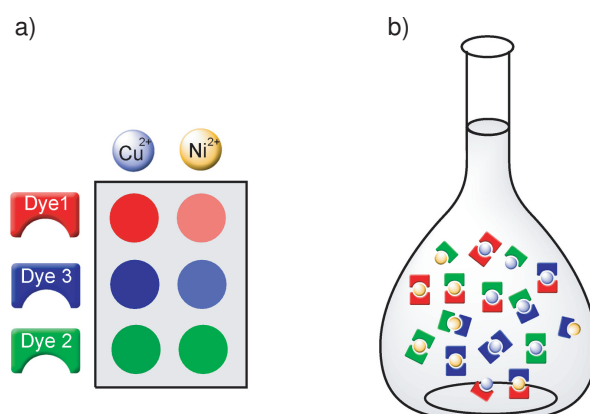


Figure 6.3 – Representation of two different systems that were compared in the last part of this work: a) a sensor array; b) a dynamic combinatorial library made of the same constituents.

7

Experimental Section

7.1 General and Instrumentation

7.1.1 General

UNLESS OTHERWISE STATED, non-aqueous reactions were performed in oven-dried glassware under an atmosphere of dry dinitrogen with standard Schlenk-line techniques. Reactions performed in aqueous environment were carried out in air, except the syntheses of macrocycles **M4**, **M5**, **M9**, and **M10**, that were performed under N₂. Solvents were of analytical grade quality, and were stored under an atmosphere of dinitrogen. When required, benzene, hexane, dichloromethane, chloroform or diethyl ether were dehydrated by filtration through activated aluminium oxide columns under dinitrogen (Innovative Technology solvent purification system). Anhydrous methanol and ethanol were obtained by distillation over magnesium. The weights of the commercial compounds given in the detailed procedures are impurity corrected, and indicated yields refer to purified and dried compounds. The indications in square brackets correspond to reactions codes in laboratory books: [SR-B100(3)] refers to the book B, reaction number 100, 3rd repetition.

7.1.2 Instrumentation

NMR spectroscopy. ¹H NMR and ¹³C NMR spectra were recorded at room temperature on a Bruker Avance DPX 400 spectrometer or on a Bruker Avance 200 spectrometer, using the residual protonated solvents as internal standards. ¹³C NMR spectra in D₂O were recorded using dioxane as internal standard. Chemical shifts δ are reported in ppm, and the multiplicity is reported as follows: s = singlet, d = doublet, t = triplet, dd = doublet of doublets, quint = quintet, sept = septuplet, m = multiplet or unresolved. Coupling constants *J* are given in Hz.

Elemental analysis. Measurement were performed by the elemental analysis service at EPFL on a EA 1110 CHN Carlo Erba, or on a Flash 2000 Organic Elemental Analyser Thermo Fisher Scientific instrument.

Mass spectrometry. High resolution mass spectra were recorded by the mass spectrometry service at EPFL on a Waters CapLC-coupled Micromass Q-ToF Ultima ESI-instrument equipped with a Z-spray type ESI source.

UV-Visible spectroscopy. UV-Visible spectra were recorded at room temperature on a Perkin-Elmer Lambda 40 spectrometer.

Fluorescence spectroscopy. Fluorescence measurements were performed with a Varian Cary Eclipse spectrophotometer equipped with a thermostatted cell holder and a stirring mechanism.

HPLC. Purifications by reversed phase HPLC were carried out using a Waters system consisting of a Waters 600 controller unit, a Waters Delta 600 pump and a Waters 2487 dual wavelength absorbance detector. A Sunfire semi-preparative C18 column (5 mm, 10 × 250 mm) was used as stationary phase, and Millipore water and acetonitrile (HPLC grade) as mobile phase.

Cyclic Voltammetry. Measurements were performed at the Laboratory of Inorganic Synthesis and Catalysis at EPFL with a computer controlled IVIUMSTAT Electrochemical Interface at a sweep rate of 50 mV/s. An aqueous Ag/AgCl electrode was used as reference electrode. The solution was purged with nitrogen prior to recording the electrochemical data, and all measurements were recorded at room temperature under a dinitrogen atmosphere.

Others. Concentrations under reduced pressure were performed at 40°C with a Büchi Rotavapor R200 rotary evaporator (unless otherwise indicated); Thin layer chromatography was performed on Merck silica gel 60 F₂₅₄ plates and flash chromatography was effectuated using silica gel 60 from Fluka; pH measurements were recorded with a Metrohm Titrino 716 DMS instrument equipped with a combined LL pH glass electrode (Metrohm Ecotrode).

7.1.3 Purchase of Compounds

The following compounds were used as received: PdCl₂ (ca. 60% Pd), RhCl₃ · 3 H₂O (37 - 42% Rh), RuCl₃ · xH₂O (40 - 43% Ru) (Precious Metals Online), 4-aminobutyric acid (99%), ammonium hydroxyde (25% solution in H₂O), Asp-Phe (95%), carnosine (β-Ala-His, 98%), dibenzylamine (98%), N,N-dimethylbenzylamine (99%), formaldehyde (37 wt% solution in H₂O, stabilized with 10-15% MeOH), HCl (25% in H₂O), N-methylpiperazine (99%), NaBH₄ (99%), NaCl (extrapure), NaOH (97%), palladium (10% Pd on activated carbon), α-terpinene (90%), Xylenol Orange (sodium salt, pure) (Acros), Ala-Ala, Ala-Phe, benzyl chloroformate (95%), Calcein Blue, Celite, coumarin (99%), Cs₂CO₃ (>99.999%), CsOH · H₂O (99.5%), dimethyl sulfate (99%), 2,3-dihydroxypyridine (98%), ethylenediamine (99%), Gly-Leu, Gly-Met, HEPES (>99%), HPTS trisodium salt (97%), human serum, KOH (extra pure), Leu-Gly, Leu-Met, Lumazine (97%), Met-Gly, N-methylantranilic

acid (95%), Methyl Calcein Blue, methyl chloroformate (99%), Met-Leu, Nuclear Fast Red, Phe-Pro, Ser-Gly, sodium (purum), Trp-Gly (Sigma-Aldrich), Calcein, $\text{CuCl}_2 \cdot 2 \text{H}_2\text{O}$ (99%), DCl (38% in D_2O), *N,N*-dimethylformamide (absolute, over molecular sieve, $\text{H}_2\text{O} < 0.01\%$), Gly-Gly, hexamethylenetetramine (99%), K_2CO_3 (99%), KH_2PO_4 (>99.5%), K_2HPO_4 (>99.5%), LiCl (99%), $\text{MgSO}_4 \cdot 6 \text{H}_2\text{O}$ (>99%), MgSO_4 (98%), NaHCO_3 (99%), Na_2SO_4 (99%), NH_4Cl (99%) (Fluka), dansyl chloride, ethyl chloroformate, human serum, 7-hydroxycoumarin (99%), 1,2,3,4,5-pentamethylcyclopentadiene, triethylamine (VWR), Arsenazo I, 1-pyrenecarboxaldehyde, trifluoroacetic acid (HPLC grade) (Alfa Aesar), Histidine methyl ester dihydrochloride (Senn Chemicals), bradykinin, Gly-Gly-Met, Gly-Met-Gly, Gly-Phe, His-Ala, kallidin, Lys-Tyr, Met-Leu-Gly, Met-Phe, Met-Phe-Gly, Val-Phe (Bachem), CHES (AppliChem), and $\text{NiCl}_2 \cdot 6 \text{H}_2\text{O}$ (Strem Chemicals).

7.1.4 Software

WinEQNMR^[293] was used to calculate equilibrium constants from NMR or fluorescence data.

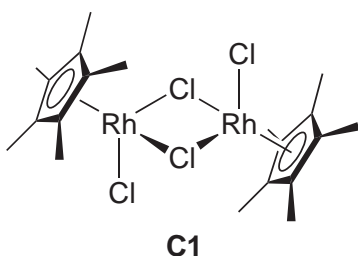
UV-Vis and fluorescence binding isotherms were fitted using a routine built in MATLAB[®] which implements the Newton-Gauss non-linear least squares fitting algorithm.^[343-345] Systat (version 11)^[342] was used to perform statistical analyses (principal component and linear discriminant analyses).

7.2 Syntheses

7.2.1 Organometallic Complexes

Organometallic complexes $[\text{Cp}^*\text{RhCl}_2]_2$ (**C1**),^[280] $[(p\text{-cymene})\text{RuCl}_2]_2$ (**C2**),^[346, 347] $[\eta^6\text{-}(\text{C}_6\text{H}_5\text{CH}_2\text{NMe}_2\text{H})\text{RuCl}_2]_2\text{Cl}_2$ (**C3**),^[291] and $[\text{PdCl}_2(\text{en})]$ (**C4**)^[348] were synthesized according to published methods. Typical procedures are given below:

$[\text{Cp}^*\text{RhCl}_2]_2$ (**C1**).^[280]



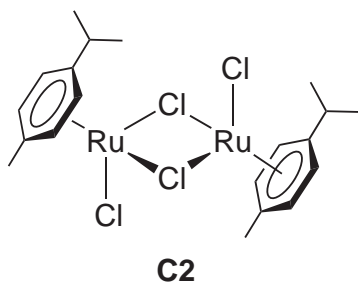
$\text{RhCl}_3 \cdot 3\text{H}_2\text{O}$ (3.45 g, 13.1 mmol) was dissolved in MeOH (100 mL). 1,2,3,4,5-Pentamethyl-1,3-cyclopentadiene was added (2.25 mL, 14.4 mmol, 1.1 equiv.) and the mixture was heated to reflux for 48 hours. The solution was left overnight at -20°C to afford red microcrystals, which were filtered off and washed with cold MeOH. Compound **C1** was obtained as a red

solid (3.29 g, 5.33 mmol, 81%) with spectral data in good agreement with literature.^[349] [SR-C224(1)].

$^1\text{H NMR}$ (CDCl_3 , 400 MHz): δ (ppm) = 1.62 (s, 30 H, CH_3).

$^{13}\text{C}\{^1\text{H}\}$ NMR (CDCl_3 , 101 MHz): δ (ppm) = 10.1 $\text{C}_5(\text{CH}_3)_5$, 94.3 $\text{C}_5(\text{CH}_3)_5$.

$[(p\text{-cymene})\text{RuCl}_2]_2$ (**C2**).^[346, 347]



$\text{RuCl}_3 \cdot x\text{H}_2\text{O}$ (ca. 41% Ru, 5.0 g, 20.3 mmol) was dissolved in a mixture of EtOH (250 mL) and water (25 mL). α -Terpinene was added (28 mL, 155 mmol, 7.6 equiv.) and the mixture was heated to reflux for 6 hours. The solution was left to cool to room temperature, and filtered through a fritte in order to remove any unreacted RuCl_3 . The solution was then

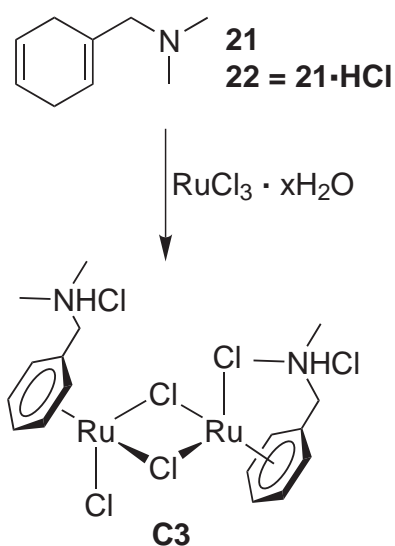
evaporated under reduced pressure to ca. 1/3 of its initial volume, and placed in a fridge for 24 hours. A red precipitate was collected by filtration, washed with Et_2O and dried under vacuum. The mother liquor could be further evaporated in order to collect a second fraction of the product. Purification of the product was performed as follows: the solid was dissolved in degassed CH_2Cl_2 , the solution was filtered through a pad of Celite and evaporated to dryness. The obtained solid was then washed with Et_2O and dried under vacuum to afford **C2** as an orange powder (4.75 g, 7.76 mmol, 76%) with

spectral data in good agreement with literature.^[347] [SR-A6(3)].

^1H NMR (CDCl_3 , 200 MHz): δ (ppm) = 1.27 (d, $^3J = 7.0$ Hz, 12 H, $\text{CH}(\text{CH}_3)_2$), 2.15 (s, 6 H, CH), 2.92 (sept, $^3J = 6.9$ Hz, 2 H, $\text{CH}(\text{CH}_3)_2$), 5.34 (d, $^3J = 5.8$ Hz, 4 H, $\text{MeC}_6\text{H}_4^i\text{Pr}$), 5.47 (d, $^3J = 5.8$ Hz, 4 H, $\text{MeC}_6\text{H}_4^i\text{Pr}$).

$^{13}\text{C}\{^1\text{H}\}$ NMR (CDCl_3 , 101 MHz): δ (ppm) = 19.1 (CH_3), 22.3 ($\text{CH}(\text{CH}_3)_2$), 30.7 ($\text{CH}(\text{CH}_3)_2$), 80.7, 81.4, 96.9, 101.3 (arene).

$[\eta^6\text{-(C}_6\text{H}_5\text{CH}_2\text{NMe}_2\text{H)RuCl}_2]_2\text{Cl}_2$ (**C3**).^[291]



(Cyclohexa-1,4-dienyl)-*N,N*-dimethylmethanamine (**21**) was obtained from *N,N*-dimethylbenzylamine by a Birch reduction.^[350, 351] A mixture of freshly distilled EtOH (40 mL) and *N,N*-dimethylbenzylamine (11.1 mL, 10.0 g, 73.1 mmol) was added to 300 mL of condensed ammonia at -70°C . Freshly cut pieces of sodium (10.0 g, 435 mmol) were slowly added, and the mixture was stirred at -70°C for 4 hours. EtOH (30 mL) was slowly added, followed by NH_4Cl (30 g). Ammonia was evaporated and H_2O (120 mL) was added. The solution was extracted with Et_2O (2×150 mL), the organic phase was dried on MgSO_4 and evaporated under reduced pressure to

afford **21** as a colorless oil that was used without further purification (7.18 g, 52.3 mmol, 72%). [SR-A58(1)].

^1H NMR (CDCl_3 , 400 MHz): δ (ppm) = 2.11 (s, 6 H, CH_3), 2.62 (m, 4 H, CH_2 (cycle)), 2.71 (s, 2 H, NCH_2), 5.53 (s, 1 H, cycle), 5.61 (d, $^3J = 12.0$ Hz, 1 H, cycle), 5.68 (d, $^3J = 12.0$ Hz, 1 H, cycle).

The diene **21** was converted to the corresponding ammonium salt **22** prior to coordination to ruthenium: A solution of **21** (3.57 g, 26.0 mmol) in CH_2Cl_2 was treated with HCl (3.9 mL of a 25% solution in H_2O , 30.0 mmol). The solvents were removed and the white solid was dried under vacuum (3.62 g, 20.8 mmol, 80%). [SR-A59(1)].

^1H NMR (D_2O , 400 MHz): δ (ppm) = 2.72 (s, 6 H, CH_3), 3.56 (s, 2 H, NCH_2), 4.69 (s, 4 H, CH_2 (cycle)), 5.66 (s, 2 H, CH (cycle)), 5.92 (s, 1 H, CH (cycle)).

$^{13}\text{C}\{^1\text{H}\}$ NMR (D_2O , 101 MHz): δ (ppm) = 26.18, 26.82 (CH_2 (cycle)), 42.14 ($\text{NH}(\text{CH}_3)_2$), 63.62 (NCH_2), 123.2, 123.9 ($-\text{CH}=\text{}$), 131.6 (quaternary).

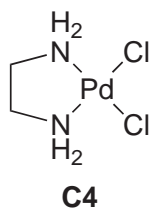
A solution of $\text{RuCl}_3 \cdot x\text{H}_2\text{O}$ (1.42 g, *ca.* 41% Ru, 5.75 mmol) in EtOH (50 mL) was prepared. Diene **22** was added (3.00 g, 17.3 mmol, 3.0 equiv.) and the mixture was heated to reflux for 5 hours. The green solid was filtered off, washed with EtOH (15 mL) followed by Et₂O (15 mL) and dried under vacuum to afford **C3** (1.61 g, 2.34 mmol, 81%) with spectral data in good agreement with literature.^[291] [SR-A60(1)].

¹H NMR (d6-DMSO, 400 MHz): δ (ppm) = 2.79 (s, 12 H, $\text{NH}(\text{CH}_3)_2$), 4.04 (s, 4 H, NCH_2), 6.09 - 6.15 (m, 6 H, aromatic *p*- and *m*-protons), 6.32 (d, ³*J* = 5.6 Hz, 4 H, aromatic *o*-protons), 11.57 (s, 2 H, NH).

¹³C{¹H} NMR (d6-DMSO, 101 MHz): δ (ppm) = 41.8 ($\text{NH}(\text{CH}_3)_2$), 57.5 (CH_2), 86.2, 88.2, 88.8, 92.1 (arene).

Elemental analysis (%) calcd (found) for $\text{C}_{18}\text{H}_{28}\text{Cl}_6\text{N}_2\text{Ru}_2 \times \text{H}_2\text{O}$: C 30.65 (30.36), H 4.40 (4.07), N 3.97 (3.93).

[PdCl₂(en)] (**C4**).^[348]



PdCl_2 (500 mg, 2.85 mmol) was dissolved in water under acidic conditions (10 mL H₂O + 3 mL HCl (37%)). The solution was heated to reflux and filtered. The pH of the solution was increased to 2 - 3 by addition of NaOH (*ca.* 20 mL of a 1.5 M solution). Ethylenediamine (0.19 mL, 2.85 mmol, 1.0 equiv.) was added dropwise, while ensuring the pH was kept under 3 (addition of HCl if necessary). The brown solution turned yellow, and was stirred at 70°C for one hour. It was then left to cool to room temperature overnight. A yellow solid was filtered off, washed with small portions of H₂O and acetone, and dried under vacuum to afford **C4** (455 mg, 1.92 mmol, 67%) with spectral data in good agreement with literature.^[352]

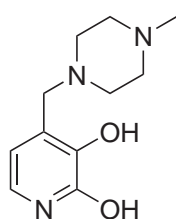
¹H NMR (d6-DMSO, 400 MHz): δ (ppm) = 2.33 (s, 4 H, CH_2), 4.88 (s, 4 H, NH_2).

¹³C{¹H} NMR (d6-DMSO, 101 MHz): δ (ppm) = 47.2 (CH_2).

7.2.2 Dihydroxypyridine-based Bridging Ligands

Commercially available 2,3-dihydroxypyridine (**L1**) was used as the starting material for the synthesis of ligands **L2** and **L3**.^[289, 290, 353] **L4** was obtained from **L3** by Pd-catalyzed hydrogenolysis, and the fluorescent ligands **L5-L10** were prepared by coupling a fluorophore to **L4**.^[22]

4-((4-Methylpiperazine)-1-yl)methyl)-2,3-dihydroxypyridine (**L2**).^[289, 290]



L2

2,3-Dihydroxypyridine (**L1**, 2.0 g, 17.1 mmol), formaldehyde (1.3 mL, 37 wt% in H₂O, 17.1 mmol, 1 equiv.) and *N*-methylpiperazine (1.9 mL, 17.1 mmol, 1 equiv.) were heated under reflux in EtOH (75 mL) for 7 hours. The mixture was stirred for an additional 12 hours at room temperature. The solution was concentrated to *ca.* 25 mL and acetone was added to afford a precipitate which was filtered off and washed with acetone. The crude product was solubilized in

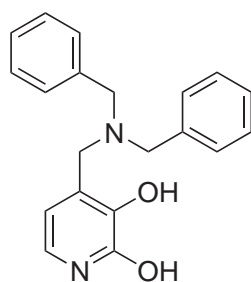
hot CHCl₃. The obtained solution was filtered through a pad of Celite and cooled down to -20°C. The precipitate was filtered off, washed with acetone and dried under vacuum to afford ligand **L2** as a white solid (1.34 g, 6.00 mmol, 35%). [SR-C232(1)].

¹H NMR (CDCl₃, 400 MHz): δ (ppm) = 2.29 (s, 3 H, CH₃), 2.58 (m, br, 8 H, NCH₂, piperazine), 3.59 (s, 2 H, NCH₂), 5.98 (d, ³J = 6.4 Hz, 1 H, pyridine), 6.92 (d, ³J = 6.4 Hz, 1 H, pyridine).

¹³C{¹H} NMR (CDCl₃, 101 MHz): δ (ppm) = 46.0, 52.8, 54.9, 59.5 (NCH₃, NCH₂), 107.7, 123.9, 125.5, 146.7, 159.8 (pyridine).

Elemental analysis (%) calcd (found) for C₁₁H₁₇N₃O₂ × 1/25 CHCl₃: C 58.15 (58.36), H 7.53 (7.63), N 18.43 (18.24).

2,3-Dihydroxy-4-(*N,N*-dibenzylaminomethyl)pyridine (**L3**).^[353]



L3

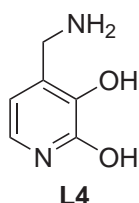
2,3-Dihydroxypyridine (**L1**, 10.0 g, 87.3 mmol), formaldehyde (7.1 mL, 37 wt% in H₂O, 87.3 mmol, 1 equiv.) and dibenzylamine (33.5 mL, 175 mmol, 2 equiv.) were heated under reflux in EtOH (700 mL) for 6 days. After the mixture was cooled down to room temperature, a solid residue was filtered off and discarded. The solution was concentrated to *ca.* 50 mL and a solid was filtered off, which was solubilized in hot CHCl₃ (400 mL). The hot solution was filtered through a pad of Celite and concentrated to 100 mL under reduced pressure. Addition of

acetone (100 mL) and storage of the mixture in the fridge afforded a white precipitate which was filtered off, washed with acetone and dried under vacuum. Ligand **L3** was obtained in 46% yield (12.8 g, 40.0 mmol) with spectral data in good agreement with literature.^[353] [SR-A30(1)].

¹H NMR (CDCl₃, 400 MHz): δ (ppm) = 3.62 (s, 2 H, NCH₂), 3.65 (s, 4 H, NCH₂Ph), 6.17 (d, ³J = 6.8 Hz, 1 H, pyridine), 6.95 (d, ³J = 6.8 Hz, 1 H, pyridine), 7.26 - 7.39 (m, 10 H, Ph), 10.04 (s, 1 H, OH), 12.95 (s, 1 H, OH).

¹³C{¹H} NMR (CDCl₃, 101 MHz): δ (ppm) = 54.0, 58.4 (NCH₂), 108.1, 123.7, 127.0, 127.8, 128.8, 129.5, 137.2, 146.0, 159.5 (pyridine, Ph).

4-Aminomethyl-DHP (**L4**).^[22]



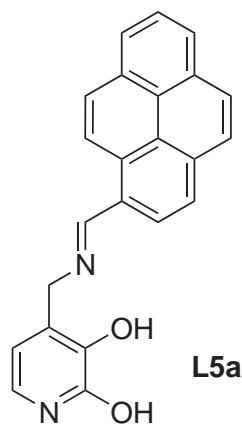
4-(Dibenzylamino)methyl-2,3-dihydroxypyridine (**L3**, 1.00 g, 3.12 mmol) was dissolved in degassed methanol (200 mL). Pd/C (0.332 g, 0.312 mmol, 10 mol%) was added and the mixture was stirred under an atmosphere of dihydrogen for 8 h. After filtration through a pad of Celite, the solvent was evaporated under reduced pressure. The residue was suspended in MeOH (10 mL), and the resulting solid was filtered off, and dried in vacuum. Yield: 305 mg (2.18 mmol, 70%). [SR-A95(2)].

¹H NMR (DCl 0.1 M in D₂O, 400 MHz): δ (ppm) = 4.11 (s, 2 H, CH₂), 6.41 (d, ³J = 6.6 Hz, 1 H, pyridine), 7.08 (d, ³J = 6.9 Hz, 1 H, pyridine).

¹³C{¹H} NMR (DCl 0.1 M in D₂O, 101 MHz): δ (ppm) = 38.3 (CH₂), 109.6 (C-H), 124.8 (C-CH₂), 125.3 (C-H), 145.4 (C-OH), 159.0 (C-OH).

m/z (ESI) 141.0665 (M + H⁺. [C₆H₉N₂O₂]⁺ requires 141.0659).

Pyrene-DHP imine (**L5a**).^[22]



4-Aminomethyl-2,3-dihydroxypyridine (**L4**, 200 mg, 1.43 mmol) and 1-pyrenecarboxaldehyde (329 mg, 1.43 mmol, 1 equiv.) were stirred in anhydrous methanol (75 mL) for 2 h. The resulting imine **L5a** was filtered off, washed with MeOH, and dried under vacuum. Yield: 372 mg (1.06 mmol, 74%). [SR-A52(3)].

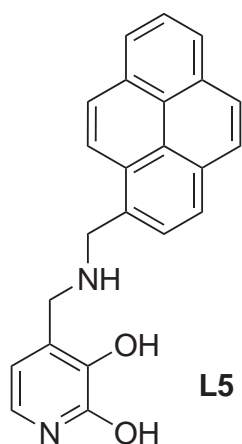
¹H NMR (d₆-DMSO, 400 MHz): δ (ppm) = 4.87 (s, 2 H, NCH₂), 6.30 (d, ³J = 6.8 Hz, 1 H, pyridine), 6.90 (d, ³J = 6.8 Hz, 1 H, pyridine), 8.12 (t, ³J = 7.6 Hz, 1 H, pyrene), 8.22 (d, ³J = 9.1 Hz, 1 H, pyrene), 8.28 (d, ³J = 8.8 Hz, 1 H, pyrene), 8.32 - 8.38 (m, 4 H, pyrene), 8.59 (d, ³J = 8.0 Hz, 1 H, pyrene), 9.12 (d, ³J = 9.6

Hz, 1 H, pyrene), 9.55 (s, 1 H, CH=N).

$^{13}\text{C}\{^1\text{H}\}$ NMR (d6-DMSO, 101 MHz): δ (ppm) = 58.2 (NCH₂), 106.5, 122.9, 123.2, 123.7, 124.0, 125.0, 125.8, 126.1, 126.4, 126.6, 127.2, 127.4, 128.4, 128.7, 128.8, 129.3, 130.1, 130.8, 132.4, 143.7 (pyrene, pyridine, CH=N), 158.1, 161.9 (pyridine).

m/z (ESI) 353.1287 (M + H⁺. [C₂₃H₁₇N₂O₂]⁺ requires 353.1290).

Pyrene-DHP amine (L5).^[22]



L5

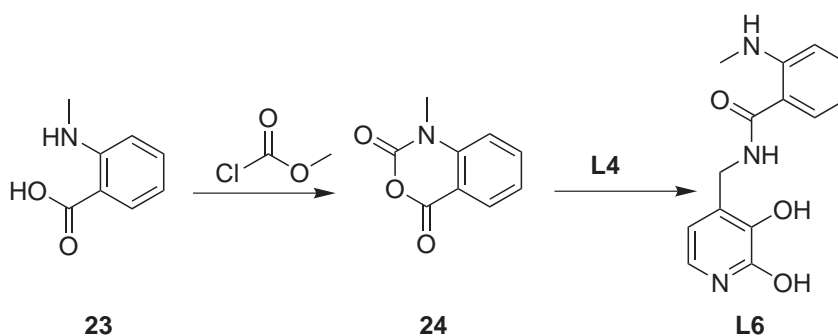
A suspension of the imine **L5a** (250 mg, 0.71 mmol) and NaBH₄ (96 mg, 2.48 mmol, 3.5 equiv.) in anhydrous methanol (50 mL) was stirred for 2 h. The off-white precipitate was filtered off, washed with MeOH, and dried in vacuum to afford the ligand **L5**. Yield: 181 mg (0.51 mmol, 72%). [SR-A2(1)].

^1H NMR (d6-DMSO, 400 MHz): δ (ppm) = 3.76 (s, 2 H, NCH₂), 4.40 (s, 2 H, NCH₂), 6.30 (d, $^3J = 7.0$ Hz, 1 H, pyridine), 6.86 (d, $^3J = 7.0$ Hz, 1 H, pyridine), 8.07 (t, $^3J = 8.0$ Hz, 1 H, pyrene), 8.10 (d, $^3J = 8.0$ Hz, 1 H, pyrene), 8.15 (m, 2 H, pyrene), 8.21 (d, $^3J = 9.0$ Hz, 1 H, pyrene), 8.26 (d, $^3J = 8.0$ Hz, 1H, pyrene), 8.29 (d, $^3J = 8.0$ Hz, 1 H, pyrene), 8.44 (d, $^3J = 9.0$ Hz, 1 H, pyrene), 11.57 (s, br, 1 H, OH).

$^{13}\text{C}\{^1\text{H}\}$ NMR (d6-DMSO, 101 MHz): δ (ppm) = 46.5, 50.2 (NCH₂), 106.4, 122.9, 123.7, 124.0, 124.1, 124.6, 125.0, 125.1, 126.2, 126.8, 127.2, 127.4, 127.9, 128.6, 129.9, 130.4, 130.8, 134.3, 144.2, 157.9 (pyrene, pyridine).

m/z (ESI) 355.1444 (M + H⁺. [C₂₃H₁₉N₂O₂]⁺ requires 355.1447).

N-Methylantranilic acid-DHP (L6).



23

24

L6

As a consequence of the poor purity of commercially available samples, N-methylisatoic anhydride (**24**) was synthesized from N-methylantranilic acid (**23**):^[354] N-Methylantranilic acid (5.0 g, 31.4 mmol) was refluxed in methyl chloroformate (50 mL) for 7 h.

The solvent was then removed under vacuum, and the obtained solid was washed with anhydrous MeOH (4×10 mL) and dried under vacuum to afford *N*-methylisatoic anhydride (**24**) as a white solid (1.98 g, 11.2 mmol, 36%) with spectral data in good agreement with literature.^[355] [SR-B115(2)].

¹H NMR (d6-DMSO, 400 MHz): δ (ppm) = 3.46 (s, 3 H, NCH₃), 7.34 (t, ³J = 7.6 Hz, 1 H, aromatic), 7.44 (d, ³J = 8.6 Hz, 1 H, aromatic), 7.86 (t, ³J = 7.8 Hz, 1 H, aromatic), 8.00 (d, ³J = 7.8 Hz, 1 H, aromatic).

¹³C{¹H} NMR (d6-DMSO, 101 MHz): δ (ppm) = 31.7 (NCH₃), 111.5, 114.8, 123.6, 129.3, 137.2, 142.2 (arene), 147.7 (O=CO), 159.0 (O=CON).

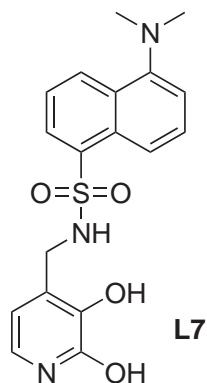
N-methylisatoic anhydride (**24**) (253 mg, 1.43 mmol) and 4-aminomethyl-2,3-dihydroxypyridine (**L4**) (1.43 mmol, 1 equiv.) were refluxed in anhydrous EtOH (8 mL) for 3 hours. The obtained precipitate was filtered off, washed with EtOH (3×3 mL) followed by Et₂O (3×3 mL), and dried under vacuum to afford the ligand **L6** as an off-white solid (352 mg, 1.29 mmol, 90%). [SR-A104(7)].

¹H NMR (d6-DMSO, 400 MHz): δ (ppm) = 2.76 (d, ³J = 5.2, 3 H, CH₃), 4.28 (d, ³J = 5.6 Hz, 2 H, NCH₂), 6.03 (d, ³J = 6.8 Hz, 1 H, pyridine), 6.56 (t, ³J = 7.4 Hz, 1 H, Ph), 6.63 (d, ³J = 8.4 Hz, 1 H, Ph), 6.82 (d, ³J = 6.8 Hz, 1 H, pyridine), 7.29 (t, ³J = 7.8 Hz, 1 H, Ph), 7.61 (d, ³J = 8.0 Hz, 1 H, Ph), 7.69 (d, ³J = 4.8 Hz, 1 H, PhNHCH₃), 8.71 (t, ³J = 5.8 Hz, 1 H, CH₂NHCO), 8.86 (s, 1 H, OH), 11.59 (s, 1 H, OH).

¹³C{¹H} NMR (d6-DMSO, 101 MHz): δ (ppm) = 29.3 (CH₃), 36.2 (CH₂), 105.1, 110.6, 113.9, 114.4, 123.1, 127.4, 128.3, 132.6, 143.2, 150.3, 157.8, 169.3 (pyridine, arene, CO).

Elemental analysis (%) calcd (found) for C₁₄H₁₅N₃O₃ \times 1/3 H₂O : C 60.21 (60.57), H 5.65 (5.26), N 15.05 (14.78).

Dansyl-DHP (**L7**).^[22]



Dansyl chloride (400 mg, 1.47 mmol) was added to a suspension of 4-aminomethyl-2,3-dihydroxypyridine (**L4**, 1150 mg, 7.40 mmol, 5.0 equiv.) in anhydrous DMF (20 mL). The mixture was stirred overnight at room temperature. The excess of 4-aminomethyl-2,3-dihydroxypyridine was filtered off and washed with CH₂Cl₂. The organic solutions were poured into 30 mL of H₂O, and evaporated under vacuum. The residual solid was purified by flash chromatography on silica gel (MeOH/CH₂Cl₂ 2:98 to 10:90) to afford **L7**. Yield: 356 mg (953 μ mol, 65%). [SR-B113(5)].

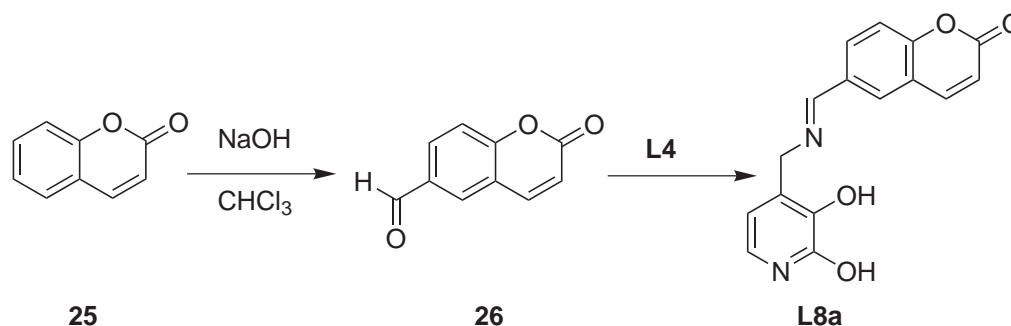
¹H NMR (d6-DMSO, 400 MHz): δ (ppm) = 2.82 (s, 6 H, N(CH₃)₂), 3.87 (s, 2 H, NCH₂), 5.97

(d, $^3J = 6.8$ Hz, 1 H, pyridine), 6.58 (br, 1 H, pyridine), 7.24 (d, $^3J = 7.6$ Hz, 1 H, dansyl), 7.54 – 7.60 (m, 2 H, dansyl), 8.09 (d, $^3J = 7.4$ Hz, 1 H, dansyl), 8.29 (d, $^3J = 8.6$ Hz, 1 H, dansyl), 8.41 (d, $^3J = 8.6$ Hz, 1 H, dansyl).

$^{13}\text{C}\{^1\text{H}\}$ NMR (d6-DMSO, 101 MHz): δ (ppm) = 39.4 (CH_2), 45.1 ($\text{N}(\text{CH}_3)_2$), 105.5, 115.1, 119.1, 122.3, 123.4, 125.0, 127.8, 128.3, 128.9, 129.0, 129.4, 135.9, 143.7 (pyridine, dansyl), 151.3, 157.8 (pyridine).

m/z (ESI) 374.1156 ($\text{M} + \text{H}^+$. [$\text{C}_{18}\text{H}_{20}\text{N}_3\text{O}_4\text{S}$] $^+$ requires 374.1175).

Coumarin-DHP imine (L8a).

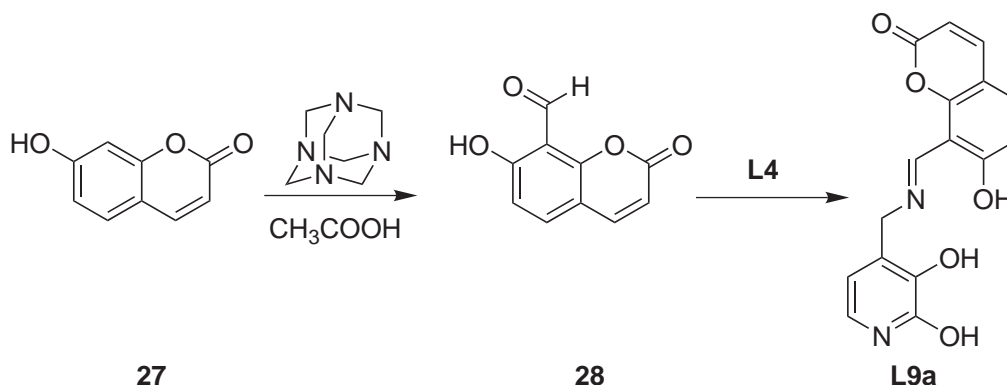


Formylation of coumarin:^[292] Coumarin (**25**, 16.0 g, 109.5 mmol) and NaOH (27.0 g, 675 mmol) were dissolved in H₂O (40 mL), and the mixture was heated to 80°C. CHCl₃ (20 mL, 250 mmol) was added over 1.5 hour and the mixture was then refluxed for 6 hours. The temperature was then decreased to 80°C, and the excess CHCl₃ was evaporated. The solution was then cooled down to room temperature, and a solid residue was filtered off and discarded. The residual mixture was acidified with HCl (37% solution in H₂O) until a red liquid started to separate. The solution was left to stand overnight, and the red solid was filtered off. Washing it with H₂O followed by extractions with hot EtOH / Et₂O 8:1 mixture (ca. 50°C, 5 × 40 mL) afforded 6-formylcoumarin (**26**) as a white solid with spectral data in good agreement with literature.^[356] Yield: 1.49 g (8.56 mmol, 8.0%). [SR-B116(1)].

^1H NMR (CDCl_3 , 400 MHz): δ (ppm) = 6.52 (d, $^3J = 9.8$ Hz, 1 H, aromatic), 7.47 (d, $^3J = 8.3$ Hz, 1 H, aromatic), 7.80 (d, $^3J = 9.8$ Hz, 1 H, aromatic), 8.04 - 8.07 (m, 2 H, aromatic), 10.04 (s, 1 H, CHO).

$^{13}\text{C}\{^1\text{H}\}$ NMR (CDCl_3 , 101 MHz): δ (ppm) = 118.1 (CH), 119.3 (CH), 128.1 (C_{10}), 130.2 (CH), 132.6 (CH), 133.0 (C-CHO), 143.0 (CH), 157.9, 159.8 (C=O, C_9), 190.2 (CHO)

Formation of imine **L8a**: A suspension of 6-formylcoumarin (**26**, 1181 mg, 6.78 mmol) and 4-aminomethyl-2,3-dihydroxypyridine (**L4**, 950 mg, 6.78 mmol, 1 equiv.) in anhy-

Hydroxycoumarin-DHP imine (**L9a**).

Preparation of 8-formyl-7-hydroxycoumarin (**28**):^[357] 7-Hydroxycoumarin (**27**, 20.0 g, 123 mmol) and hexamethylenetetramine (40.0 g, 285 mmol, 2.3 equiv.) were added to glacial acetic acid (150 mL). The solution was heated to 95°C for 5.5 hours. Dilute hydrochloric acid (HCl-H₂O = 84:100 (v/v), 300 mL) was added, and the solution was heated to reflux for 30 minutes. The mixture was poured into H₂O (1500 mL) and extracted with Et₂O (4 × 500 mL). The organic fractions were dried over MgSO₄ and the solvent was removed under reduced pressure to afford 8-formyl-7-hydroxycoumarin (**28**) as a pale yellow solid (3.80 g, 20.0 mmol, 16%) with spectral data in good agreement with literature.^[357] [SR-B183(1)].

¹H NMR (d₆-DMSO, 400 MHz): δ (ppm) = 6.37 (d, ³J = 9.6 Hz, 1 H, coumarin), 6.96 (d, ³J = 8.8 Hz, 1 H, coumarin), 7.87 (d, ³J = 8.8 Hz, 1 H, coumarin), 8.03 (d, ³J = 9.6 Hz, 1 H, coumarin), 10.43 (s, 1 H, CHO).

¹³C{¹H} NMR (d₆-DMSO, 101 MHz): δ (ppm) = 109.2, 111.2, 112.6, 114.0, 136.3, 144.6, 155.7, 159.1, 163.9 (coumarin), 190.9 (CHO).

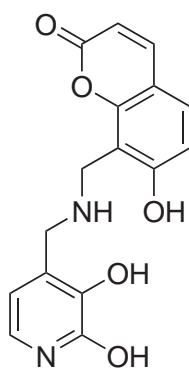
Formation of the imine **L9a**: A suspension of 8-formyl-7-hydroxycoumarin (**28**, 570 mg, 3.0 mmol) and 4-aminomethyl-2,3-dihydroxypyridine (**L4**, 420 mg, 3.0 mmol, 1.0 equiv.) in anhydrous MeOH (50 mL) was stirred at room temperature for 2 hours. The precipitate was filtered off, washed with MeOH, and dried under vacuum. The imine **L9a** was obtained as a pale orange powder (514 mg, 1.65 mmol, 55%). [SR-B176(2)].

¹H NMR (d₆-DMSO, 400 MHz): δ (ppm) = 4.77 (s, 2 H, NCH₂), 6.11 - 6.18 (m, 2 H, pyridine, coumarin), 6.55 (d, ³J = 9.2 Hz, 1 H, coumarin), 6.90 (d, ³J = 6.8 Hz, 1 H, pyridine), 7.54 (d, ³J = 9.2 Hz, 1 H, coumarin), 7.88 (d, ³J = 9.2 Hz, 1 H, coumarin), 9.02 (s, 1 H, CH=N).

$^{13}\text{C}\{^1\text{H}\}$ NMR (d6-DMSO, 101 MHz): δ (ppm) = 57.9 (NCH₂), 103.9, 106.1, 106.4, 108.7, 118.6, 123.7, 123.8, 134.0, 144.8, 145.2, 156.2, 157.9, 159.8, 160.5, 174.4 (coumarin, pyridine, CHN).

Elemental analysis (%) calcd (found) for C₁₆H₁₂N₂O₅ × 0.75 H₂O: C 58.99 (58.67), H 4.18 (4.35), N 8.60 (8.34).

Hydroxycoumarin-DHP amine (L9).



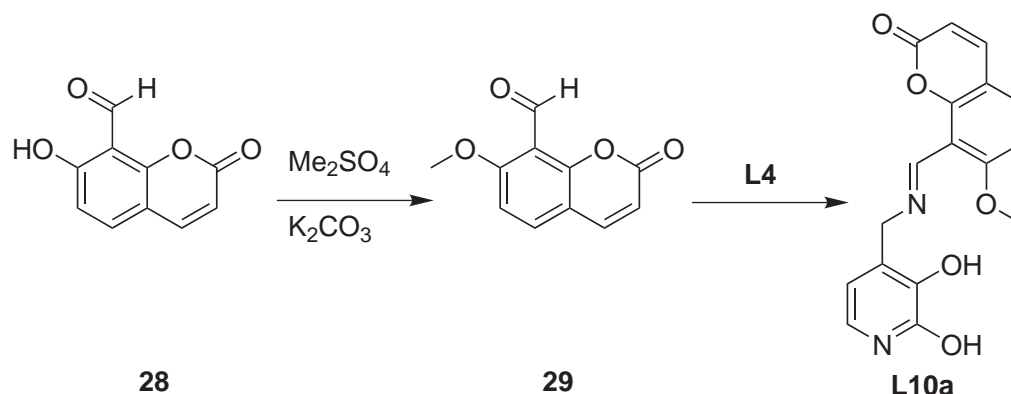
L9

A suspension of the imine **L9a** (744 mg, 2.38 mmol) and NaBH₄ (315 mg, 8.33 mmol, 3.5 equiv.) in anhydrous methanol (120 mL) was stirred for 3 h. An orange powder was filtered off and discarded, and the solvent was removed under reduced pressure. The obtained solid was dissolved in MeOH (15 mL), and Et₂O was added to precipitate the product. The final purification was performed by reversed phase HPLC (H₂O/CH₃CN + 0.1% TFA, gradient 92:8 to 82:18 in 10 minutes, λ_{max} = 254 nm, sample: 1 mL H₂O/CH₃CN 92:8, 10.0 mg crude material, R_f = 8.1 min). Yield (**L9** × **TFA**): 172 mg (0.400 mmol, 17%). [SR-B181(3)].

^1H NMR (D₂O, 400 MHz): δ (ppm) = 4.23 (s, 2 H, NCH₂), 4.49 (s, 2 H, NCH₂), 6.23 (d, 3J = 7.2 Hz, 1 H, pyridine), 6.30 (d, 3J = 9.2 Hz, 1 H, coumarin), 6.89 - 6.92 (m, 2 H, coumarin, pyridine), 7.53 (d, 3J = 8.8 Hz, 1 H, coumarin), 7.91 (d, 3J = 9.6 Hz, 1 H, coumarin).

$^{13}\text{C}\{^1\text{H}\}$ NMR (d6-DMSO, 101 MHz): δ (ppm) = 38.6, 44.2 (NCH₂), 105.3, 106.4, 111.3, 111.6, 112.4, 119.1, 123.6, 130.6, 144.8, 146.2, 154.1, 157.8, 159.7, 160.3 (coumarin, pyridine).

m/z (ESI) 315.0995 (M + H⁺. [C₁₆H₁₅N₂O₅]⁺ requires 315.0981).

Methoxycoumarin-DHP imine (**L10a**).

Preparation of 8-formyl-7-methoxycoumarin (**29**):^[357, 358] 8-Formyl-7-hydroxycoumarin (**28**, 2.77 g, 14.6 mmol), K_2CO_3 (11.1 g, 80.3 mmol, 5.5 equiv.), and dimethyl sulfate (22.2 mL, 235 mmol, 16 equiv.) were heated to reflux in anhydrous acetone (300 mL). After 8 hours, the solution was cooled down to room temperature, and poured into 500 mL H_2O . The solid residue was filtered off, washed with 25 mL of a NH_4OH aqueous solution (3%), followed by water (50 mL), and dried under vacuum. 8-Formyl-7-methoxycoumarin (**29**) was obtained without further purification as a pale yellow solid (1.31 g, 6.42 mmol, 44%) with spectral data in good agreement with literature.^[359] [SR-C194(4)].

^1H NMR (CDCl_3 , 400 MHz): δ (ppm) = 4.02 (s, 3 H, OCH_3), 6.33 (d, $^3J = 9.6$ Hz, 1 H, coumarin), 6.95 (d, $^3J = 8.8$ Hz, 1 H, coumarin), 7.62 - 7.66 (m, 2 H, coumarin), 10.67 (s, 1 H, CHO).

$^{13}\text{C}\{^1\text{H}\}$ NMR (CDCl_3 , 101 MHz): δ (ppm) = 56.9 (OCH_3), 108.3 (CH), 112.8 (C-CHO and C_{10}), 114.1 (CH), 134.3 (CH), 143.2 (CH), 156.2 (C_9), 159.6, 163.3 (C=O, C- OCH_3), 187.0 (CHO).

Formation of the imine **L10a**: 8-Formyl-7-methoxycoumarin (**29**, 408 mg, 2.00 mmol) and 4-aminomethyl-2,3-dihydroxypyridine (**L4**, 280 mg, 2.00 mmol) were stirred for 3 h in anhydrous methanol (20 mL). The resulting imine **L10a** was filtered off, washed with methanol, and dried under vacuum. Yield: 490 mg (1.50 mmol, 75%). [SR-C206(4)].

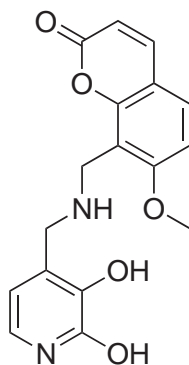
^1H NMR (d_6 -DMSO, 400 MHz): δ (ppm) = 3.94 (s, 3 H, OCH_3), 4.69 (s, 2 H, NCH_2), 6.29 (d, $^3J = 6.8$ Hz, 1 H, pyridine), 6.33 (d, $^3J = 9.5$ Hz, 1 H, coumarin), 6.83 (d, $^3J = 6.8$ Hz, 1 H, pyridine), 7.17 (d, $^3J = 8.8$ Hz, 1 H, coumarin), 7.78 (d, $^3J = 8.8$ Hz, 1 H, coumarin), 8.02 (d, $^3J = 9.5$ Hz, 1 H, coumarin), 8.67 (s, 1 H, CHN), 8.83 (s, br, 1 H, OH), 11.55 (s, br, 1 H, OH).

$^{13}\text{C}\{^1\text{H}\}$ NMR (d_6 -DMSO, 101 MHz): δ (ppm) = 56.6 (CH_2), 58.9 (CH_3), 106.2, 108.5, 112.2, 112.8, 112.9, 122.9, 127.13, 131.1, 143.3, 144.5, 152.6, 155.6, 157.9, 159.9, 160.9 (pyridine,

coumarin, CHN).

m/z (ESI) 327.0979 ($M + H^+$. $[C_{17}H_{15}N_2O_5]^+$ requires 327.0975).

Methoxycoumarin-DHP amine (L10).^[22]



L10

Excess $NaBH_4$ (166 mg, 4.39 mmol, 3.5 equiv.) was added to a suspension of the imine **L10a** (409 mg, 1.25 mmol, 1 equiv.) in anhydrous methanol (50 mL). After stirring the mixture for 3 h, the solvent was evaporated. The crude product was purified by reversed phase HPLC (H_2O/CH_3CN , gradient 88:12 to 76:24 in 16 minutes, $\lambda_{max} = 254$ nm, sample: 1 mL, 20 mg crude material, $R_f = 14.5$ min). Yield: 197 mg (0.60 mmol, 48%). [SR-208(2)]

1H NMR (DCl 0.1 M in D_2O , 400 MHz): δ (ppm) = 3.88 (s, 3 H, OCH_3), 4.11 (s, 2 H, NCH_2), 4.43 (s, 2 H, NCH_2), 6.11 (d, $^3J = 6.8$ Hz, 1 H, pyridine), 6.26 (d, $^3J = 9.5$ Hz, 1 H, coumarin), 6.83 (d, $^3J = 6.9$

Hz, 1 H, pyridine), 6.99 (d, $^3J = 9.1$ Hz, 1 H, coumarin), 7.60 (d, $^3J = 8.8$ Hz, 1 H, coumarin), 7.87 (d, $^3J = 9.5$ Hz, 1H, coumarin).

$^{13}C\{^1H\}$ NMR (DCl 0.1 M in D_2O , 101 MHz): δ (ppm) = 39.6 (NCH_2), 45.6 (NCH_2), 57.1 (OCH_3), 106.2, 109.1, 109.6, 112.8, 113.6, 122.4, 124.9, 132.4, 145.7, 146.6, 153.4, 158.5, 161.8, 163.9 (pyridine, coumarin).

m/z (ESI) 329.1121 ($M + H^+$. $[C_{17}H_{17}N_2O_5]^+$ requires 329.1132).

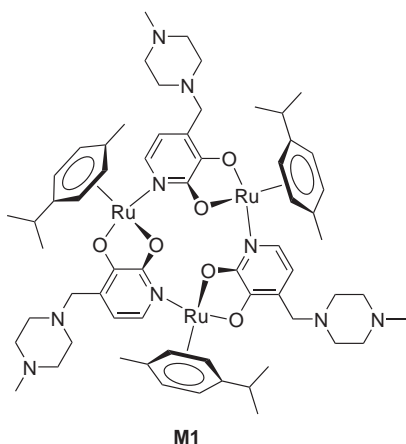
7.2.3 Syntheses of Trimeric Complexes

The general procedure for the preparation of neutral 12-metallacrown-3 trimeric complexes was described in the literature.^[267, 274] Appropriate amounts of metal fragments and bridging ligands were mixed in methanol in the presence of a base (cesium carbonate or hydroxyde). After 2 hours, the solvent was removed under reduced pressure, and CH_2Cl_2 was used to extract the product from the salts. Addition of hexane generally resulted in the precipitation of the product.

Syntheses of macrocycles based on (*p*-cymene)Ru fragments with dansyl or coumarin derivatives **L7**, **L8**, **L9** and **L10** were not attempted, owing to the poor solubility observed for macrocycles **M2** and **M3**. The fragment ($\eta^6\text{-C}_6\text{H}_5\text{CH}_2\text{NMe}_2$)Ru was used for the synthesis of macrocycles **M4** - **M10**. The hydroxycoumarin-based ligand **L9** was not suitable for the self-assembly process, and no macrocycle was isolated, which contained **L9**. Furthermore, the macrocycles **M1**, **M4**, **M5**, **M9**, and **M10** could be obtained by self-assembly directly in H_2O , in the presence of a buffer (phosphate buffer, pH 7.0 - 8.0).

Neutral 12-Metallacrown-3 Complexes based on the (*p*-cymene)Ru Fragment

$[(p\text{-cymene})\text{Ru}(\text{L2-2H}^+)]_3$ (**M1**).^[267]



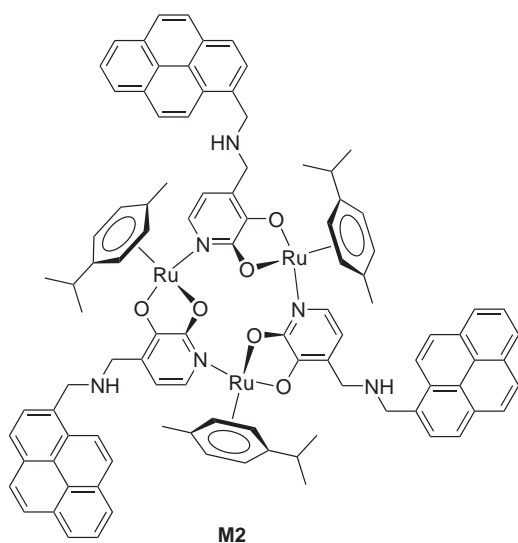
A suspension of $[(p\text{-cymene})\text{RuCl}_2]_2$ (**C2**, 612 mg, 1.00 mmol), ligand **L2** (447 mg, 2.00 mmol, 2 equiv.) and Cs_2CO_3 (1.60 g, 5.00 mmol, 5 equiv.) in degassed MeOH (40 mL) was stirred for 2 h at room temperature. After evaporation of the solvent under reduced pressure, the product was extracted with hot hexane (1×300 mL and 3×125 mL). The solution was concentrated (15 mL) and cooled down to -18°C for 1 h. The precipitate was filtered and dried under vacuum. The product **M1** was obtained as an orange powder in 58% yield (539 mg, 0.39 mmol) with spectral data in good agreement with literature.^[267]

^1H NMR (CDCl_3 , 400 MHz): δ (ppm) = 1.25 (d, $^3J = 7.2$ Hz, 9 H, $\text{CH}(\text{CH}_3)_2$), 1.33 (d, $^3J = 6.8$ Hz, 9 H, $\text{CH}(\text{CH}_3)_2$), 2.00 (s, 9 H, $\text{C}_6\text{H}_4\text{CH}_3$), 2.23 (s, 9 H, NCH_3), 2.25 - 2.55 (m, br, 24 H, NCH_2 , piperazine), 2.75 (sept, $^3J = 6.9$ Hz, 3 H, $\text{CH}(\text{CH}_3)_2$), 3.25 (d, $^2J = 13.2$ Hz, 3 H, NCH_2), 3.33 (d, $^2J = 13.6$ Hz, 3 H, NCH_2), 5.07 (d, $^3J = 5.6$ Hz, 3 H, $\text{MeC}_6\text{H}_4^i\text{Pr}$), 5.25 (d, $^3J = 6.0$ Hz,

3 H, MeC₆H₄^{*i*}Pr), 5.38 (d, ³J = 5.6 Hz, 3 H, MeC₆H₄^{*i*}Pr), 5.66 (d, ³J = 5.6 Hz, 3 H, MeC₆H₄^{*i*}Pr), 5.69 (d, ³J = 6.4 Hz, 3 H, pyridine), 6.50 (d, ³J = 6.4 Hz, 3 H, pyridine).

¹³C{¹H} NMR (CDCl₃, 101 MHz): δ (ppm) = 18.4, 22.6, 23.4 (CH₃, CH(CH₃)₂) 31.2 (CH(CH₃)₂), 46.2 (NCH₃), 53.4, 55.4, 55.5 (NCH₂), 77.4, 79.7, 81.9, 82.3, 96.5, 97.9 (C, CH, *p*-cymene), 110.8, 123.9, 131.2, 154.9, 170.5 (C, CH, C-O, pyridine).

[(*p*-cymene)Ru(L5-2H⁺)]₃ (M2).^[22]



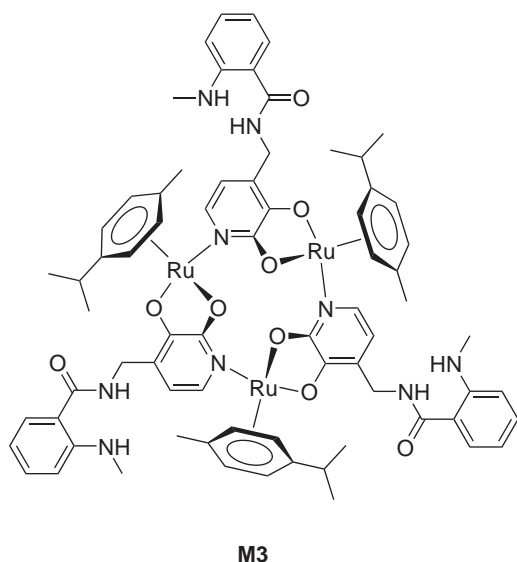
A mixture of [(*p*-cymene)RuCl₂]₂ (**C2**, 86.3 mg, 141 μmol), ligand **L5** (100 mg, 282 μmol, 2 equiv.), and CsOH (94.7 mg, 564 μmol, 4 equiv.) in 10 mL of degassed methanol was stirred for 2 h. The precipitate was filtered off, washed with cold methanol and dried under vacuum. Yield: 132 mg (74.9 μmol, 80%). [SR-A11(1)].

¹H NMR (C₆D₆, 400 MHz): δ (ppm) = 1.07 (d, ³J = 6.8 Hz, 9 H, CH(CH₃)₂), 1.10 (d, ³J = 7.1 Hz, 9 H, CH(CH₃)₂), 1.76 (s, 9 H, CH₃), 2.63 (sept, ³J = 6.8 Hz, 3 H, CH(CH₃)₂), 3.88 (d, ²J = 13.2 Hz, 3 H, NCH₂), 3.94 (d, ²J = 13.2

Hz, 3 H, NCH₂), 4.15 (d, ²J = 13.4 Hz, 3 H, NCH₂), 4.19 (d, ²J = 13.4 Hz, 3 H, NCH₂), 4.58 (d, ³J = 5.6 Hz, 3 H, MeC₆H₄^{*i*}Pr), 5.13 (d, ³J = 5.6 Hz, 3 H, MeC₆H₄^{*i*}Pr), 5.25 (d, ³J = 5.6 Hz, 3 H, MeC₆H₄^{*i*}Pr), 5.61 (d, ³J = 5.6 Hz, 3 H, MeC₆H₄^{*i*}Pr), 5.90 (d, ³J = 6.1 Hz, 3 H, pyridine), 6.96 (d, ³J = 6.1 Hz, 3 H, pyridine), 7.70 – 7.75 (m, 9 H, pyrene), 7.83 – 7.90 (m, 12 H, pyrene), 8.00 (d, ³J = 7.8 Hz, 3 H, pyrene), 8.28 (d, ³J = 9.3 Hz, 3 H, pyrene).

m/z (ESI) 882.7197 (M + 2 H⁺). [C₉₉H₉₂N₆O₆Ru₃]²⁺ requires 882.7131.

$[(p\text{-cymene})\text{Ru}(\text{L6-2H}^+)]_3$ (**M3**).



A mixture of $[(p\text{-cymene})\text{RuCl}_2]_2$ (**C2**, 224 mg, 0.366 mmol), ligand **L6** (200 mg, 0.732 mmol, 2 equiv.), and CsOH (3.0 mL of a 1.0 M stock solution in MeOH, 3.00 mmol, 8 equiv.) in 15 mL of degassed methanol was stirred for 2 h. The solvent was removed under reduced pressure, and the obtained solid was extracted with CHCl_3 (30 mL). Hexane (60 mL) was added, and the volume reduced to ca. 10 mL. The precipitate was filtered off, washed with hexane, and dried under vacuum. The macrocycle **M3** was obtained as a red powder. Yield: 231 mg (0.152 mmol, 62%). [SR-A109(5)].

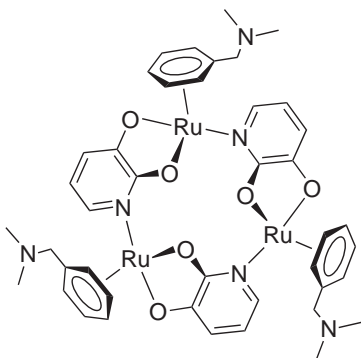
^1H NMR (CDCl_3 , 400 MHz): δ (ppm) = 1.28 (d, $^3J = 6.8$ Hz, 9 H, $\text{CH}(\text{CH}_3)_2$), 1.33 (d, $^3J = 6.9$ Hz, 9 H, $\text{CH}(\text{CH}_3)_2$), 1.96 (s, 9 H, CH_3), 2.78 (sept, $^3J = 7.0$ Hz, 3 H, $\text{CH}(\text{CH}_3)_2$), 2.83 (s, 9 H, NHCH_3), 4.14 (d, $^2J = 15.4$ Hz, 3 H, NCH_2), 4.34 (d, $^2J = 15.4$ Hz, 3 H, NCH_2), 4.95 (d, $^3J = 5.9$ Hz, 3 H, $\text{MeC}_6\text{H}_4^i\text{Pr}$), 5.25 (d, $^3J = 5.6$ Hz, 3 H, $\text{MeC}_6\text{H}_4^i\text{Pr}$), 5.38 (d, $^3J = 5.6$ Hz, 3 H, $\text{MeC}_6\text{H}_4^i\text{Pr}$), 5.51 (d, $^3J = 6.1$ Hz, 3 H, pyridine), 5.67 (d, $^3J = 5.6$ Hz, 3 H, $\text{MeC}_6\text{H}_4^i\text{Pr}$), 6.50 (d, $^3J = 6.4$ Hz, 3 H, pyridine), 6.59 (br, 3 H, arene), 6.65 (d, $^3J = 8.3$ Hz, 3 H, arene), 7.30 (t, $^3J = 7.8$ Hz, 3 H, arene), 7.47 (d, $^3J = 7.8$ Hz, 3 H, arene).

$^{13}\text{C}\{^1\text{H}\}$ NMR (CDCl_3 , 101 MHz): δ (ppm) = 18.4, 22.4, 23.6 (CH_3 , $\text{CH}(\text{CH}_3)_2$), 29.7 (NCH_3), 31.4 ($\text{CH}(\text{CH}_3)_2$), 40.7 (NCH_2), 76.1, 79.0, 82.8, 82.9, 97.7, 97.8 (C, CH, cymene), 111.1, 111.4, 114.2, 116.3, 123.3, 127.6, 131.6, 132.5, 150.5, 154.7, 169.4, 170.3 (pyridine, arene, C=O).

Elemental analysis (%) calcd (found) for $\text{C}_{72}\text{H}_{81}\text{N}_9\text{O}_9\text{Ru}_3 \times \text{H}_2\text{O} \times 4\text{CHCl}_3$: C 45.30 (44.98), H 4.35 (4.33), N 6.26 (6.32).

Neutral 12-Metallacrown-3 Complexes based on the (η^6 -C₆H₅CH₂NMe₂)Ru Fragment

$[(\eta^6\text{-C}_6\text{H}_5\text{CH}_2\text{NMe}_2)\text{Ru}(\text{L1-2H}^+)]_3$ (**M4**).



M4

A mixture of $[(\eta^6\text{-C}_6\text{H}_5\text{CH}_2\text{NMe}_2\text{H})\text{RuCl}_2]_2\text{Cl}_2$ (**C3**, 344 mg, 0.50 mmol), ligand **L1** (117 mg, 1.00 mmol, 2 equiv.) and CsOH (504 mg, 3.00 mmol, 6 equiv.) was stirred in degassed methanol (40 mL) for 2 hours. The solvent was then removed under vacuum and the solid was extracted with degassed CH₂Cl₂ (2 × 20 mL). Hexane was added (80 mL) and the volume was reduced to ca. 20 mL. The precipitate was filtered off, washed with hexane, and dried under vacuum to afford the macrocycle **M4** as a red powder (255 mg,

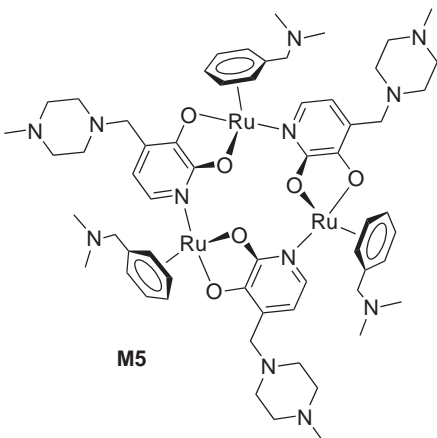
0.246 mmol, 74 %). [SR-A74(1)].

¹H NMR (CDCl₃, 400 MHz): δ (ppm) = 2.37 (s, 18 H, N(CH₃)₂), 3.35 (d, ²J = 13.2 Hz, 3 H, NCH₂), 3.46 (d, ²J = 12.8 Hz, 3 H, NCH₂), 5.37 - 5.41 (m, 6 H, arene), 5.48 (d, ³J = 5.4 Hz, 3 H, arene), 5.53 - 5.59 (m, 6 H, arene), 5.69 (t, ³J = 6.7 Hz, 3 H, pyridine), 6.16 (dd, ⁴J = 1.4 Hz, ³J = 7.1 Hz, 3 H, pyridine), 6.61 (dd, ⁴J = 1.5 Hz, ³J = 6.1 Hz, 3 H, pyridine).

¹³C{¹H} NMR (MeOD, 101 MHz): δ (ppm) = 45.5 (N(CH₃)₂), 62.8 (NCH₂), 76.8, 80.5, 81.8, 83.2, 84.7, 94.6 (arene), 110.9, 116.2, 134.1, 156.3, 172.0 (pyridine).

Elemental analysis (%) calcd (found) for C₄₂H₄₈N₆O₆Ru₃ × 2 H₂O × 2 CH₂Cl₂ : C 42.55 (42.37), H 4.54 (4.17), N 6.77 (6.96).

$[(\eta^6\text{-C}_6\text{H}_5\text{CH}_2\text{NMe}_2)\text{Ru}(\text{L2-2H}^+)]_3$ (**M5**).



M5

A mixture of $[(\eta^6\text{-C}_6\text{H}_5\text{CH}_2\text{NMe}_2\text{H})\text{RuCl}_2]_2\text{Cl}_2$ (**C3**, 154 mg, 0.224 mmol), ligand **L2** (100 mg, 0.448 mmol, 2 equiv.) and Cs₂CO₃ (538 mg, 1.65 mmol, 7.5 equiv.) was stirred in degassed methanol (20 mL) for 2 hours. The solvent was then removed under vacuum and the solid was extracted with degassed CH₂Cl₂ (2 × 20 mL). Hexane was added (50 mL) and the volume was reduced to ca. 15 mL. The precipitate was filtered off, washed with hexane, and dried under vacuum to afford the macrocycle **M5** as

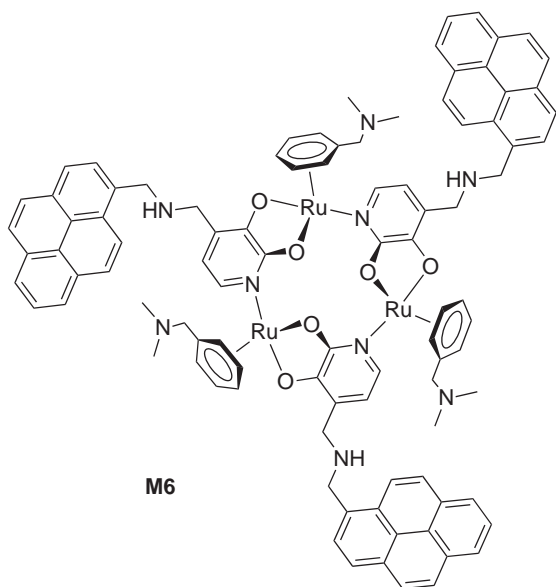
a red powder (136 mg, 0.099 mmol, 66%). [SR-C235(1)].

^1H NMR (CDCl_3 , 400 MHz): δ (ppm) = 2.23 (s, 9 H, NCH_3), 2.35 (s, 18 H, $\text{N}(\text{CH}_3)_2$), 2.27 - 2.80 (m, br, 24 H, piperazine), 3.22 (d, $^2J = 13.3$ Hz, 3 H, NCH_2), 3.30 (d, $^2J = 13.3$ Hz, 3 H, NCH_2), 3.33 (d, $^2J = 13.7$ Hz, 3 H, NCH_2), 3.43 (d, $^2J = 13.3$ Hz, 3 H, NCH_2), 5.28 (d, $^3J = 5.4$ Hz, 3 H, arene), 5.40 - 5.42 (m, 6 H, arene), 5.56 - 5.60 (m, 6 H, arene), 5.69 (d, $^3J = 6.3$ Hz, 3 H, pyridine), 6.51 (d, $^3J = 6.2$ Hz, 3 H, pyridine).

$^{13}\text{C}\{^1\text{H}\}$ NMR (CDCl_3 , 101 MHz): δ (ppm) = 45.7 ($\text{N}(\text{CH}_3)_2$), 46.2 (NCH_3), 50.9, 53.5, 55.5 (NCH_2 (piperazine)), 61.8 (NCH_2 (π -ligand)), 78.7, 79.9, 80.8, 83.9, 84.4, 94.9 (π -ligand), 111.2, 124.5, 131.8, 154.6, 170.5 (pyridine).

m/z (ESI) 1375.3773 ($\text{M} + \text{H}^+$. [$\text{C}_{60}\text{H}_{85}\text{N}_{12}\text{O}_6\text{Ru}_3$] $^+$ requires 1375.3790).

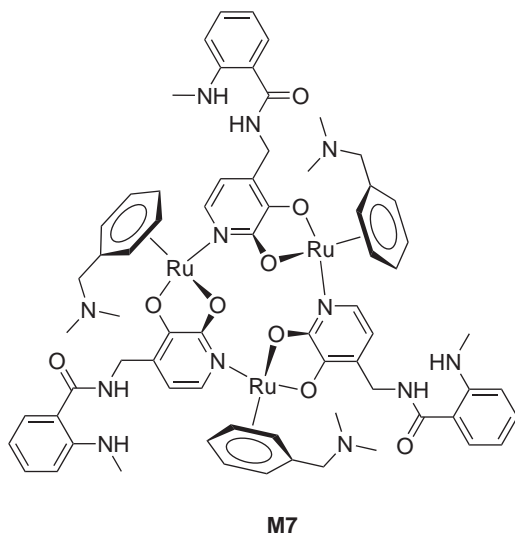
$[(\eta^6\text{-C}_6\text{H}_5\text{CH}_2\text{NMe}_2)\text{Ru}(\text{L5-2H}^+)]_3$ (M6**).**



Ligand **L5** (90.0 mg, 0.254 mmol, 2 equiv.), $[(\eta^6\text{-C}_6\text{H}_5\text{CH}_2\text{NMe}_2\text{H})\text{RuCl}_2]_2\text{Cl}_2$ (**C3**, 87.3 mg, 0.127 mmol) and CsOH (0.76 mL of a 1.0 M solution in MeOH, 0.76 mmol, 6 equiv.) were stirred in degassed methanol (20 mL) for 2 hours. The precipitate was filtered off, washed with cold MeOH, and dried under vacuum. The macrocycle **M6** was obtained as an orange powder (91 mg, 0.052 mmol, 61%). The compound was found to be insoluble in many solvents, except in hot benzene. [SR-C266(1)].

^1H NMR (C_6D_6 , 400 MHz): δ (ppm) = 2.01 (s, 18 H, $\text{N}(\text{CH}_3)_2$), 3.18 (d, $^2J = 14.1$ Hz, 3 H, NCH_2), 3.36 (d, $^2J = 13.3$ Hz, 3 H, NCH_2), 3.92 (s, 6 H, NCH_2), 4.16 (d, $^2J = 13.7$ Hz, 3 H, NCH_2), 4.23 (d, $^2J = 13.3$ Hz, 3 H, NCH_2), 4.98 (d, $^3J = 5.5$ Hz, 3 H, arene), 5.08 - 5.15 (m, 6 H, arene), 5.27 (d, $^3J = 5.5$ Hz, 3 H, arene), 5.47 (t, $^3J = 5.1$ Hz, 3 H, arene), 5.92 (d, $^3J = 5.8$ Hz, 3 H, pyridine), 7.00 (d, $^3J = 6.3$ Hz, 3 H, pyridine), 7.70 - 7.74 (m, 9 H, pyrene), 7.83 - 7.89 (m, 12 H, pyrene), 8.00 (d, $^3J = 7.8$ Hz, 3 H, pyrene), 8.26 (d, $^3J = 9.4$ Hz, 3 H, pyrene).

Elemental analysis (%) calcd (found) for $\text{C}_{96}\text{H}_{87}\text{N}_9\text{O}_6\text{Ru}_3 \times \text{MeOH}$: C 64.80 (64.82), H 5.10 (5.04), N 7.01 (6.93).

$$[(\eta^6\text{-C}_6\text{H}_5\text{CH}_2\text{NMe}_2)\text{Ru}(\text{L6-2H}^+)]_3 \text{ (M7)}.$$


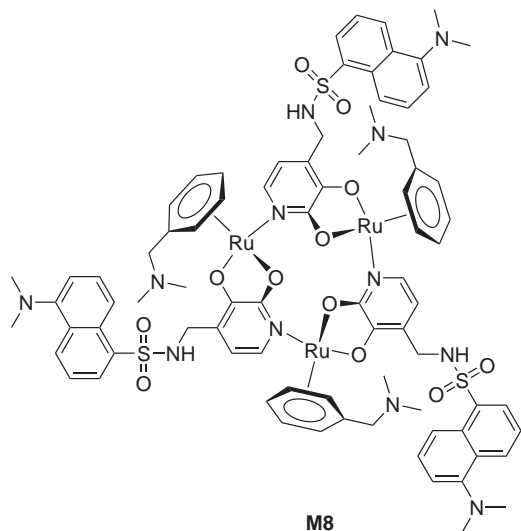
Ligand **L6** (200.0 mg, 0.732 mmol, 2 equiv.), $[(\eta^6\text{-C}_6\text{H}_5\text{CH}_2\text{NMe}_2\text{H})\text{RuCl}_2]_2\text{Cl}_2$ (**C3**, 252 mg, 0.366 mmol) and CsOH (3.7 mL of a 1.0 M solution in MeOH, 3.7 mmol, 10 equiv.) were stirred in degassed methanol (15 mL) for 4 hours. The solvent was evaporated under reduced pressure and the obtained solid was extracted with CH_2Cl_2 (2×15 mL). Hexane (60 mL) was added, and the volume of the solution was reduced to ca. 10 mL. The precipitate was filtered off, washed with hexane, and dried under vacuum. The macrocycle **M7** was obtained

as a red powder (190 mg, 0.125 mmol, 51%). [SR-B114(4)].

$^1\text{H NMR}$ (CDCl_3 , 400 MHz): δ (ppm) = 2.34 (s, 18 H, $\text{N}(\text{CH}_3)_2$), 2.84 (s, 9 H, NCH_3), 3.36 (d, $^2J = 13.2$ Hz, 3 H, NCH_2), 3.47 (d, $^2J = 13.2$ Hz, 3 H, NCH_2), 4.14 (d, $^2J = 15.2$ Hz, 3 H, NCH_2), 4.35 (d, $^2J = 15.2$ Hz, 3 H, NCH_2), 5.27 - 5.30 (m, 3 H, η^6 -arene), 5.41 - 5.53 (m, 15 H, η^6 -arene, pyridine), 6.49 (d, $^3J = 6.1$ Hz, 3 H, pyridine), 6.61 - 6.66 (m, 6 H, Ph), 7.31 (d, $^3J = 6.6$ Hz, 3 H, Ph), 7.47 (d, $^3J = 7.6$ Hz, 3 H, Ph), 7.59 (s, br, 3 H, PhNHCH_3), 8.14 (s, br, 3 H, CH_2NHCO).

$^{13}\text{C}\{^1\text{H}\}$ NMR (CDCl_3 , 101 MHz): δ (ppm) = 29.7 (NCH_3), 45.7, 45.8 ($\text{N}(\text{CH}_3)_2$), 61.5, 64.5 (NCH_2), 79.2, 80.6, 81.0, 83.5, 84.0, 94.8 (η^6 -arene), 111.2, 114.5, 124.0, 127.6, 128.4, 129.3, 132.0, 132.6, 150.6, 154.4, 169.5, 170.4 (pyridine, Ph, $\text{C}=\text{O}$).

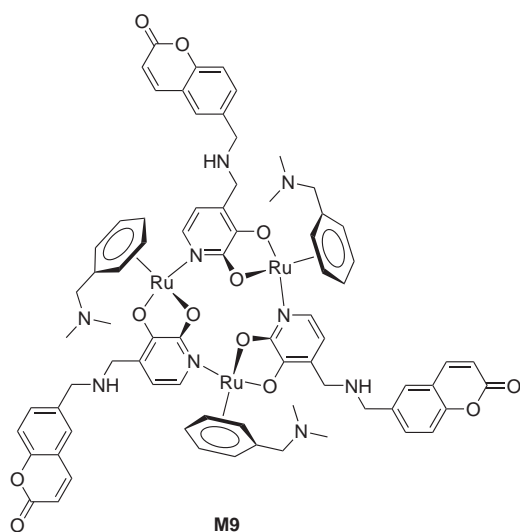
m/z (ESI) 509.0765 ($\text{M} + 3\text{H}^+$. [$\text{C}_{69}\text{H}_{81}\text{N}_{12}\text{O}_9\text{Ru}_3$] $^{3+}$ requires 509.1108).

$[(\eta^6\text{-C}_6\text{H}_5\text{CH}_2\text{NMe}_2)\text{Ru}(\text{L7-2H}^+)]_3$ (**M8**).


A mixture of ligand **L7** (100 mg, 0.268 mmol), $[(\eta^6\text{-C}_6\text{H}_5\text{CH}_2\text{NMe}_2\text{H})\text{RuCl}_2]_2\text{Cl}_2$ (92 mg, 0.134 mmol), and Cs_2CO_3 (329 mg, 1.01 mmol) in degassed methanol (15 mL) was stirred for 3 h. The solvent was removed under vacuum, and the solid residue was extracted with CH_2Cl_2 (2×15 mL). Hexane (60 mL) was added to the orange solution, and the volume was reduced to 30 mL under reduced pressure. The precipitate was filtered off, washed with hexane, and dried under vacuum. Yield: 129 mg (0.071 mmol, 79%). [SR-B125(4)].

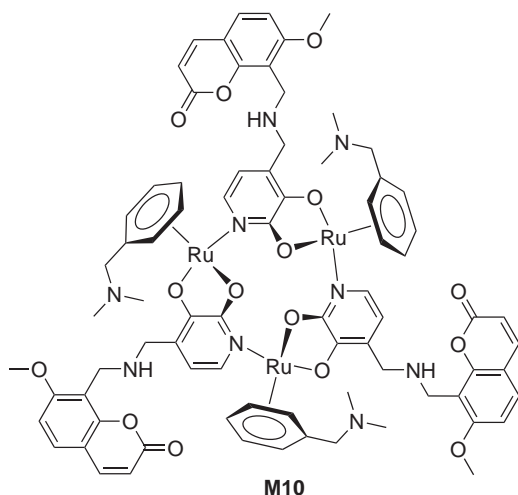
^1H NMR (MeOD, 400 MHz): δ (ppm) = 2.36 (s, 18 H, $\text{N}(\text{CH}_3)_2$), 2.89 (s, 18 H, $\text{N}(\text{CH}_3)_2$ (dansyl)), 3.35 (m, 6 H, NCH_2), 3.68 (s, 6 H, NCH_2), 5.40 – 5.53 (m, 15 H, arene and pyridine), 5.62 (t, $^3J = 5.5$ Hz, 3 H, arene), 6.20 (d, $^3J = 6.4$ Hz, 3 H, pyridine), 7.28 (d, $^3J = 7.3$ Hz, 3 H, dansyl), 7.52 (t, $^3J = 7.9$ Hz, 3 H, dansyl), 7.60 (t, $^3J = 8.1$ Hz, 3 H, dansyl), 8.13 (d, $^3J = 7.2$ Hz, 3 H, dansyl), 8.36 (d, $^3J = 8.8$ Hz, 3 H, dansyl), 8.55 (d, $^3J = 8.6$ Hz, 3 H, dansyl).

m/z (ESI) 912.6633 ($M + 2\text{H}^+$. [$\text{C}_{81}\text{H}_{92}\text{N}_{12}\text{O}_{12}\text{S}_3\text{Ru}_3$] $^{2+}$ requires 912.6647).

 $[(\eta^6\text{-C}_6\text{H}_5\text{CH}_2\text{NMe}_2)\text{Ru}(\text{L8-2H}^+)]_3$ (**M9**) - Attempted synthesis.


No pure product could be isolated, neither when the reaction was performed in MeOH in the presence of a base, nor in H_2O in the presence of a phosphate buffer. In the next section, the ^1H NMR spectrum corresponding to a solution of **M9** in buffered D_2O is given.

$[(\eta^6\text{-C}_6\text{H}_5\text{CH}_2\text{NMe}_2)\text{Ru}(\text{L10-2H}^+)]_3$ (**M10**).



A mixture of ligand **L10** (4.9 mg, 15 μmol , 2 equiv.), $[(\eta^6\text{-C}_6\text{H}_5\text{CH}_2\text{NMe}_2\text{H})\text{RuCl}_2]_2\text{Cl}_2$ (5.2 mg, 7.5 μmol) and Cs_2CO_3 (0.19 mL of a 0.3 M solution in MeOH, 57 μmol , 7.6 equiv.) in degassed MeOH (1 mL) was stirred for 3 h. The solvent was removed in vacuum, and the solid residue was extracted with CH_2Cl_2 (2×1 mL). Hexane (4 mL) was added to the orange solution, and the volume was reduced to ca. 0.5 mL. The precipitate was filtered off, washed with hexane, and dried under vacuum. Yield: 5.5 mg (3.3 μmol , 65%). [SR-C222(1)].

$^1\text{H NMR}$ (CDCl_3 , 400 MHz): δ (ppm) = 2.25 (s, 18 H, $\text{N}(\text{CH}_3)_2$), 3.18 (d, $^2J = 13.2$ Hz, 3 H, NCH_2), 3.25 (d, $^2J = 13.2$ Hz, 3 H, NCH_2), 3.35 (d, $^2J = 12.8$ Hz, 3 H, NCH_2), 3.51 (d, $^2J = 12.8$ Hz, 3 H, NCH_2), 3.81 (s, 9 H, OCH_3), 3.95 (d, $^2J = 12.4$ Hz, 3 H, NCH_2), 3.99 (d, $^2J = 12.4$ Hz, 3 H, NCH_2), 5.33 (d, $^3J = 4.8$ Hz, 3 H, arene), 5.40 (d, $^3J = 5.2$ Hz, 3 H, arene), 5.52 (d, $^3J = 6.0$ Hz, 3 H, pyridine), 5.63 (t, $^3J = 5.2$ Hz, 3 H, arene), 5.75 (t, $^3J = 5.0$ Hz, 3 H, arene), 6.16 (t, $^3J = 5.2$ Hz, 3 H, arene), 6.23 (d, $^3J = 9.6$ Hz, 3 H, pyridine), 6.46 (d, $^3J = 6.0$ Hz, 3 H, coumarin), 6.83 (d, $^3J = 8.4$ Hz, 3 H, coumarin), 7.35 (d, $^3J = 8.4$ Hz, 3 H, coumarin), 7.64 (d, $^3J = 9.6$ Hz, 3 H, coumarin).

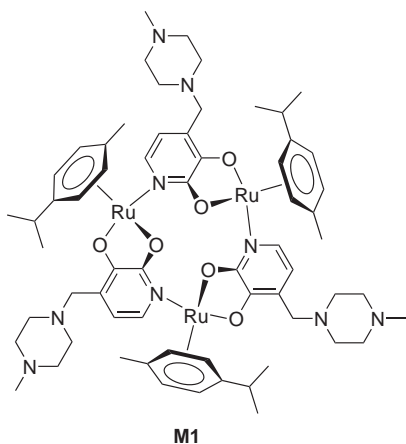
$^{13}\text{C}\{^1\text{H}\}$ NMR (D_2O pD 8.0, 101 MHz): δ (ppm) = 37.9 (NCH_2), 43.2, 43.4 ($\text{N}(\text{CH}_3)_2$), 45.5 (NCH_2), 56.9 (OCH_3), 60.1 (NCH_2), 80.0, 82.8, 84.1, 87.8, 106.5, 109.1 (arene), 111.3, 112.4, 113.4, 118.8, 129.9, 131.4, 132.2, 133.8, 146.3, 153.0, 154.4, 161.3, 163.0, 170.8 (coumarin, pyridine).

m/z (ESI) 845.1574 ($\text{M} + 2\text{H}^+$. $[\text{C}_{78}\text{H}_{83}\text{N}_9\text{O}_{15}\text{Ru}_3]^{2+}$ requires 845.1588).

Self-Assembly and LiCl Adducts of 12-Metallacrown-3 Complexes in Water

The macrocycles **M1**, **M4**, **M5**, **M9**, and **M10** are water soluble, and can be synthesized in water in the presence of a buffer, following this general procedure: appropriate amounts of $[(p\text{-cymene})\text{RuCl}_2]_2$ (**C2**, 4.6 mg, 7.5 μmol) or $[(\text{C}_6\text{H}_5\text{CH}_2\text{NHMe}_2)\text{RuCl}_2]_2\text{Cl}_2$ (**C3**, 5.2 mg, 7.5 μmol) and respective bridging ligand (15 μmol , 2 equiv.) were mixed for 2 hours in D_2O (100 mM phosphate buffer, pD 7.0 or 8.0), to afford solutions containing 5.0 mM of macrocycles (for experiments with lower receptor concentration (2.0 mM), the amounts of building blocks were varied accordingly). ^1H NMR spectra were recorded directly thereafter. LiCl adducts were obtained by adding an excess of LiCl (2 equiv.) to the solution during self-assembly of the macrocycle. They could be identified on ^1H NMR spectra, appearing slightly shifted relative to signals corresponding to empty macrocycles, and displaying broader peaks.

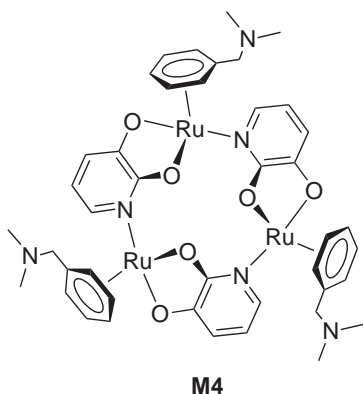
$[(p\text{-cymene})\text{Ru}(\text{L2-2H}^+)]_3$ (**M1**).



^1H NMR (D_2O , pD 7.0, phosphate buffer (100 mM), 400 MHz): δ (ppm) = 1.25 (d, $^3J = 6.8$ Hz, 9 H, $\text{CH}(\text{CH}_3)_2$), 1.28 (d, $^3J = 6.4$ Hz, 9 H, $\text{CH}(\text{CH}_3)_2$), 1.80 (s, 9 H, $\text{C}_6\text{H}_4\text{CH}_3$), 2.53 (s, 9 H, NCH_3), 2.55 - 3.00 (m, 27 H, NCH_2 (piperazine), $\text{CH}(\text{CH}_3)_2$), 3.33 (d, $^2J = 13.2$ Hz, 3 H, NCH_2), 3.66 (d, $^2J = 12.8$ Hz, 3 H, NCH_2), 5.23 (d, $^3J = 5.6$ Hz, 3 H, $\text{MeC}_6\text{H}_4^i\text{Pr}$), 5.48 (d, $^3J = 5.6$ Hz, 3 H, $\text{MeC}_6\text{H}_4^i\text{Pr}$), 5.76 - 5.79 (m, 6 H, $\text{MeC}_6\text{H}_4^i\text{Pr}$, pyridine), 6.03 (d, $^3J = 5.6$ Hz, 3 H, $\text{MeC}_6\text{H}_4^i\text{Pr}$), 6.65 (d, $^3J = 6.4$ Hz, 3 H, pyridine).

$[(p\text{-cymene})\text{Ru}(\text{L2-2H}^+)]_3 \times \text{LiCl}$ (**M1** \times **LiCl**).

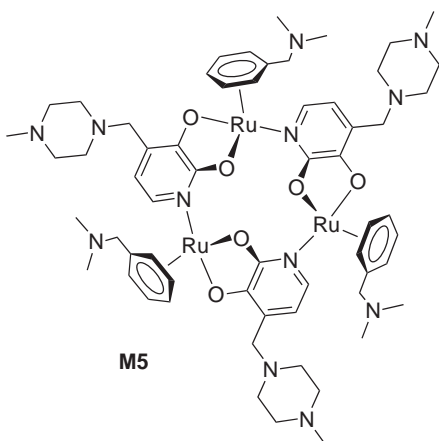
^1H NMR (D_2O , pD 7.0, phosphate buffer (100 mM), 400 MHz): δ (ppm) = 1.23 (d, $^3J = 7.2$ Hz, 9 H, $\text{CH}(\text{CH}_3)_2$), 1.27 (d, $^3J = 7.2$ Hz, 9 H, $\text{CH}(\text{CH}_3)_2$), 1.74 (s, 9 H, $\text{C}_6\text{H}_4\text{CH}_3$), 2.40 - 2.80 (m, 36 H, NCH_3 , NCH_2 (piperazine), $\text{CH}(\text{CH}_3)_2$), 3.33 (d, $^2J = 13.2$ Hz, 3 H, NCH_2), 3.58 (d, $^2J = 13.2$ Hz, 3 H, NCH_2), 5.23 (br, 3 H, $\text{MeC}_6\text{H}_4^i\text{Pr}$), 5.67 (d, $^3J = 5.6$ Hz, 3 H, $\text{MeC}_6\text{H}_4^i\text{Pr}$), 5.99 (d, $^3J = 6.0$ Hz, 3 H, $\text{MeC}_6\text{H}_4^i\text{Pr}$), 6.03 (d, $^3J = 6.8$ Hz, 3 H, pyridine), 6.15 (br, 3 H, $\text{MeC}_6\text{H}_4^i\text{Pr}$), 6.77 (d, $^3J = 6.0$ Hz, 3 H, pyridine).

$[(\eta^6\text{-C}_6\text{H}_5\text{CH}_2\text{NMe}_2)\text{Ru}(\text{L1-2H}^+)]_3$ (**M4**).


^1H NMR (D_2O , phosphate buffer (100 mM) pD 8.0, 400 MHz): δ (ppm) = 2.29 (s, 18 H, $\text{N}(\text{CH}_3)_2$), 3.05 (d, $^2J = 12.7$ Hz, 3 H, NCH_2), 3.18 (d, $^2J = 12.7$ Hz, 3 H, NCH_2), 5.42 (d, $^3J = 5.8$ Hz, 3 H, arene), 5.63 (t, $^3J = 5.5$ Hz, 3 H, arene), 5.70 (d, $^3J = 5.6$ Hz, 3 H, arene), 5.77 - 5.83 (m, 6 H, arene), 6.06 (t, $^3J = 5.6$ Hz, 3 H, pyridine), 6.23 (d, $^3J = 6.8$ Hz, 3 H, pyridine), 6.63 (d, $^3J = 5.9$ Hz, 3 H, pyridine). [SR-A74(1)].

 $[(\eta^6\text{-C}_6\text{H}_5\text{CH}_2\text{NMe}_2)\text{Ru}(\text{L1-2H}^+)]_3 \times \text{LiCl}$ (**M4** \times **LiCl**).

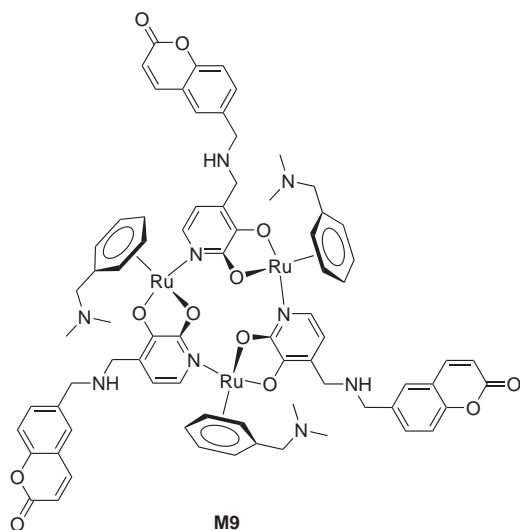
^1H NMR (D_2O , phosphate buffer (100 mM) pD 8.0, 400 MHz): δ (ppm) = 2.27 (s, 18 H, $\text{N}(\text{CH}_3)_2$), 2.91 (d, $^2J = 11.5$ Hz, 3 H, NCH_2), 3.06 (d, $^2J = 11.5$ Hz, 3 H, NCH_2), 5.53 (s, br, 3 H, arene), 5.77 (t, $^3J = 5.7$ Hz, 3 H, arene), 5.83 (s, 3 H, arene), 6.00 (t, $^3J = 6.7$ Hz, 3 H, arene), 6.05 (t, $^3J = 5.7$ Hz, 3 H, arene), 6.20 (s, br, 3 H, pyridine), 6.46 (d, $^3J = 7.1$ Hz, 3 H, pyridine), 6.73 (d, $^3J = 6.1$ Hz, 3 H, pyridine). [SR-A86(1)].

 $[(\eta^6\text{-C}_6\text{H}_5\text{CH}_2\text{NMe}_2)\text{Ru}(\text{L2-2H}^+)]_3$ (**M5**).


^1H NMR (D_2O , phosphate buffer (100 mM) pD 8.0, 400 MHz): δ (ppm) = 2.60 (s, 18 H, $\text{N}(\text{CH}_3)_2$), 2.67 (s, 9 H, NCH_3), 2.50 - 3.10 (m, br, 24 H, NCH_2 (piperazine)), 3.36 (d, $^2J = 13.2$ Hz, 3 H, NCH_2), 3.51 (s, 6 H, NCH_2), 3.60 (d, $^2J = 13.2$ Hz, 3 H, NCH_2), 5.67 (d, $^3J = 5.9$ Hz, 3 H, arene), 5.81 - 5.86 (m, 9 H, arene, pyridine), 5.92 (t, $^3J = 5.6$ Hz, 3 H, arene), 6.12 (t, $^3J = 5.7$ Hz, 3 H, arene), 6.62 (d, $^3J = 6.4$ Hz, 3 H, pyridine). [SR-A63(1)].

$[(\eta^6\text{-C}_6\text{H}_5\text{CH}_2\text{NMe}_2)\text{Ru}(\text{L2-2H}^+)]_3 \times \text{LiCl}$ (**M5** \times **LiCl**). In the presence of LiCl, the spectrum broadens considerably, leaving only a few peaks clearly identifiable. ^1H NMR (D_2O , phosphate buffer (100 mM) pD 8.0, 400 MHz): δ (ppm) = 2.25 - 3.30 (m, br, 39 H, CH_2 (piperazine), NCH_3 , NCH_2), 2.70 (s, 18 H, $\text{N}(\text{CH}_3)_2$), 3.39 (d, $^2J = 12.9$ Hz, 3 H, NCH_2), 3.61 (d, $^2J = 13.2$ Hz, 3 H, NCH_2), 5.55 - 6.20 (m, br, 12 H, arene), 6.07 (d, $^3J = 5.6$ Hz, 3 H, pyridine), 6.25 (t, $^3J = 5.4$ Hz, 3 H, arene), 6.76 (d, $^3J = 6.1$ Hz, 3 H, pyridine). [SR-A63(2)].

$[(\eta^6\text{-C}_6\text{H}_5\text{CH}_2\text{NMe}_2)\text{Ru}(\text{L8-2H}^+)]_3$ (**M9**).



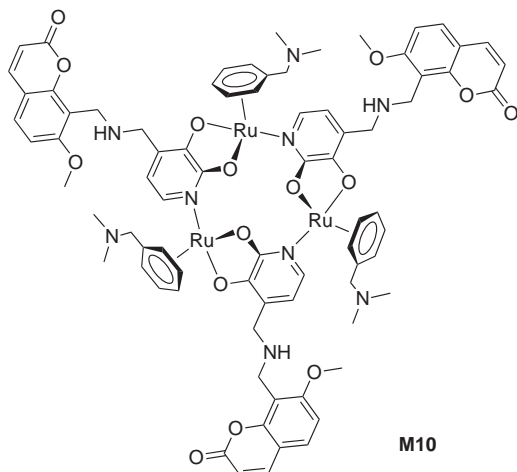
The spectrum contains characteristic signals indicating the formation of a macrocycle (such as diastereotopic protons) but contains many other signals, making a clear assignment difficult. The situation worsens in the presence of lithium.

$^1\text{H NMR}$ (D_2O , phosphate buffer (100 mM) pD 8.0, 400 MHz): δ (ppm) = 2.59 (s, 18 H, $\text{N}(\text{CH}_3)_2$), 3.32 (d, $^2J = 13.6$ Hz, 3 H, NCH_2), 3.52 (d, $^2J = 12.8$ Hz, 3 H, NCH_2), 3.58 (d, 2J

= 12.8 Hz, 3 H, NCH_2), 3.74 - 3.80 (m, 9 H, NCH_2), 5.61 - 5.95 (m, 15 H, arene, pyridine), 6.12 (m, 3 H, arene), 6.29 (d, $^3J = 9.2$ Hz, 3 H, coumarin), 6.72 (d, $^3J = 6.0$ Hz, 3 H, pyridine), 6.78 (s, br, 6 H, coumarin), 7.20 (s, 3 H, coumarin), 7.67 (d, $^3J = 9.6$ Hz, 3 H, coumarin). [SR-B168(3)].

$[(\eta^6\text{-C}_6\text{H}_5\text{CH}_2\text{NMe}_2)\text{Ru}(\text{L8-2H}^+)]_3 \times \text{LiCl}$ (**M9** \times **LiCl**). $^1\text{H NMR}$ (D_2O , phosphate buffer (100 mM) pD 8.0, 400 MHz): δ (ppm) = 2.57 (s, 18 H, $\text{N}(\text{CH}_3)_2$), 3.20 (d, $^2J = 13.6$ Hz, 3 H, NCH_2), 3.66 - 3.77 (m, 12 H, NCH_2), 3.87 (d, $^2J = 13.3$ Hz, 3 H, NCH_2), 5.65 - 6.27 (m, br, 21 H, arene, pyridine, coumarin), 6.70 (s, br, 6 H, coumarin), 6.86 (d, $^3J = 5.6$ Hz, 3 H, pyridine), 7.15 (s, 3 H, coumarin), 7.64 (d, $^3J = 9.6$ Hz, 3 H, coumarin). [SR-B168(3)].

$[(\eta^6\text{-C}_6\text{H}_5\text{CH}_2\text{NMe}_2)\text{Ru}(\text{L10-2H}^+)]_3$ (**M10**).



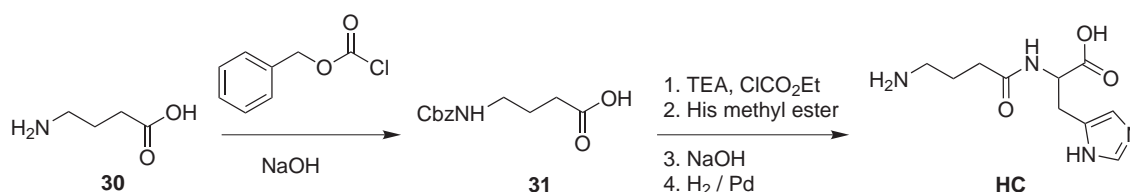
In absence of LiCl, the ^1H NMR spectrum contains well-defined signals with very few impurities. Upon addition of lithium, the peaks broaden and the spectrum becomes more difficult to interpret.

^1H NMR (D_2O , phosphate buffer (100 mM) pD 8.0, 400 MHz): δ (ppm) = 2.60 (s, 18 H, $\text{N}(\text{CH}_3)_2$), 3.59 - 3.64 (m, 6 H, NCH_2), 3.68 (s, 9 H, OCH_3), 3.77 - 4.02 (m, 12 H, NCH_2), 5.72 (d, $^3J = 5.6$ Hz, 3 H, arene), 5.83 - 5.90 (m, 9 H, arene), 5.94 (t, $^3J = 5.6$ Hz, 3 H,

arene), 6.06 - 6.11 (m, 6 H, arene, coumarin), 6.78 (d, $^3J = 6.4$ Hz, 3 H, pyridine), 6.89 (d, $^3J = 9.2$ Hz, 3 H, coumarin), 7.52 (d, $^3J = 8.8$ Hz, 3 H, coumarin), 7.76 (d, $^3J = 9.2$ Hz, 3 H, coumarin). [SR-C213(5)].

$[(\eta^6\text{-C}_6\text{H}_5\text{CH}_2\text{NMe}_2)\text{Ru}(\text{L10-2H}^+)]_3 \times \text{LiCl}$ (**M10** \times **LiCl**). ^1H NMR (D_2O , phosphate buffer (100 mM) pD 8.0, 400 MHz): δ (ppm) = 2.50 - 2.80 (m, br, 18 H, $\text{N}(\text{CH}_3)_2$), 3.50 - 4.05 (m, 18 H, NCH_2), 3.63 (s, 9 H, OCH_3), 5.60 - 6.20 (m, 21 H, arene, pyridine, coumarin), 6.87 (d, $^3J = 8.8$ Hz, 3 H, coumarin), 6.92 (d, $^3J = 6.4$ Hz, 3 H, pyridine), 7.50 (d, $^3J = 8.8$ Hz, 3 H, coumarin), 7.74 (d, $^3J = 9.6$ Hz, 3 H, coumarin). [SR-C213(5)].

7.2.4 Other Syntheses

Homocarnosine (HC)^[360]

Synthesis of N-carboxybenzyl-γ-aminobutyric acid (**31**):^[361, 362] 4-Aminobutyric acid (**30**, 5.20 g, 50 mmol) was dissolved in aqueous NaOH (25 mL, 2 M), and the mixture was cooled in an ice bath. A solution of benzyl chloroformate (7.5 mL, 50 mmol, 1 equiv.) in toluene (5.0 mL), and a solution of NaOH (4.0 M, 12.5 mL) were simultaneously added dropwise. After the addition was complete, the solution was stirred for further 10 minutes. The toluene layer was separated, and the aqueous phase was extracted with Et₂O (100 mL). The aqueous solution was cooled in an ice bath, and HCl (37% in H₂O) was slowly added to precipitate the product. The obtained solid was dissolved in hot ethyl acetate, filtered, and hexane was added. The solution was left overnight in a freezer, which resulted in the precipitation of the product. It was filtered off, washed with hexane, and dried under vacuum. Yield: 8.39 g (35.4 mmol, 71%). [SR-D382(1)].

¹H NMR (CDCl₃, 400 MHz): δ (ppm) = 1.75 (quint, ³J = 6.9 Hz, 2 H, CH₂CH₂CH₂), 2.31 (t, ³J = 7.2 Hz, 2 H, CH₂COOH), 3.17 (m, br, 2 H, CH₂NH), 4.85 (s, br, 1 H, NH), 5.01 (s, br, 2 H, OCH₂Ph), 7.21 - 7.27 (m, 5 H, Ph).

Synthesis of Homocarnosine sulfate: Cbz-4-aminobutyric acid (**31**, 5.93 g, 25 mmol) was suspended in CH₂Cl₂ (125 mL). Triethylamine (TEA) was added (3.5 mL, 25 mmol, 1 equiv.) and the mixture was cooled to -5°C in an CaCl₂/ice bath. To this solution was added ethyl chloroformate (2.4 mL, 25 mmol, 1 equiv.) followed, after 10 minutes, by cold CH₂Cl₂ (125 mL, 0°C) containing histidine methyl ester × 2 HCl (6.08 g, 25 mmol, 1 equiv.) and TEA (10.5 mL). The mixture was stirred at room temperature for 24 h. It was then washed with H₂O (200 mL), followed by aqueous NaHCO₃ (200 mL, 1 M) and dried over Na₂SO₄. Solvents were removed under reduced pressure, and the residue was solubilized in MeOH (50 mL), and aqueous NaOH (50 mL, 1 M) was added. The solution was stirred at room temperature for 3 h, acidified to pH 5 by addition of dilute H₂SO₄, and evaporated under reduced pressure. The residue was extracted with hot EtOH (2 × 50 mL), and H₂O (50 mL) was added to the extracts. Pd/C was added (0.5 g, 10% Pd), and the mixture was stirred under an atmosphere of dihydrogen for 9 h. When the reaction was complete, the mixture was filtered over Celite and evaporated

under reduced pressure. The residue was dissolved in H₂O, acidified to pH 3.0 (dilute H₂SO₄) and EtOH (200 mL) was added. The solution was left in a freezer for 72 h. The precipitate was filtered off and recrystallized from H₂O/EtOH to afford homocarnosine sulfate as a white solid. Yield: 5.40 g (16.0 mmol, 64%). [SR-D391(1)].

¹H NMR (D₂O, 400 MHz): δ (ppm) = 1.89 (quint, ³J = 7.6 Hz, 2 H, CH₂CH₂CH₂), 2.38 (t, ³J = 7.6 Hz, 2 H, CH₂CONH), 2.97 (t, ³J = 7.0 Hz, 2 H, CH₂NH₂), 3.16 (m, 1 H, CH₂CH), 3.33 (m, 1 H, CH₂CH), 4.71 (m, 1 H, CH₂CH), 7.31 (s, 1 H, CH, imidazole), 8.62 (s, 1 H, CH, imidazole).

¹³C{¹H} NMR (D₂O, 101 MHz): δ (ppm) = 23.4, 26.9 (CH₂, His- and γ-aminobutyryl side-chains) 32.7, 39.4 (CH₂, γ-aminobutyryl side-chain), 52.7 (CH, C^α), 117.8, 129.5, 134.7 (CH, imidazole), 174.5, 175.4 (C=O).

Elemental analysis (%) calcd (found) for C₁₀H₁₈N₄O₇S × 1/2 H₂O: C 34.58 (34.85), H 5.51 (5.45), N 16.13 (15.67).

7.3 Lithium Detection with Conjugate 12-Metallacrown-3 Complexes

7.3.1 NMR Studies for K_a Determination

General procedure for K_a determination by NMR measurements: 5.0 mM solutions of the respective macrocycles were prepared, either by dissolving the isolated compound in the appropriate deuterated solvent, or by *in situ* self-assembly in D_2O (pD 8.0, 100 mM phosphate). The solutions also contained 10.0 mM LiCl (2 equiv.) and were equilibrated for 2 h (when necessary, lower concentrations were employed, but there was always a twofold excess of Li^+ ions). The binding constants K_a were determined by integration of suited 1H NMR signals of the free and complexed receptor. When many baseline-resolved signals were available, their integration values were averaged and used for calculations.

In order to determine K_a , it is necessary to know the equilibrium concentrations of macrocycle $[M]$, $[Li^+]$, and adduct $[MLi^+]$:

$$K_a = \frac{[MLi^+]}{[M] \cdot [Li^+]} \quad (7.1)$$

The total concentrations of macrocycle and lithium are known from the experimental conditions:

$$[M]_{tot} = [M] + [MLi^+] \quad (7.2)$$

$$[Li^+]_{tot} = [Li^+] + [MLi^+] \quad (7.3)$$

The ratio R between the concentrations of adduct $[MLi^+]$ and macrocycle $[M]$ can be determined by analyzing the NMR integrations:

$$R = \frac{[MLi^+]}{[M]} \quad (7.4)$$

K_a can thus be expressed as a function of R :

$$K_a = \frac{R}{[Li^+]} \quad (7.5)$$

From Eq. 7.2, one can write:

$$\frac{[M]_{tot}}{[M]} = \frac{[M]}{[M]} + \frac{[MLi^+]}{[M]} \quad (7.6)$$

Therefore

$$[M] = \frac{[M]_{\text{tot}}}{R + 1} \quad (7.7)$$

Combining this expression with Eq. 7.2 gives:

$$[M_{\text{tot}}] = \frac{[M]_{\text{tot}}}{R + 1} + [MLi^+] \quad (7.8)$$

Therefore,

$$[MLi^+] = [M]_{\text{tot}} - \frac{[M]_{\text{tot}}}{R + 1} \quad (7.9)$$

Combining Eq. 7.9 and Eq. 7.3 gives:

$$[Li^+] = [Li^+]_{\text{tot}} - [M]_{\text{tot}} + \frac{[M]_{\text{tot}}}{R + 1} \quad (7.10)$$

K_a can be expressed by combining the latter equation with Eq. 7.5:

$$K_a = \frac{R}{[Li^+]_{\text{tot}} - [M]_{\text{tot}} + \frac{[M]_{\text{tot}}}{R + 1}} \quad (7.11)$$

7.3.2 Fluorescence Measurements

Measurements in Water/MeOH systems

For ^1H NMR measurements, macrocycle **M7** was dissolved in CD_3OD , and an equal volume of D_2O (containing 100 mM phosphate buffer, pH 7.0) was added. The final concentrations were $[\text{M7}] = 2.0$ mM, $[\text{phosphate}] = 50$ mM. Another solution was prepared similarly, which contained additional 2.0 equivalents (4.0 mM) of LiCl. Both solutions were stirred at room temperature for 2 h before fluorescence and NMR measurements were performed. [SR-B122(3)].

Macrocycles **M7** and **M8** were dissolved in MeOH, and H_2O (containing 100 mM phosphate buffer, pH 7.0) was added in the following quantities: 1:1 ratio for complex **M7**, final phosphate concentration: 50 mM; 10% v/v H_2O for complex **M8**, final phosphate concentration: 10 mM. Final volumes were 3.0 mL, and concentrations of macrocycles were 2.0 mM. Fluorescence spectra were recorded (**M7**: $\lambda_{\text{ex}} = 350$ nm, [SR-B122(3)]; **M8**: $\lambda_{\text{ex}} = 360$ nm, [SR-B132(5)]) 5 minutes after each addition of LiCl (μL amounts of a 1.0 M solution in MeOH).

Measurements in Water

Macrocycles **M9** and **M10** were synthesized in H₂O (pH 8.0, 100 mM phosphate buffer) and their fluorescence response was immediately studied. General procedure: A 2.0 mM solution of complex (**M9** or **M10**) was prepared in H₂O (pH 8.0, 100 mM phosphate buffer). The solution was filtered and an aliquot of 3.0 mL was placed in a cuvette for fluorescence measurements. The solution was stirred and its temperature equilibrated to 20°C. The fluorescence was measured (**M9**: $\lambda_{\text{ex}} = 495 \text{ nm}$, $\lambda_{\text{em}} = 523 \text{ nm}$, [SR-B170(6)]; **M10**: $\lambda_{\text{ex}} = 382 \text{ nm}$, $\lambda_{\text{em}} = 480 \text{ nm}$, [SR-C213(12)-(15)]) in a kinetic fashion every 4 seconds during one minute, or until the signal was stabilized. The solution was then titrated with μL amounts of a 1.10 M solution of LiCl (respectively NaCl or MgCl₂ for selectivity tests) in H₂O. After each addition, the solution was equilibrated as long as required (usually, 1 minute was enough), and fluorescence was recorded for one minute every 4 seconds (15 measurements that were averaged) before the next addition of analyte took place. The data were fitted with the non-linear least square curve-fitting program WinEQNMR^[293] using a 1:1 binding model to calculate the association constant $K_a(\text{Li}^+)$.

Measurements with Complex M10 in Human Serum

Serum preparation:^[294] 5.0 mL of HPLC-grade acetonitrile were added to 2.5 mL serum. The suspension was vigorously mixed for 5 min at room temperature, then centrifuged at 4000 rpm for 30 minutes. 6.0 mL of the supernatant were removed and lyophilized. The residue was dissolved in 2.0 mL H₂O (pH 8.0, 100 mM phosphate buffer) to obtain reconstituted serum.

Lithium titration in reconstituted serum: the reconstituted serum solution was filtered and 1.5 mL was added to 0.5 mL of a solution of the receptor **M10** (8.0 mM in H₂O pH 8.0, 100 mM phosphate buffer). The resulting mixture was equilibrated (as indicated by a stable fluorescence signal), and titrated with LiCl (μL doses of a 0.30 M stock solution) while fluorescence was recorded under the same conditions as in plain water. The final concentration of complex **M10** was 2.0 mM, whereas all serum constituents were diluted to 75% of their initial value. [SR-C242(7)].

7.4 Lithium Detection with Supramolecular Assays

7.4.1 Assay based on the HPTS Fluorophore

Buffers. Phosphate buffer (pH 7.0, 20 mM) was prepared by dissolution of appropriate amounts of KH_2PO_4 and K_2HPO_4 in bidistilled water. HEPES buffer (pH 7.0, 20 mM) was prepared by dissolving an appropriate amount of HEPES in bidistilled water, and the pH was adjusted to 7.0 by adding KOH.

Interaction between complex **M1 and HPTS:** In order to determine the association constant between complex **M1** and HPTS, fluorescence titration experiments were performed. A solution of complex **M1** (1.0 mM) was prepared *in situ* by mixing appropriate amounts of $[(p\text{-cymene})\text{RuCl}_2]_2$ (**C2**) and ligand **L2** in HEPES buffer (20 mM, pH 7.0). Aliquots of this solution were mixed with a solution of HPTS to prepare a series of solutions with a constant HPTS concentration of 50 μM and variable concentrations of complex **M1** (0 – 1000 μM). The fluorescence spectra ($\lambda_{\text{ex}} = 462 \text{ nm}$) were measured after equilibration for 16 h at room temperature. The titration data ($\lambda_{\text{em}} = 520 \text{ nm}$) were fitted to a 1:1 binding algorithm to give an association constant of $K_a = 3.4 (\pm 0.3) \cdot 10^4 \text{ M}^{-1}$. The data for the Job plot analysis were obtained by recording the fluorescence emission intensity at 520 nm ($\lambda_{\text{ex}} = 462 \text{ nm}$) of solutions (20 mM HEPES buffer, pH 7.0) containing different ratios of complex **M1** and HPTS and a constant total concentration of $[\text{complex } \mathbf{M1} + \text{HPTS}]_{\text{tot}} = 100 \mu\text{M}$. The solutions for the ^1H NMR spectra were prepared with buffered D_2O (20 mM phosphate buffer, pD = 7.0).

Assay in buffered water: Various amounts of a LiCl stock solution (100 mM) were added to a solution containing HPTS (final concentration = 0.5 mM), $[(p\text{-cymene})\text{RuCl}_2]_2$ (final concentration = 1.5 mM), and ligand **L2** (final concentration = 3.0 mM) in H_2O (100 mM HEPES buffer, pH 7.0). The fluorescence spectrum was measured ($\lambda_{\text{ex}} = 462 \text{ nm}$) after equilibration for 16 h at room temperature.

Assay in deproteinized serum: Preparation of reconstituted, deproteinized serum: HPLC-grade acetonitrile (30 mL) was added to serum (15 mL). The suspension was vigorously mixed for 5 min at room temperature, and then centrifuged at 4000 rpm for 30 min. 36 mL of the supernatant were removed and lyophilized. The residue was dissolved in 12 mL of HEPES buffer (100 mM, pH 7.0) and filtered through a 0.45 μm Millipore filter. Fluorescence measurements: reconstituted serum (1.5 mL) was added to 0.5 mL of a solution containing HPTS (final concentration = 0.5 mM), $[(p\text{-cymene})\text{RuCl}_2]_2$ (final concentration = 1.5 mM), ligand **L2** (final concentration = 3.0 mM), and LiCl (final concentration = 0 – 20 mM) in H_2O (100 mM HEPES buffer, pH 7.0).

The fluorescence spectrum was measured ($\lambda_{\text{ex}} = 462 \text{ nm}$) after equilibration for 16 h at room temperature.

7.4.2 Assay based on the Calcein Blue Fluorophore

General. The macrocycle **M1** was prepared as described in the section about synthesis of trimeric complexes (p. 123). Phosphate buffer (20 mM, pH 7.0) was prepared in bidistilled water and used for all experiments. Stock solutions of Calcein Blue (CAB) and metal salts were prepared in buffer and stored at 4°C. Solutions of macrocycle **M1** were freshly prepared in buffer prior to each experiment. Fluorescence measurements were recorded at 25°C. All NMR and UV/Vis spectra were recorded at room temperature.

Fluorescence titration of CAB by the macrocycle M1. A fixed amount of the dye and a variable amount of the complex (**M1**) were dissolved in buffered water (pH 7.0, 20 mM phosphate buffer). The final concentrations were $[\text{CAB}] = 30 \mu\text{M}$, and $[\text{Ru}] = 0 - 400 \mu\text{M}$. The solutions were equilibrated at room temperature for 24 h in the dark before measurement. The resulting fluorescence spectra were recorded with an excitation wavelength of 364 nm. The binding constant was obtained by fitting of the binding isotherm using a routine built in MATLAB which implements the Newton-Gauss non-linear least squares fitting algorithm.^[343-345] The minimum error of the binding constant was estimated to be 10%. [SR-E442(1)].

Detection of Li⁺. An aqueous solution (pH 7.0, 20 mM phosphate buffer) containing macrocycle **M1** (2.0 mM) in the presence of a definite amount of LiCl (0 – 20 mM) was stirred at room temperature. After 2 h, a 50 μL portion was poured into 2950 μL of a Calcein Blue solution in water (pH 7.0, 20 mM phosphate buffer). The final concentrations were $[\text{M1}] = 33.3 \mu\text{M}$, $[\text{CAB}] = 75 \mu\text{M}$ and the solution was stirred at room temperature for 5.5 h before fluorescence measurement was performed ($\lambda_{\text{ex}} = 364 \text{ nm}$). The fluorescence measurements need to be performed after a reaction time comprised between 5.5 and 6.5 hours in order to keep maximal accuracy [SR-E438(11)]. The apparent binding constant was obtained as indicated above. For selectivity experiments, LiCl was replaced by the appropriate chloride salts.

NMR measurements. Macrocycle **M1** was dissolved in D₂O at neutral pH (20 mM phosphate buffer, pH 7.0). The concentration was $[\text{M1}] = 4.0 \text{ mM}$. A second solution was prepared, which contained 2 equivalents of LiCl ($[\text{Li}^+] = 8.0 \text{ mM}$) in addition to

complex **M1**. Both solutions were equilibrated for 2 hours at room temperature under an atmosphere of dinitrogen. An equivalent volume of a Calcein Blue solution (12 mM in 20 mM phosphate buffer, pH 7.0) was then added to the solutions of **M1**. ^1H NMR measurements were performed directly after the solutions were mixed, and pursued at regular time intervals for 12 hours. The concentrations at $t = 0$ min were: [**M1**] (or [**M1** + Li^+]) = 2.0 mM; [CAB] = 6.0 mM. [SR-E438].

UV/Vis measurements. UV/Vis measurements were performed in the same fashion as the fluorescence measurements described above: An aqueous solution (pH 7.0, 20 mM phosphate buffer) containing macrocycle **M1** (2.0 mM) in the presence of a definite amount of LiCl (0 or 20 mM) was stirred at room temperature. After 2 h, a 50 μL portion was poured into 2950 μL of a Calcein Blue solution in water (pH 7.0, 20 mM phosphate buffer). The final concentrations were [**M1**] or [**M1** + Li^+] = 33.3 μM , [CAB] = 75 μM . UV/Vis measurements were started immediately, and performed at regular intervals during 10 hours in the range 250 - 600 nm.

7.5 Sensor Arrays for Small Peptides

7.5.1 General

Homocarnosine (HC) and the metal complexes $[\text{Cp}^*\text{RhCl}_2]_2$ (C1), $[(p\text{-cymene})\text{RuCl}_2]_2$ (C2) and $[(\text{en})\text{PdCl}_2]$ (C4) were prepared as described in the Syntheses section (p. 110). Phosphate buffer (100 mM, pH 7.0) was prepared with bidistilled H_2O and used for all experiments. Stock solutions of dyes, metal complexes, and peptides were prepared in buffer and stored at 4°C . Fluorescence measurements were recorded at 25°C .

7.5.2 Metal/Dye Titrations

Fluorescence titration experiments were performed in buffered aqueous solution (100 mM phosphate buffer, pH 7.0) with a fixed amount of the dye and a variable amount of the metal complex (Table 7.1). The solutions were equilibrated at room temperature for 48 h in the dark before measurement. The binding constants were obtained by fitting of the binding isotherm using a routine built in MATLAB which implements the Newton-Gauss non-linear least squares fitting algorithm.^[343-345] The minimum error of the binding constants was estimated to be 10%. [SR-C262, C269, C272, C276, D302, D303, D304, E407].

Table 7.1 – Concentrations of dyes and organometallic complexes for titration experiments.

Fluorescent Dye	Metal	Fluorescent Dye [μM]	Metal [μM]
CAL	Rh	25	0 - 40
CAB	Rh	2.5	0-20
MCB	Rh	25	0 - 200
NFR	Rh	25	0 - 500
CAL	Ru	25	0 - 40
CAB	Ru	25	0 - 40
MCB	Ru	25	0 - 200
NFR	Ru	50	0 - 200
CAL	Pd	25	0 - 400
CAB	Pd	25	0 - 400
MCB	Pd	25	0 - 400
NFR	Pd	25	0 - 125
LUM	Pd	25	0 - 600
MAA	Pd	25	0 - 5000

7.5.3 Fluorescence Assays with Dipeptides

Stock solutions of the respective dipeptide and the dye were diluted with buffered water. The fluorescence signal was measured in a time-resolved fashion at the maximum emission intensity until it stabilized; this ensured the homogeneity and thermal stability of the solution. The reaction was then started by adding a stock solution of the respective metal complex. The final volume was 3.0 mL; the final concentrations were: [dipeptide] = 50 or 20 μM , [dye] = 25 μM , [metal] = 25 μM , [phosphate buffer] = 100 mM. Each of the ten dipeptides was treated with each of the 14 metal–dye combinations indicated in Table 7.1, and a blank (with no peptide) was also recorded. The experiments were repeated four times (when [dipeptide] = 50 μM or for the blank) or six times (when [dipeptide] = 20 μM), totalling 784 experiments. Fluorescence intensities that were recorded 5, 20, and 60 min after addition of the metal complex were used for multivariate analyses. [SR-C282-C293, D309-D379].

Reduced sensor array: The component loading to factor 1 (PC1) of the three measurements at 4, 20 and 60 min of each metal–dye mixture were combined, thus affording fourteen contributions. A comparison of the resulting values allowed us to identify the six metal–dye combinations that contribute most significantly to the discriminating power: Pd/NFR, Pd/CAB, Rh/NFR, Rh/CAL, Pd/MCB and Rh/CAB. Fluorescence data obtained from these six combinations in the presence of various dipeptides were used for multivariate analyses.

7.5.4 Fluorescence Assays with Bradykinin (BK) and Kallidin (KD)

Sensor subset determination: A selection was performed by comparing the fluorescence signals obtained when a metal complex stock solution was added to a solution containing the respective peptide (BK or KD) and dye. The final concentrations were: [metal] = 10 μM , [dye] = 10 μM (for the cases in which the metal was Rh or Ru), [metal] = 20 μM , [dye] = 20 μM (for the cases where the metal was Pd) and [peptide] = 50 μM in a phosphate buffer (100 mM).

These concentrations were experimentally determined, and are explainable according to two conditions: a) the weak affinity of the peptides to the metal receptors led to the use of an excess of peptide; b) in order to obtain exploitable kinetic data, higher concentrations were necessary for the Pd-based sensors than for the Rh- or Ru-based ones (Pd binds dyes with lower equilibrium constants than Rh or Ru). Each experiment was monitored by fluorescence spectroscopy, and for every metal–dye combination, the intensity difference between mixtures containing KD or BK was calculated after 5,

30 and 60 minutes of reaction time. The results were summed up for each metal-dye combination, allowing an estimation of how good any metal-dye combination is for the discrimination of KD from BK. The results are shown in Figure 7.1. The five metal-dye combinations displaying the biggest differences were chosen for subsequent analyses, whereas Rh/NFR was eliminated because it was displaying constant signals over time. Rh/CAL was utilized instead as the sixth combination.

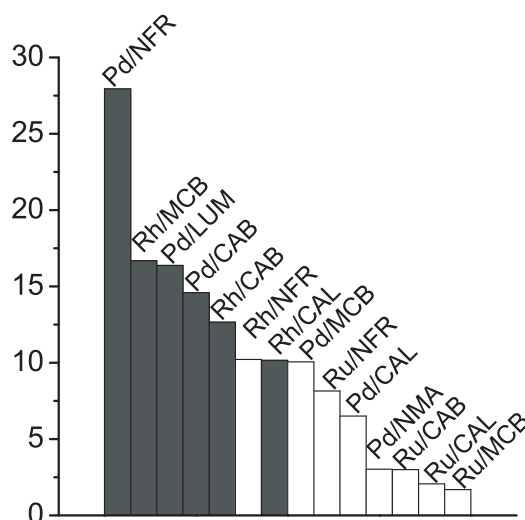


Figure 7.1 – Differences in the fluorescence responses between reactions involving bradykinin or kallidin together with the indicated metal-dye combinations: the values (in percent) were obtained by addition of the fluorescence differences recorded after 5, 30 and 60 minutes of reaction time. The combinations, which were selected for the differentiation experiments are shown in grey.

Differentiation of mixtures of KD and BK: Stock solutions of the peptides and the dyes were diluted with buffered H₂O. The fluorescence signal was measured in a time-resolved fashion at its maximum emission intensity until it stabilized; this ensured the homogeneity and thermal stability of the solution. The reaction was then started by adding a solution of the respective metal complex. The final volume was 3.0 mL; the final concentrations were: [total peptide] = 50 μM, [phosphate buffer] = 100 mM; when the metal complex was Rh: [dye] = [Rh] = 10 μM; when the metal receptor was Pd: [dye] = [Pd] = 20 μM. Six mixtures containing different KD/BK ratios (100:0; 80:20; 60:40; 40:60; 20:80; 0:100) and a blank were measured with the six metal-dye combinations indicated above. Each reaction was repeated four times, totalling to 168 experiments. The fluorescence intensities were recorded 2.5, 5, and 10 min after the reaction was initiated when Rh was the receptor, and after 40, 50, and 60 min when Pd was the receptor. These data were used as input values for multivariate analyses. [SR-E410-E429].

7.5.5 Fluorescence Assays with Carnosine and Homocarnosine

Serum preprocessing: Two volumes of HPLC-grade MeCN were added to one volume of serum. The mixture was vigorously shaken for 5 min at room temperature, then centrifuged for 30 min at 4000 rpm. The supernatant was removed, filtered, and stored at 4°C.

Fluorescence measurements: The six metal–dye combinations, which were successfully used for the differentiation of the ten dipeptides, were employed again (*i.e.*, Pd/NFR, Pd/CAB, Rh/NFR, Rh/CAL, Pd/MCB and Rh/CAB). Stock solutions of the respective peptide and the dye were added to a mixture of serum (prepared as described above) and buffer. The fluorescence signal was measured in a time-resolved fashion at its maximum emission intensity until it was stabilized; this ensured the homogeneity and thermal stability of the solution. The reaction was then started by adding a solution of the respective metal complex. The final volume was 3.0 mL and contained 25% serum, 50% MeCN, and 25% buffered H₂O. The final concentrations were: [peptide] = 25, 50, 75 or 100 μM, [dye] = 25 μM, [phosphate buffer] = 25 mM. The final metal concentration was 500 μM for Pd/NFR, Pd/CAB, Rh/NFR and Rh/CAL mixtures, 300 μM for Pd/MCB mixtures, and 200 μM for Rh/CAB mixtures. Four different concentrations of each dipeptide were reacted with each of the six metal–dye combinations indicated above, and a blank (with no peptide) was also recorded. The experiments were repeated four times, totalling to 216 experiments. The fluorescence intensities that were recorded 5, 20, and 60 min after the reaction was initiated were used for multivariate analyses. [SR-E398-E406].

7.5.6 Data Processing

The fluorescence data, recorded after given reaction times (indicated above for each system) at the emission maxima (Table 4.2, p. 75), were normalized relative to the fluorescence intensity measured before addition of the metal complex (*i. e.*, before quenching occurs). The multivariate analyses (LDA and PCA) were performed with the help of the SYSTAT software package (version 11).^[342]

7.6 Sensor Arrays versus Dynamic Combinatorial Libraries

7.6.1 General

Stock solution of CHES buffer (286 mM, pH 8.4) was prepared with bidistilled H₂O and used for all experiments (the pH was adjusted by addition of NaOH). Stock solutions of dyes (MCB: 0.60 mM; AI: 0.30 mM; XO: 0.15 mM), metal salts (NiCl₂: 1.0 mM; CuCl₂: 1.0 mM), and peptides (5.0 mM) were prepared in plain water and stored at 4°C. UV/Vis measurements were performed at room temperature.

7.6.2 Sensing of Peptides with DCL Sensors

Aliquots of stock solutions of Methylcalcein Blue (83.3 μL), Arsenazo I (83.3 μL), Xylenol Orange (83.3 μL), CuCl₂ (100 μL), NiCl₂ (100 μL), CHES buffer (350 μL), and the respective peptide (200 μL) were mixed in a UV/Vis cuvette. The final concentrations were [MCB] = 50 μM, [AI] = 25 μM, [XO] = 12.5 μM, [NiCl₂] = [CuCl₂] = 100 μM, [peptide] = 1.0 mM, and [CHES] = 100 mM, and the final volume was 1.0 mL. The solution was equilibrated for 30 min at 60°C, cooled to room temperature, and its UV/Vis spectrum was recorded between 332 and 700 nm. The experiment was repeated 10 times for each peptide. An analogous procedure was employed for DCL sensors of reduced complexity (smaller number of dyes and/or metal complexes). In these cases, the library components to be omitted were replaced by bidistilled water. [SR-E443-E582, F583-F736].

Data Analysis

The UV/Vis data obtained for each DCL sensor were analyzed as follows: For each measurement, 93 data points (absorbance values in the region $\lambda = 332 - 700$ nm, with intervals of 4.0 nm) were used as input. To determine the wavelengths, which contribute most to the differentiation of the peptides, a variable selection algorithm was applied. Six wavelengths were selected for each data set. The selected variables were then utilized to calculate the LDA classification functions and to generate the score plots. The commercial software package Systat^[342] (version 11) was employed for the variable selections, the linear discriminant analyses, and the calculation of the *F*-values.

7.6.3 Sensing of Peptides with the Sensor Array

First, we have determined the wavelengths, at which the largest spectral changes occurred for each metal-dye combination. For that purpose, the UV/Vis spectra of buffered aqueous solutions containing the free dye were compared with the spectra of solutions containing a mixture of MCl_2 (100 μM) and the dye (50 μM for MCB, 25 μM for Al, or 12.5 μM for XO). The largest differences were observed at the following wavelengths: MCB/Cu: 372 nm, Al/Cu: 492 nm, XO/Cu: 584 nm, MCB/Ni: 376 nm, Al/Ni: 532 nm, and XO/Ni: 592 nm. The assays were carried out in a similar manner as the measurements with the DCL sensors: mixtures of the respective dye (50 μM for MCB, 25 μM for Al, or 12.5 μM for XO), metal chloride (100 μM), and peptide (1.0 mM) in water (pH 8.4, CHES buffer) were heated at 60°C for 30 min. After cooling to room temperature, UV/Vis measurements were performed (10 independent measurements for each peptide).

Data Analysis

The six individual sensors were analyzed at the wavelengths given above. The absorbances for the $2 \times 3 \times 13$ metal-dye-peptide combinations (10 replicates per combination) were used as input to calculate the LDA classification functions with Systat.^[342]

A

Cross-Reactive Sensor Arrays for
the Detection of Peptides in
Aqueous Solution by
Fluorescence Spectroscopy

A.1 Fluorescence Titration Experiments

Fluorescence titration data for the Rh complex and Calcein

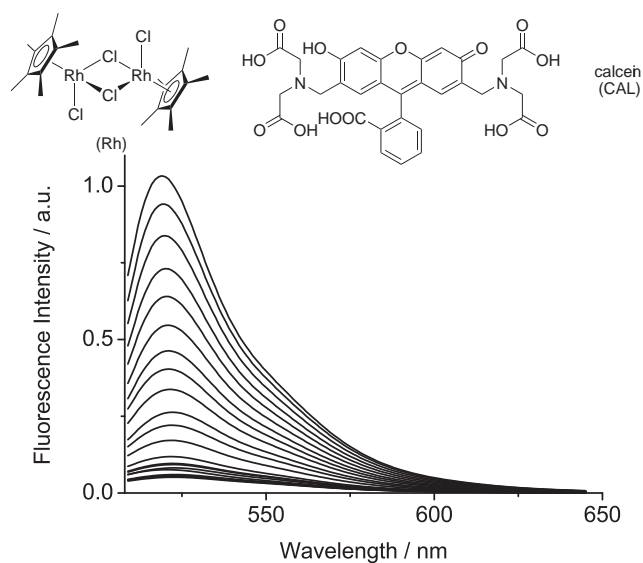


Figure A.1 – Fluorescence emission spectra of a solution of Calcein (25 μM) upon addition of complex $[\text{Cp}^*\text{RhCl}_2]_2$ ($[\text{Rh}] = 0 - 40 \mu\text{M}$). The excitation wavelength was 493 nm. The spectra were recorded in H_2O (100 mM phosphate buffer, pH 7.0) after equilibration for two days in the dark.

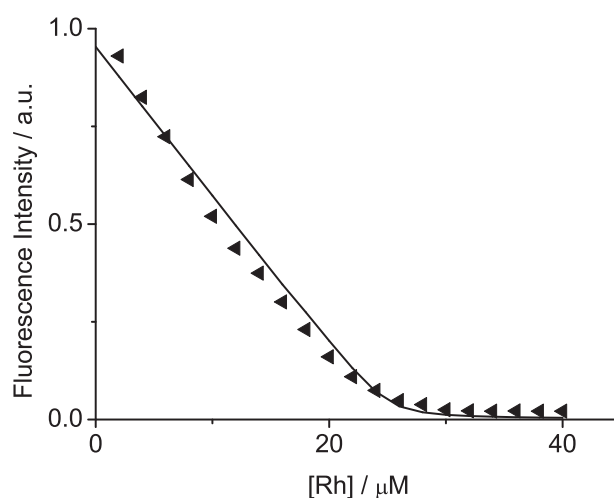


Figure A.2 – Fluorescence emission intensity at 520 nm of a solution of Calcein (25 μM) upon addition of complex $[\text{Cp}^*\text{RhCl}_2]_2$ ($[\text{Rh}] = 0 - 40 \mu\text{M}$). The curve was obtained by fitting the data to a 1:1 binding model ($K_1 = 7.6 (\pm 0.8) \cdot 10^6 \text{ M}^{-1}$).

Fluorescence titration data for the Rh complex and Calcein Blue

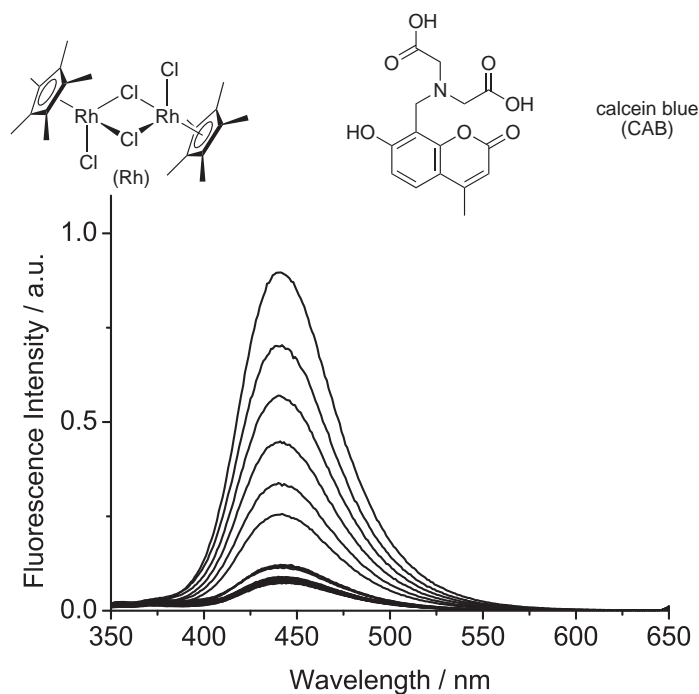


Figure A.3 – Fluorescence emission spectra of a solution of Calcein Blue (2.5 μM) upon addition of complex [Cp*RhCl₂]₂ ([Rh] = 0 – 20 μM). The excitation wavelength was 336 nm. The spectra were recorded in H₂O (100 mM phosphate buffer, pH 7.0) after equilibration for two days in the dark.

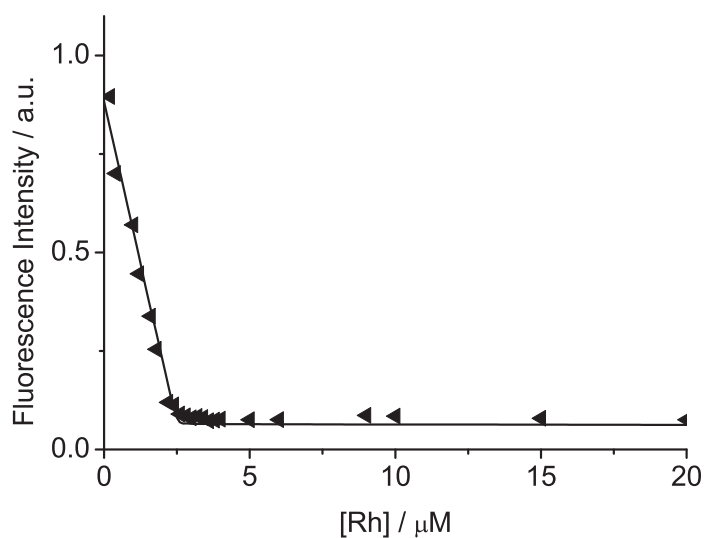


Figure A.4 – Fluorescence emission intensity at 440 nm of a solution of Calcein Blue (2.5 μM) upon addition of complex [Cp*RhCl₂]₂ ([Rh] = 0 – 20 μM). The curve was obtained by fitting the data to a 1:1 binding model ($K_1 = 1.3 (\pm 0.5) \cdot 10^9 \text{ M}^{-1}$).

Fluorescence titration data for the Rh complex and Methylcalcein Blue

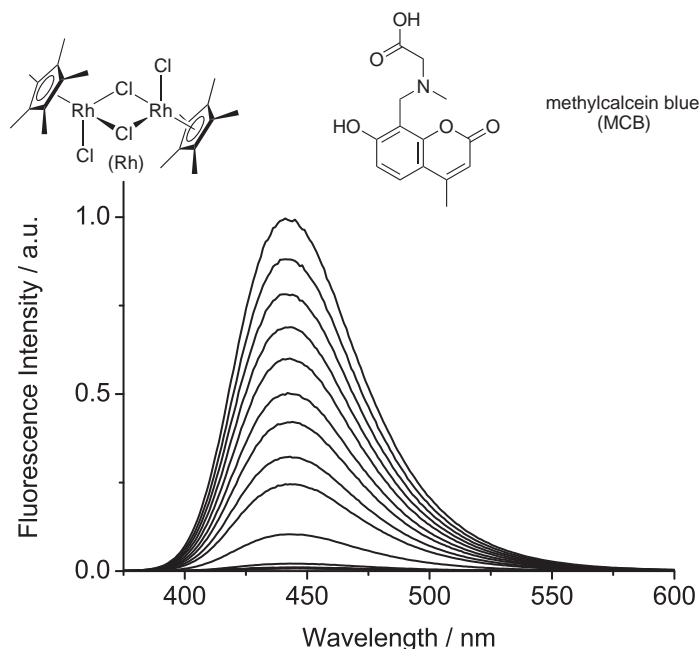


Figure A.5 – Fluorescence emission spectra of a solution of Methylcalcein Blue (25 μM) upon addition of complex $[\text{Cp}^*\text{RhCl}_2]_2$ ($[\text{Rh}] = 0 - 200 \mu\text{M}$). The excitation wavelength was 363 nm. The spectra were recorded in H_2O (100 mM phosphate buffer, pH 7.0) after equilibration for two days in the dark.

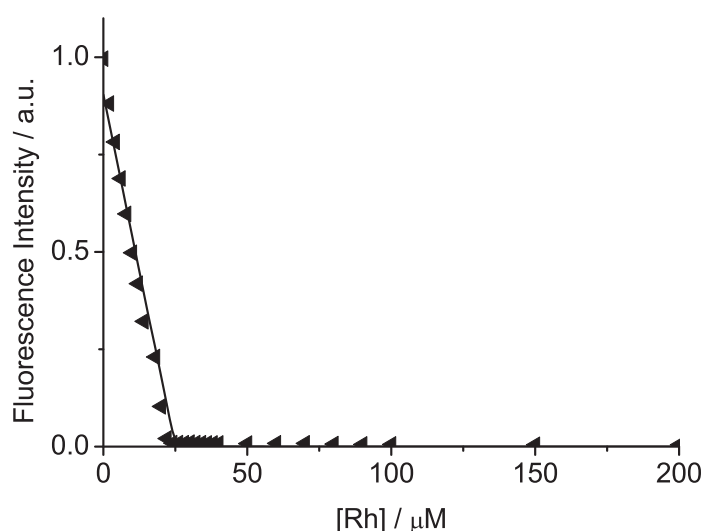


Figure A.6 – Fluorescence emission intensity at 445 nm of a solution of Methylcalcein Blue (25 μM) upon addition of complex $[\text{Cp}^*\text{RhCl}_2]_2$ ($[\text{Rh}] = 0 - 200 \mu\text{M}$). The curve was obtained by fitting the data to a 1:1 binding model ($K_1 = 1.8 (\pm 0.8) \cdot 10^8 \text{ M}^{-1}$).

Fluorescence titration data for the Rh complex and Nuclear Fast Red

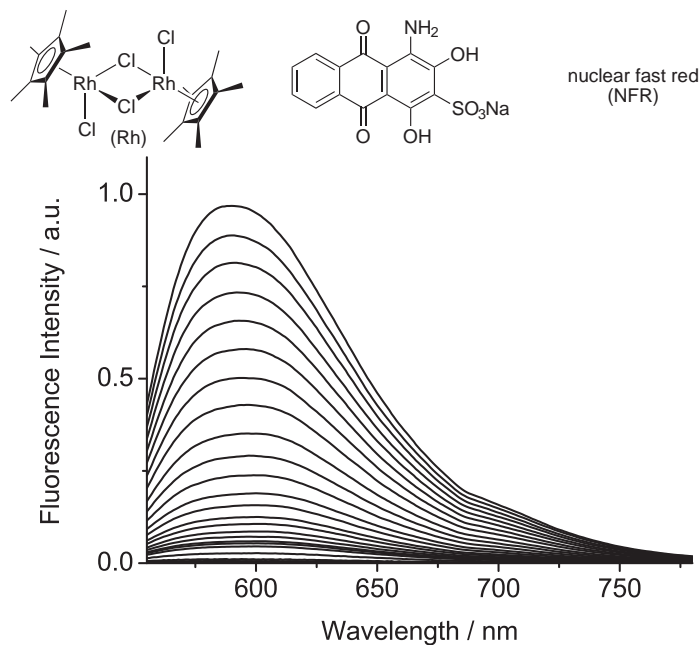


Figure A.7 – Fluorescence emission spectra of a solution of Nuclear Fast Red (25 μM) upon addition of complex $[\text{Cp}^*\text{RhCl}_2]_2$ ($[\text{Rh}] = 0 - 500 \mu\text{M}$). The excitation wavelength was 540 nm. The spectra were recorded in H_2O (100 mM phosphate buffer, pH 7.0) after equilibration for two days in the dark.

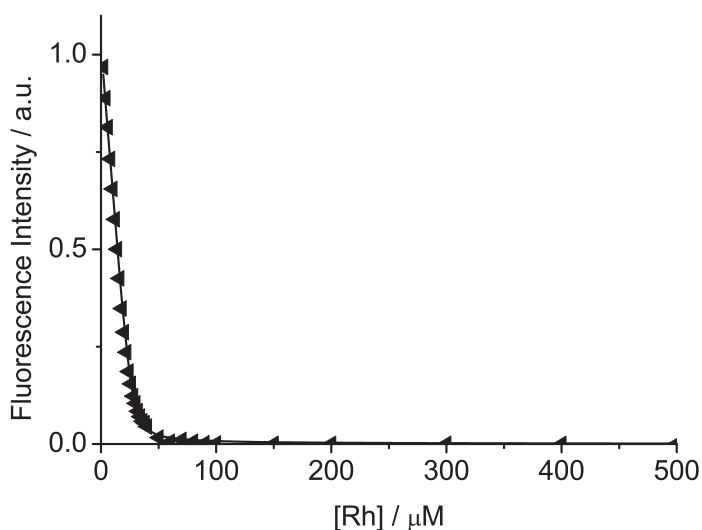


Figure A.8 – Fluorescence emission intensity at 590 nm of a solution of Nuclear Fast Red (25 μM) upon addition of complex $[\text{Cp}^*\text{RhCl}_2]_2$ ($[\text{Rh}] = 0 - 500 \mu\text{M}$). The curve was obtained by fitting the data to a 1:1 binding model ($K_1 = 1.6 (\pm 0.2) \cdot 10^6 \text{ M}^{-1}$).

Fluorescence titration data for the Ru complex and Calcein

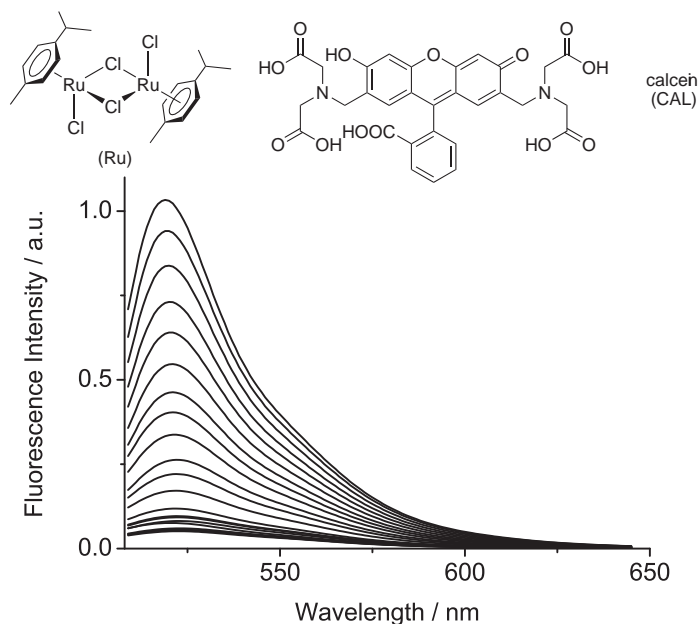


Figure A.9 – Fluorescence emission spectra of a solution of Calcein (25 μM) upon addition of complex $[(p\text{-cymene})\text{RuCl}_2]_2$ ($[\text{Ru}] = 0 - 40 \mu\text{M}$). The excitation wavelength was 493 nm. The spectra were recorded in H_2O (100 mM phosphate buffer, pH 7.0) after equilibration for two days in the dark.

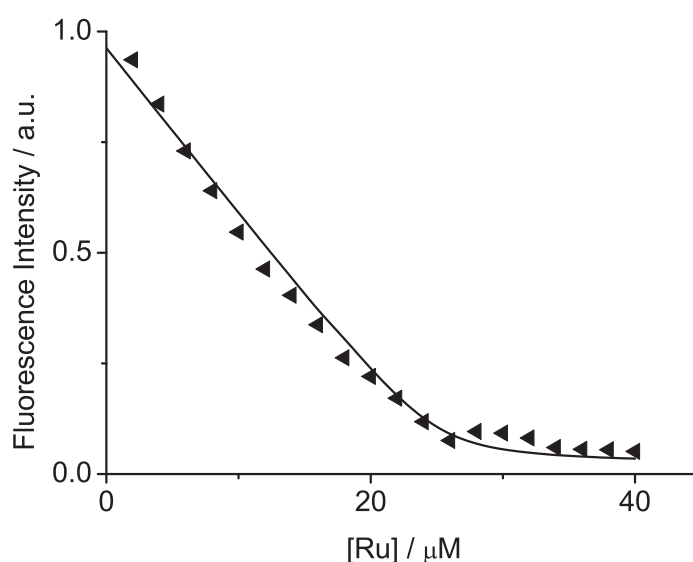


Figure A.10 – Fluorescence emission intensity at 520 nm of a solution of Calcein (25 μM) upon addition of complex $[(p\text{-cymene})\text{RuCl}_2]_2$ ($[\text{Ru}] = 0 - 40 \mu\text{M}$). The curve was obtained by fitting the data to a 1:1 binding model ($K_1 = 1.9 (\pm 0.2) \cdot 10^6 \text{ M}^{-1}$).

Fluorescence titration data for the Ru complex and Calcein Blue

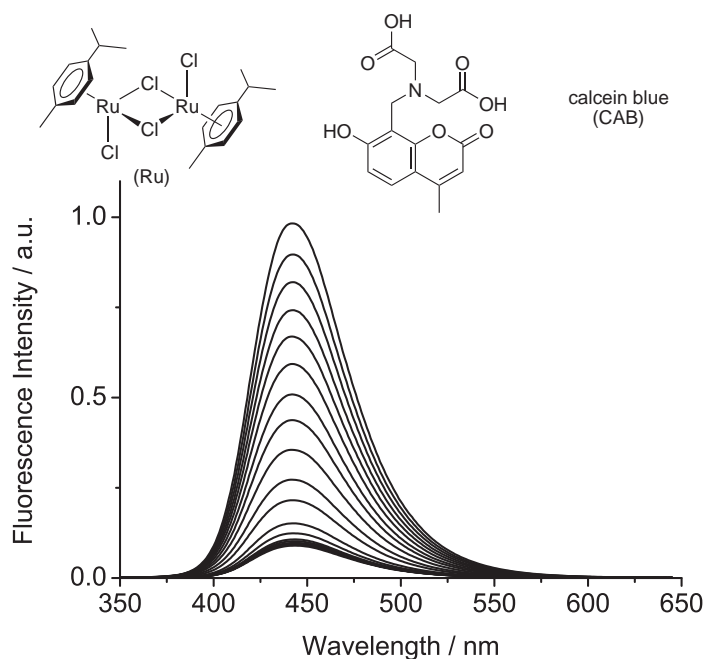


Figure A.11 – Fluorescence emission spectra of a solution of Calcein Blue ($25 \mu\text{M}$) upon addition of complex $[(p\text{-cymene})\text{RuCl}_2]_2$ ($[\text{Ru}] = 0 - 40 \mu\text{M}$). The excitation wavelength was 336 nm . The spectra were recorded in H_2O (100 mM phosphate buffer, $\text{pH } 7.0$) after equilibration for two days in the dark.

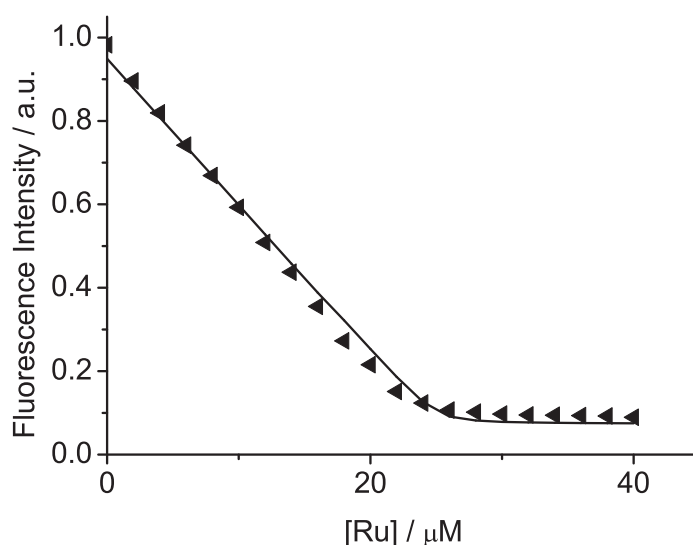


Figure A.12 – Fluorescence emission intensity at 440 nm of a solution of Calcein Blue ($25 \mu\text{M}$) upon addition of complex $[(p\text{-cymene})\text{RuCl}_2]_2$ ($[\text{Ru}] = 0 - 40 \mu\text{M}$). The curve was obtained by fitting the data to a 1:1 binding model ($K_1 = 1.6 (\pm 0.2) \cdot 10^6 \text{ M}^{-1}$).

Fluorescence titration data for the Ru complex and Methylcalcein Blue

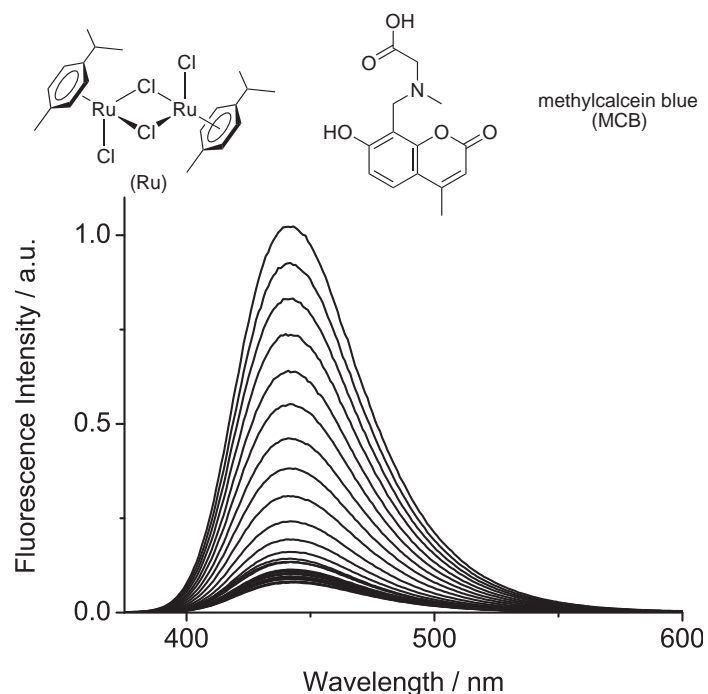


Figure A.13 – Fluorescence emission spectra of a solution of Methylcalcein Blue (25 μM) upon addition of complex $[(p\text{-cymene})\text{RuCl}_2]_2$ ($[\text{Ru}] = 0 - 200 \mu\text{M}$). The excitation wavelength was 363 nm. The spectra were recorded in H_2O (100 mM phosphate buffer, pH 7.0) after equilibration for two days in the dark.

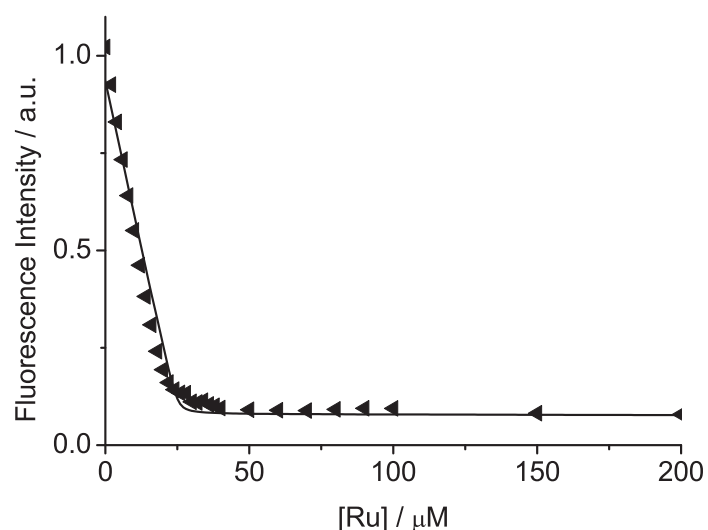


Figure A.14 – Fluorescence emission intensity at 445 nm of a solution of Methylcalcein Blue (25 μM) upon addition of complex $[(p\text{-cymene})\text{RuCl}_2]_2$ ($[\text{Ru}] = 0 - 200 \mu\text{M}$). The curve was obtained by fitting the data to a 1:1 binding model ($K_1 = 1.8 (\pm 0.2) \cdot 10^7 \text{ M}^{-1}$).

Fluorescence titration data for the Ru complex and Nuclear Fast Red

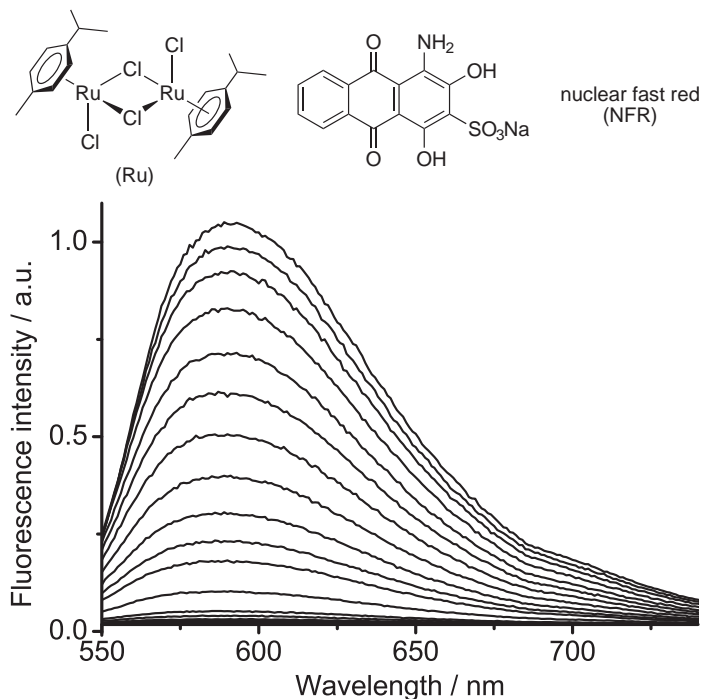


Figure A.15 – Fluorescence emission spectra of a solution of Nuclear Fast Red ($50 \mu\text{M}$) upon addition of complex $[(p\text{-cymene})\text{RuCl}_2]_2$ ($[\text{Ru}] = 0 - 200 \mu\text{M}$). The excitation wavelength was 540 nm . The spectra were recorded in H_2O (100 mM phosphate buffer, $\text{pH } 7.0$) after equilibration for two days in the dark.

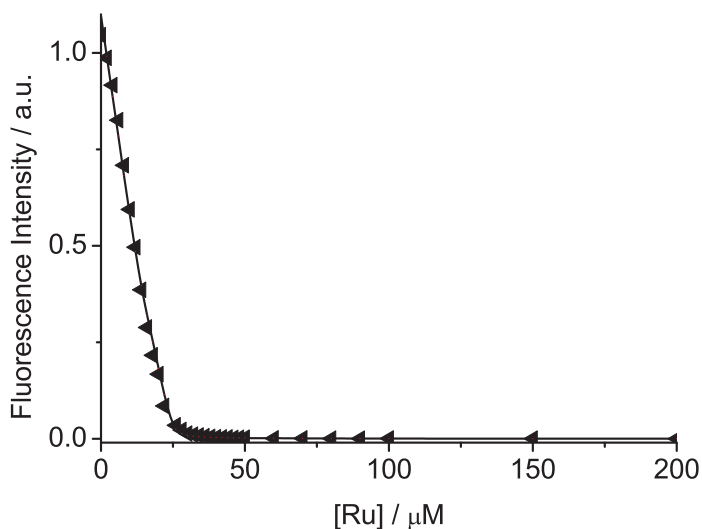


Figure A.16 – Fluorescence emission intensity at 590 nm of a solution of Nuclear Fast Red ($50 \mu\text{M}$) upon addition of complex $[(p\text{-cymene})\text{RuCl}_2]_2$ ($[\text{Ru}] = 0 - 200 \mu\text{M}$). The curve was obtained by fitting the data to a 1:2 binding model ($K_1 = 7.4 (\pm 2.1) \cdot 10^8 \text{ M}^{-1}$; $K_2 = 1.6 (\pm 0.8) \cdot 10^6 \text{ M}^{-1}$).

Fluorescence titration data for the Pd complex and Calcein

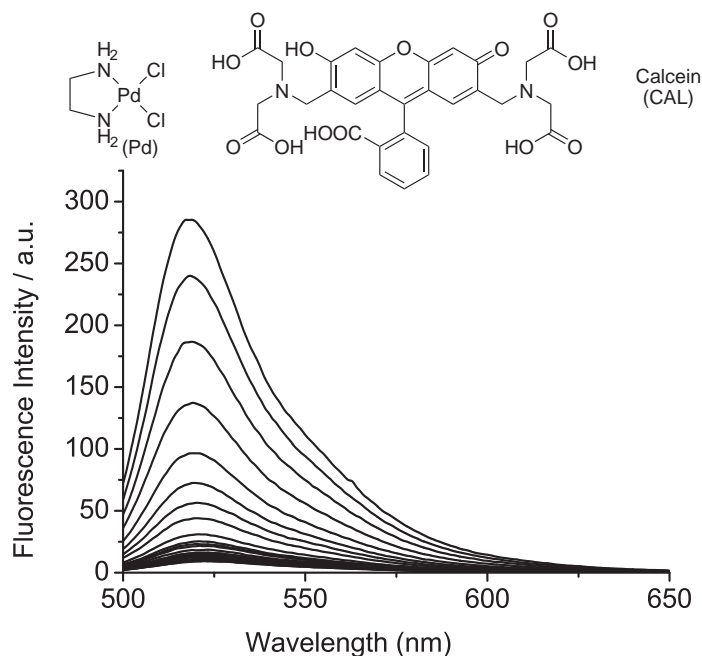


Figure A.17 – Fluorescence emission spectra of a solution of Calcein (25 μM) upon addition of complex $[(\text{en})\text{PdCl}_2]$ (0 – 400 μM). The excitation wavelength was 493 nm. The spectra were recorded in H_2O (100 mM phosphate buffer, pH 7.0) after equilibration for two days in the dark.

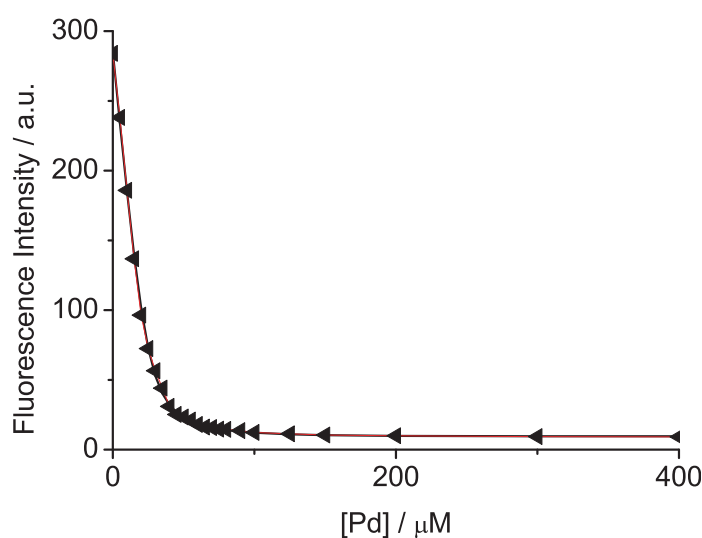


Figure A.18 – Fluorescence emission intensity at 520 nm of a solution of Calcein (25 μM) upon addition of complex $[(\text{en})\text{PdCl}_2]$ (0 – 400 μM). The curve was obtained by fitting the data to a 1:2 binding model ($K_1 = 6.2 (\pm 0.6) \cdot 10^5 \text{ M}^{-1}$; $K_2 = 1.0 (\pm 0.8) \cdot 10^4 \text{ M}^{-1}$).

Fluorescence titration data for the Pd complex and Calcein Blue

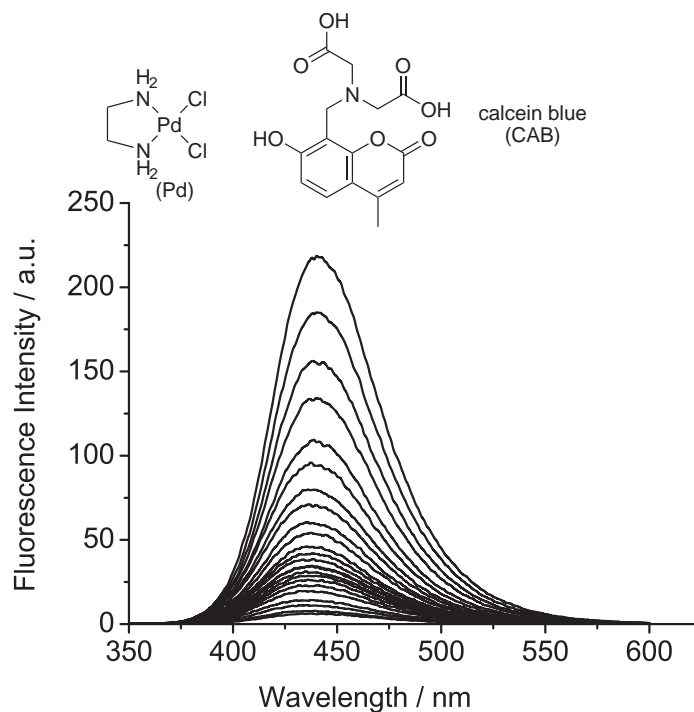


Figure A.19 – Fluorescence emission spectra of a solution of Calcein Blue (25 μM) upon addition of complex $[(en)PdCl_2]$ (0 – 400 μM). The excitation wavelength was 336 nm. The spectra were recorded in H_2O (100 mM phosphate buffer, pH 7.0) after equilibration for two days in the dark.

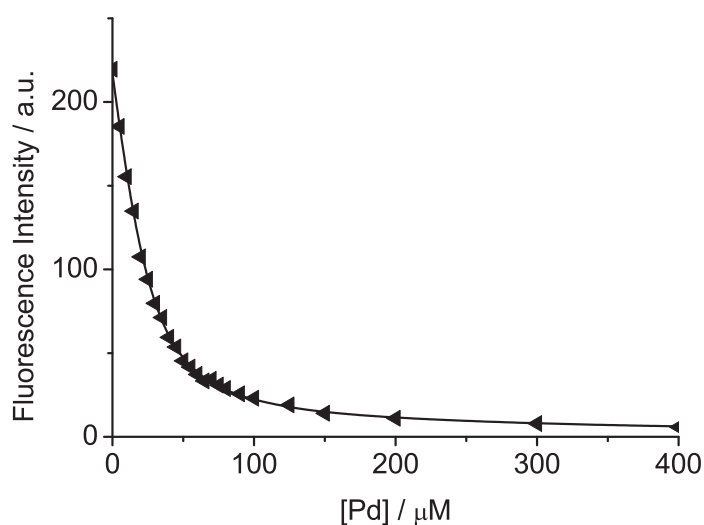


Figure A.20 – Fluorescence emission intensity at 440 nm of a solution of Calcein Blue (25 μM) upon addition of complex $[(en)PdCl_2]$ (0 – 400 μM). The curve was obtained by fitting the data to a 1:1 binding model ($K_1 = 1.2 (\pm 0.1) \cdot 10^5 M^{-1}$).

Fluorescence titration data for the Pd complex and Methylcalcein Blue

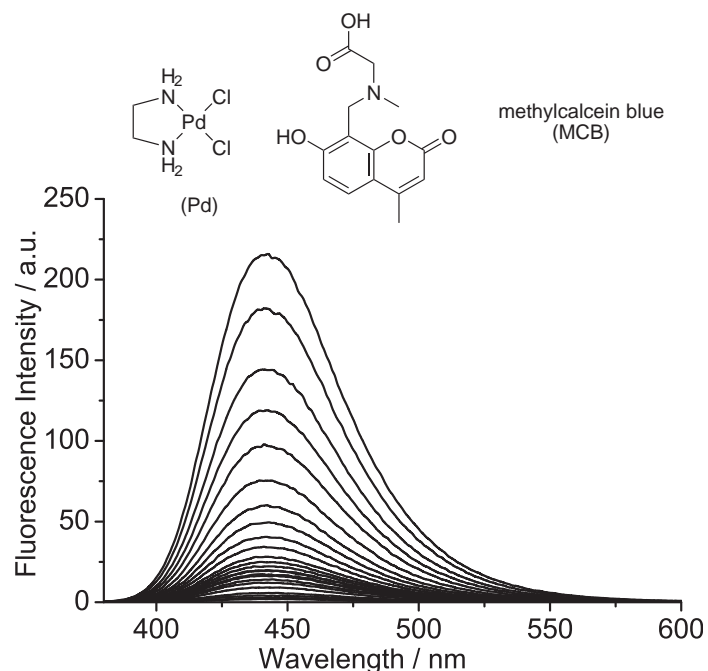


Figure A.21 – Fluorescence emission spectra of a solution of Methylcalcein Blue (25 μM) upon addition of complex $[(en)PdCl_2]$ (0 – 400 μM). The excitation wavelength was 363 nm. The spectra were recorded in H_2O (100 mM phosphate buffer, pH 7.0) after equilibration for two days in the dark.

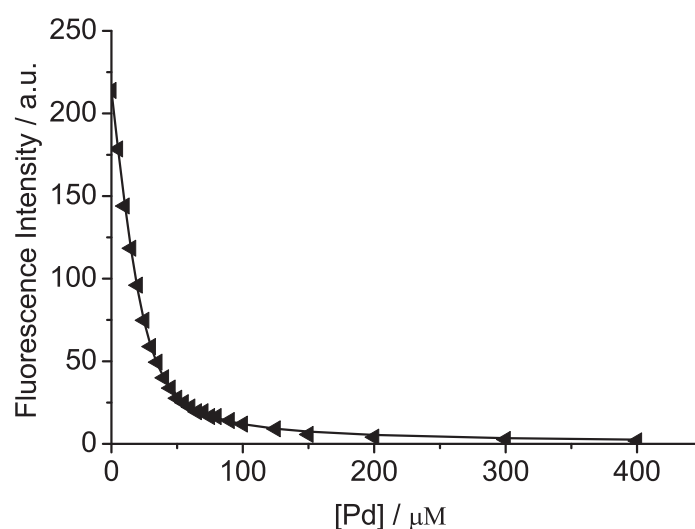


Figure A.22 – Fluorescence emission intensity at 445 nm of a solution of Methylcalcein Blue (25 μM) upon addition of complex $[(en)PdCl_2]$ (0 – 400 μM). The curve was obtained by fitting the data to a 1:1 binding model ($K_1 = 2.2(\pm 0.2) \cdot 10^5 \text{ M}^{-1}$).

Fluorescence titration data for the Pd complex and Nuclear Fast Red

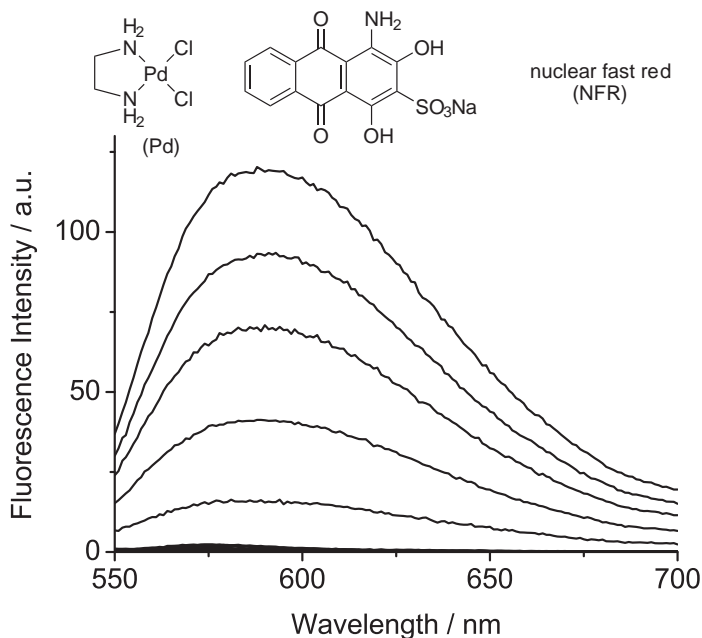


Figure A.23 – Fluorescence emission spectra of a solution of Nuclear Fast Red (25 μM) upon addition of complex $[(en)PdCl_2]$ (0 – 125 μM). The excitation wavelength was 540 nm. The spectra were recorded in H_2O (100 mM phosphate buffer, pH 7.0) after equilibration for two days in the dark.

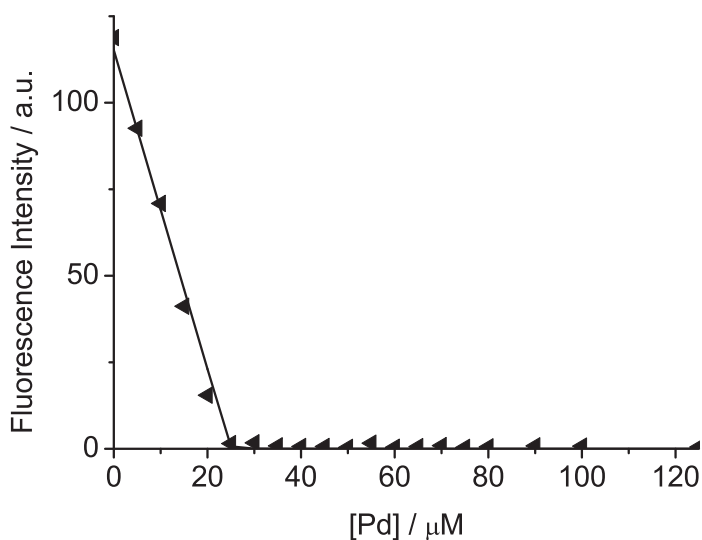


Figure A.24 – Fluorescence emission intensity at 590 nm of a solution of Nuclear Fast Red (25 μM) upon addition of complex $[(en)PdCl_2]$ (0 – 125 μM). The curve was obtained by fitting the data to a 1:1 binding model ($K_1 = 9.5(\pm 9.5) \cdot 10^8 \text{ M}^{-1}$).

Fluorescence titration data for the Pd complex and Lumazine

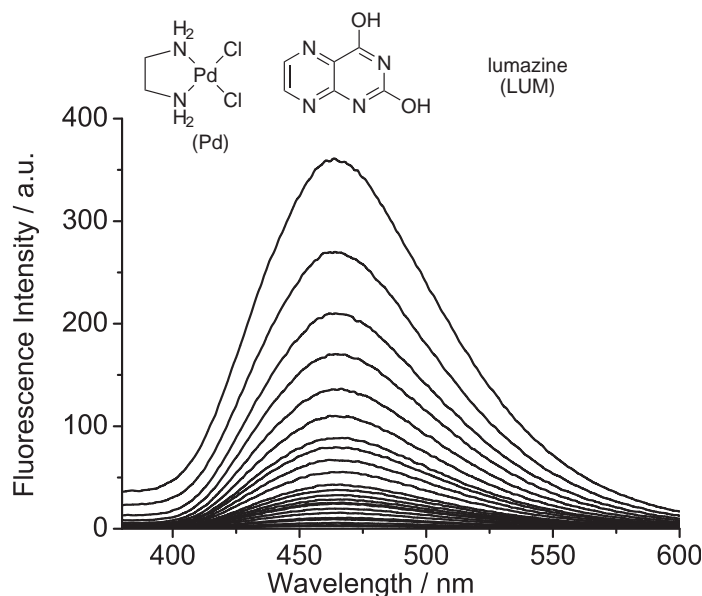


Figure A.25 – Fluorescence emission spectra of a solution of Lumazine (25 μM) upon addition of complex [(en)PdCl₂] (0 – 600 μM). The excitation wavelength was 328 nm. The spectra were recorded in H₂O (100 mM phosphate buffer, pH 7.0) after equilibration for two days in the dark.

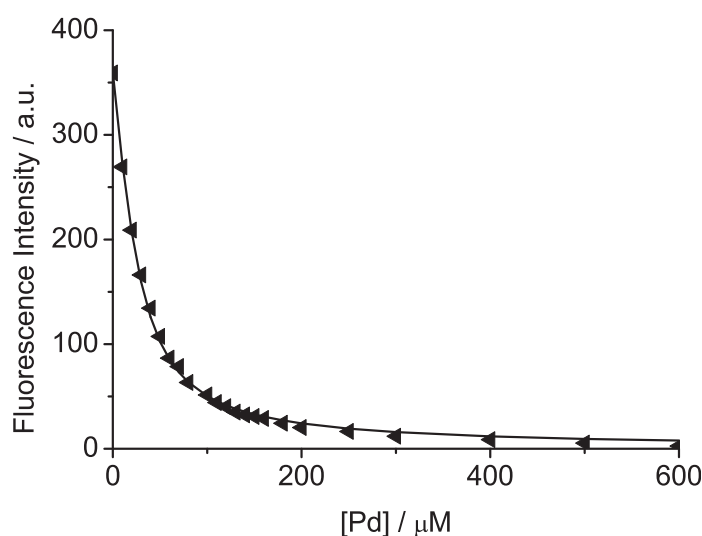


Figure A.26 – Fluorescence emission intensity at 460 nm of a solution of Lumazine (25 μM) upon addition of complex [(en)PdCl₂] (0 – 600 μM). The curve was obtained by fitting the data to a 1:1 binding model ($K_1 = 7.8 (\pm 0.8) \cdot 10^4 \text{ M}^{-1}$).

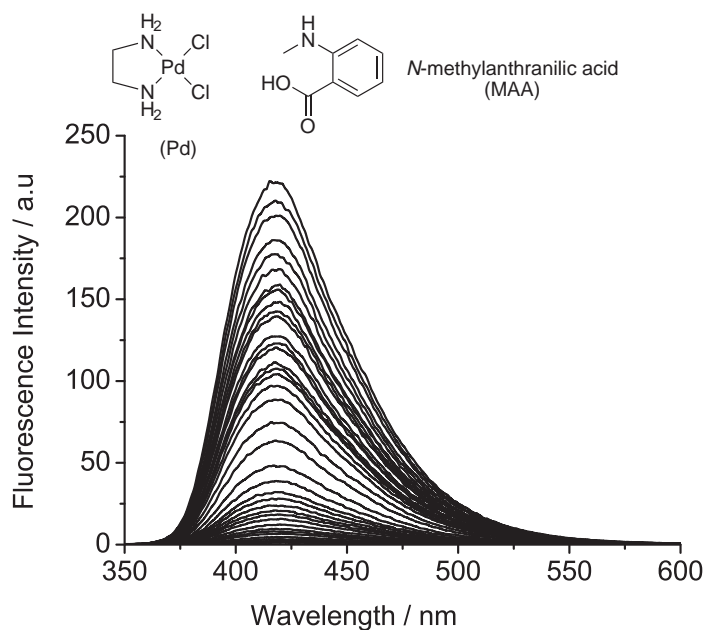
Fluorescence titration data for the Pd complex and *N*-Methylantranilic Acid

Figure A.27 – Fluorescence emission spectra of a solution of *N*-Methylantranilic Acid (25 μM) upon addition of complex $[(\text{en})\text{PdCl}_2]$ (0 – 5000 μM). The excitation wavelength was 325 nm. The spectra were recorded in H_2O (100 mM phosphate buffer, pH 7.0) after equilibration for two days in the dark.

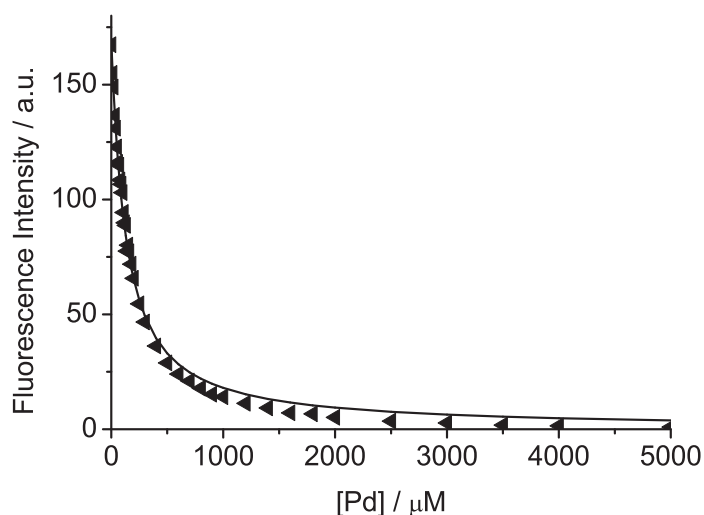


Figure A.28 – Fluorescence emission intensity at 439 nm of a solution of *N*-Methylantranilic Acid (25 μM) upon addition of complex $[(\text{en})\text{PdCl}_2]$ (0 – 5000 μM). The curve was obtained by fitting the data to a 1:1 binding model ($K_1 = 8.6 (\pm 0.9) \cdot 10^3 \text{ M}^{-1}$).

A.2 Multivariate Analyses

A.2.1 Sensing of Ten Dipeptides in Water

Principal Component Analysis (Figure 4.7)

Table A.1 – Correlation matrix

Eigenvalue	35.09	2.70	1.74	0.87	0.60
Variance explained by components	83.54	6.42	4.13	2.06	1.42
Total variance explained (%)	83.54	89.96	94.09	96.15	97.57

Table A.2 – Variables contributions to PC₁, calculated as the square of the corresponding component loading (only principal component 1 was taken into account, since it represents more than 80% of the total variance).

variable	PC ₁	variable	PC ₁
Ru/MCB, 5 min	0.687241	Rh/NFR, 5 min	0.877969
Ru/MCB, 20 min	0.749956	Rh/NFR, 20 min	0.857476
Ru/MCB, 60 min	0.748225	Rh/NFR, 60 min	0.861184
Rh/MCB, 5 min	0.802816	Pd/NFR, 5 min	0.795664
Rh/MCB, 20 min	0.833569	Pd/NFR, 20 min	0.956484
Rh/MCB, 60 min	0.833776	Pd/NFR, 60 min	0.923521
Ru/CAB, 5 min	0.624100	Pd/CAL, 5 min	0.588289
Ru/CAB, 20 min	0.801025	Pd/CAL, 20 min	0.904401
Ru/CAB, 60 min	0.872356	Pd/CAL, 60 min	0.972196
Rh/CAB, 5 min	0.937024	Pd/MCB, 5 min	0.859329
Rh/CAB, 20 min	0.940900	Pd/MCB, 20 min	0.958441
Rh/CAB, 60 min	0.933156	Pd/MCB, 60 min	0.940900
Ru/CAL, 5 min	0.603729	Pd/CAB, 5 min	0.724201
Ru/CAL, 20 min	0.783225	Pd/CAB, 20 min	0.958441
Ru/CAL, 60 min	0.877969	Pd/CAB, 60 min	0.946729
Rh/CAL, 5 min	0.889249	Pd/LUM, 5 min	0.698896
Rh/CAL, 20 min	0.912025	Pd/LUM, 20 min	0.859329
Rh/CAL, 60 min	0.925444	Pd/LUM, 60 min	0.727609
Ru/NFR, 5 min	0.777924	Pd/NMA, 5 min	0.826281
Ru/NFR, 20 min	0.831744	Pd/NMA, 20 min	0.919681
Ru/NFR, 60 min	0.863041	Pd/NMA, 60 min	0.680625

Table A.3 – Sum of each metal-dye combination contributions to PC1 reported in Table A.2. In bold, the 6 most important contributors which were selected to build the reduced sensor array (see A.2.2 and A.2.4 for examples involving this reduced array).

Metal/dye combination	PC1	Metal/dye combination	PC1
Ru/MCB	2.185422	Rh/NFR	2.596629
Rh/MCB	2.490161	Pd/NFR	2.675669
Ru/CAB	2.297481	Pd/CAL	2.464886
Rh/CAB	2.811080	Pd/MCB	2.758670
Ru/CAL	2.264923	Pd/CAB	2.629371
Rh/CAL	2.726718	Pd/LUM	2.285834
Ru/NFR	2.472709	Pd/NMA	2.426587

Linear Discriminant Analysis

The linear discriminant analysis was performed using a stepwise variable selection algorithm based on the statistical significance of each variable in the discrimination between groups. Selected variables and related classification function coefficients are shown in section A.3 (p. 181).

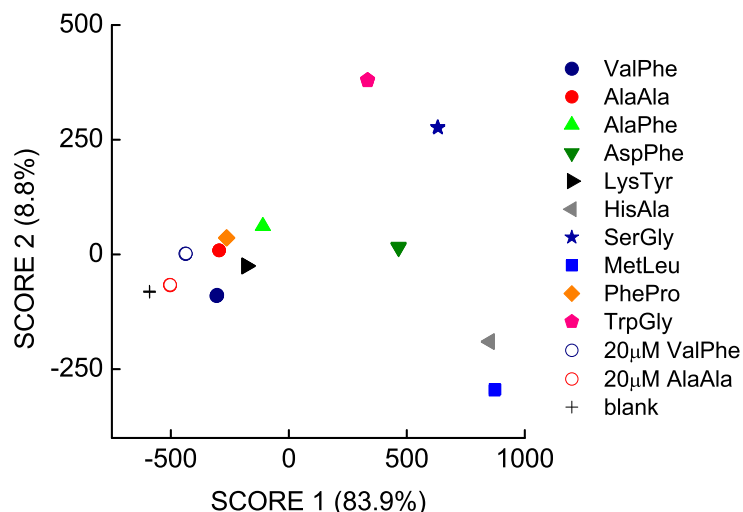


Figure A.29 – Two-dimensional LDA score plot for the discrimination of 10 dipeptides. The peptide concentrations were 50 μM (filled symbols) or 20 μM (open symbols). The input data for the LDA was obtained from a sensor array composed of the 14 metal-dye combinations listed in Table 4.1 (p. 73), and was the same as the input data used for the PCA analysis that produced Figure 4.7 of Section 4.3.1.

Table A.4 – Classification matrix (cases in row categories classified into columns). Unless otherwise indicated, the concentrations of peptides were 50 μ M.

	20 AA	20 VF	AA	AF	DF	HA	KY	ML	FP	SG	WG	VF	Blank	% correct
20 μ M AA	6	0	0	0	0	0	0	0	0	0	0	0	0	100
20 μ M VF	0	6	0	0	0	0	0	0	0	0	0	0	0	100
AA	0	0	4	0	0	0	0	0	0	0	0	0	0	100
AF	0	0	0	4	0	0	0	0	0	0	0	0	0	100
DF	0	0	0	0	4	0	0	0	0	0	0	0	0	100
HA	0	0	0	0	0	4	0	0	0	0	0	0	0	100
KY	0	0	0	0	0	0	4	0	0	0	0	0	0	100
ML	0	0	0	0	0	0	0	4	0	0	0	0	0	100
FP	0	0	0	0	0	0	0	0	4	0	0	0	0	100
SG	0	0	0	0	0	0	0	0	0	4	0	0	0	100
WG	0	0	0	0	0	0	0	0	0	0	4	0	0	100
VF	0	0	0	0	0	0	0	0	0	0	0	4	0	100
Blank	0	0	0	0	0	0	0	0	0	0	0	0	4	100
Total	6	6	4	4	4	4	4	4	4	4	4	4	4	100

Table A.5 – Jack-knifed classification matrix (each measurement was omitted at a time and then classified). Unless otherwise indicated, the concentrations of peptides were 50 μ M.

	20 AA	20 VF	AA	AF	DF	HA	KY	ML	FP	SG	WG	VF	Blank	% correct
20 μ M AA	6	0	0	0	0	0	0	0	0	0	0	0	0	100
20 μ M VF	0	6	0	0	0	0	0	0	0	0	0	0	0	100
AA	0	0	4	0	0	0	0	0	0	0	0	0	0	100
AF	0	0	0	4	0	0	0	0	0	0	0	0	0	100
DF	0	0	0	0	4	0	0	0	0	0	0	0	0	100
HA	0	0	0	0	0	4	0	0	0	0	0	0	0	100
KY	0	0	0	0	0	0	4	0	0	0	0	0	0	100
ML	0	0	0	0	0	0	0	4	0	0	0	0	0	100
FP	0	0	0	0	0	0	0	0	4	0	0	0	0	100
SG	0	0	0	0	0	0	0	0	0	4	0	0	0	100
WG	0	0	0	0	0	0	0	0	0	0	4	0	0	100
VF	0	0	0	0	0	0	0	0	0	0	0	4	0	100
Blank	0	0	0	0	0	0	0	0	0	0	0	0	4	100
Total	6	6	4	4	4	4	4	4	4	4	4	4	4	100

Table A.6 – Correlation matrix

Eigenvalue	327940	34500	11492	8778	4808	917	...
Variance explained	83.9	8.8	2.9	2.3	1.2	0.3	...
Total variance explained (%)	83.9	92.7	95.6	97.9	99.1	99.4	...

A.2.2 Sensor Array Reduction

The following results were obtained by using the six metal/dye combination determined in table Table A.3 (Pd/NFR, Pd/CAB, Rh/NFR, Rh/CAL, Pd/MCB and Rh/CAB).

Principal Component Analysis

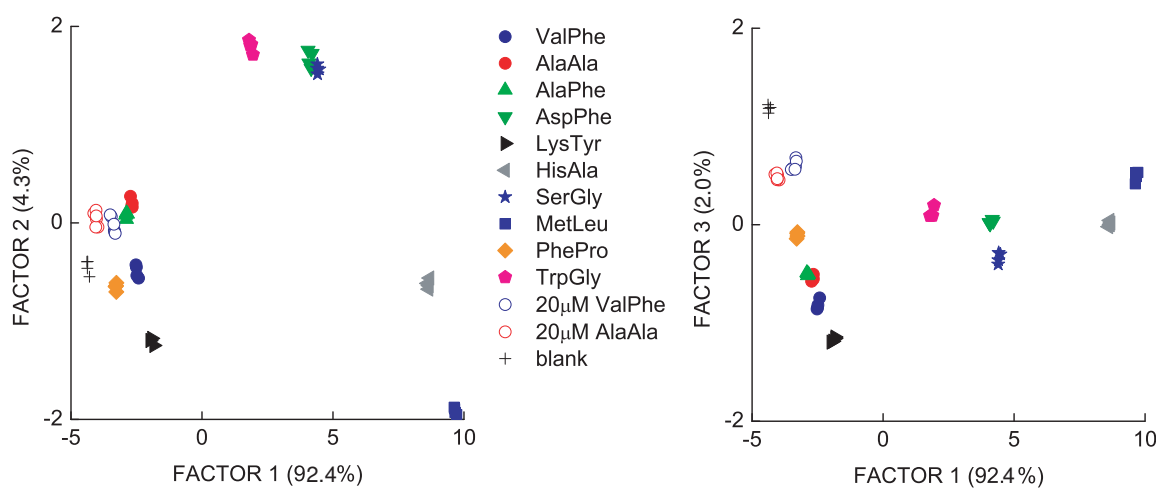


Figure A.30 – Two-dimensional PCA score plots for the discrimination of 10 dipeptides. The input data for the PCA was obtained from a sensor array composed of the following six metal-dye combinations: Pd/NFR, Pd/CAB, Rh/NFR, Rh/CAL, Pd/MCB, and Rh/CAB. The fluorescence was measured after 5, 20 and 60 minutes and the peptides concentrations were 50 μM (filled symbols) or 20 μM (open symbols).

Table A.7 – Correlation matrix

Eigenvalue	16.63	0.77	0.37	0.09	0.05	...
Variance explained by components	92.38	4.27	2.04	0.53	0.28	...
Total variance explained (%)	92.38	96.65	98.69	99.22	99.50	...

Table A.8 – Variables contributions to PC1 and PC2, calculated as the square of the corresponding component loadings.

variable	PC1	PC2	variable	PC1	PC2
Rh/CAB, 5 min	0.96236	0.02132	Pd/NFR, 5 min	0.82446	0.12745
Rh/CAB, 20 min	0.98605	0.00792	Pd/NFR, 20 min	0.97220	0.00160
Rh/CAB, 60 min	0.98406	0.00084	Pd/NFR, 60 min	0.92544	0.01563
Rh/CAL, 5 min	0.92544	0.04623	Pd/MCB, 5 min	0.86118	0.10304
Rh/CAL, 20 min	0.96432	0.02403	Pd/MCB, 20 min	0.92930	0.02856
Rh/CAL, 60 min	0.97812	0.00176	Pd/MCB, 60 min	0.89681	0.00020
Rh/NFR, 5 min	0.94090	0.04580	Pd/CAB, 5 min	0.75690	0.20160
Rh/NFR, 20 min	0.92737	0.05712	Pd/CAB, 20 min	0.95063	0.02822
Rh/NFR, 60 min	0.92930	0.05664	Pd/CAB, 60 min	0.91776	0.00063

Linear Discriminant Analysis

The linear discriminant analysis was performed using a stepwise variable selection algorithm based on the statistical significance of each variable in the discrimination between groups. Selected variables and related classification function coefficients are shown in section A.3.

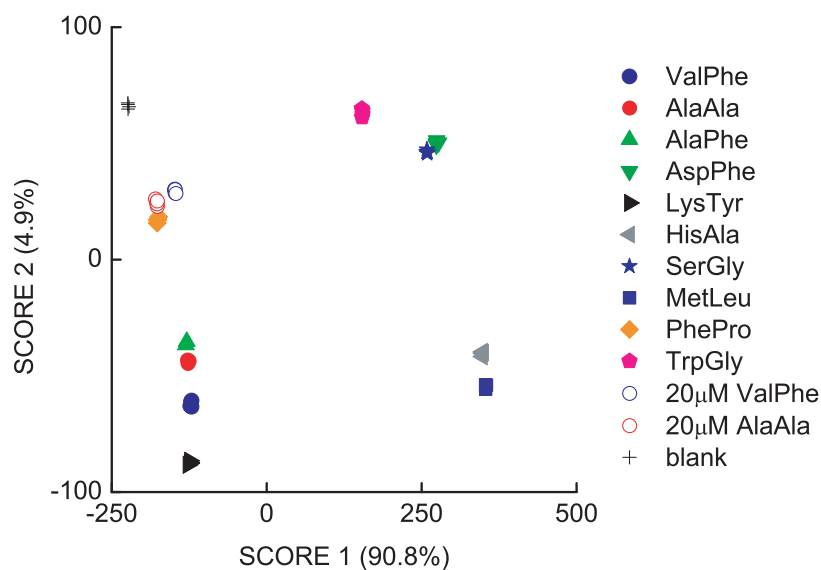


Figure A.31 – Two-dimensional LDA score plot for the discrimination of 10 dipeptides. The input data for the LDA was obtained from a sensor array composed of the following six metal-dye combinations: Pd/NFR, Pd/CAB, Rh/NFR, Rh/CAL, Pd/MCB, and Rh/CAB. The fluorescence was measured after 5, 20 and 60 minutes and the peptides concentrations were 50 μM (filled symbols) or 20 μM (open symbols).

Table A.9 – Classification matrix (cases in row categories classified into columns). Unless otherwise indicated, the concentrations of peptides were 50 μ M.

	20 AA	20 VF	AA	AF	DF	HA	KY	ML	FP	SG	WG	VF	Blank	% correct
20 μ M AA	6	0	0	0	0	0	0	0	0	0	0	0	0	100
20 μ M VF	0	6	0	0	0	0	0	0	0	0	0	0	0	100
AA	0	0	4	0	0	0	0	0	0	0	0	0	0	100
AF	0	0	0	4	0	0	0	0	0	0	0	0	0	100
DF	0	0	0	0	4	0	0	0	0	0	0	0	0	100
HA	0	0	0	0	0	4	0	0	0	0	0	0	0	100
KY	0	0	0	0	0	0	4	0	0	0	0	0	0	100
ML	0	0	0	0	0	0	0	4	0	0	0	0	0	100
FP	0	0	0	0	0	0	0	0	4	0	0	0	0	100
SG	0	0	0	0	0	0	0	0	0	4	0	0	0	100
WG	0	0	0	0	0	0	0	0	0	0	4	0	0	100
VF	0	0	0	0	0	0	0	0	0	0	0	4	0	100
Blank	0	0	0	0	0	0	0	0	0	0	0	0	4	100
Total	6	6	4	4	4	4	4	4	4	4	4	4	4	100

Table A.10 – Jack-knifed classification matrix (each measurement was omitted at a time and then classified). Unless otherwise indicated, the concentrations of peptides were 50 μ M.

	20 AA	20 VF	AA	AF	DF	HA	KY	ML	FP	SG	WG	VF	Blank	% correct
20 μ M AA	6	0	0	0	0	0	0	0	0	0	0	0	0	100
20 μ M VF	0	6	0	0	0	0	0	0	0	0	0	0	0	100
AA	0	0	4	0	0	0	0	0	0	0	0	0	0	100
AF	0	0	0	4	0	0	0	0	0	0	0	0	0	100
DF	0	0	0	0	4	0	0	0	0	0	0	0	0	100
HA	0	0	0	0	0	4	0	0	0	0	0	0	0	100
KY	0	0	0	0	0	0	4	0	0	0	0	0	0	100
ML	0	0	0	0	0	0	0	4	0	0	0	0	0	100
FP	0	0	0	0	0	0	0	0	4	0	0	0	0	100
SG	0	0	0	0	0	0	0	0	0	4	0	0	0	100
WG	0	0	0	0	0	0	0	0	0	0	4	0	0	100
VF	0	0	0	0	0	0	0	0	0	0	0	4	0	100
Blank	0	0	0	0	0	0	0	0	0	0	0	0	4	100
Total	6	6	4	4	4	4	4	4	4	4	4	4	4	100

Table A.11 – Correlation matrix

Eigenvalue	59247	3244	2400	158	110	84	...
Variance explained	90.8	4.9	3.7	0.2	0.2	0.1	...
Total variance explained (%)	90.8	95.7	99.4	99.6	99.8	99.9	...

Cross-validation

The data from the previous experiment were used but this time 40% of the data was taken out randomly (not involved in building the linear discriminant functions) and then reclassified.

Table A.12 – Classification matrix (cases used to build the discriminant functions). Unless otherwise indicated, the concentrations of peptides were 50 μM .

	20 AA	20 VF	AA	AF	DF	HA	KY	ML	FP	SG	WG	VF	Blank	% correct
20 μM AA	3	0	0	0	0	0	0	0	0	0	0	0	0	100
20 μM VF	0	5	0	0	0	0	0	0	0	0	0	0	0	100
AA	0	0	1	0	0	0	0	0	0	0	0	0	0	100
AF	0	0	0	3	0	0	0	0	0	0	0	0	0	100
DF	0	0	0	0	3	0	0	0	0	0	0	0	0	100
HA	0	0	0	0	0	3	0	0	0	0	0	0	0	100
KY	0	0	0	0	0	0	2	0	0	0	0	0	0	100
ML	0	0	0	0	0	0	0	3	0	0	0	0	0	100
FP	0	0	0	0	0	0	0	0	3	0	0	0	0	100
SG	0	0	0	0	0	0	0	0	0	3	0	0	0	100
WG	0	0	0	0	0	0	0	0	0	0	2	0	0	100
VF	0	0	0	0	0	0	0	0	0	0	0	2	0	100
Blank	0	0	0	0	0	0	0	0	0	0	0	0	1	100
Total	3	5	1	3	3	3	2	3	3	3	2	2	1	100

Table A.13 – Classification of cases with zero weight or frequency: these observations were not used to determine discriminant functions but were classified into groups afterwards. Unless otherwise indicated, the concentrations of peptides were 50 μM .

	20 AA	20 VF	AA	AF	DF	HA	KY	ML	FP	SG	WG	VF	Blank	% correct
20 μM AA	3	0	0	0	0	0	0	0	0	0	0	0	0	100
20 μM VF	0	1	0	0	0	0	0	0	0	0	0	0	0	100
AA	0	0	3	0	0	0	0	0	0	0	0	0	0	100
AF	0	0	0	1	0	0	0	0	0	0	0	0	0	100
DF	0	0	0	0	1	0	0	0	0	0	0	0	0	100
HA	0	0	0	0	0	1	0	0	0	0	0	0	0	100
KY	0	0	0	0	0	0	2	0	0	0	0	0	0	100
ML	0	0	0	0	0	0	0	1	0	0	0	0	0	100
FP	0	0	0	0	0	0	0	0	1	0	0	0	0	100
SG	0	0	0	0	0	0	0	0	0	1	0	0	0	100
WG	0	0	0	0	0	0	0	0	0	0	2	0	0	100
VF	0	0	0	0	0	0	0	0	0	0	0	2	0	100
Blank	0	0	0	0	0	0	0	0	0	0	0	0	3	100
Total	3	1	3	1	1	1	1	2	1	1	2	2	3	100

Table A.14 – Correlation matrix

Eigenvalue	57281	4239	2321	123	74	...
Variance explained	89.3	6.6	3.7	0.2	0.1	...
Total variance explained (%)	89.3	95.9	99.6	99.8	99.9	...

A.2.3 Sensing of Bradykinin and Kallidin

Principal Component Analysis (see also Figure 4.8)

All measurements were performed with the six metal-dye combinations determined by pre-screening (Rh/MCB, Rh/CAB, Rh/CAL, Pd/CAB, Pd/NFR, and Pd/LUM), see 7.5.4, p. 144.

Table A.15 – Correlation matrix

Eigenvalue	10.85	6.22	0.58	0.14	0.05	...
Variance explained by components	60.25	34.54	3.22	0.80	0.28	...
Total variance explained (%)	60.25	94.79	98.01	98.81	99.09	...

Table A.16 – Variables contributions to PC1 and PC2, calculated as the square of the corresponding component loadings.

variable	PC1	PC2	variable	PC1	PC2
Rh/MCB, 2.5 min	0.85008	0.14063	Pd/LUM, 40 min	0.40323	0.55950
Rh/MCB, 5 min	0.83723	0.15288	Pd/LUM, 50 min	0.27248	0.70224
Rh/MCB, 10 min	0.81000	0.17223	Pd/LUM, 60 min	0.23232	0.74304
Rh/CAL, 2.5 min	0.78410	0.20430	Pd/NFR, 40 min	0.35522	0.60996
Rh/CAL, 5 min	0.70224	0.27353	Pd/NFR, 50 min	0.00230	0.47197
Rh/CAL, 10 min	0.62410	0.33408	Pd/NFR, 60 min	0.35760	0.60528
Rh/CAB, 2.5 min	0.76738	0.19184	Pd/CAB, 40 min	0.79388	0.18318
Rh/CAB, 5 min	0.78146	0.19536	Pd/CAB, 50 min	0.76913	0.22278
Rh/CAB, 10 min	0.77440	0.18576	Pd/CAB, 60 min	0.72420	0.26729

Table A.18 – Jack-knifed classification matrix (each measurement was omitted at a time and then classified).

	0 KD 50 BK	10 KD 40 BK	20 KD 30 BK	30 KD 20 BK	40 KD 10 BK	50 KD 0 BK	Blank	% correct
0 KD 50 BK	4	0	0	0	0	0	0	100
10 KD 40 BK	0	4	0	0	0	0	0	100
20 KD 30 BK	0	0	4	0	0	0	0	100
30 KD 20 BK	0	0	0	4	0	0	0	100
40 KD 10 BK	0	0	0	0	4	0	0	100
50 KD 0 BK	0	0	0	0	0	4	0	100
Blank	0	0	0	0	0	0	4	100
Total	4	4	4	4	4	4	4	100

Table A.19 – Correlation matrix.

Eigenvalue	1078	467	4.39	2.00	1.85	0.10
Variance explained	69.4	30.1	0.2	0.2	0.1	0.0
Total variance explained (%)	69.4	99.5	99.7	99.9	100	100

A.2.4 Sensing of Carnosine and Homocarnosine in Serum

The following results were obtained by using the six metal-dye combination determined in section A.2.2. (Pd/NFR, Pd/CAB, Rh/NFR, Rh/CAL, Pd/MCB and Rh/CAB) with modified metal concentrations ($[\text{Metal}] = 500 \mu\text{M}$ for Pd/NFR, Pd/CAB, Rh/NFR, and Rh/CAL mixtures, $300 \mu\text{M}$ for Pd/MCB mixtures, and $200 \mu\text{M}$ for Rh/CAB mixtures).

Principal Component Analysis (see also Figure 4.9)

Table A.20 – Correlation matrix.

Eigenvalue	8.84	6.64	1.08	0.56	0.42	0.26	...
Variance explained by components	49.1	36.9	6.0	3.1	2.3	1.4	...
Total variance explained (%)	49.1	86.0	92.0	95.1	97.4	98.8	...

Table A.21 – Variables contributions to PC1 and PC2, calculated as the square of the corresponding component loadings.

variable	PC1	PC2	variable	PC1	PC2
Rh/CAB, 5 min	0.32262	0.44622	Pd/MCB, 5 min	0.48025	0.40323
Rh/CAB, 20 min	0.47886	0.41990	Pd/MCB, 20 min	0.56250	0.27144
Rh/CAB, 60 min	0.32718	0.61152	Pd/MCB, 60 min	0.53582	0.26112
Rh/CAL, 5 min	0.54908	0.26832	Pd/CAB, 40 min	0.51840	0.38564
Rh/CAL, 20 min	0.68228	0.20521	Pd/CAB, 50 min	0.54170	0.30914
Rh/CAL, 60 min	0.70896	0.16403	Pd/CAB, 60 min	0.55354	0.25402
Rh/NFR, 5 min	0.64642	0.11903	Pd/NFR, 5 min	0.20160	0.72250
Rh/NFR, 20 min	0.77792	0.10049	Pd/NFR, 20 min	0.15445	0.77088
Rh/NFR, 60 min	0.78500	0.13323	Pd/NFR, 60 min	0.01082	0.79388

Table A.23 – Jack-knifed classification matrix (each measurement was omitted at a time and then classified).

	100 Car	100 HCar	75 Car	75 HCar	50 Car	50 HCar	25 Car	25 HCar	Blank	% correct
100 Car	4	0	0	0	0	0	0	0	0	100
100 HCar	0	4	0	0	0	0	0	0	0	100
75 Car	0	0	4	0	0	0	0	0	0	100
75 HCar	0	0	0	4	0	0	0	0	0	100
50 Car	0	0	0	0	4	0	0	0	0	100
50 HCar	0	0	0	0	0	4	0	0	0	100
25 Car	0	0	0	0	0	0	4	0	0	100
25 HCar	0	0	0	0	0	0	0	4	0	100
Blank	0	0	0	0	0	0	0	0	4	100
Total	4	4	4	4	4	4	4	4	4	100

Table A.24 – Correlation matrix.

Eigenvalue	1083	191.7	169.4	20.33	6.38	3.57	1.37
Variance explained	73.4	13.0	11.4	1.4	0.4	0.3	0.1
Total variance explained (%)	73.4	86.4	97.8	99.2	99.6	99.9	100

Cross-validation

The data from the previous experiment were used but this time 20% of the data was taken out randomly (not involved in building the linear discriminant functions) and then reclassified.

Table A.25 – Classification matrix (cases used to build the discriminant functions).

	100 Car	100 HCar	75 Car	75 HCar	50 Car	50 HCar	25 Car	25 HCar	Blank	% correct
100 Car	3	0	0	0	0	0	0	0	0	100
100 HCar	0	3	0	0	0	0	0	0	0	100
75 Car	0	0	2	0	0	0	0	0	0	100
75 HCar	0	0	0	4	0	0	0	0	0	100
50 Car	0	0	0	0	3	0	0	0	0	100
50 HCar	0	0	0	0	0	2	0	0	0	100
25 Car	0	0	0	0	0	0	4	0	0	100
25 HCar	0	0	0	0	0	0	0	3	0	100
Blank	0	0	0	0	0	0	0	0	4	100
Total	3	3	2	4	3	2	4	3	4	100

Table A.26 – Classification of cases with zero weight or frequency: these observations were not used to determine discriminant functions but were classified into groups afterwards.

	100 Car	100 HCar	75 Car	75 HCar	50 Car	50 HCar	25 Car	25 HCar	Blank	% correct
100 Car	1	0	0	0	0	0	0	0	0	100
100 HCar	0	1	0	0	0	0	0	0	0	100
75 Car	0	0	2	0	0	0	0	0	0	100
75 HCar	0	0	0	0	0	0	0	0	0	-
50 Car	0	0	0	0	1	0	0	0	0	100
50 HCar	0	0	0	0	0	2	0	0	0	100
25 Car	0	0	0	0	0	0	0	0	0	-
25 HCar	0	0	0	0	0	0	0	1	0	100
Blank	0	0	0	0	0	0	0	0	0	-
Total	1	1	2	0	1	2	0	1	0	100

Table A.27 – Correlation matrix.

Eigenvalue	671.7	114.8	55.8	21.3	2.5	...
Variance explained	77.5	13.2	6.5	2.4	0.3	...
Total variance explained (%)	77.5	90.7	97.2	99.6	99.9	...

A.3 Linear Discriminant Functions provided by the LDAs

Linear Discriminant Functions, also called canonical roots, are created as a linear combination of discriminating (independent) variables, such as:

$$F_z = A + \sum_{b=1}^p c_b \cdot Z_b \quad (\text{A.1})$$

Where A represents a constant, c the classification coefficients and Z the variables (in the case where p variables are used).

Linear discriminant functions describe the best fit parameters to separate different clusters (analytes). The cross-validation (jack-knifed matrix) routine is then used to test the predictability of the sensor array by leaving one observation out of the set at the time, and uses the rest of the data as a training set to generate the linear discriminant functions. The linear discriminant functions are then used to place the excluded observation (data point) within the correct cluster. This is performed for each observation, and the overall ability to classify the observations describes the quality and predictability of the array.

Table A.28 – Linear discrimination functions for the analysis of 10 dipeptides (cf. A.2.1, p. 166).

	20 AA	20 VF	AA	AF	DF	HA	KY	ML	FP	SG	WG	VF	Blank
Constant	-2115861	-2130020	-2266113	-2294806	-3116715	-3906599	-2344979	-4228655	-2106248	-3081226	-2567908	-2371773	-2035679
Ru/MCB, 5min	-118675	-39935	-77479	-39093	8729	62071	-60175	-140899	-22801	414683	369206	-240787	-141372
Ru/MCB, 20min	585119	497113	525398	418897	641566	930959	535356	982716	442437	493816	278097	557913	554863
Ru/MCB, 60min	619114	633637	683149	749787	586394	442334	679614	624541	684582	380424	543073	810961	644017
Rh/MCB, 5min	934115	943737	967368	964917	1033147	1072026	967746	1154521	932962	968294	944368	994515	903552
Rh/MCB, 20min	-1239291	-1158280	-1125559	-1057655	-1089912	-1118438	-1109207	-1236722	-1083359	-814696	-767193	-1231652	-1252731
Rh/MCB, 60min	206440	167932	172301	274012	431175	573453	220929	583354	258539	387404	240049	212882	229959
Ru/CAB, 5min	1184307	1158013	1070286	1083892	1212248	1018823	993847	1177061	1116889	832564	863470	1158326	1245738
Ru/CAB, 20min	-7435	-11678	-94861	-253575	-615980	-735671	-122755	-837779	-167475	-625970	-462398	-126722	30184
Ru/CAB, 60min	-157253	-162120	-77245	34743	214292	402787	-4686	449574	-34722	278780	159040	-30923	-186961
Rh/CAB, 5min	-992244	-982562	-992895	-993116	-1134403	-1151407	-987335	-1253484	-968605	-999457	-953901	-1050643	-975964
Rh/CAB, 20min	-94669	-35774	46697	133993	606348	800127	108796	690103	53964	980964	737031	-41880	-201033
Rh/CAB, 60min	110962	88767	59150	85773	-151649	-161629	73250	-84036	102954	-404485	-280408	146111	194945
Ru/CAL, 5min	750671	719364	865570	894577	1026814	1210997	954476	1329346	774435	998713	892159	988145	694784
Ru/CAL, 20min	-674008	-654100	-889699	-1016647	-1269801	-1487987	-1020136	-1660778	-795026	-1243751	-1087036	-1050081	-597290
Ru/CAL, 60min	649277	655807	752799	892349	1097566	1199847	803893	1312541	774791	1017251	901884	816794	639989
Rh/CAL, 5min	-571365	-592466	-566062	-610897	-675620	-615890	-570879	-672850	-601256	-580201	-610352	-616543	-587818
Rh/CAL, 20min	-282531	-72006	-9312	273587	491168	394045	11856	317530	129998	1005553	1035416	-136907	-318810
Rh/CAL, 60min	1011400	807219	718314	470462	333276	403620	696764	556840	611379	-321616	-348010	909845	1067367
Ru/NFR, 5min	15665	47407	61728	132794	237965	327414	102189	296034	111426	312255	260329	47949	12873
Ru/NFR, 20min	-1277732	-1271073	-1253343	-1227340	-1324489	-1091969	-1145629	-1338111	-1204838	-937029	-1048514	-1372463	-1305081
Ru/NFR, 60min	884136	869325	862901	829011	845958	834842	794549	931946	829361	709429	691855	909154	894204

Table A.29 – Linear discrimination functions for the analysis of 10 dipeptides with a reduced sensor array (cf. A.2.2, p. 170).

	20AA	20VF	AA	AF	DF	HA	KY	ML	FP	SG	WG	VF	Blank
Constant	-98222	-105827	-148972	-144522	-307640	-381883	-164046	-390669	-104781	-322763	-247487	-151482	-69146
Rh/CAB, 5min													
Rh/CAB, 20min	37737	46939	51024	49778	145486	127662	45854	127596	40095	193468	168753	47191	29586
Rh/CAB, 60min	-63659	-71030	-79273	-78226	-142795	-108579	-70934	-106695	-66962	-202018	-176578	-71747	-49216
Rh/CAL, 5min	26016	27783	37591	36322	19739	16338	30038	16932	28501	34061	37220	28370	22249
Rh/CAL, 20min													
Rh/CAL, 60min	-17783	-20065	-28585	-28403	-6555	3710	-21536	3787	-21569	-23487	-32611	-19925	-15857
Rh/NFR, 5min													
Rh/NFR, 20min	26885	44901	27502	30082	283422	283641	13009	282103	25899	269958	219970	23453	17799
Rh/NFR, 60min	-18069	-22574	-22921	-22739	-79757	-85379	-21597	-87704	-17291	-79689	-67384	-22574	-15138
Pd/NFR, 5min													
Pd/NFR, 20min													
Pd/NFR, 60min	144894	146969	182535	177026	161682	194934	189902	200096	139779	178282	168662	186485	118601
Pd/MCB, 5min													
Pd/MCB, 20min													
Pd/MCB, 60min	82937	83966	98606	98890	116878	126057	109938	125657	93888	123300	106037	100281	76069
Pd/CAB, 5min													
Pd/CAB, 20min													
Pd/CAB, 60min	135347	139938	166544	164433	206642	234465	175532	240663	139345	216901	194263	168148	110383

Table A.30 – Linear discrimination functions for the analysis of kallidin and bradykinin (cf. section A.2.3, p. 175).

	50 μ M KD	40 μ M KD	30 μ M KD	20 μ M KD	10 μ M KD		Blank
		+	+	+	+		
		10 μ M BK	20 μ M BK	30 μ M BK	40 μ M BK	50 μ M BK	
Constant	108996	111945	115779	119795	124859	-126886	-93646
Rh/MCB, 2.5 min	183145	186226	191548	198828	203999	204401	198426
Rh/MCB, 5 min	67737	63905	54917	46425	39482	35516	23659
Rh/MCB, 10 min	-181545	-182939	-182597	-183118	-184309	-182129	-166274
Rh/CAL, 2.5 min							
Rh/CAL, 5 min							
Rh/CAL, 10 min							
Rh/CAB, 2.5 min	-74667	-73953	-72922	-73190	-72432	-71669	-68473
Rh/CAB, 5 min							
Rh/CAB, 10 min	138783	137670	136444	137568	136665	135547	124908
Pd/LUM, 40 min	59795	60995	62152	62389	64265	65289	50962
Pd/LUM, 50 min							
Pd/LUM, 60 min	74228	75970	78183	80578	83424	84265	75798
Pd/NFR, 40 min							
Pd/NFR, 50 min							
Pd/NFR, 60 min	-17780	-16317	-14111	-13462	-12021	-10744	-16522
Pd/CAB, 40 min							
Pd/CAB, 50 min	51839	51606	51495	52794	52497	52236	47673
Pd/CAB, 60 min	54442	57658	62219	64591	68887	71394	50495

Table A.31 – Linear discrimination functions for the analysis of carnosine and homocarnosine (cf. section A.2.4, p. 178).

	100 μ M Car	100 μ M HCar	25 μ M HCar	25 μ M Car	50 μ M Car	50 μ M HCar	75 μ M HCar	75 μ M Car	Blank
Constant	-178164	-176360	-161825	-163059	-170198	-170021	-166591	-174938	-175199
Rh/CAB, 5 min	399074	410692	391176	385964	395041	401448	394346	397081	403874
Rh/CAB, 20 min	-411043	-402472	-385950	-386494	-402409	-398577	-383059	-406854	-424968
Rh/CAB, 60 min	96840	73711	76372	82804	91456	80165	69228	94288	109418
Rh/CAL, 5 min	192376	202590	180576	182580	185263	190886	195758	189272	183846
Rh/CAL, 20 min	-177095	-216599	-166475	-164698	-163908	-185199	-204628	-171241	-143477
Rh/CAL, 60 min	56725	84712	54143	50954	49425	64322	77170	53680	35024
Rh/NFR, 5 min	54846	47375	50068	52314	54393	50379	46143	54866	60524
Rh/NFR, 20 min									
Rh/NFR, 60 min									
Pd/NFR, 5 min	206584	207066	201394	200252	203824	205091	201526	206092	205644
Pd/NFR, 20 min	-32211	-31894	-33656	-32836	-32927	33682	-31344	-32186	-30286
Pd/NFR, 60 min	41120	45283	40185	39616	38975	42375	43989	39990	33058
Pd/MCB, 5 min	-84630	-80161	-81638	-82346	-85102	-82241	-77802	-85559	-98487
Pd/MCB, 20 min	70393	69016	66682	67476	69153	68498	66578	70026	72881
Pd/MCB, 60 min	-17273	-12917	-15111	-16191	-18017	-14599	-12444	-18387	-29890
Pd/CAB, 5 min	87376	78757	80586	81076	85985	681889	75708	86891	96977
Pd/CAB, 20 min	-2152	3406	950	-417	-2128	852	4441	-2122	-8950
Pd/CAB, 60 min	-21166	-20665	-22079	-20909	-20788	-22302	-20715	-21050	-18619

A.4 Kinetic Profiles

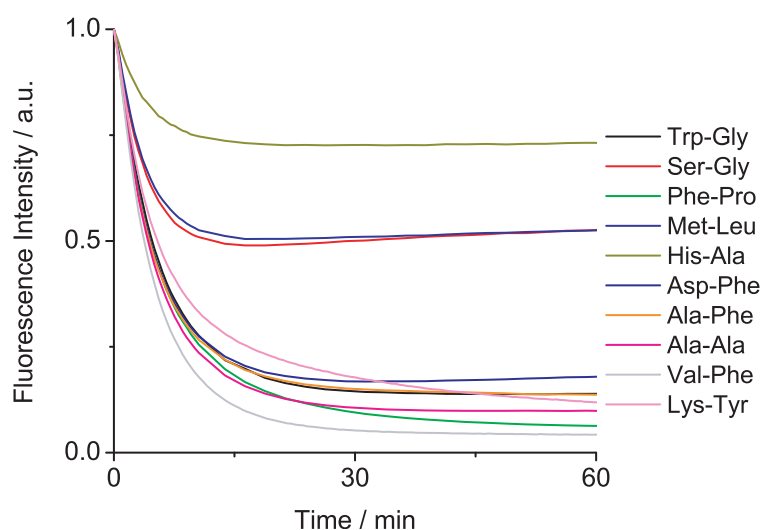


Figure A.34 – Relative fluorescence emission intensity at 590 nm for the reaction of $[(p\text{-cymene})\text{RuCl}_2]_2$ ($25\ \mu\text{M}$) and Nuclear Fast Red ($25\ \mu\text{M}$) in the presence of different dipeptides. The data were obtained at 25°C in H_2O (100 mM phosphate buffer, pH 7.0). The excitation wavelength was 540 nm.

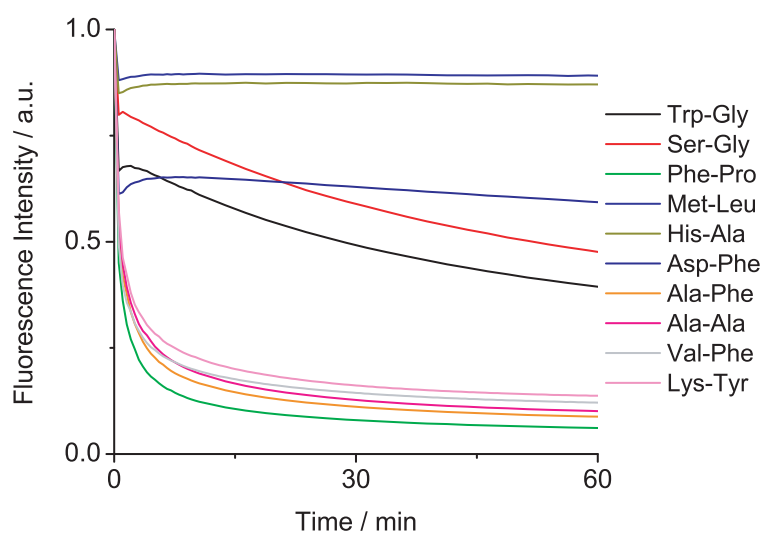


Figure A.35 – Relative fluorescence emission intensity at 440 nm for the reaction of $[\text{Cp}^*\text{RhCl}_2]_2$ ($25\ \mu\text{M}$) and Calcein Blue ($25\ \mu\text{M}$) in the presence of different dipeptides. The data were obtained at 25°C in H_2O (100 mM phosphate buffer, pH 7.0). The excitation wavelength was 336 nm.

B

Pattern-Based Sensing with
Metal-Dye Complexes: Sensor
Arrays versus Dynamic
Combinatorial Libraries

B.1 LDA Score Plots

Here are presented the linear discriminant analysis score plots not displayed in Chapter 5. They appear by order of decreasing quality of discrimination, as classified in Table 5.1, p. 94.

In all cases, the concentration of analyte was [peptide] = 1.0 mM, the concentration of the dyes were [MCB] = 50 μ M, [Al] = 25 μ M, [XO] = 12.5 μ M, and the concentration of metal cations were [Cu²⁺] = [Ni²⁺] = 100 μ M. When one or several of the members of the DCL was/were omitted, bidistilled water was used instead. The pH was maintained at 8.4 (100 mM of a CHES buffer).

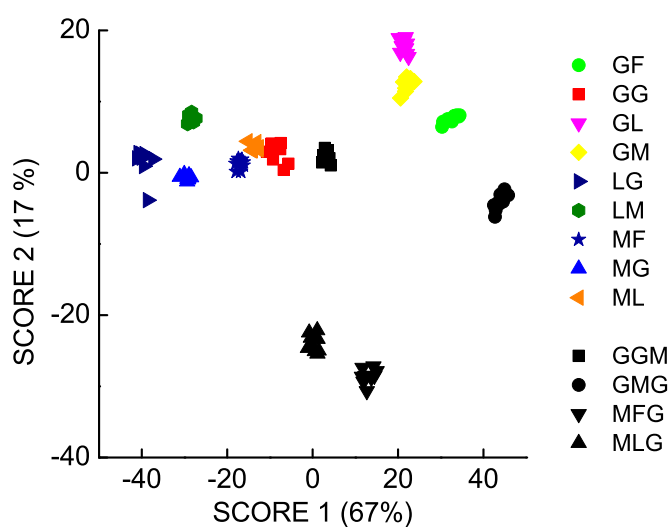


Figure B.1 – LDA score plot generated from the data of a sensor made from Al, XO, CuCl₂ and NiCl₂. The sensor was used for the differentiation of 13 di- and tripeptides in buffered aqueous solution at a concentration of 1.0 mM. Cross-validation afforded 100% correct classification, and the *F*-value associated to the LDA model is 510.

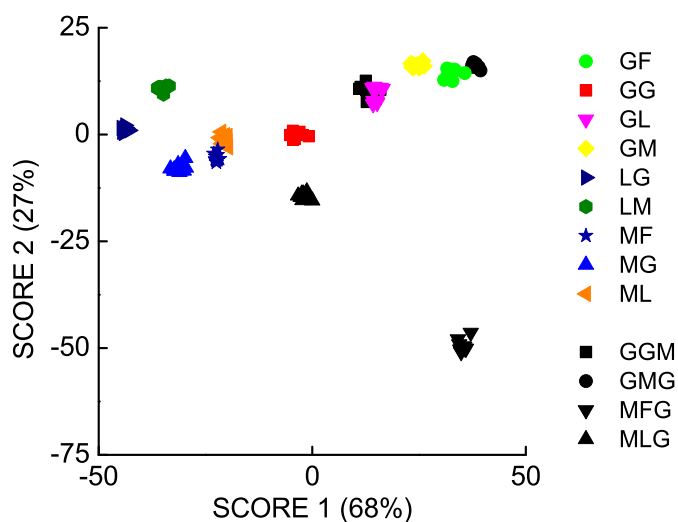


Figure B.2 – LDA score plot generated from the data of a sensor made from MCB, Al, XO, and NiCl₂. The sensor was used for the differentiation of 13 di- and tripeptides in buffered aqueous solution at a concentration of 1.0 mM. Cross-validation afforded 100% correct classification, and the *F*-value associated to the LDA model is 423.

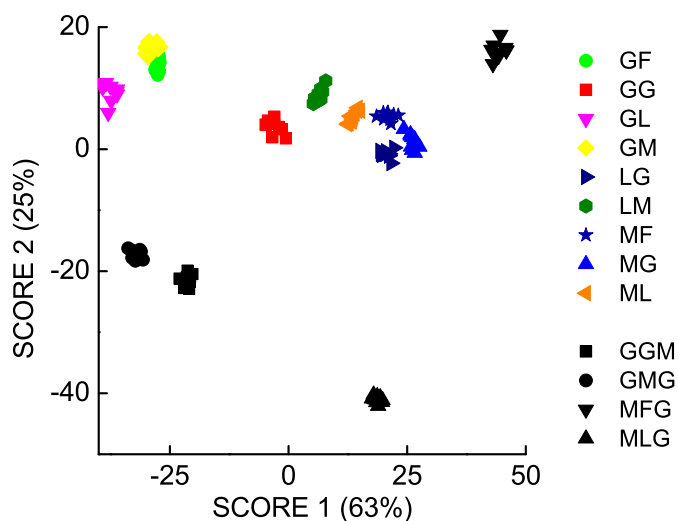


Figure B.3 – LDA score plot generated from the data of a sensor made from MCB, XO, CuCl₂ and NiCl₂. The sensor was used for the differentiation of 13 di- and tripeptides in buffered aqueous solution at a concentration of 1.0 mM. Cross-validation afforded 100% correct classification, and the *F*-value associated to the LDA model is 325.

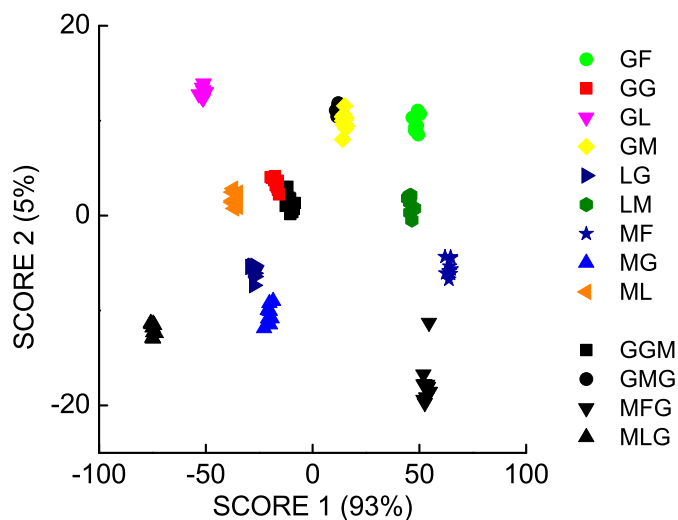


Figure B.4 – LDA score plot generated from the data of a sensor made from MCB, XO, and CuCl_2 . The sensor was used for the differentiation of 13 di- and tripeptides in buffered aqueous solution at a concentration of 1.0 mM. Cross-validation afforded 100% correct classification, and the *F*-value associated to the LDA model is 220.

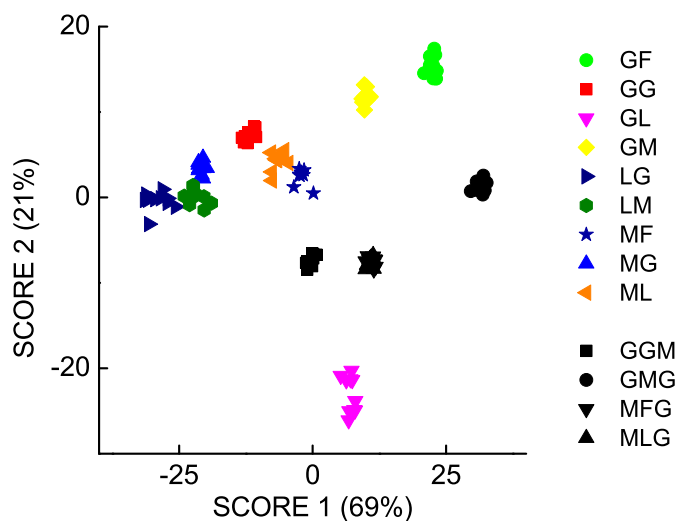


Figure B.5 – LDA score plot generated from the data of a sensor made from Al, CuCl_2 and NiCl_2 . The sensor was used for the differentiation of 13 di- and tripeptides in buffered aqueous solution at a concentration of 1.0 mM. Cross-validation afforded 100% correct classification, and the *F*-value associated to the LDA model is 209.

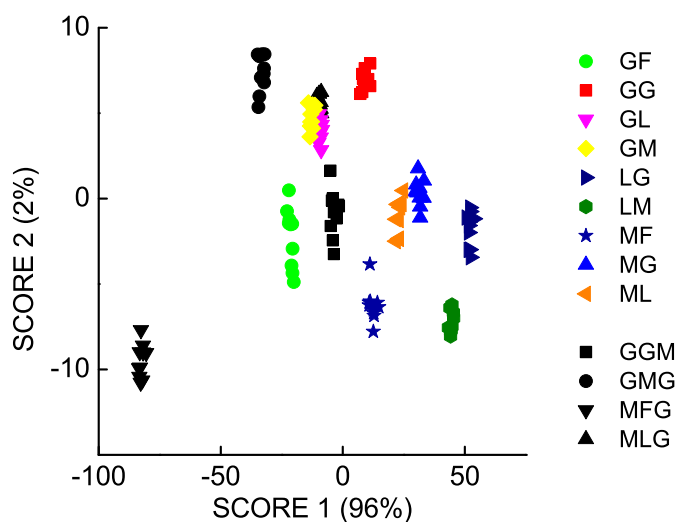


Figure B.6 – LDA score plot generated from the data of a sensor made from MCB, Al and NiCl₂. The sensor was used for the differentiation of 13 di- and tripeptides in buffered aqueous solution at a concentration of 1.0 mM. Cross-validation afforded 100% correct classification, and the *F*-value associated to the LDA model is 154.

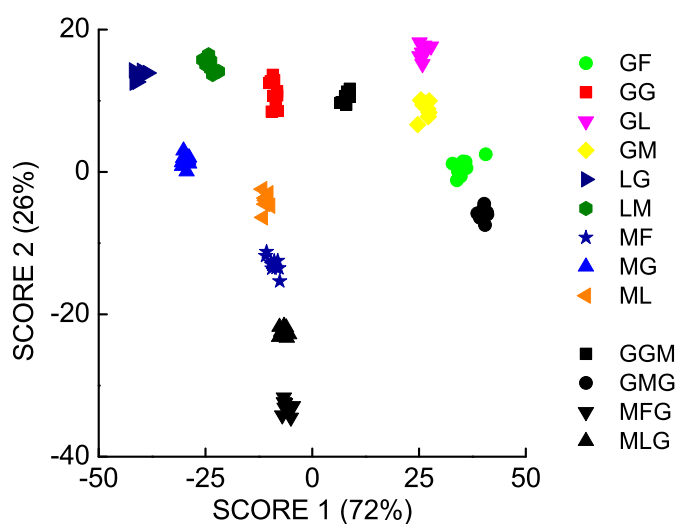


Figure B.7 – LDA score plot generated from the data of a sensor made from Al, XO and NiCl₂. The sensor was used for the differentiation of 13 di- and tripeptides in buffered aqueous solution at a concentration of 1.0 mM. Cross-validation afforded 100% correct classification, and the *F*-value associated to the LDA model is 154.

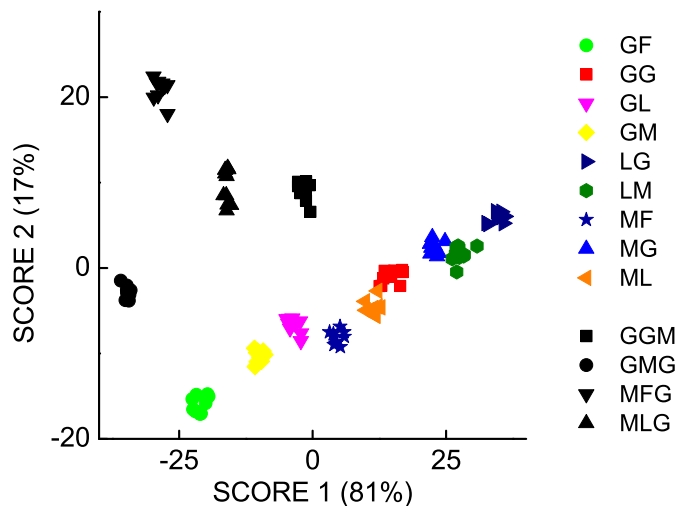


Figure B.8 – LDA score plot generated from the data of a sensor made from Al and NiCl₂. The sensor was used for the differentiation of 13 di- and tripeptides in buffered aqueous solution at a concentration of 1.0 mM. Cross-validation afforded 100% correct classification, and the *F*-value associated to the LDA model is 141.

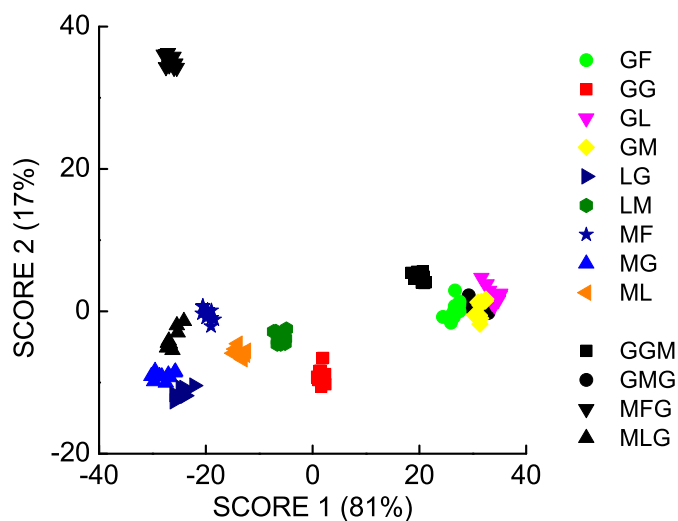


Figure B.9 – LDA score plot generated from the data of a sensor made from MCB, XO and NiCl₂. The sensor was used for the differentiation of 13 di- and tripeptides in buffered aqueous solution at a concentration of 1.0 mM. Cross-validation afforded 100% correct classification, and the *F*-value associated to the LDA model is 133.

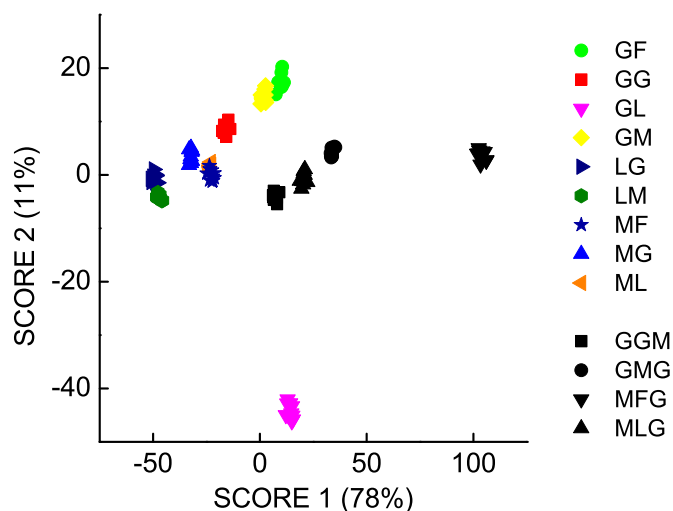


Figure B.10 – LDA score plot generated from the data of a sensor made from MCB, Al, CuCl₂ and NiCl₂. The sensor was used for the differentiation of 13 di- and tripeptides in buffered aqueous solution at a concentration of 1.0 mM. Cross-validation afforded 99% correct classification, and the *F*-value associated to the LDA model is 661.

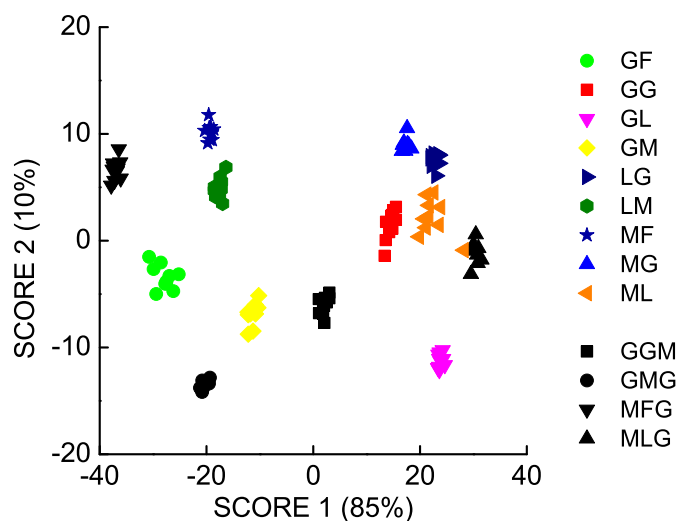


Figure B.11 – LDA score plot generated from the data of a sensor made from MCB, Al, XO and CuCl₂. The sensor was used for the differentiation of 13 di- and tripeptides in buffered aqueous solution at a concentration of 1.0 mM. Cross-validation afforded 99% correct classification, and the *F*-value associated to the LDA model is 230.

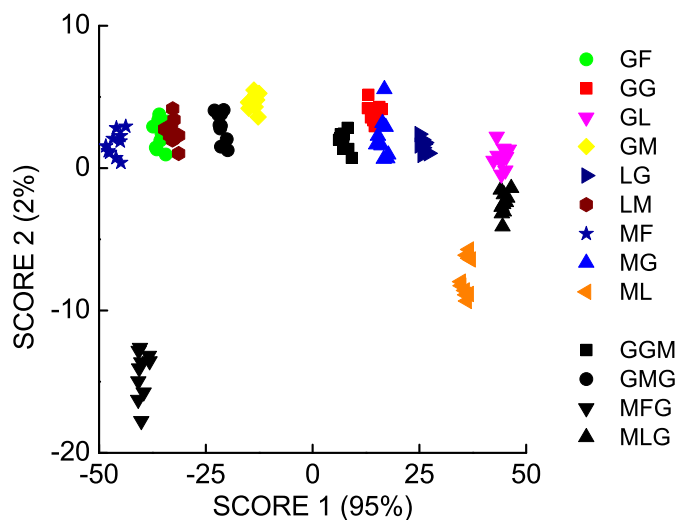


Figure B.12 – LDA score plot generated from the data of a sensor made from MCB, Al and CuCl_2 . The sensor was used for the differentiation of 13 di- and tripeptides in buffered aqueous solution at a concentration of 1.0 mM. Cross-validation afforded 99% correct classification, and the *F*-value associated to the LDA model is 190.

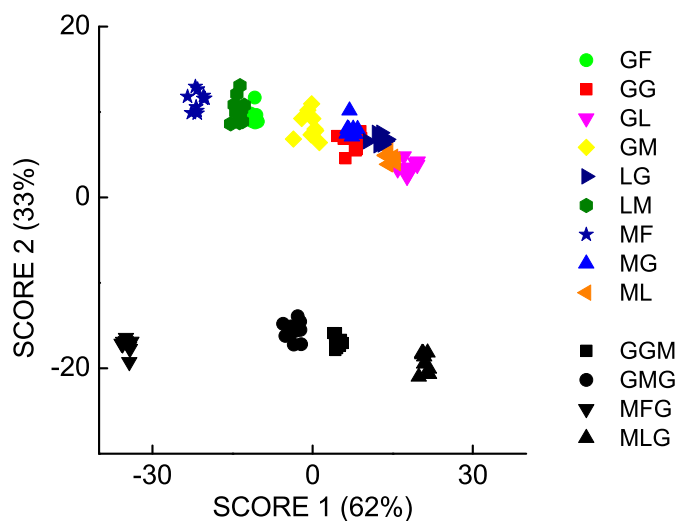


Figure B.13 – LDA score plot generated from the data of a sensor made from MCB and CuCl_2 . The sensor was used for the differentiation of 13 di- and tripeptides in buffered aqueous solution at a concentration of 1.0 mM. Cross-validation afforded 99% correct classification, and the *F*-value associated to the LDA model is 121.

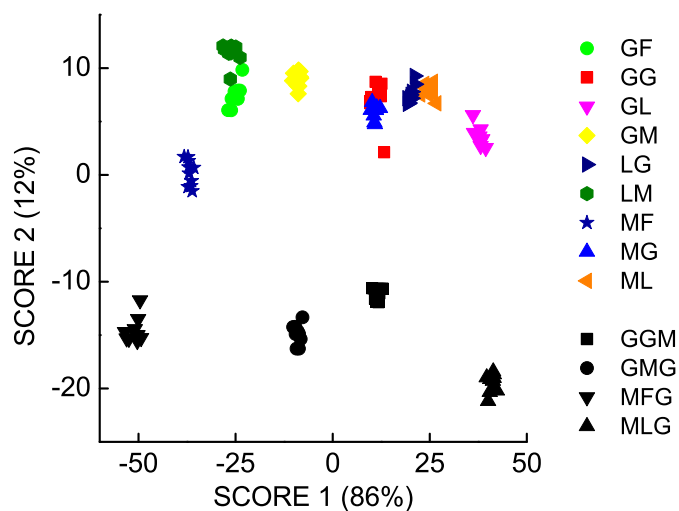


Figure B.14 – LDA score plot generated from the data of a sensor made from A1 and CuCl_2 . The sensor was used for the differentiation of 13 di- and tripeptides in buffered aqueous solution at a concentration of 1.0 mM. Cross-validation afforded 98% correct classification, and the *F*-value associated to the LDA model is 209.

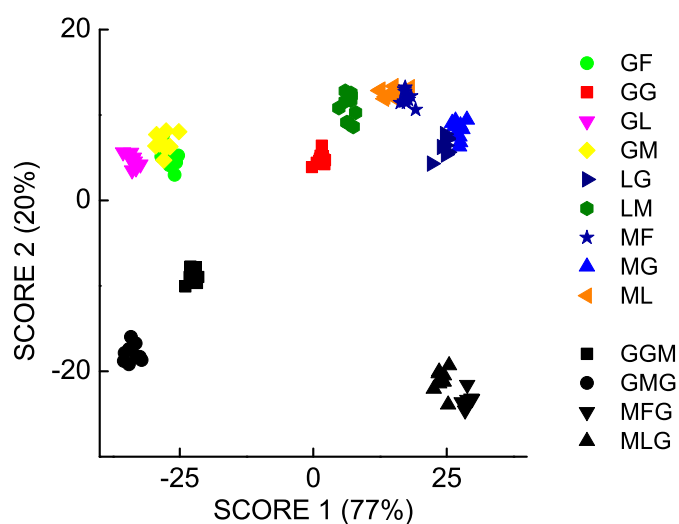


Figure B.15 – LDA score plot generated from the data of a sensor made from XO, CuCl_2 and NiCl_2 . The sensor was used for the differentiation of 13 di- and tripeptides in buffered aqueous solution at a concentration of 1.0 mM. Cross-validation afforded 98% correct classification, and the *F*-value associated to the LDA model is 194.

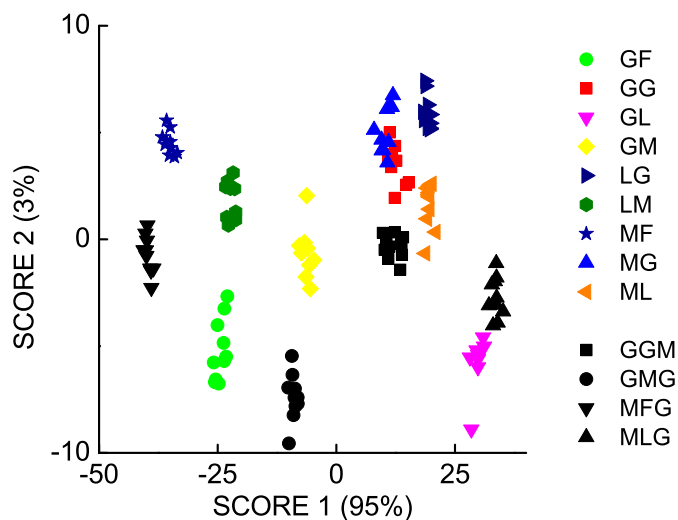


Figure B.16 – LDA score plot generated from the data of a sensor made from AI, XO and CuCl_2 . The sensor was used for the differentiation of 13 di- and tripeptides in buffered aqueous solution at a concentration of 1.0 mM. Cross-validation afforded 98% correct classification, and the *F*-value associated to the LDA model is 105.

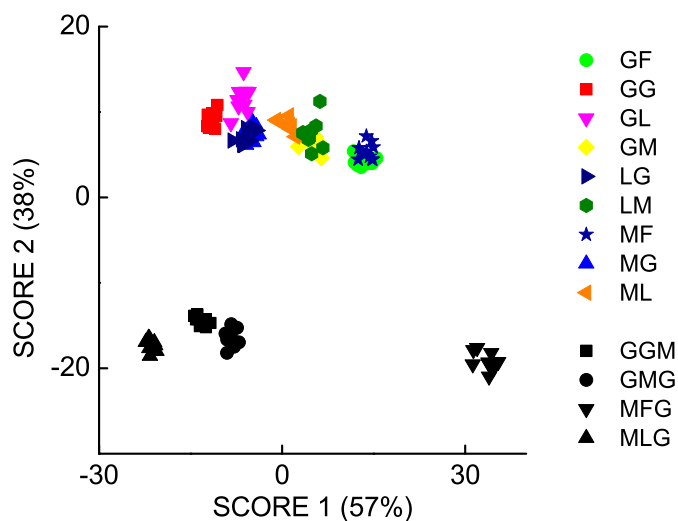


Figure B.17 – LDA score plot generated from the data of a sensor made from MCB, CuCl_2 and NiCl_2 . The sensor was used for the differentiation of 13 di- and tripeptides in buffered aqueous solution at a concentration of 1.0 mM. Cross-validation afforded 96% correct classification, and the *F*-value associated to the LDA model is 161.

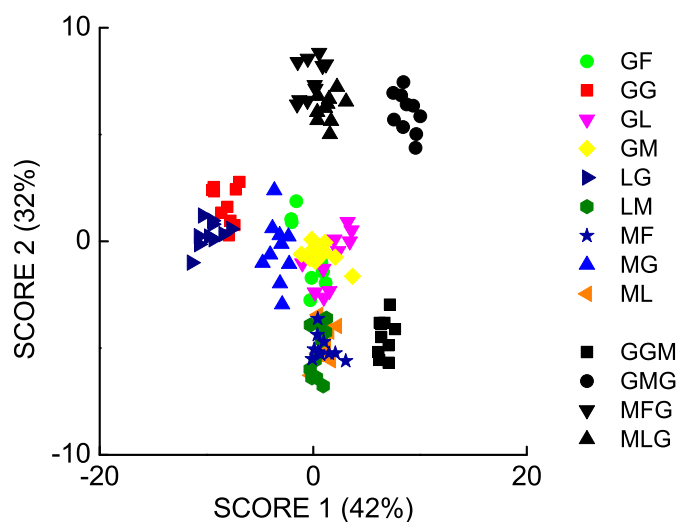


Figure B.18 – LDA score plot generated from the data of a sensor made from XO and CuCl_2 . The sensor was used for the differentiation of 13 di- and tripeptides in buffered aqueous solution at a concentration of 1.0 mM. Cross-validation afforded 87% correct classification, and the *F*-value associated to the LDA model is 63.

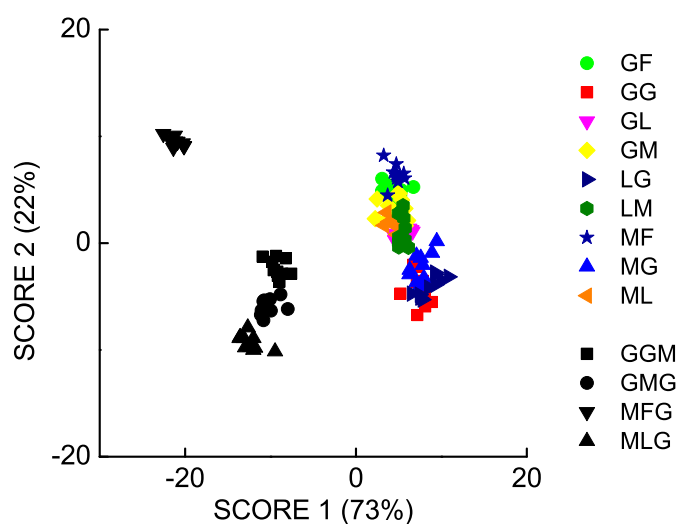


Figure B.19 – LDA score plot generated from the data of a sensor made from MCB and NiCl_2 . The sensor was used for the differentiation of 13 di- and tripeptides in buffered aqueous solution at a concentration of 1.0 mM. Cross-validation afforded 81% correct classification, and the *F*-value associated to the LDA model is 60.

Bibliography

- [1] E. V. Anslyn, *J. Org. Chem.* **2007**, *72*, 687–699.
- [2] A. P. de Silva, T. S. Moody, G. D. Wright, *Analyst* **2009**, *134*, 2385–2393.
- [3] B. T. Nguyen, E. V. Anslyn, *Coord. Chem. Rev.* **2006**, *250*, 3118–3127.
- [4] F. Mancin, E. Rampazzo, P. Tecilla, U. Tonellato, *Chem. Eur. J.* **2006**, *12*, 1844–1854.
- [5] T. W. Bell, N. M. Hext, *Chem. Soc. Rev.* **2004**, *33*, 589–598.
- [6] G. W. Gokel, W. M. Leevy, M. E. Weber, *Chem. Rev.* **2004**, *104*, 2723–2750.
- [7] R. Martínez-Máñez, F. Sancenón, *Chem. Rev.* **2003**, *103*, 4419–4476.
- [8] C. Suksai, T. Tuntulani, *Chem. Soc. Rev.* **2003**, *32*, 192–202.
- [9] P. D. Beer, J. Cadman, *Coord. Chem. Rev.* **2000**, *205*, 131–155.
- [10] L. Fabbrizzi, M. Licchelli, G. Rabaioli, A. Taglietti, *Coord. Chem. Rev.* **2000**, *205*, 85–108.
- [11] B. Valeur, I. Leray, *Coord. Chem. Rev.* **2000**, *205*, 3–40.
- [12] A. W. Czarnik, *Acc. Chem. Res.* **1994**, *27*, 302–308.
- [13] R. A. Bissell, A. P. de Silva, H. Q. N. Gunaratne, P. L. M. Lynch, G. E. M. Maguire, K. R. A. S. Sandanayake, *Chem. Soc. Rev.* **1992**, *21*, 187–195.
- [14] H.-G. Löhr, F. Vögtle, *Acc. Chem. Res.* **1985**, *18*, 65–72.
- [15] A. P. de Silva, H. Q. N. Gunaratne, T. Gunnlaugsson, A. J. M. Huxley, C. P. McCoy, J. T. Rademacher, T. E. Rice, *Chem. Rev.* **1997**, *97*, 1515–1566.
- [16] Y. Kubo, K. Tsuruzoe, S. Okuyama, R. Nishiyabu, T. Fujihara, *Chem. Commun.* **2010**, *46*, 3604–3606.
- [17] T. W. Bell, Z. Hou, Y. Luo, M. G. B. Drew, E. Chapoteau, B. P. Czech, A. Kumar, *Science* **1995**, *269*, 671–674.

- [18] R. A. Bissell, A. P. de Silva, H. Q. N. Gunaratne, P. L. M. Lynch, G. E. M. Maguire, C. P. McCoy, K. R. A. S. Samankumara, *Top. Curr. Chem.* **1993**, 168, 223–264.
- [19] K. Rurack, U. Resch-Genger, *Chem. Soc. Rev.* **2002**, 31, 116–127.
- [20] F. Pina, M. A. Bernardo, E. García-España, *Eur. J. Inorg. Chem.* **2000**, 2143–2157.
- [21] R. Bergonzi, L. Fabbrizzi, M. Licchelli, C. Mangano, *Coord. Chem. Rev.* **1998**, 170, 31–46.
- [22] S. Rochat, Z. Grote, K. Severin, *Org. Biomol. Chem.* **2009**, 7, 1147–1153.
- [23] F. Cheng, N. Tang, *Inorg. Chem. Commun.* **2008**, 11, 400–403.
- [24] D. Citterio, J. Takeda, M. Kosugi, H. Hisamoto, S.-i. Sasaki, H. Komatsu, K. Suzuki, *Anal. Chem.* **2007**, 79, 1237–1242.
- [25] T. Gunnlaugsson, B. Bichell, C. Nolan, *Tetrahedron* **2004**, 60, 5799–5806.
- [26] T. Gunnlaugsson, B. Bichell, C. Nolan, *Tetrahedron Lett.* **2002**, 43, 4989–4992.
- [27] A. P. de Silva, H. Q. N. Gunaratne, T. Gunnlaugsson, M. Nieuwenhuizen, *Chem. Commun.* **1996**, 1967–1968.
- [28] L. Fabbrizzi, A. Poggi, *Chem. Soc. Rev.* **1995**, 24, 197–202.
- [29] G. Grynkiewicz, M. Poenie, R. Y. Tsien, *J. Biol. Chem.* **1985**, 260, 3440–3450.
- [30] S. Voutsadaki, G. K. Tsikalas, E. Klontzas, G. E. Froudakis, H. E. Katerinopoulos, *Chem. Commun.* **2010**, 46, 3292–3294.
- [31] D. W. Domaille, L. Zeng, C. J. Chang, *J. Am. Chem. Soc.* **2010**, 132, 1194–1195.
- [32] I. Leray, B. Valeur, *Eur. J. Inorg. Chem.* **2009**, 3525–3535.
- [33] L. Jiao, J. Li, S. Zhang, C. Wei, E. Hao, M. G. H. Vicente, *New J. Chem.* **2009**, 33, 1888–1893.
- [34] G. Ambrosi, S. Ciattini, M. Formica, V. Fusi, L. Giorgi, E. Macedi, M. Micheloni, P. Paoli, P. Rossi, G. Zappia, *Chem. Commun.* **2009**, 7039–7041.
- [35] X. Peng, J. Du, J. Fan, J. Wang, Y. Wu, J. Zhao, S. Sun, T. Xu, *J. Am. Chem. Soc.* **2007**, 129, 1500–1501.
- [36] N. C. Lim, J. V. Schuster, M. C. Porto, M. A. Tanudra, L. Yao, H. C. Freake, C. Brückner, *Inorg. Chem.* **2005**, 44, 2018–2030.
- [37] Y. Ma, W. Luo, P. J. Quinn, Z. Liu, R. C. Hider, *J. Med. Chem.* **2004**, 47, 6349–6362.
- [38] N. C. Lim, C. Brückner, *Chem. Commun.* **2004**, 1094–1095.

- [39] S. C. Burdette, G. K. Walkup, B. Spingler, R. Y. Tsien, S. J. Lippard, *J. Am. Chem. Soc.* **2001**, 123, 7831–7841.
- [40] L. Prodi, F. Bolletta, M. Montalti, N. Zaccheroni, *Eur. J. Inorg. Chem.* **1999**, 455–460.
- [41] E. Kimura, T. Koike, *Chem. Soc. Rev.* **1998**, 27, 179–184.
- [42] T. Gunnlaugsson, H. D. P. Ali, M. Glynn, P. E. Kruger, G. M. Hussey, F. M. Pfeffer, C. M. G. dos Santos, J. Tierney, *J. Fluoresc.* **2005**, 15, 287–299.
- [43] M. E. Huston, E. U. Akkaya, A. W. Czarnik, *J. Am. Chem. Soc.* **1989**, 111, 8735–8737.
- [44] D. H. Vance, A. W. Czarnik, *J. Am. Chem. Soc.* **1994**, 116, 9397–9398.
- [45] T. James, S. Shinkai, *Top. Curr. Chem.* **2002**, 218, 159–200.
- [46] R. E. Gawley, H. Mao, M. M. Haque, J. B. Thorne, J. S. Pharr, *J. Org. Chem.* **2007**, 72, 2187–2191.
- [47] R. E. Gawley, S. Pinet, C. M. Cardona, P. K. Datta, T. Ren, W. C. Guida, J. Nydick, R. M. Leblanc, *J. Am. Chem. Soc.* **2002**, 124, 13448–13453.
- [48] M. Inouye, K.-i. Hashimoto, K. Isagawa, *J. Am. Chem. Soc.* **1994**, 116, 5517–5518.
- [49] K. N. Koh, K. Araki, A. Ikeda, H. Otsuka, S. Shinkai, *J. Am. Chem. Soc.* **1996**, 118, 755–758.
- [50] S. L. Wiskur, H. Aït-Haddou, J. J. Lavigne, E. V. Anslyn, *Acc. Chem. Res.* **2001**, 34, 963–972.
- [51] L. Fabbrizzi, M. Licchelli, A. Taglietti, *Dalton Trans.* **2003**, 3471–3479.
- [52] L. Fabbrizzi, N. Marcotte, F. Stomeo, A. Taglietti, *Angew. Chem. Int. Ed.* **2002**, 41, 3811–3814.
- [53] K. Severin, *Top. Organomet. Chem.* **2006**, 17, 123–142.
- [54] J. J. Lavigne, E. V. Anslyn, *Angew. Chem. Int. Ed.* **1999**, 38, 3666–3669.
- [55] A. M. Piątek, Y. J. Bomble, S. L. Wiskur, E. V. Anslyn, *J. Am. Chem. Soc.* **2004**, 126, 6072–6077.
- [56] K. Niikura, A. Metzger, E. V. Anslyn, *J. Am. Chem. Soc.* **1998**, 120, 8533–8534.
- [57] S. E. Schneider, S. N. O'Neil, E. V. Anslyn, *J. Am. Chem. Soc.* **2000**, 122, 542–543.
- [58] S. Atilgan, E. U. Akkaya, *Tetrahedron Lett.* **2004**, 45, 9269–9271.
- [59] V. Amendola, G. Bergamaschi, A. Buttafava, L. Fabbrizzi, E. Monzani, *J. Am. Chem. Soc.* **2010**, 132, 147–156.

- [60] P. P. Neelakandan, M. Hariharan, D. Ramaiah, *J. Am. Chem. Soc.* **2006**, 128, 11334–11335.
- [61] C. Siering, H. Kerschbaumer, M. Nieger, S. R. Waldvogel, *Org. Lett.* **2006**, 8, 1471–1474.
- [62] H. Aït-Haddou, S. L. Wiskur, V. M. Lynch, E. V. Anslyn, *J. Am. Chem. Soc.* **2001**, 123, 11296–11297.
- [63] M. Bonizzoni, L. Fabbrizzi, G. Piovani, A. Taglietti, *Tetrahedron* **2004**, 60, 11159–11162.
- [64] J. F. Folmer-Andersen, V. M. Lynch, E. V. Anslyn, *Chem. Eur. J.* **2005**, 11, 5319–5326.
- [65] A. Buryak, K. Severin, *Angew. Chem. Int. Ed.* **2004**, 43, 4771–4774.
- [66] M. A. Hortalá, L. Fabbrizzi, N. Marcotte, F. Stomeo, A. Taglietti, *J. Am. Chem. Soc.* **2003**, 125, 20–21.
- [67] A. T. Wright, E. V. Anslyn, *Org. Lett.* **2004**, 6, 1341–1344.
- [68] J. Veliscek Carolan, S. J. Butler, K. A. Jolliffe, *J. Org. Chem.* **2009**, 74, 2992–2996.
- [69] B. P. Morgan, S. He, R. C. Smith, *Inorg. Chem.* **2007**, 46, 9262–9266.
- [70] C. Yin, F. Gao, F. Huo, P. Yang, *Chem. Commun.* **2004**, 934–935.
- [71] S. L. Tobey, E. V. Anslyn, *Org. Lett.* **2003**, 5, 2029–2031.
- [72] M. Su Han, D. H. Kim, *Angew. Chem. Int. Ed.* **2002**, 41, 3809–3811.
- [73] M. K. Coggins, A. M. Parker, A. Mangalum, G. A. Galdamez, R. C. Smith, *Eur. J. Org. Chem.* **2009**, 343–348.
- [74] M. J. McDonough, A. J. Reynolds, W. Y. G. Lee, K. A. Jolliffe, *Chem. Commun.* **2006**, 2971–2973.
- [75] T. Zhang, E. V. Anslyn, *Tetrahedron* **2004**, 60, 11117–11124.
- [76] Z. Zhong, E. V. Anslyn, *Angew. Chem. Int. Ed.* **2003**, 42, 3005–3008.
- [77] P. A. Gale, L. J. Twyman, C. I. Handlin, J. L. Sessler, *Chem. Commun.* **1999**, 1851–1852.
- [78] T. Zhang, E. V. Anslyn, *Org. Lett.* **2006**, 8, 1649–1652.
- [79] T. Zhang, E. V. Anslyn, *Org. Lett.* **2007**, 9, 1627–1629.
- [80] K. Kacprzak, J. Grajewski, J. Gawronski, *Tetrahedron: Asymmetry* **2006**, 17, 1332–1336.

- [81] L. Zhu, E. V. Anslyn, *J. Am. Chem. Soc.* **2004**, *126*, 3676–3677.
- [82] L. Fabbrizzi, F. Foti, A. Taglietti, *Org. Lett.* **2005**, *7*, 2603–2606.
- [83] M. Boiocchi, M. Bonizzoni, L. Fabbrizzi, G. Piovani, A. Taglietti, *Angew. Chem. Int. Ed.* **2004**, *43*, 3847–3852.
- [84] S. L. Wiskur, J. J. Lavigne, A. Metzger, S. L. Tobey, V. Lynch, E. V. Anslyn, *Chem. Eur. J.* **2004**, *10*, 3792–3804.
- [85] A. Metzger, V. M. Lynch, E. V. Anslyn, *Angew. Chem. Int. Ed. Engl.* **1997**, *36*, 862–865.
- [86] L. Fabbrizzi, A. Leone, A. Taglietti, *Angew. Chem. Int. Ed.* **2001**, *40*, 3066–3069.
- [87] Z. Zhong, E. V. Anslyn, *J. Am. Chem. Soc.* **2002**, *124*, 9014–9015.
- [88] D. H. Kim, M. Su Han, *Bioorg. Med. Chem. Lett.* **2003**, *13*, 2543–2546.
- [89] M. H. Lim, C. Kuang, S. J. Lippard, *ChemBioChem* **2006**, *7*, 1571–1576.
- [90] S. A. Hilderbrand, M. H. Lim, S. J. Lippard, *J. Am. Chem. Soc.* **2004**, *126*, 4972–4978.
- [91] J. F. Folmer-Andersen, V. M. Lynch, E. V. Anslyn, *J. Am. Chem. Soc.* **2005**, *127*, 7986–7987.
- [92] D. Leung, J. F. Folmer-Andersen, V. M. Lynch, E. V. Anslyn, *J. Am. Chem. Soc.* **2008**, *130*, 12318–12327.
- [93] S. H. Shabbir, C. J. Regan, E. V. Anslyn, *Proc. Natl. Acad. Sci. U.S.A.* **2009**, *106*, 10487–10492.
- [94] E. Fischer, *Ber. Dtsch. Chem. Ges.* **1894**, *27*, 2985–2993.
- [95] J. J. Lavigne, E. V. Anslyn, *Angew. Chem. Int. Ed.* **2001**, *40*, 3118–3130.
- [96] K. J. Albert, N. S. Lewis, C. L. Schauer, G. A. Sotzing, S. E. Stitzel, T. P. Vaid, D. R. Walt, *Chem. Rev.* **2000**, *100*, 2595–2626.
- [97] K. Persaud, G. Dodd, *Nature* **1982**, *299*, 352–355.
- [98] D. James, S. M. Scott, Z. Ali, W. T. O'Hare, *Microchim. Acta* **2005**, *149*, 1–17.
- [99] N. S. Lewis, *Acc. Chem. Res.* **2004**, *37*, 663–672.
- [100] K. S. Suslick, *MRS Bulletin* **2004**, *29*, 720–725.
- [101] B. A. Suslick, L. Feng, K. S. Suslick, *Anal. Chem.* **2010**, *82*, 2067–2073.
- [102] M. Peris, L. Escuder-Gilabert, *Anal. Chim. Acta* **2009**, *638*, 1–15.
- [103] F. Röck, N. Barsan, U. Weimar, *Chem. Rev.* **2008**, *108*, 705–725.

- [104] A. K. Deisingh, D. C. Stone, M. Thompson, *Int. J. Food. Sci. Technol.* **2004**, 39, 587-604.
- [105] T. Nakamoto, A. Fukuda, T. Moriizumi, *Sens. Actuators B* **1993**, 10, 85-90.
- [106] A. Rudnitskaya, A. Legin, *J. Ind. Microbiol. Biotechnol.* **2008**, 35, 443-451.
- [107] S. H. Lim, L. Feng, J. W. Kemling, C. J. Musto, K. S. Suslick, *Nat. Chem.* **2009**, 1, 562-567.
- [108] S. H. Lim, J. W. Kemling, L. Feng, K. S. Suslick, *Analyst* **2009**, 134, 2453-2457.
- [109] Q. Ameer, S. B. Adeloju, *Sens. Actuators B* **2005**, 106, 541-552.
- [110] P. C. Jurs, G. A. Bakken, H. E. McClelland, *Chem. Rev.* **2000**, 100, 2649-2678.
- [111] N. A. Rakow, K. S. Suslick, *Nature* **2000**, 406, 710-713.
- [112] L. Feng, C. J. Musto, J. W. Kemling, S. H. Lim, K. S. Suslick, *Chem. Commun.* **2010**, 46, 2037-2039.
- [113] L. Feng, C. J. Musto, K. S. Suslick, *J. Am. Chem. Soc.* **2010**, 132, 4046-4047.
- [114] R. Paolesse, L. Lvova, S. Nardis, C. Di Natale, A. D'Amico, F. Lo Castro, *Microchim. Acta* **2008**, 163, 103-112.
- [115] M. L. Rodríguez-Méndez, V. Parra, C. Apetrei, S. Villanueva, M. Gay, N. Prieto, J. Martinez, J. A. de Saja, *Microchim. Acta* **2008**, 163, 23-31.
- [116] M. Scampicchio, D. Ballabio, A. Arecchi, S. M. Cosio, S. Mannino, *Microchim. Acta* **2008**, 163, 11-21.
- [117] F. Winquist, *Microchim. Acta* **2008**, 163, 3-10.
- [118] A. Gutés, F. Céspedes, M. del Valle, *Anal. Chim. Acta* **2007**, 600, 90-96.
- [119] P. Ciosek, W. Wróblewski, *Analyst* **2007**, 132, 963-978.
- [120] P. Ciosek, Z. Brzózka, W. Wróblewski, *Sens. Actuators B* **2004**, 103, 76-83.
- [121] C. Krantz-Rülcker, M. Stenberg, F. Winquist, I. Lundström, *Anal. Chim. Acta* **2001**, 426, 217-226.
- [122] B. E. Collins, A. T. Wright, E. V. Anslyn, *Top. Curr. Chem.* **2007**, 277, 181-218.
- [123] S. Otto, K. Severin, *Top. Curr. Chem.* **2007**, 277, 267-288.
- [124] A. T. Wright, E. V. Anslyn, *Chem. Soc. Rev.* **2006**, 35, 14-28.
- [125] L. A. Baumes, M. Buaki Sogo, P. Montes-Navajas, A. Corma, H. Garcia, *Tetrahedron Lett.* **2009**, 50, 7001-7004.

- [126] M. S. Maynor, T. K. Deason, T. L. Nelson, J. J. Lavigne, *Supramol. Chem.* **2009**, *21*, 310 – 315.
- [127] Z. Wang, M. A. Palacios, P. Anzenbacher Jr., *Anal. Chem.* **2008**, *80*, 7451–7459.
- [128] M. A. Palacios, Z. Wang, V. A. Montes, G. V. Zyryanov, P. Anzenbacher Jr., *J. Am. Chem. Soc.* **2008**, *130*, 10307–10314.
- [129] J.-S. Lee, J. W. Lee, Y.-T. Chang, *J. Comb. Chem.* **2007**, *9*, 926–928.
- [130] L. Basabe-Desmonts, F. van der Baan, R. Zimmerman, D. Reinhoudt, M. Crego-Calama, *Sensors* **2007**, *7*, 1731–1746.
- [131] J. W. Lee, J.-S. Lee, M. Kang, A. I. Su, Y.-T. Chang, *Chem. Eur. J.* **2006**, *12*, 5691–5696.
- [132] T. Carofiglio, C. Fregonese, G. J. Mohr, F. Rastrelli, U. Tonellato, *Tetrahedron* **2006**, *62*, 1502–1507.
- [133] R. Zimmerman, L. Basabe-Desmonts, F. van der Baan, D. N. Reinhoudt, M. Crego-Calama, *J. Mater. Chem.* **2005**, *15*, 2772–2777.
- [134] I. Yoshimura, Y. Miyahara, N. Kasagi, H. Yamane, A. Ojida, I. Hamachi, *J. Am. Chem. Soc.* **2004**, *126*, 12204–12205.
- [135] D. Mikami, T. Ohki, K. Yamaji, S. Ishihara, D. Citterio, M. Hagiwara, K. Suzuki, *Anal. Chem.* **2004**, *76*, 5726–5733.
- [136] A. P. Goodey, J. T. McDevitt, *J. Am. Chem. Soc.* **2003**, *125*, 2870–2871.
- [137] T. Mayr, C. Igel, G. Liebsch, I. Klimant, O. S. Wolfbeis, *Anal. Chem.* **2003**, *75*, 4389–4396.
- [138] A. Goodey, J. J. Lavigne, S. M. Savoy, M. D. Rodriguez, T. Curey, A. Tsao, G. Simmons, J. Wright, S.-J. Yoo, Y. Sohn, E. V. Anslyn, J. B. Shear, D. P. Neikirk, J. T. McDevitt, *J. Am. Chem. Soc.* **2001**, *123*, 2559–2570.
- [139] H. Prestel, A. Gahr, R. Niessner, *Fresenius J. Anal. Chem.* **2000**, *368*, 182–191.
- [140] J. J. Lavigne, S. Savoy, M. B. Clevenger, J. E. Ritchie, B. McDoniel, S.-J. Yoo, E. V. Anslyn, J. T. McDevitt, J. B. Shear, D. Neikirk, *J. Am. Chem. Soc.* **1998**, *120*, 6429–6430.
- [141] M. A. Palacios, R. Nishiyabu, M. Marquez, P. Anzenbacher Jr., *J. Am. Chem. Soc.* **2007**, *129*, 7538–7544.
- [142] G. V. Zyryanov, M. A. Palacios, P. Anzenbacher Jr., *Angew. Chem. Int. Ed.* **2007**, *46*, 7849–7852.
- [143] B. García-Acosta, R. Martínez-Máñez, F. Sancenón, J. Soto, K. Rurack, M. Spieles, E. García-Breijo, L. Gil, *Inorg. Chem.* **2007**, *46*, 3123–3135.

- [144] S. Yamaguchi, I. Yoshimura, T. Kohira, S.-i. Tamaru, I. Hamachi, *J. Am. Chem. Soc.* **2005**, *127*, 11835–11841.
- [145] B. García-Acosta, X. Albiach-Martí, E. García, L. Gil, R. Martínez-Mañez, K. Rurack, F. Sancenón, J. Soto, *Chem. Commun.* **2004**, 774–775.
- [146] H. Liu, J. He, J. Tang, H. Liu, P. Pang, D. Cao, P. Krstic, S. Joseph, S. Lindsay, C. Nuckolls, *Science* **2010**, *327*, 64–67.
- [147] P. Montes-Navajas, L. A. Baumes, A. Corma, H. Garcia, *Tetrahedron Lett.* **2009**, *50*, 2301–2304.
- [148] M. S. Maynor, T. L. Nelson, C. O'Sullivan, J. J. Lavigne, *Org. Lett.* **2007**, *9*, 3217–3220.
- [149] T. L. Nelson, I. Tran, T. G. Ingallinera, M. S. Maynor, J. J. Lavigne, *Analyst* **2007**, *132*, 1024–1030.
- [150] T. L. Nelson, C. O'Sullivan, N. T. Greene, M. S. Maynor, J. J. Lavigne, *J. Am. Chem. Soc.* **2006**, *128*, 5640–5641.
- [151] N. T. Greene, K. D. Shimizu, *J. Am. Chem. Soc.* **2005**, *127*, 5695–5700.
- [152] C. Zhang, K. S. Suslick, *J. Am. Chem. Soc.* **2005**, *127*, 11548–11549.
- [153] N. T. Greene, S. L. Morgan, K. D. Shimizu, *Chem. Commun.* **2004**, 1172–1173.
- [154] L. A. Baumes, M. Buaki Sogo, P. Montes-Navajas, A. Corma, H. Garcia, *Chem. Eur. J.* **2010**, *16*, 4489–4495.
- [155] M. Kitamura, S. H. Shabbir, E. V. Anslyn, *J. Org. Chem.* **2009**, *74*, 4479–4489.
- [156] J. Viljanen, J. Larsson, A. Larsson, K. S. Broo, *Bioconjugate Chem.* **2007**, *18*, 1935–1945.
- [157] S. L. Wiskur, P. N. Floriano, E. V. Anslyn, J. T. McDevitt, *Angew. Chem. Int. Ed.* **2003**, *42*, 2070–2072.
- [158] S. C. McCleskey, P. N. Floriano, S. L. Wiskur, E. V. Anslyn, J. T. McDevitt, *Tetrahedron* **2003**, *59*, 10089–10092.
- [159] S. L. Wiskur, E. V. Anslyn, *J. Am. Chem. Soc.* **2001**, *123*, 10109–10110.
- [160] M. E. Germain, M. J. Knapp, *J. Am. Chem. Soc.* **2008**, *130*, 5422–5423.
- [161] A. Ponnu, N. Y. Edwards, E. V. Anslyn, *New J. Chem.* **2008**, *32*, 848–855.
- [162] A. D. Hughes, I. C. Glenn, A. D. Patrick, A. Ellington, E. V. Anslyn, *Chem. Eur. J.* **2008**, *14*, 1822–1827.
- [163] J. Gao, A. Granzhan, X. Qian, K. Severin, *Chem. Commun.* **2010**, *46*, 5515–5517.

- [164] Z. Yao, X. Feng, W. Hong, C. Li, G. Shi, *Chem. Commun.* **2009**, 4696–4698.
- [165] A. Schiller, B. Vilozny, R. A. Wessling, B. Singaram, *Anal. Chim. Acta* **2008**, 627, 203–211.
- [166] A. Buryak, A. Pozdnoukhov, K. Severin, *Chem. Commun.* **2007**, 2366–2368.
- [167] S. C. McCleskey, M. J. Griffin, S. E. Schneider, J. T. McDevitt, E. V. Anslyn, *J. Am. Chem. Soc.* **2003**, 125, 1114–1115.
- [168] E. G. Green, M. J. Olah, T. Abramova, L. R. Williams, D. Stefanovic, T. Worgall, M. N. Stojanović, *J. Am. Chem. Soc.* **2006**, 128, 15278–15282.
- [169] M. N. Stojanović, E. G. Green, S. Semova, D. B. Nikić, D. W. Landry, *J. Am. Chem. Soc.* **2003**, 125, 6085–6089.
- [170] R. Pei, A. Shen, M. J. Olah, D. Stefanovic, T. Worgall, M. N. Stojanović, *Chem. Commun.* **2009**, 3193–3195.
- [171] C. J. Musto, S. H. Lim, K. S. Suslick, *Anal. Chem.* **2009**, 81, 6526–6533.
- [172] R. B. C. Jagt, R. F. Gómez-Biagi, M. Nitz, *Angew. Chem. Int. Ed.* **2009**, 48, 1995–1997.
- [173] S. H. Lim, C. J. Musto, E. Park, W. Zhong, K. S. Suslick, *Org. Lett.* **2008**, 10, 4405–4408.
- [174] A. Schiller, R. A. Wessling, B. Singaram, *Angew. Chem. Int. Ed.* **2007**, 46, 6457–6459.
- [175] N. Y. Edwards, T. W. Sager, J. T. McDevitt, E. V. Anslyn, *J. Am. Chem. Soc.* **2007**, 129, 13575–13583.
- [176] F. Zaubitzer, A. Buryak, K. Severin, *Chem. Eur. J.* **2006**, 12, 3928–3934.
- [177] Y. Koshi, E. Nakata, H. Yamane, I. Hamachi, *J. Am. Chem. Soc.* **2006**, 128, 10413–10422.
- [178] J. W. Lee, J.-S. Lee, Y.-T. Chang, *Angew. Chem. Int. Ed.* **2006**, 45, 6485–6487.
- [179] J. F. Folmer-Andersen, M. Kitamura, E. V. Anslyn, *J. Am. Chem. Soc.* **2006**, 128, 5652–5653.
- [180] A. Buryak, K. Severin, *J. Am. Chem. Soc.* **2005**, 127, 3700–3701.
- [181] S. Rochat, J. Gao, X. Qian, F. Zaubitzer, K. Severin, *Chem. Eur. J.* **2010**, 16, 104–113.
- [182] T. Zhang, N. Y. Edwards, M. Bonizzoni, E. V. Anslyn, *J. Am. Chem. Soc.* **2009**, 131, 11976–11984.

- [183] F. Zaubitzer, T. Riis-Johannessen, K. Severin, *Org. Biomol. Chem.* **2009**, *7*, 4598–4603.
- [184] B. E. Collins, E. V. Anslyn, *Chem. Eur. J.* **2007**, *13*, 4700–4708.
- [185] A. T. Wright, N. Y. Edwards, E. V. Anslyn, J. T. McDevitt, *Angew. Chem. Int. Ed.* **2007**, *46*, 8212–8215.
- [186] A. Buryak, K. Severin, *J. Comb. Chem.* **2006**, *8*, 540–543.
- [187] A. T. Wright, E. V. Anslyn, J. T. McDevitt, *J. Am. Chem. Soc.* **2005**, *127*, 17405–17411.
- [188] A. Buryak, K. Severin, *Angew. Chem. Int. Ed.* **2005**, *44*, 7935–7938.
- [189] H. Li, G. C. Bazan, *Adv. Mat.* **2009**, *21*, 964–967.
- [190] D. C. González, E. N. Savariar, S. Thayumanavan, *J. Am. Chem. Soc.* **2009**, *131*, 7708–7716.
- [191] S. Jiwpanich, B. S. Sandanaraj, S. Thayumanavan, *Chem. Commun.* **2009**, 806–808.
- [192] D. Margulies, A. D. Hamilton, *Angew. Chem. Int. Ed.* **2009**, *48*, 1771–1774.
- [193] M. De, S. Rana, H. Akpınar, O. R. Miranda, R. R. Arvizo, U. H. F. Bunz, V. M. Rotello, *Nat. Chem.* **2009**, *1*, 461–465.
- [194] E. N. Savariar, S. Ghosh, D. C. González, S. Thayumanavan, *J. Am. Chem. Soc.* **2008**, *130*, 5416–5417.
- [195] O. R. Miranda, C.-C. You, R. Phillips, I.-B. Kim, P. S. Ghosh, U. H. F. Bunz, V. M. Rotello, *J. Am. Chem. Soc.* **2007**, *129*, 9856–9857.
- [196] C.-C. You, O. R. Miranda, B. Gider, P. S. Ghosh, I.-B. Kim, B. Erdogan, S. A. Krovi, U. H. F. Bunz, V. M. Rotello, *Nat. Nanotechnol.* **2007**, *2*, 318–323.
- [197] B. S. Sandanaraj, R. Demont, S. Thayumanavan, *J. Am. Chem. Soc.* **2007**, *129*, 3506–3507.
- [198] H. Zhou, L. Baldini, J. Hong, A. J. Wilson, A. D. Hamilton, *J. Am. Chem. Soc.* **2006**, *128*, 2421–2425.
- [199] A. T. Wright, M. J. Griffin, Z. Zhong, S. C. McCleskey, E. V. Anslyn, J. T. McDevitt, *Angew. Chem. Int. Ed.* **2005**, *44*, 6375–6378.
- [200] M. M. Reddy, T. Kodadek, *Proc. Natl. Acad. Sci. U.S.A.* **2005**, *102*, 12672–12677.
- [201] L. Baldini, A. J. Wilson, J. Hong, A. D. Hamilton, *J. Am. Chem. Soc.* **2004**, *126*, 5656–5657.
- [202] C. Zhang, K. S. Suslick, *J. Agric. Food Chem.* **2007**, *55*, 237–242.

- [203] A. Bajaj, O. R. Miranda, R. Phillips, I.-B. Kim, D. J. Jerry, U. H. F. Bunz, V. M. Rotello, *J. Am. Chem. Soc.* **2010**, 132, 1018–1022.
- [204] A. Bajaj, O. R. Miranda, I.-B. Kim, R. L. Phillips, D. J. Jerry, U. H. F. Bunz, V. M. Rotello, *Proc. Natl. Acad. Sci. U.S.A.* **2009**, 106, 10912–10916.
- [205] *Dynamic Combinatorial Chemistry*, (Eds.: J. N. H. Reek, S. Otto), Wiley-VCH, Weinheim, **2010**.
- [206] S. Ladame, *Org. Biomol. Chem.* **2008**, 6, 219–226.
- [207] R. F. Ludlow, S. Otto, *Chem. Soc. Rev.* **2008**, 37, 101–108.
- [208] J.-M. Lehn, *Chem. Soc. Rev.* **2007**, 36, 151–160.
- [209] P. T. Corbett, J. Leclaire, L. Vial, K. R. West, J.-L. Wietor, J. K. M. Sanders, S. Otto, *Chem. Rev.* **2006**, 106, 3652–3711.
- [210] S. J. Rowan, S. J. Cantrill, G. R. L. Cousins, J. K. M. Sanders, J. F. Stoddart, *Angew. Chem. Int. Ed.* **2002**, 41, 898–952.
- [211] P.-K. Müller-Graff, H. Szelke, K. Severin, R. Krämer, *Org. Biomol. Chem.* **2010**, 8, 2327–2331.
- [212] A. Buryak, F. Zaubitzer, A. Pozdnoukhov, K. Severin, *J. Am. Chem. Soc.* **2008**, 130, 11260–11261.
- [213] S. Rochat, K. Severin, *J. Comb. Chem.* **2010**, 12, 595–599.
- [214] P. K. Hopke, *Anal. Chim. Acta* **2003**, 500, 365–377.
- [215] A. C. Rencher, *Methods of Multivariate Analysis*, John Wiley & Sons, New York, **1995**.
- [216] P. B. Mitchell, D. Hadzi-Pavlovic, *B. World Health Organ.* **2000**, 78, 515–517.
- [217] J. F. J. Cade, *Med. J. Australia* **1949**, 2, 349–351.
- [218] A. C. Corcoran, R. D. Taylor, I. H. Page, *J. Am. Med. Assoc.* **1949**, 139, 685–688.
- [219] G. Johnson, S. Gershon, *Aust. NZ J. Psychiat.* **1999**, 33, S48–S53.
- [220] N. J. Birch in *Metal Ions in Biological Systems, Vol. 41* (Eds.: A. Sigel, H. Sigel), Marcel Dekker, Inc., Basel, **2004**, pp. 305–332.
- [221] R. S. McIntyre, D. A. Mancini, S. Parikh, S. H. Kennedy, *Can. J. Psychiat.* **2001**, 46, 322–327.
- [222] N. J. Birch, *Chem. Rev.* **1999**, 99, 2659–2682.
- [223] I. Daly, *Lancet* **1997**, 349, 1157–1160.

- [224] F. Fornai, P. Longone, L. Cafaro, O. Kastsuchenka, M. Ferrucci, M. L. Manca, G. Lazzeri, A. Spalloni, N. Bellio, P. Lenzi, N. Modugno, G. Siciliano, C. Isidoro, L. Murri, S. Ruggieri, A. Paparelli, *Proc. Natl. Acad. Sci. U.S.A.* **2008**, 105, 2052--2057.
- [225] F. Fornai, P. Longone, M. Ferrucci, P. Lenzi, C. Isidoro, S. Ruggieri, A. Paparelli, *Autophagy* **2008**, 4, 527--530.
- [226] J. Zhong, W.-H. Lee, *Expert Opin. Drug Saf.* **2007**, 6, 375--383.
- [227] B. De Strooper, J. Woodgett, *Nature* **2003**, 423, 392--393.
- [228] C. J. Phiel, C. A. Wilson, V. M.-Y. Lee, P. S. Klein, *Nature* **2003**, 423, 435--439.
- [229] H. R. Pilcher, *Nature* **2003**, 425, 118--120.
- [230] G. D. Christian, *Sensors* **2002**, 2, 432--435.
- [231] G. D. Christian, *J. Pharmaceut. Biomed. Anal.* **1996**, 14, 899--908.
- [232] R. A. Bartsch, V. Ramesh, R. O. Bach, T. Shono, K. Kimura in *Lithium Chemistry: A Theoretical and Experimental Overview* (Eds.: A.-M. Sapse, P. v. R. Schleyer), John Wiley & Sons, New York, **1995**, pp. 393--476.
- [233] D. Mota de Freitas, M. M. C. A. Castro, C. F. G. C. Geraldés, *Acc. Chem. Res.* **2006**, 39, 283--291.
- [234] F. A. Cotton, G. Wilkinson, C. A. Murillo, M. Bochmann, *Advanced Inorganic Chemistry*, John Wiley & Sons, New York, 6th ed., **1999**.
- [235] *Geigy Scientific Tables*, Vol. 3, (Ed.: C. Lentner), Ciba-Geigy, Basel, 8th ed., **1984**, p. 65.
- [236] M. Cametti, L. Ilander, K. Rissanen, *Inorg. Chem.* **2009**, 48, 8632--8637.
- [237] N. Wanichecheva, J. S. Benco, C. R. Lambert, W. G. McGimpsey, *Photochem. Photobiol.* **2006**, 82, 268--273.
- [238] K. Hiratani, M. Kaneyama, Y. Nagawa, E. Koyama, M. Kanetsato, *J. Am. Chem. Soc.* **2004**, 126, 13568--13569.
- [239] J. S. Benco, H. A. Nienaber, W. G. McGimpsey, *J. Photochem. Photobiol. A* **2004**, 162, 289--296.
- [240] W. Qin, S. O. Obare, C. J. Murphy, S. M. Angel, *Anal. Chem.* **2002**, 74, 4757--4762.
- [241] G. G. Talanova, V. S. Talanov, H.-S. Hwang, B. A. Eliasi, R. A. Bartsch, *J. Chem. Soc. Perkin Trans. 2* **2002**, 1869--1874.
- [242] S. Tsuchiya, Y. Nakatani, R. Ibrahim, S. Ogawa, *J. Am. Chem. Soc.* **2002**, 124, 4936--4937.

- [243] J.-A. Chen, J.-L. Lai, G. H. Lee, Y. Wang, J. K. Su, H.-C. Yeh, W.-Y. Lin, M.-k. Leung, *Org. Lett.* **2001**, *3*, 3999–4002.
- [244] S. O. Obare, C. J. Murphy, *Inorg. Chem.* **2001**, *40*, 6080–6082.
- [245] L. A. Paquette, J. Tae, *J. Am. Chem. Soc.* **2001**, *123*, 4974–4984.
- [246] L. A. Paquette, J. Tae, E. R. Hickey, R. D. Rogers, *Angew. Chem. Int. Ed.* **1999**, *38*, 1409–1411.
- [247] M. Ciampolini, M. Formica, V. Fusi, A. Saint-Mauricec, M. Micheloni, N. Nardi, R. Pontellini, F. Pina, P. Romani, A. M. Sabatini, B. Valtancoli, *Eur. J. Inorg. Chem.* **1999**, 2261–2268.
- [248] Ç. Erk, A. Göçmen, M. Bulut, *Supramol. Chem.* **1999**, *11*, 49 – 56.
- [249] C. R. Chenthamarakshan, A. Ajayaghosh, *Tetrahedron Lett.* **1998**, *39*, 1795–1798.
- [250] S. Inokuma, M. Takezawa, H. Satoh, Y. Nakamura, T. Sasaki, J. Nishimura, *J. Org. Chem.* **1998**, *63*, 5791–5796.
- [251] F. Bockstahl, E. Graf, M. W. Hosseini, D. Suhr, A. De Cian, J. Fischer, *Tetrahedron Lett.* **1997**, *38*, 7539–7542.
- [252] H. Tsukube, S. Shinoda, Y. Mizutani, M. Okano, K. Takagi, K. Hori, *Tetrahedron* **1997**, *53*, 3487–3496.
- [253] K. Kobiro, *Coord. Chem. Rev.* **1996**, *148*, 135–149.
- [254] S. Faulkner, R. Katakly, D. Parker, A. Teasdale, *J. Chem. Soc. Perkin Trans. 2* **1995**, 1761–1769.
- [255] D. J. Cram, R. A. Carmack, R. C. Helgeson, *J. Am. Chem. Soc.* **1988**, *110*, 571–577.
- [256] W. Liu, J.-H. Lu, Y. Ji, J.-L. Zuo, X.-Z. You, *Tetrahedron Lett.* **2006**, *47*, 3431–3434.
- [257] A. Caballero, R. Tormos, A. Espinosa, M. D. Velasco, A. Tárraga, M. A. Miranda, P. Molina, *Org. Lett.* **2004**, *6*, 4599–4602.
- [258] Y. Ando, Y. Hiruta, D. Citterio, K. Suzuki, *Analyst* **2009**, *134*, 2314–2319.
- [259] J.-M. Tarascon, *Nat. Chem.* **2010**, *2*, 510.
- [260] S. Rochat, K. Severin, *Chimia* **2010**, *64*, 150–152.
- [261] T. B. Rauchfuss, K. Severin in *Organic Nanostructures* (Eds.: J. L. Atwood, J. W. Steed), Wiley-VCH, Weinheim, **2008**, pp. 179–203.
- [262] G. Mezei, C. M. Zaleski, V. L. Pecoraro, *Chem. Rev.* **2007**, *107*, 4933–5003.
- [263] K. Severin, *Chem. Commun.* **2006**, 3859–3867.

- [264] K. Severin, *Coord. Chem. Rev.* **2003**, 245, 3--10.
- [265] Z. Grote, H.-D. Witzemann, R. Scopelliti, K. Severin, *Z. Anorg. Allg. Chem.* **2007**, 633, 858--864.
- [266] I. Saur, K. Severin, *Chem. Commun.* **2005**, 1471--1473.
- [267] Z. Grote, R. Scopelliti, K. Severin, *J. Am. Chem. Soc.* **2004**, 126, 16959--16972.
- [268] Z. Grote, M.-L. Lehaire, R. Scopelliti, K. Severin, *J. Am. Chem. Soc.* **2003**, 125, 13638--13639.
- [269] M.-L. Lehaire, A. Schulz, R. Scopelliti, K. Severin, *Inorg. Chem.* **2003**, 42, 3576--3581.
- [270] M.-L. Lehaire, R. Scopelliti, H. Piotrowski, K. Severin, *Angew. Chem. Int. Ed.* **2002**, 41, 1419--1422.
- [271] M.-L. Lehaire, R. Scopelliti, K. Severin, *Inorg. Chem.* **2002**, 41, 5466--5474.
- [272] M.-L. Lehaire, R. Scopelliti, K. Severin, *Chem. Commun.* **2002**, 2766--2767.
- [273] H. Piotrowski, K. Severin, *Proc. Natl. Acad. Sci. U.S.A.* **2002**, 99, 4997--5000.
- [274] H. Piotrowski, G. Hilt, A. Schulz, P. Mayer, K. Polborn, K. Severin, *Chem. Eur. J.* **2001**, 7, 3196--3208.
- [275] H. Piotrowski, K. Polborn, G. Hilt, K. Severin, *J. Am. Chem. Soc.* **2001**, 123, 2699--2700.
- [276] S. Katsuta, T. Imoto, Y. Kudo, Y. Takeda, *Anal. Sci.* **2008**, 24, 1215--1217.
- [277] S. Katsuta, Y. Iwabe, Y. Kato, Y. Kudo, Y. Takeda, *Inorg. Chim. Acta* **2008**, 361, 103--108.
- [278] L. Mimassi, C. Cordier, C. Guyard-Duhayon, B. E. Mann, H. Amouri, *Organometallics* **2007**, 26, 860--864.
- [279] L. Mimassi, C. Guyard-Duhayon, M. N. Rager, H. Amouri, *Inorg. Chem.* **2004**, 43, 6644--6649.
- [280] C. White, A. Yates, P. M. Maitlis, *Inorg. Synth.* **1992**, 29, 228--234.
- [281] M. A. Bennett, *Coord. Chem. Rev.* **1997**, 166, 225--254.
- [282] J. W. Hull Jr., W. L. Gladfelter, *Organometallics* **1984**, 3, 605--613.
- [283] F. A. Dunand, L. Helm, A. E. Merbach, *Adv. Inorg. Chem.* **2003**, Volume 54, 1--69.
- [284] L. Dadci, H. Elias, U. Frey, A. Hörnig, U. Koelle, A. E. Merbach, H. Paulus, J. S. Schneider, *Inorg. Chem.* **1995**, 34, 306--315.

- [285] M. S. Lah, V. L. Pecoraro, *J. Am. Chem. Soc.* **1989**, *111*, 7258–7259.
- [286] M. S. Lah, M. L. Kirk, W. Hatfield, V. L. Pecoraro, *J. Chem. Soc. Chem. Commun.* **1989**, 1606–1608.
- [287] A. Nakamura, S. Kamiya, *Chem. Pharm. Bull.* **1968**, *16*, 1466–1471.
- [288] A. G. Osborne, L. Jackson, P. D. Taylor, *Spectrochim. Acta Part A* **1993**, *49*, 1703–1708.
- [289] M. K. Patel, R. Fox, P. D. Taylor, *Tetrahedron* **1996**, *52*, 1835–1840.
- [290] K.-W. Chi, Y. S. Ahn, T. H. Park, J. S. Ahn, H. A. Kim, J. Y. Park, *J. Korean Chem. Soc.* **2001**, *45*, 51–60.
- [291] C. Scolaro, T. J. Geldbach, S. Rochat, A. Dorcier, C. Gossens, A. Bergamo, M. Cocchietto, I. Tavernelli, G. Sava, U. Röthlisberger, P. J. Dyson, *Organometallics* **2006**, *25*, 756–765.
- [292] R. Sen, D. Chakravarty, *J. Am. Chem. Soc.* **1928**, *50*, 2428–2436.
- [293] M. J. Hynes, *J. Chem. Soc. Dalton Trans.* **1993**, 311–312.
- [294] A. J. Alpert, A. K. Shukla, *ABRF 2003: Translating biology using proteomics and functional genomics (Denver)* **2003**, Poster P111–W.
- [295] O. S. Wolfbeis, E. Furlinger, H. Kroneis, H. Marsoner, *Fresenius Z. Anal. Chem.* **1983**, *314*, 119–124.
- [296] J. Gao, S. Rochat, X. Qian, K. Severin, *Chem. Eur. J.* **2010**, *16*, 5013–5017.
- [297] M. Kruppa, C. Mandl, S. Miltschitzky, B. König, *J. Am. Chem. Soc.* **2005**, *127*, 3362–3365.
- [298] M. E. Bush, N. D. Bouley, A. R. Urbach, *J. Am. Chem. Soc.* **2005**, *127*, 14511–14517.
- [299] J. Will, A. Kyas, W. S. Sheldrick, D. Wolters, *J. Biol. Inorg. Chem.* **2007**, *12*, 883–894.
- [300] R. Stodt, S. Gencaslan, A. Frodl, C. Schmidt, W. S. Sheldrick, *Inorg. Chim. Acta* **2003**, *355*, 242–253.
- [301] W. Hoffmüller, M. Maurus, K. Severin, W. Beck, *Eur. J. Inorg. Chem.* **1998**, 729–731.
- [302] K. Severin, R. Bergs, W. Beck, *Angew. Chem. Int. Ed.* **1998**, *37*, 1634–1654.
- [303] R. Krämer, M. Maurus, K. Polborn, K. Sünkel, C. Robl, W. Beck, *Chem. Eur. J.* **1996**, *2*, 1518–1526.
- [304] W. Beck, R. Krämer, *Angew. Chem. Int. Ed. Engl.* **1991**, *30*, 1467–1469.

- [305] M. T. Ma, H. N. Hoang, C. C. G. Scully, T. G. Appleton, D. P. Fairlie, *J. Am. Chem. Soc.* **2009**, 131, 4505–4512.
- [306] H. N. Hoang, G. K. Bryant, M. J. Kelso, R. L. Beyer, T. G. Appleton, D. P. Fairlie, *Inorg. Chem.* **2008**, 47, 9439–9449.
- [307] M. J. Kelso, R. L. Beyer, H. N. Hoang, A. S. Lakdawala, J. P. Snyder, W. V. Oliver, T. A. Robertson, T. G. Appleton, D. P. Fairlie, *J. Am. Chem. Soc.* **2004**, 126, 4828–4842.
- [308] X.-j. Sun, L. Zhang, Y. Zhang, G.-s. Yang, Z.-j. Guo, L.-g. Zhu, *New. J. Chem.* **2003**, 27, 818–822.
- [309] N. M. Milović, N. M. Kostić, *J. Am. Chem. Soc.* **2002**, 124, 4759–4769.
- [310] L. Zhu, N. M. Kostić, *Inorg. Chim. Acta* **2002**, 339, 104–110.
- [311] M. I. Djuran, S. U. Milinković, *Polyhedron* **2000**, 19, 959–963.
- [312] P. Tsiveriotis, N. Hadjiliadis, *J. Chem. Soc. Dalton Trans.* **1999**, 459–466.
- [313] L. Zhu, R. Bakhtiar, N. M. Kostić, *J. Biol. Inorg. Chem.* **1998**, 3, 383–391.
- [314] T. N. Parac, N. M. Kostić, *Inorg. Chem.* **1998**, 37, 2141–2144.
- [315] S. U. Milinković, T. N. Parac, M. I. Djuran, Kostić, *J. Chem. Soc. Dalton Trans.* **1997**, 2771–2776.
- [316] T. N. Parac, N. M. Kostić, *J. Am. Chem. Soc.* **1996**, 118, 51–58.
- [317] T. N. Parac, N. M. Kostić, *J. Am. Chem. Soc.* **1996**, 118, 5946–5951.
- [318] L. Zhu, N. M. Kostić, *Inorg. Chim. Acta* **1994**, 217, 21–28.
- [319] L. D. Pettit, M. Bezer, *Coord. Chem. Rev.* **1985**, 61, 97–114.
- [320] A. Ahluwalia, M. Perretti, *Trends Pharmacol. Sci.* **1999**, 20, 100–104.
- [321] K. D. Bhoola, C. D. Figueroa, K. Worthy, *Pharmacol. Rev.* **1992**, 44, 1–80.
- [322] A. Kuoppala, K. A. Lindstedt, J. Saarinen, P. T. Kovanen, J. O. Kokkonen, *Am. J. Physiol.* **2000**, 278, H1069–H1074.
- [323] R. Kohen, Y. Yamamoto, K. C. Cundy, B. N. Ames, *Proc. Natl. Acad. Sci. U.S.A.* **1988**, 85, 3175–3179.
- [324] A. A. Boldyrev, A. M. Dupin, A. Y. Bunin, M. A. Babizhaev, S. E. Severin, *Biochem. Int.* **1987**, 15, 1105–1113.
- [325] O. I. Aruoma, M. J. Laughton, B. Halliwell, *Biochem. J.* **1989**, 264, 863–869.

- [326] G. R. Lenz, A. E. Martell, *Biochemistry* **1964**, 3, 750–753.
- [327] R. D. Vaughan-Jones, K. W. Spitzer, P. Swietach, *Prog. Biophys. Mol. Biol.* **2006**, 90, 207–224.
- [328] T. L. Perry, S. Hansen, D. L. Love, *Lancet* **1968**, 291, 1229–1230.
- [329] S. M. Willi, Y. Zhang, J. B. Hill, M. C. Phelan, R. C. Michaelis, K. R. Holden, *Pediatr. Res.* **1997**, 41, 210–213.
- [330] G. G. Kramarenko, E. D. Markova, I. A. Ivanova-Smolenskaya, A. A. Boldyrev, *Bull. Exp. Biol. Med.* **2001**, 132, 996–999.
- [331] H. A. Lunde, L. R. Gjessing, O. Sjaastad, *Neurochem. Res.* **1986**, 11, 825–838.
- [332] J. F. Lenney, S. C. Peppers, C. M. Kucera, O. Sjaastad, *Clin. Chim. Acta* **1983**, 132, 157–165.
- [333] T. L. Perry, S. Hansen, B. Tischler, R. Bunting, K. Berry, *N. Engl. J. Med.* **1967**, 277, 1219–1227.
- [334] S. P. Bessman, R. Baldwin, *Science* **1962**, 135, 789–791.
- [335] W. S. Wassif, R. A. Sherwood, A. Amir, B. Idowu, B. Summers, N. Leigh, T. J. Peters, *Clin. Chim. Acta* **1994**, 225, 57–64.
- [336] *Geigy Scientific Tables*, Vol. 3, (Ed.: C. Lentner), Ciba-Geigy, Basel, 8th ed., **1984**, pp. 89–106.
- [337] S. Zhang, T. E. Glass, *Tetrahedron Lett.* **2010**, 51, 112–114.
- [338] J. P. Leonard, C. M. G. dos Santos, S. E. Plush, T. McCabe, T. Gunnlaugsson, *Chem. Commun.* **2007**, 129–131.
- [339] J. P. Plante, T. E. Glass, *Org. Lett.* **2006**, 8, 2163–2166.
- [340] J. Lattin, J. D. Carroll, P. E. Green, *Analyzing Multivariate Data*, Brooks/Cole, Pacific Grove, USA, **2003**.
- [341] S. Tufféry, *Data Mining et Statistique Décisionnelle*, Editions TECHNIP, Paris, **2007**.
- [342] *Systat (version 11)*, Systat Software Inc., Chicago, Illinois, USA.
- [343] M. Maeder, Y.-M. Neuhold in *Practical Data Analysis in Chemistry* (Eds.: S. Rutan, B. Walczak), Elsevier Publishing Co., Amsterdam, **2007**.
- [344] H. Gampp, M. Maeder, C. J. Meyer, A. D. Zuberbühler, *Talanta* **1985**, 32, 1133–1139.
- [345] H. Gampp, M. Maeder, C. J. Meyer, A. D. Zuberbühler, *Talanta* **1986**, 33, 943–951.
- [346] M. A. Bennett, A. K. Smith, *J. Chem. Soc. Dalton Trans.* **1974**, 233–241.

- [347] M. A. Bennett, T.-N. Huang, T. W. Matheson, A. K. Smith, *Inorg. Synth.* **1982**, 21, 74–78.
- [348] H. Hohmann, R. Van Eldik, *Inorg. Chim. Acta* **1990**, 174, 87–92.
- [349] H. El Amouri, M. Gruselle, G. Jaouen, *Synth. React. Inorg. Met.-Org. Chem.* **1994**, 24, 395 – 400.
- [350] A. J. Birch, *J. Chem. Soc.* **1950**, 1551–1556.
- [351] M. E. Kuehne, B. F. Lambert, *J. Am. Chem. Soc.* **1959**, 81, 4278–87.
- [352] H. S. Sahoo, D. K. Chand, S. Mahalakshmi, M. Hedayetullah Mir, R. Raghunathan, *Tetrahedron Lett.* **2007**, 48, 761–765.
- [353] C. Olivier, E. Solari, R. Scopelliti, K. Severin, *Inorg. Chem.* **2008**, 47, 4454–4456.
- [354] J. Bergman, S. Bergman, *J. Org. Chem.* **1985**, 50, 1246–1255.
- [355] B. Coxon, A. J. Fatiadi, L. T. Sniegowski, H. S. Hertz, R. Schaffer, *J. Org. Chem.* **1977**, 42, 3132–3140.
- [356] H. E. Gottlieb, R. Alves de Lima, F. delle Monache, *J. Chem. Soc. Perkin Trans. 2* **1979**, 435–437.
- [357] M. Black, J. I. G. Cadogan, H. McNab, A. D. MacPherson, V. P. Roddam, C. Smith, H. R. Swenson, *J. Chem. Soc. Perkin Trans. 1* **1997**, 2483–2494.
- [358] P. W. Chow, A. M. Duffield, P. R. Jefferies, *Aust. J. Chem.* **1966**, 19, 483–488.
- [359] A. Gillmore, C. Lauret, S. M. Roberts, *Tetrahedron* **2003**, 59, 4363–4375.
- [360] J. J. Pisano, J. D. Wilson, L. Cohen, D. Abraham, S. Udenfriend, *J. Biol. Chem.* **1961**, 236, 499–502.
- [361] R. Evans, F. Irreverre, *J. Org. Chem.* **1959**, 24, 863–864.
- [362] H. E. Carter, R. L. Frank, H. W. Johnston, *Organic Syntheses Coll. Vol. 3* **1955**, 167–169.

Curriculum Vitae

Sébastien Rochat

Avenue d'Yverdon 2
1004 Lausanne
Switzerland

0041 (0)76 503 44 41
sebastien.rochat@a3.epfl.ch

Education

Ecole Polytechnique Fédérale de Lausanne (EPFL)
PhD student in the doctoral program of chemistry and chemical engineering

Lausanne, Switzerland
May 2006 - present

Ecole Polytechnique Fédérale de Lausanne (EPFL)
Master of Science (MSc) in molecular and biological chemistry

Lausanne, Switzerland
2001-2006

Final grade: 5.67/6.00 (95%)

Research Experience

Laboratory of Supramolecular Chemistry, EPFL
Metal-based chemosensors for important bioanalytes

Lausanne, Switzerland
May 2006 - present

Thesis advisor: Prof. Kay Severin

Catalysis and Advanced Materials group, Imperial College London

London, UK

MSc thesis in supramolecular chemistry (coordination networks)

Oct. 2005 - March 2006

Supervisor: Prof. Nicholas J. Long

Laboratory of Biomolecular Magnetic Resonance, EPFL

Lausanne, Switzerland

Internship in NMR spectroscopy (slow diffusion measurements through singlet-state studies of coupled protons systems)

Aug. - Sept. 2005

Supervisor: Prof. Geoffrey Bodenhausen

Laboratory of Glycochemistry and Asymmetric Synthesis, EPFL

Lausanne, Switzerland

Semester project (new transition metal-catalysed carbon-carbon couplings)

Feb. - June 2005

Supervisor: Prof. Pierre Vogel

Laboratory of Organometallic and Medicinal Chemistry, EPFL

Lausanne, Switzerland

Semester project (synthesis and reactivity towards DNA of new ruthenium(II) complexes)

Oct. 2004 - Feb. 2005

Supervisor: Prof. Paul J. Dyson

Teaching Experience

Practical Inorganic Chemistry	2006 - 2008
BSc level, average class 12 students Responsible for the organisation of the course (total 45 students)	
Project in Supramolecular Chemistry	2006
MSc level (Master's thesis), individual supervision	
General practical chemistry	2005 - 2008
BSc level, average class 15 students	

Skills

Chemical Techniques: synthesis of organic and inorganic molecules, handling of air- and moisture-sensitive compounds (Schlenk and glovebox techniques), chromatography, distillation. Analytical techniques: NMR, IR, UV-visible and fluorescence spectroscopies, mass spectrometry, HPLC, GC, GC-MS, LC-MS.

Computer skills: MS Office, EndNote, LaTeX, Systat, ChemDraw, Winnmr, Xwinmr, TopSpin, Cary Eclipse Softwares.

Languages: French (mother tongue), English (fluent), German (working knowledge).

Scientific Achievements

Scientific Publications

6. S. Rochat, K. Severin, *J. Comb. Chem.* **2010**, 12, 595-599.
5. S. Rochat, K. Severin, *Chimia* **2010**, 64, 150-152.
4. J. Gao, S. Rochat, X. Qian, K. Severin, *Chem. Eur. J.* **2010**, 16, 5013-5017.
3. S. Rochat, J. Gao, X. Qian, F. Zaubitzer K. Severin, *Chem. Eur. J.* **2010**, 16, 104-113.
2. S. Rochat, Z. Grote, K. Severin, *Org. Biomol. Chem.* **2009**, 7, 1147-1153.
1. C. Scolaro, T. J. Geldbach, S. Rochat, A. Dorcier, C. Gossens, A. Bergamo, M. Cocchietto, I. Tavernelli, G. Sava, U. Röthlisberger, P. J. Dyson, *Organometallics* **2006**, 25, 756-765.

Attended Conferences & Presentations

3rd EuCheMS Chemistry Congress	Nürnberg, Germany
Poster presentation	2010
Swiss Chemical Society Fall Meeting	Lausanne, Switzerland
Oral presentation	2009

International Symposium in Macrocyclic and Supramolecular Chemistry	Maastricht, The Netherlands
<i>Poster presentation</i>	2009
Swiss Chemical Society Fall Meeting	Zürich, Switzerland
<i>Poster presentation</i>	2008
CUSO séminaire hors-ville “The Challenge of Future Energy Sources”	Villars, Switzerland
<i>Poster presentation</i>	2008
Swiss Chemical Society Fall Meeting	Lausanne, Switzerland
<i>Poster presentation</i>	2007
CHUV (University Hospital) Research Day “Biomedical Imaging”	Lausanne, Switzerland
<i>Poster presentation</i>	2007
CUSO séminaire hors-ville “Bottom-up Approach to Nanotechnology”	Villars, Switzerland
<i>Poster presentation</i>	2007
Swiss Chemical Society Fall Meeting	Zürich, Switzerland
<i>Poster presentation</i>	2006

Awards & Honors

SCNAT Chemistry Travel Award from the Swiss Academy of Sciences	2010
Mettler-Toledo Prize for the best oral presentation in Inorganic Chemistry, Swiss Chemical Society Fall Meeting, Lausanne	2009
Proficiency Prize for teaching activities, Section of Chemistry and Chemical Engineering, EPFL	2008
Pelet Award for the best general average grade of the Bachelor cycle in the Section of Chemistry and Chemical Engineering, EPFL	2004

“But it was all right, everything was all right, the struggle was finished.”

G. Orwell, *Nineteen Eighty-Four*